SCALE-UP STUDY OF SUSPENSION POLYMERISATION IN AN OSCILLATORY BAFFLED REACTOR

Greig Nelson

Thesis submitted for the degree of

Doctor of Philosophy

To Heriot-Watt University, Edinburgh, U.K.

On the completion of research in the

Centre for Oscillatory Baffled Reactor Applications (C.O.B.R.A.),

Department of Mechanical and Chemical Engineering

August 2001

DECLARATION

This is to declare that the thesis is an account of the author's work carried out at Heriot-Watt University, Edinburgh, except where aknowledgement is made, and has not been submitted for any other degrees.

Greig Nelson (Candidate)

Prof. Xiongwei Ni (Supervisor)

CONTENTS

CONTENTS I

LIST OF FIGURES IX

LIST OF TABLES XIII

AKNOWLEDGEMENTS XIV

NOMENCLATURE XV

ABSTRACT XX

1 INTRODUCTION 1

1.1 General Introduction 1

1.2 Objectives and Scope of Project 2

1.3 Structure of Thesis 3

2 LITERATURE REVIEW 4

2.1 Oscillatory Flow Mixing 4

2.1.1 Background 4

2.1.2 Fluid Mechanics 4

2.1.3 Baffle Geometry 8

2.1.4 Applications 10

2.1.5 Power Requirements 11

2.1.6 Summary 13

2.2 Liquid-Liquid Dispersion 13

2.2.1 Introduction 13

2.2.1 Minimum Agitation Intensity for Complete Dispersion 14

2.2.3 Influence of Fluid Mechanics on Drop Size 17

2.2.3.1 Fluid Mechanics of Turbulent Liquid-Liquid Dispersions 17

2.2.3.2 Droplet Breakage Mechanism 19

2.2.3.3 Droplet Coalescence Mechanism 21

2.2.4 Techniques for Droplet Size Measurement 23

2.2.4.1 Photographic Techniques 24

2.2.4.2 Droplet Stabilisation Techniques 25

2.2.4.3 Other Techniques 26

2.2.5 Experimental Investigations into Drop Size 27

2.2.5.1 Effect of System Parameters on Drop Size 27

2.2.5.2 Scale-Up Characteristics 30

2.2.5.3 Summary of Experimental Work 30

2.2.6 Modelling of Dynamic Droplet Behaviour 31

2.2.7 Summary 33

2.3 Suspension Polymerisation 34

2.3.1 Introduction 34

2.3.1.1 Polymerisation Processes 34

2.3.1.2 Types of Suspension Polymerisation 35

2.3.1.3 Stabilisers 36

2.3.1.4 Advantages and Disadvantages 37

2.3.1.5 Factors Affecting Product Quality 38

2.3.2 Reaction Kinetics 39

2.3.2.1 Kinetic Mechanism 40

2.3.2.2 Factors Affecting Chain Length 42

2.3.3 Suspension Polymerisation Reactors 42

2.3.3.1 Reactor Requirements 42

2.3.3.2 Stirred Tank Reactor 43

2.3.3.3 Stirred Tank with Draft Tube 44

2.3.3.4 Loop Reactor 44

2.3.3.5 Stirred Tank with Pre-Mixer 45

2.3.3.6 Oscillatory Baffled Reactor 46

2.3.3.7 Other Techniques 46

2.3.4 Control of Particle Size Distribution 47

2.3.4.1 Introduction 47

2.3.4.2 Effect of Agitation Intensity 48

2.3.4.3 Effect of Stabiliser Concentration 52

2.3.4.4 Effect of Phase Fraction 53

2.3.5 Evolution of Droplet Population during Reaction 54

2.3.6 Summary 56

3 EXPERIMENTAL APPARATUS AND FACILITIES **58**

3.1 The Perspex OBC 58

3.2 The Stainless Steel OBC 61

3.2.1 The Column 61

3.2.2 The Baffle Oscillation Mechanism 62

3.2.3 The Heating/Cooling System 62

3.2.4 The Data Acquisition System 64

4 FLOW VISUALISATION **65**

4.1 Introduction 65

4.2 Experimental Apparatus and Procedures 65

4.3 Results and Discussion 66

4.3.1 Effect of Oscillation Frequency and Amplitude 66

4.3.2 Effect of Orifice Diameter 67

4.3.3 Effect of Baffle Spacing 68

4.4 Conclusions 69

5 OIL-WATER DISPERSION **79**

5.1 Introduction 79

5.2 Experimental Apparatus and Procedures 79

5.3 Results and Discussion 82

5.3.1 Effect of Oscillation Time 82

5.3.2 Effect of Operating Conditions on Degree of Oil-Water Dispersion 83

5.3.3 Minimum Frequency for Complete Dispersion 86

5.3.3.1 Definition 86

5.3.3.2 Effect of Amplitude and Baffle Geometry on f_{min} 87

5.3.3.3 Effect of Oil Phase Fraction 89

5.3.4 Effect of Energy Dissipation 90

5.3.5 Scale-Up 91

5.3.5.1 Effect of Scale-Up on Minimum Energy Dissipation 91

5.3.5.2 Effect of Scale-Up on Minimum Oscillatory Velocity 94

5.3.5.3 Scale-Up Correlation 95

5.4 Conclusions 100

6 HEAT TRANSFER **102**

6.1 Introduction 102

6.2 Experimental Apparatus and Procedures 102

6.3 Results and Discussion 103

6.3.1 Heat Loss from the System 103

6.3.2 Effect of Oscillation on Temperature Uniformity 104

6.3.3 Shell Side Correlation 106

6.3.4 Tube Side Correlation 109

6.3.5Scale-Up 114

6.4 Conclusions 115

7 DROPLET SIZE DISTRIBUTION 117

7.1 Introduction 117

7.2 Experimental Apparatus and Procedures 118

7.2.1 Apparatus and Materials 118

7.2.2 Droplet Measurement Technique 118

7.2.2.1 Sampling and Stabilisation 118

7.2.2.2 Image Analysis 119

7.3 results and Discussion 120

7.3.1 Droplet Number 120

7.3.2 Repeatability 121

7.3.3 Uniformity 122

7.3.4 Effect of Oscillation Time 124

7.3.5 Effect of Oscillatory Conditions 125

7.3.5.1 Effect of Oscillation Frequency 125

7.3.5.2 Effect of Oscillation Amplitude 127

7.3.5.3 Effect of Oscillatory Velocity 129

7.3.6 Effect of Baffle Geometry 130

7.3.6.1 Effect of Baffle Free Area 130

7.3.6.2 Effect of Baffle spacing 132

7.3.7 Effect of Energy Dissipation 134

7.4 Scale-Up Characteristics 135

7.5 Conclusions 138

8 BREAKAGE AND COALESCENCE MODELLING **140**

8.1 Introduction 140

8.2 The model 140

8.2.1 General Assumptions 141

8.2.2 Droplet Discretisation 142

8.2.3 The Continuity Equation for Volume Fraction 143

8.2.3.1 Breakage Equations 144

8.2.3.2 Coalescence Equations 145

8.2.2.3 The Combined Model 150

8.3 Experimental Facilities and Procedures 152

8.3.1 Experimental Set-Up 152

8.3.2 Procedures 153

8.3.2.1 Breakage-Only Experiments 153

8.3.2.2 Experiments with Breakage and Coalescence 153

8.4 Results and Discussion 154

8.4.1 Breakage-Only Experiments 154

8.4.2 Experiments with Breakage and Coalescence 156

8.4.3 Model Validation and Robustness Tests 158

8.4.3.1 DSD Reconstruction 158

8.4.3.2 Robustness of The Model 159

8.4.4 Comparison of Scale-Up 162

8.5 Conclusions 164

9 SUSPENSION POLYMERISATION **166**

9.1 Introduction 166

9.2 Experimental Apparatus and Procedures 166

9.2.1 Apparatus and Materials 166

9.2.2 Procedures 167

9.2.2.1 Reaction Procedure 167

9.2.2.2 Product Recovery 168

9.2.2.3 Analysis of Results 169

9.2.2.4 Range of Operating Conditions Studied 169

9.3 Results and Discussion 170

9.3.1 Temperature Profile of Reaction 170

9.3.2 Oversize Fraction 171

9.3.3 Effect of Operating Parameters on Particle Size 171

9.3.3.1 Effect of Oscillation Frequency 171

9.3.3.2 Effect of Oscillation Amplitude 173

9.3.3.3 Effect of Oscillatory Velocity 175

9.3.4 Effect of Baffle Geometry 176

9.3.4.1 Effect of Baffle Free Area 176

9.3.4.2 Effect of Baffle Spacing 178

9.3.5 Effect of Energy Dissipation 180

9.3.6 Comparison of Final Particle Size with Initial Drop Size 181

9.3.7 Effect of Scale-Up on Particle Size

9.3.8 Other Product Properties 185

9.3.8.1 Molecular Weight Distribution 185

9.3.8.2 Residual BPO Content 185

9.4 Fouling Problems 187

9.5 Conclusions 188

10 CONCLUSIONS **190**

10.1 Mixing Characteristics 190

10.2 Application of OBC to Suspension Polymerisation 191

10.2.1 Heat Transfer Study 191

10.2.2 Droplets Size Distribution 192

10.2.3 Suspension Polymerisation 193

11 RECOMMENDATIONS FOR FUTURE WORK 195

11.1 Oil-Water Dispersion 195

11.2 Heat Transfer 195

11.3 Droplet Size Distribution 196

11.4 Suspension Polymerisation 196

APPENDIX 1 - OIL-WATER DISPERSION RESULTS 197

APPENDIX 2 - HEAT TRANSFER RESULTS 202

Appendix 2.1 Experimental and Calculated Results for Continuous Operation 202

Appendix 2.2 Recorded Temperature Data for Batch Operation 203

Appendix 2.3 Calculated Heat Transfer Data 215

APPENDIX 3 - DROPLET SIZE DISTRIBUTION RESULTS 216

Appendix 3.1 DSD Data Collected at Various Operating Conditions 216

Appendix 3.2 Data Used for Breakage and Coalescence Modelling 225

Appendix 3.2.1 Data form Breakage Only Experiments 225

Appendix 3.2.2 Data from Experiments with Breakage and Coalescence 230

APPENDIX 4 – POLYMERISATION RESULTS 235

Appendix 4.1 Particle Size Distribution Data 235

Appendix 4.2 Molecular Weight Data 241

Appendix 4.3 Residual BPO Content 243

REFERENCES 244

LIST OF FIGURES

Figure 2.1: Fluid mechanics of oscillatory baffled flow

Figure 3.1: The Perspex oscillatory baffled column

Figure 3.2: Stainless steel OBC

Figure 3.3: Heating cooling system

Figure 4.1: Effect of oscillation frequency on flow patterns (A) 0.25 Hz, (B) 0.5 Hz, (C) 0.75 Hz, (x_o = 100 mm, α = 25%, L = 600 mm)

Figure 4.2: Effect of oscillation amplitude on flow patterns (A) 100 mm, (B) 140 mm, (C) 180 mm, (f = 0.5 Hz, α = 25 %, L = 600 mm)

Figure 4.3: Effect of baffle free area on flow patterns (A) α = 20%, (B) α = 25%, (C) α = 31% (f = 0.25 Hz, x_o = 140 mm, L = 600 mm)

Figure 4.4: Effect of baffle spacing on flow patterns (A) L = 500 mm, (B) L = 600 mm, (C) L = 800 mm (f = 0.25 Hz, x_o = 100 mm, α = 25%)

Figure 4.5: Effect of baffle spacing on flow patterns (A) L = 500 mm, (B) L = 600 mm, (C) L = 800 mm (f = 0.25 Hz, x_o = 140 mm, α = 25%)

Figure 4.6: Effect of baffle spacing on flow patterns (A) L = 500 mm, (B) L = 600 mm, (C) L = 800 mm (f = 0.25 Hz, x_o = 180 mm, α = 25%)

Figure 5.1: Location of sampling point

Figure 5.2: Effect of time and frequency on level of oil-water dispersion achieved

Figure 5.3: Effect of oscillatory velocity on f_r (α=31%, L=600mm)

Figure 5.4: Effect of oscillatory velocity and α on f_r (L=600mm)

Figure 5.5: Effect of oscillatory velocity and baffle spacing on f_r (α=25%)

Figure 5.6: Effect of amplitude and α on f_{min} (L=600mm)

Figure 5.7: Effect of amplitude and L on f_{min} (α=25%)

Figure 5.8: Effect of oil phase fraction on f_{min} (x_o=140mm, α=25%, L=600mm)

Figure 5.9: Effect of energy dissipation on f_r

Figure 5.10: Minimum energy dissipation for complete dispersion

Figure 5.11: Minimum oscillation frequency for complete dispersion

Figure 5.12: Effect of column diameter on f_{min}

Figure 5.13: Comparison of correlation with experimental data

Figure 6.1: Temperature drop due to heat loss by natural convection

Figure 6.2: Temperature profile without oscillation

Figure 6.3: Temperature profile with oscillation (f = 1Hz, x_o = 75mm, α = 25%, L = 315mm)

Figure 6.4: Correlation between 1/U and $1/(Re_s^{0.45})$

Figure 6.5: Effect of frequency and amplitude on tube side heat transfer coefficient

Figure 6.6: Heat transfer correlation

Figure 6.7: Scale-Up correlation for heat transfer coefficient

Figure 7.1: Typical droplet image

Figure 7.2: Effect of droplet number on drop size distribution

Figure 7.3: Repeatability test (f=1.0Hz, x_o=75mm, α=25%, L=315mm)

Figure 7.4: Effect of sample location on drop size distribution (f=1.0Hz, x_o=75mm, α=25%, L=315mm)

Figure 7.5: Effect of oscillation time on drop size distribution (f=1.0Hz, x_o=75mm, α=20%, L=315mm)

Figure 7.6: Effect of oscillation time on Suater mean droplet diameter (f=1.0Hz, x_o=75mm, α=20%, L=315mm)

Figure 7.7: Effect of frequency drop size distribution (x_o=100mm, α=25%, L=315mm)

Figure 7.8: Effect of oscillation frequency on d_{32} (α=25%, L=315mm)

Figure 7.9: Effect of amplitude on drop size distribution (f=0.8Hz, α=25%, L=315mm)

Figure 7.10: Effect of oscillation amplitude on d_{32} (f=0.8Hz, α=25%, L=315mm)

Figure 7.11: Effect of frequency and amplitude, at constant oscillatory velocity on drop size distribution (α=25%, L=315mm)

Figure 7.12: Effect of oscillatory velocity on d_{32} (α=25%, L=315mm)

Figure 7.13: Effect of baffle free area on drop size distribution (f=1.0Hz, x_o=75mm, L=315mm)

Figure 7.14: Effect of x_of and α on d_{32} (L=315mm)

Figure 7.15: Effect of baffle spacing on drop size distribution (f=1.0Hz, x_o=75mm, α=25%)

Figure 7.16: Effect of x_of and L on d_{32} (α=25%)

Figure 7.17: Effect of energy dissipation on d_{32}

Figure 7.18: Comparison of the effect of energy dissipation on d_{32} in OBCs of 50mm and 213mm in diameter

Figure 8.1: The discretised volume bins of droplets used in the model

Figure 8.2: Effect of frequency on breakage rate (x_o = 75 mm)

Figure 8.3: Effect of amplitude on breakage rate (f = 1.0Hz)

Figure 8.4: Effect of frequency on the evaluated breakage rate (x_o = 75 mm)

Figure 8.5: Effect of amplitude on coalescence rate (f = 0.8 Hz)

Figure 8.6: Individual coalescence rates evaluated for each type of drop interaction (f = 0.8 Hz, x_o = 75 mm)

Figure 8.7: Comparison of DSDs between reconstructed and experimental measured (f = 0.6 Hz, x_o = 75 mm)

Figure 8.8: Comparison of breakage rate between the target and the extracted ones (Robustness test 1)

Figure 8.9: Comparison of coalescence rates between the target and the extracted ones (Robustness test 1)

Figure 8.10: Comparison of breakage and coalescence rates (Robustness test 2)

Figure 8.11: Comparison of breakage rates between bench and pilot scale OBRs

Figure 8.12: Comparison of coalescence rates between bench and pilot scale OBRs

Figure 9.1: Reaction temperature profile (f=1.0Hz, x_o=75mm, α=25%, L=315mm)

Figure 9.2: Effect of oscillation frequency on PSD (x_o=100mm, α=20%, L=315mm)

Figure 9.3: Effect of oscillation frequency on mean particle diameter (x_o=100mm, α=20%, L=315mm)

Figure 9.4: Effect of oscillation amplitude on PSD (f=1.2Hz, α=20%, L=315mm)

Figure 9.5: Effect of oscillation amplitude on mean particle diameter (f=1.2Hz, α=20%, L=315mm)

Figure 9.6: Effect of oscillatory velocity on mean particle size (α=20%, L=315mm)

Figure 9.7: Effect of baffle free area on PSD (f=1.0Hz, x_o=100mm, L=315mm)

Figure 9.8: Effect of x_of and α on mean particle size (L=315mm)

Figure 9.9: Effect of baffle spacing on PSD (f=1.0Hz, x_o=75mm, α=25%)

Figure 9.10: Effect of oscillatory velocity and baffle spacing on mean particle size (α=20%)

Figure 9.11: Effect of energy dissipation on mean particle size

Figure 9.12: Comparison of mean droplet at particle sizes

LIST OF TABLES

Table 4.1: Effect of oscillation frequency and amplitude on the length to which eddies propagate through the baffled cavity (baffle spacing = 800 mm)

Table 4.2: Effect of oscillation frequency and amplitude on the length to which eddies propagate through the baffled cavity (baffle spacing = 600 mm)

Table 4.3: Effect of oscillation frequency and amplitude on the length to which eddies propagate through the baffled cavity (baffle spacing = 500 mm)

Table 7.1: Sauter mean droplet diameters obtained from repeatability test

Table 7.2: Effect of sample location on Sauter mean droplet diameter

Table 7.3: Comparison of correlation for d_{32} in different devices

Table 8.1: Specification of MMA Recipes

Table 8.2: Range of operating parameters studied in experiments to determine breakage and coalescence rates

Table 9.1: Correlations for mean drop size and mean particle size in OBCs of 213mm and 50mm in diameter

AKNOWLEDGEMENTS

My sincere thanks goes to my supervisor, Professor X. Ni, for his continued guidance and encouragement throughout the duration of this project. I am also grateful to my industrial supervisor, Dr I. Mustafa of Ineos Acrylics Ltd, for his advice on technical matters arising during the study. I would also like to thank the technical staff at Heriot-Watt University, especially Mr R. Kinsella, Mr J. Thompson, Mr C. McCluckie, Mr I. Galloway and Mr A. Haston, for their efforts in constructing the apparatus required and also Mr L. Morris for his guidance on carrying out the required photography. In addition, I would like to thank Dr S. Abed-Ali of Ineos Acrylics for his time and effort in solving some technical problems and for valuable discussion on a number of matters during the course of this work.

Finally, I would like to thank the Engineering and Physical Sciences Research Council (EPSRC) and Ineos Acrylics Ltd. for supporting me financially throughout this project.

NOMENCLATURE

a	Constant in equation (4.4)
A	Heat transfer area, m^2
$\boldsymbol{A}$	Mass matrix derived from vector **g** and matrix β
$A(h_o)$	Constant
b	Constant in equation (4.4)
B_i^+	Birth rate of drops in bin i due to coalescence, s^{-1}
B_i^-	Death rate of drops in bin i due to coalescence, s^{-1}
C	Constant
C_D	Orifice discharge coefficient (= 0.7)
C_i^+	Birth rate of drops in bin i due to coalescence, s^{-1}
C_i^-	Death rate of drops in bin i due to coalescence, s^{-1}
const	Constant
Cp_c	Specific heat capacity of cooling water, J kg^{-1} K^{-1}
Cp_h	Specific heat capacity of hot water, J kg^{-1} K^{-1}
d	Droplet diameter, m
D	Column diameter, m
	Impeller diameter, m
D_m	Hydraulic mean diameter, m
D_s	Column diameter on shell side, m
d_{32}	Sauter mean droplet diameter, m
d_i	Average droplet diameter of bin class i, m
d_{max}	Maximum droplet diameter, m
d_{min}	Minimum droplet diameter, m

$d_{v,0.5}$ Particle diameter at 50% cumulative volume fraction, m

E_a Adhesion energy, J

E_t Energy of turbulence, J

f Oscillation frequency, s^{-1}

f_i Volume fraction of dispersed phase droplets in bin i

f_{min} Minimum oscillation frequency for complete dispersion, s^{-1}

F Viscous force, N

$\boldsymbol{g}$ Vector of breakage rates

g_i Breakage rate of droplets in bin (I), s^{-1}

h_o Interfacial film thickness between droplets, m

ΔH_R Heat of reaction, kJ mol^{-1}

h_s Shell side heat transfer coefficient, W m^{-2} K^{-1}

h_t Tube side heat transfer coefficient, W m^{-2} K^{-1}

k constant

Thermal conductivity, W m^{-1} K^{-1}

$k_{b,1}$ Fraction of drops allocated to bin (j+1) from type (b) coalescence $\left(=1-\frac{1}{2\sqrt{2}}\right)$

$k_{b,2}$ Fraction of drops allocated to bin (j+2) from type (b) coalescence $\left(=\frac{1}{2\sqrt{2}}\right)$

$kc_{,1}$ Fraction of drops allocated to bin (j+1) from type (c) coalescence $\left(=\frac{3}{2}-\sqrt{2}\right)$

$kc_{,2}$ Fraction of drops allocated to bin (j+2) from type (c) coalescence $\left(=\sqrt{2}-\frac{1}{2}\right)$

K_1 Term in equation (4.7) (= UA/m_cCp_c)

k_t Thermal conductivity of tube material, W m^{-1} K^{-1}

L Baffle spacing, m

M	Mass, kg
m_c	mass flowrate of cooling water, kg s^{-1}
m_h	mass flowrate of hot water, kg s^{-1}
N	Number of baffle per unit length, m^{-1}
	Stirrer speed, s^{-1}
n_i	Number of droplets in bin class i
N_{min}	Minimum impeller speed for complete dispersion, s^{-1}
Nu_t	Tube side Nusselt number (=h_tD/k)
P	Power, W
Pr	Prandtl number (= $Cp\mu/k$)
Q	Heat transfer rate, W
r	Distance between two given points in a flow field, m
Re_n	Net flow Reynold's number (= uD/ν)
Re_o	Oscillatory Reynold's number (= $\omega x_o/\nu$)
Re_s	Shell side Reynold's number (= uD_m/ν)
Re_{ST}	Stirred tank Reynold's number, (= D^2N/ν_c)
St	Strouhal number (= $D/4\pi x_o$)
t	time, s
T	Temperature, K
$T_{c_{in}}$	Temperature of inlet cooling water, K
$T_{c_{out}}$	Temperature of outlet cooling water, K
$T_{h_{in}}$	Temperature of inlet hot water, K
$T_{h_{out}}$	Temperature of outlet hot water, K
ΔT_m	Log mean temperature difference, K

u	Velocity, m s^{-1}
U	Overall heat transfer coefficient, kW m^{-2} K^{-1}
u_t	Terminal settling velocity, m s^{-1}
u(r)	Mean velocity between two point a distance r apart, m s^{-1}
V	Volume, m^3
V_d	Dispersed phase volume, m^3
We	Weber number
We_{crit}	Critical Weber number
We_T	Impeller Weber number
x_o	Oscillation amplitude, m

Greek Letters

α	Fractional baffle free area
β	Vector of coalescence rates
$\beta_{i,j}$	Rate of coalescence between drops in bin (i) and drops in bin (j), s^{-1}
ε	Energy dissipation rate, W kg^{-1}
ϕ	Phase fraction of the dispersed phase
η	Microscale of turbulence, m
μ	Dynamic viscosity, kg m^{-1} s^{-1}
μ_c	Dynamic viscosity of the continuous phase, kg m^{-1} s^{-1}
μ_d	Dynamic viscosity of the dispersed phase, kg m^{-1} s^{-1}
μ_w	Dynamic viscosity in the vicinity of the wall, kg m^{-1} s^{-1}
σ	Surface tension, N m^{-1}
ν	Kinematic viscosity, m^2 s^{-1}

ν_c	Kinematic viscosity of the continuous phase, $m^2\ s^{-1}$
ρ	Density, kg m^3
ρ_c	Density of the continuous phase, kg m^3
ω	Angular frequency of oscillation ($=2\pi f$), rad s^{-1}

ABSTRACT

Suspension polymerisation methodology is widely used throughout the chemical industry for the production of a variety of products, and is traditionally operated in stirred tank reactors. Recent laboratory scale studies show that oscillatory baffled reactors (OBRs) may potentially be a viable alternative to stirred tanks for suspension polymerisation, as it offers greater controllability and better repeatability. The objective of the present study is, therefore, to determine the feasibility of the oscillatory baffled reactor as a relatively new technology for carrying out suspension polymerisation on an industrial scale, and the model reaction chosen for this work is the suspension polymerisation of methylmethacrylate (MMA).

Experimental investigations into the characteristics of mixing, heat transfer, liquid-liquid dispersion and suspension polymerisation of methylmethacrylate were performed in oscillatory baffled columns of 380mm and 213mm internal diameter. A range of oscillation frequencies and amplitudes, baffle spacings and baffle free areas were investigated and correlations have been established for each of the processes studied. The results were compared with those previously reported for similar studies in bench scale devices and scale-up characteristics have been determined. The significant findings from this work are that the behaviour of large and small scale OBR devices are similar in terms of both fluid mechanical conditions and reactor performance and only a linear scale up of the reactor geometry is required when OBRs are applied to any industrial scale.

1 INTRODUCTION

1.1 General Introduction

Suspension polymerisation is a common industrial process and is used for the production of a wide variety of polymer products. These include commodity species, such as polyvinylchloride, polystyrene and polyacrylamide; moderate tonnage products, such as cation and anion exchange resins; and specialities such as HPLC packings and dental materials, just to name but a few. In these processes, one or more water insoluble monomers are dispersed as discrete drops in an aqueous medium to form a suspension and the droplets in the suspension are then polymerised to form polymer beads. The particle size distribution (PSD) is an important parameter in such processes as it determines the product quality and processing ability of the polymer. Therefore, it is desirable for chemical engineers to control the PSD in any polymerisation process. Traditionally the suspension is formed by mixing the two phases by means of mechanical agitation, normally in a stirred tank vessel. The particle size distribution is controlled by the agitation intensity, which depends on factors such as the rotational speed of the impeller and the geometrical configuration of the impeller and tank. It is well known, however, that the scale up correlation for stirred tank reactors is generally poor, resulting in difficulties in predicting and controlling the PSD in large scale reactors.

An alternative mixing device to the stirred tank is the oscillatory baffled tube of Mackley (1987) in which efficient eddy mixing is generated by superimposing oscillations onto a fluid in a tube that contains periodically spaced annular baffles. In such a device,

the flow patterns and mixing intensity can be controlled by varying the tube and baffle geometry and the oscillation frequency and amplitude. Recently, liquid-liquid dispersion and suspension polymerisation of methylmethacrylate (MMA) were studied in a bench 50mm diameter oscillatory baffled reactor (OBR) of fixed baffle and tube geometry (Ni et al., 1998b,1999). It was found that by varying the oscillatory conditions (i.e. the oscillation frequency and amplitude), the mean droplet size of the dispersed phase and subsequently the mean particle size of the polymer produced can be controlled accurately. It was also found that a strong correlation existed between the two parameters, indicating that the mean droplet size can be used as a control measure for determining the final particle size. However, as these studies were carried out on a small scale, further work was required to investigate and quantify the effect of scale up on such processes, and this was the motivation for the present work.

1.2 Objectives and Scope of the Project

The primary objective of this project was to study the scale up criteria of the oscillatory baffled reactor using suspension polymerisation of MMA as the model reaction. This project was essentially an extension of the previous work in a bench scale column (Zhang, 1998). In order to carry out the study, two oscillatory baffled columns had to be constructed, one of Perspex of 380 mm in diameter and 2.04 m in height, the largest one in the U.K., and one made of stainless steel of 213 mm in diameter. Experimental work was required to study characteristics of mixing and oil-water dispersion in the 380 mm diameter column and heat transfer, liquid-liquid dispersion and suspension polymerisation of MMA in the 213 mm diameter column, from which scale up characteristics could be determined

by comparison with results from small scale studies. The project also involved computational modeling of drop breakage and coalescence rates in order to gain scientific insights on drop interactions and formation in the OBR.

1.3 Structure of Thesis

Following this introduction, the thesis commences in Chapter 2 with a survey of the background literature relevant to OBR, droplet size distribution, particle size distribution and suspension polymerisation. Chapter 3 introduces the experimental apparatus that has been constructed for the scale-up study. In order to characterise the fluid mechanical conditions, a flow visualisation study is initially used to compare flow conditions for experiments under different conditions, which is reported in Chapter 4. This is then followed by an investigation of oil-water dispersion characteristics in Chapter 5, which was carried out over a range of operating conditions. Chapter 6 describes the heat transfer study, which investigated the effect of operating parameters on heat transfer rates. The droplet study is outlined in Chapters 7 and 8, which involved measuring drop size distributions and mean droplet sizes and the effect of operating conditions and scale-up on them. Discretised population balance equations were also used to model the droplet breakage and coalescence rates. The model reactions were performed in the 213 mm diameter OBR for various oscillation frequencies, amplitudes, baffle spacings and baffle free areas and a scale-up correlation was established. Details of this study are given in Chapter 9. The overall conclusions from the project are given in Chapter 10 and Chapter 11 states some recommendations for future work.

2 LITERATURE REVIEW

In suspension polymerisation processes polymer particles are produced from dispersed monomer droplets that are initially formed by fluid agitation, which in the present case was induced by oscillatory flow mixing. Therefore, the three key areas of interest in this project are: (i) oscillatory flow mixing, (ii) liquid-liquid dispersion and (iii) suspension polymerisation, and the relevant literature relating to each of these topics is reviewed in turn in this chapter.

2.1 Oscillatory Flow Mixing

2.1.1 Background

The principle of oscillatory flow mixing was first introduced by Van Dijick (1935) who proposed the pulsed sieve plate (PSP) column as a device for liquid-liquid extraction. This design was later modified by Karr (1959) to yield the reciprocating plate column (RPC) in which perforated plates are oscillated inside the column as opposed to fluid oscillation which is used by PSPs. The development of RPCs and PSPs for liquid-liquid extraction has since been extended by a number of researchers (Richard and Babb, 1969; Karr and Lo, 1971; Lo and Karr, 1972; Kim and Baird, 1976; Hazef et al., 1979, 1980; Baird et al., 1992) and has also been successfully applied to other areas of chemical engineering such as gas-liquid mass transfer (Yang et al., 1986a,b; Baird and Rama Rao, 1998) and absorption (Baird et al., 1989). Other oscillatory flow devices that have emerged include the pulsed

packed column of Baird et al (1986) and the multi-disk vibratory column (MDVC) of Miyanami et al (1973) both of which have been further developed in recent decades (Spaay et al., 1971; Miyanami et al., 1975; Tojo et al., 1975, 1976a,b, 1980). In the 1970's Bellhouse et al (1973) carried out pioneering work using oscillatory flow in furrowed channels to enhance the performance of a membrane blood oxygenator. Sobey (1980) modelled oscillatory flow in this geometry and found that the increased mass transfer can be attributed to the formation of eddies in each of the furrows which are subsequently ejected into the main body of fluid on flow reversal. This mechanism is repeated for each cycle of the oscillation which ensures that a well mixed flow regime exists. Similar finding were reported by Knott and Mackley (1980) from a flow visualisation study of oscillatory flow from a sharp edged tube. The oscillatory baffled tube was first proposed by Mackley (1987) and consisted of a cylindrical tube, containing periodically spaced annular baffles, in which the fluid is oscillated. This device has the advantage of being simple in construction yet can achieve efficient eddy mixing similar to that reported in other OFM devices (Brunold et al., 1989). It has also been show that similar mixing characteristics can be obtained if the baffles are oscillated instead of the fluid (Gough et al., 1997).

2.1.2 Fluid Mechanics

Oscillatory flow mixing is based on the fact that if a fluid flows around a sharp object with a high enough velocity then flow separation occurs and a vortex is formed in the wake of the object (Mackley, 1991). This mechanism is illustrated in Figure 2.1, which shows, schematically, the formation of eddies downstream of baffles as the fluid is pushed through

an oscillatory baffled tube. When the direction of the flow is reversed, vortex generation occurs again but in the opposite direction. This continual generation of eddies, and their interaction with each other, results in a very complex and time dependent flow regime in which there is excellent radial and axial mixing within each inter-baffle cavity.

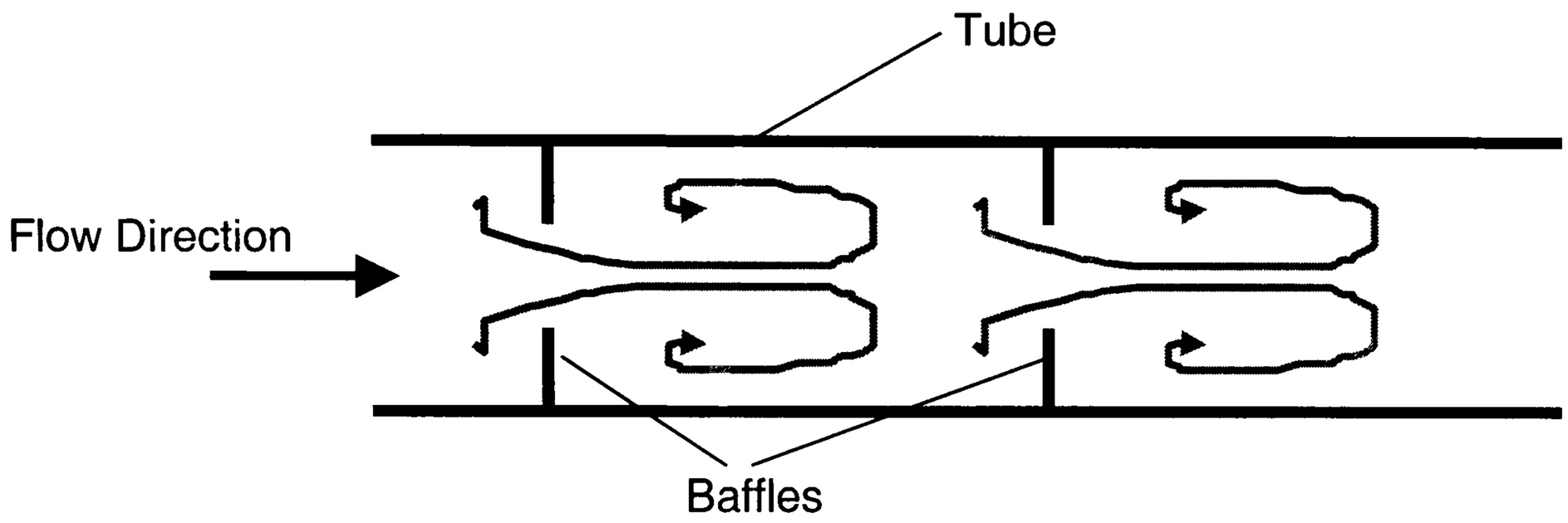

Figure 2.1: Fluid Mechanics of Oscillatory Baffled Flow

The fluid mechanics of oscillatory baffled flow is characterised by two dimensionless groups, namely the oscillatory Reynolds number and the Strouhal number as defined by equations 2.1 and 2.2 respectively.

$$\mathrm{Re}_o = \frac{x_o \omega D}{\nu} \tag{2.1}$$

$$St = \frac{D}{4\pi x_o} \tag{2.2}$$

Where x_o is the centre-to-peak oscillation amplitude (m), ω is the angular frequency of oscillation (=2πf) (rad s^{-1}), f is the oscillation frequency (Hz), D is the tube or column diameter (m) and ν is the kinematic viscosity of the fluid (m^2 s^{-1}). The oscillatory Reynolds number contains the oscillatory velocity term and so defines the level of mixing intensity in the system. The Strouhal number represents the ratio of tube diameter to amplitude and determines the propagation length of vortices generated. If there is also a net flow along the tube then the net flow Reynolds number (as defined by equation 2.3) is also applicable,

$$\mathrm{Re}_n = \frac{uD}{\nu} \tag{2.3}$$

where u is the superficial velocity of the fluid in the tube (m s^{-1}).

The effects of these dimensionless groups on the fluid mechanical conditions have been studied by a number of researchers. It has been shown, from numerical simulation, that a Reynolds number in the order of 100 is required to cause flow separation to occur, resulting in the formation of symmetrical vortices about the centreline (Mackay et al., 1991; Wang et al., 1994). At higher Re_o (>300) however the symmetry is broken and a more chaotic and well-mixed flow regime is observed (Howes et al., 1991). This is also in reasonably good agreement with Mackay et al (1991) who, from flow visualisation, put the value at Re_o = 200, independent of Strouhal number.

2.1.3 Baffle Goemetry

As pointed out by Ni and Gough (1997), the dimensionless groups used to characterise the flow do not take into account the effects of the baffle geometry (baffle spacing, L, and orifice diameter), which would be expected to have some effect on the fluid mechanical conditions. The baffle spacing determines the room available for eddies to expand and propagate within the inter-baffle cavity. Therefore, if the spacing is too large then the eddies will diminish within the cavity resulting in stagnant zone. If, on the other hand, the spacing is too small then there will be insufficient room for the vortices to develop properly and channeling of the fluid could result. The baffle orifice diameter is equally significant and determines the width of eddies generated within the tube. An orifice diameter that is too small would result in eddies being confined to the centre of the tube while an orifice that is too large confines eddies to the region in the vicinity of the tube wall and channeling occurs in the centre of the tube. The baffle orifice size is also important from the point of view that it governs the velocity at which the fluid passes through the orifice, therefore, using a smaller orifice results in higher fluid velocity and hence more intensive mixing. It is desirable to operate with a baffle geometry that optimises the mixing characteristics in the system and work has been carried out a number of researchers to try to identify what these optimal conditions are.

Brunold et al (1989) were the first to investigate baffle geometry and identified the optimum baffle spacing as 1.5 times the tube diameter from a flow visualisation study. Ni and Gao (1996a), however, found that a value of 1.8 tube diameters maximised the performance of a mass transfer process. The effect of baffle geometry on oil-water dispersion characteristics was studied by Zhang et al (1996), who reported that a baffle

spacing of 1.5 times the column diameter and a baffle free area of 20% resulted in the best mixing conditions. Gough et al (1997) studied flow patterns in a OBC, in which the baffles were oscillated rather than the fluid, and identified the optimal baffle free area to be in the region of 32 – 39 %. They also observed that good mixing could be achieved at baffle spacing of up to 2 column diameters provided that an appropriate amplitude was used and the optimal amplitude was identified as one quarter of the baffle spacing. A comprehensive, quantitative investigation into baffle geometry was recently carried out by Ni et al (1998a) covering baffle spacings of 1 – 2.5 tube diameters, baffle free areas of 11 – 51 % and baffles ticknesses of 1 – 48 mm in columns using both oscillating fluid and oscillating baffles. They identified the optimal baffle spacing as 1.8 column diameters for oscillating fluid and 2 column diameters for oscillating baffles. It was also observed that the optimal baffle free area is in the region 20 – 22 % and that baffle thickness should be 2 – 3 mm.

As well as annular baffles, other baffle designs have also been investigated, for example disk and helical baffles (Hewgill et al., 1993). It has been observed from flow visualisation and numerical simulation that annular baffles provide the very good global mixing throughout each baffle cavity. Disk baffles, on the other hand, produce poorer global mixing but generate higher shear rates in the vicinity of the wall (Howes et al., 1991), indicating potential application for processes like membrane filtration where the concentration gradient at the wall adds significantly to the overall resistance of the process. Helical baffles were shown to provide better overall mixing than disk baffles but to a lesser extent than annular baffles.

2.1.4 Applications

Oscillatory baffled flow (OBF) has been applied to a number of chemical engineering operations with promising results, for example heat transfer (Mackley et al., 1990; Mackley and Stonestreet, 1995; Ni et al., 1997), mass transfer (Hewgill et al., 1993; Ni et al., 1995a,b; Ni and Gao, 1996a,b), aeration (Mackley et al., 1998), chemical reactions (Ni and Mackley, 1993), membrane filtration (Howell et al., 1993), liquid-liquid dispersion (Zhang et al., 1996), particle suspension (Mackley et al., 1993) and crystalisation (Perry, 1997; Ventoura, 1997). Recent work has also shown that OBF can be used to control the droplet size distribution in a liquid-liquid dispersion (Ni et al., 1998b) and subsequently the particle size distribution in suspension polymerisation reactions (Ni et al., 1999). Another active area of research is the study of fluid dispersion in continuous oscillatory baffled tubes (Dickens et al., 1989; Howes and Mackley, 1990; Mackley and Ni, 1991, 1993; Ni, 1994, 1995; Ni and Pereira, 2000). These devices allow the mixing intensity to be controlled independently of the net flow and it has been shown that residence time distributions characteristic of plug flow can be achieved, indicating that they have potential applications as plug flow reactors.

The research that has been carried out to date in oscillatory baffled tubes and columns indicates that these devices have potential application in many areas of chemical engineering. However, previous studies have focused on small, laboratory scale apparatus, therefore a driving force exists to develop this technology in terms of scale-up studies and pilot trials.

2.1.5 Power Consumption

A critical aspect of any chemical engineering operation is power requirements. In oscillatory baffled flow (OBF), energy dissipation (ε) in the system can be calculated from equation (2.4).

$$\varepsilon = \frac{P}{\rho V} \tag{2.4}$$

Where (P/V) is the power density in the system (W m^{-3}) and can be calculated using one of two models. The first model is the quasi-steady equation of Jealous and Johnson (1955) defined in equation (2.5).

$$\frac{P}{V} = \frac{2\rho N}{3\pi C_D^2}\left(\frac{1-\alpha^2}{\alpha^2}\right)x_o^3\omega^3 \tag{2.5}$$

Where N is the number of baffles per unit length (m^{-1}), C_D is an orifice discharge coefficient (usually taken as 0.7) and α is the fractional free area of the baffles used. Equation (2.5) is based on the assumption that the instantaneous pressure drop across an orifice plate at any given time is equal to that if it was operating under fully developed, steady flow conditions. The second model that can be used to evaluate power density in an oscillatory baffled column (OBC) is the eddy enhancement model of Baird and Stonstreet (1995), as defined by equation (2.6)

$$\frac{P}{V} = 1.5 \frac{\rho \omega^3 x_o^2 l}{L_b \alpha} \tag{2.6}$$

where l is a mixing length (m) (an adjustable parameter that is the same order of magnitude as the tube or column diameter) and L_b is the baffle spacing.

The most reliable model for predicting the power density depends on the oscillation amplitude being used. Baird and Stonestreet (1995) measured power dissipation in an OBC of 12 mm in diameter and identified that the range of oscillation amplitudes in which the quasi-steady model applied was $x_o > 5$ mm. For oscillation amplitudes in the range of 1 – 5 mm, the eddy enhancement model was found to be more accurate. The same ranges of oscillation amplitude were also reported by Baird and Rama Rao (1995), from a study of power dissipation in OBCs of 15 and 19 cm in diameter, which indicates that this model selection criteria is applicable to any OBC, independent of column diameter, although further study is required to verify if this is the case. Based on this observation, the quasi-steady model was chosen to evaluate power density in the present work as the oscillation amplitudes used were in the range of 50 – 200 mm.

Energy dissipation has been determined for the application of oscillatory baffled columns to processes such as chemical reaction (Ni and Mackley, 1993) and mass transfer (Ni and Gao, 1996a), from which it was found that the energy requirements of the OBC were lower than that required to achieve the same results in a stirred tank. These results indicate that OBF may potentially be a more energy efficient mixing technique than stirred tanks but further investigation into this matter is required.

2.1.6 Summary

The above discussion has highlighted the potential of oscillatory baffled tube/columns for application to chemical engineering operations. The technique offers a good degree of control over the fluid mechanical conditions and allows excellent global mixing to be achieved in the system. Such criteria are the core requirements for suspension polymerisation processes and the applicability of the OBR to such processes has already been demonstrated on a bench scale. Scale-up studies are needed, however, and this is addressed by the present study.

2.2 Liquid-Liquid Dispersion

2.2.1 Introduction

Liquid-liquid dispersion is common to many chemical engineering processes such as liquid-liquid extraction, emulsion polymerisation and suspension polymerisation. In such processes one liquid is dispersed in another by applying mechanical agitation, usually by means of an impeller in a stirred tank. The key areas of interest in this field are determining minimum agitation for complete dispersion and the prediction, measurement and modeling of drop size distribution, each of which are discussed in turn in this section.

2.2.2 Minimum Agitation Intensity for Complete Dispersion.

In liquid-liquid processes it is important to achieve complete dispersion in order to maximise the performance of the system. In mechanically agitated stirred tanks this is done by increasing the stirrer speed to the point at which complete dispersion is achieved. A number of researchers have investigated the minimum stirrer speed required for complete dispersion and there are two methods by which this has been done, 1: visualisation method and 2: sampling method. The visualisation method is the most commonly used method and involves adding a dye to the dispersed phase and determining the stirrer speed at which complete dispersion occurs by visual observation. This method has the advantage of being non-intrusive and simple to do but suffers from draw backs, for example, the observers possible bias and the requirement for transparent vessels. The sampling method involves taking a sample of the dispersion from various points in the vessel to determine if complete dispersion has been reached. This method overcomes the disadvantages of the visualisation method but requires a more complicated experimental procedure.

Van Heuven and Beek (1971) used the visualisation method to investigate the effect of fluid physical properties and dispersed phase fraction on the minimum impeller speed and proposed the correlation given in equation (2.7)

$$\frac{N_{min}^2 D}{g} = 22\left(\frac{N_{min} D^2}{\nu}\right)^{-3/5}\left(\frac{\rho \nu^2}{\sigma D}\right)^{-1/5}\left(\frac{\Delta\rho}{\rho}\right)(1+2.5\Phi)^{1/3} \qquad (2.7)$$

where N_{min} is the minimum stirrer speed for complete dispersion (s^{-1}), D is the impeller diameter (m), g is the gravitational constant (= 9.81 m s^{-2}), ν is the kinematic viscosity of

the continuous phase (m^2 s^{-1}), ρ is the density of the continuous phases (kg m^{-3}), σ is the interfacial tension between the dispersed and continuous phases (N m^{-1}), $\Delta\rho$ is the density difference between the dispersed and continuous phases (kg m^{-3}) and Φ is the phase fraction of the dispersed phase. This correlation fitted the experimental data reasonably well although there was some scatter observed. Selland and Saksaria (1978) also used the visualisation method to investigate the behaviour of liquid-liquid dispersions over a range of fluid physical properties and impeller designs. They observed that there existed several mixing regimes depending, on impeller location and number of impellers, which exhibited various phenomena such as phase inversion and air entrainment. The correlation for N_{min} that they proposed is defined by equation (2.8),

$$\frac{D^{1/2}N_{\min}}{g^{1/2}} = C_1\left(\frac{T}{D}\right)^{\alpha}\left(\frac{\mu_c}{\mu_d}\right)^{1/9}\left(\frac{\Delta\rho}{\rho_c}\right)^{0.25}\left(\frac{\sigma}{D^2\rho_c g}\right)^{0.3} \qquad (2.8)$$

where C_1 is a constant, T is the tank diameter (m), μ is the dynamic viscosity of the fluid (kg m^{-1} s^{-1}) and the subscripts c and d on the physical property terms indicate continuous phase and dispersed phase respectively. Equation (2.8) provided a good fit to their data over the entire range of parameters studied. This work was later extended by Skellend and Ramsay (1987) who correlated N_{min} with fluid physical properties, phase fraction and geometry using 251 experimental data points obtained from their own work plus the data of Skelland and Saksaria and Van Hueven and Beek. They proposed a correlation that incorporates average values of density and viscosity and is defined in equation (2.9),

$$N_{\min} = C\left(\frac{T}{D}\right)^{\alpha} \frac{g^{0.42}\Delta\rho^{0.42}\mu_m^{0.08}\sigma^{0.04}\Phi^{0.05}}{D^{0.71}\rho_m^{0.54}} \qquad (2.9)$$

where μ_m and ρ_m are the mean viscosity and mean density of the dispersion respectively. This equation was found to fit the experimental data very well. Work on the minimum stirrer speed has since been further extended, by Skelland and Kanel (1992), to systems containing non-Newtonian fluids and it was found that equation (2.8) is sufficient provided that an apparent viscosity is used. Armenante and Huang (1992) used the sampling technique to study the effect of stirrer speed on the level of liquid-liquid dispersion achieved and developed an unbiased mathematical technique that can be used to determine N_{min} from experimental data. Results obtained using this technique compare well with those determined by the visualisation method.

The minimum power input for complete dispersion has also been studied (Esch et al., 1971) and it was reported that power requirements can be evaluated from the normal power number vs Reynolds number curve of Bates et al (1963), provided that mean values of viscosity and density are used in the evaluation of the dimensionless groups.

A similar topic is the minimum stirrer speed for uniform dispersion which is defined as the speed required to produce a dispersion in which the concentration of the dispersed phase is the same at all points in the vessel. Skelland and Lee (1978) investigated this using the sampling technique and found that equation (2.9) provided a good fit to the data although the stirrer speed required to achieve uniform dispersion was generally slightly higher (typically about 8%), which was expected.

The only investigation of this type in oscillatory baffled column was carried out by Zhang et al (1996). They replaced the minimum stirrer speed by a minimum oscillation frequency and studied the effects of amplitude, baffle geometry, oil phase fraction and presence of surfactants and colloids in the system on this parameter using the visualisation method. They reported that increasing the amplitude reduced the minimum oscillation frequency and found the optimal baffle geometry to be $\alpha = 19\%$ and $L = 1.5Di$. It should be noted however that this conclusion was based on minimum oscillation frequency and not minimum power input. f_{min} was also reported to be reduced by the presence of colloids or surfactants and to be unaffected by changes in the phase fraction.

2.2.3 Influence of Fluid Mechanics on Drop Size Distribution

The droplet size distribution of a liquid-liquid dispersion is an important parameter as it determines the performance of a number of aspects of the system, such as, mass transfer rate, reaction rate and particle size distribution. The behaviour of dispersed phase droplets in a liquid-liquid dispersion is dependent on the fluid mechanical conditions within the existing flow field and equations based on theoretical models have been developed for the various interactions that can occur.

2.2.3.1 Fluid Mechanics of Turbulent Liquid-Liquid Dispersions

Overall mixing between the two phases is governed by events on the macro scale, i.e. large eddies generated by the impeller that transport the liquid around the vessel. The droplet

size, on the other hand, is governed by events on the micro scale which are determined by the way in which these large eddies disperse and diminish. As most liquid-liquid mixing processes operate in the turbulant flow regime, Kolmogoroff's theory of isotropic turbulence can be applied. This states that, at high Reynold's numbers, large eddies initially diminish into smaller intermediate eddies and then further into very small eddies without loss of energy. The energy in these small eddies is then dissipated as heat by viscous effects. It is assumed that the events occurring on this micro scale are independent of events in the main flow i.e. the flow is locally isotropic. Under such conditions Kolmogoroff (1941) proposed that the size of the small eddies (η) was dependent on only the energy dissipation rate (ε) and the kinematic viscosity of the fluid (ν). From dimensional reasoning he derived the following equation:

$$\eta = \left(\frac{\nu^3}{\varepsilon} \right)^{0.25} \tag{2.10}$$

In such a flow field the mean square relative velocity (u^2) between two points a distance r apart is given by (Batchelor, 1982):

$$u^2(r) = const(\varepsilon r)^{2/3} \tag{2.11}$$

The way in which droplets interact with each other and with the eddies in the system determines the nature of the droplet breakage and coalescence processes and hence controls the drop size distribution.

2.2.3.2 Droplet Breakage Mechanism

In turbulent liquid-liquid dispersions, droplet breakage occurs due to forces acting on the droplet that stretch and deform it. Hinze (1955) pointed out that there are two mechanism by which this can happen, depending on the diameter of the droplet (d). If $d >> \eta$ then viscous forces can be neglected and droplet deformation occurs as a result of dynamic pressure fluctuations in the region around the drop, caused by eddies colliding with the drop. In the case where $d << \eta$, eddies will only act to carry the drops and breakage is caused by viscous shear effects.

For a droplet of $d >> \eta$ to break, the kinetic energy applied in the deformation $[\rho.u^2(d).d^3]$ must exceed the surface energy which acts to hold the drop together $[\sigma.d^2]$. The ratio of these two terms is the Weber number (We), as shown by equation (2.12).

$$We = \frac{\rho u^2(d) d^3}{\sigma d^2} \qquad (2.12)$$

If locally isotropic conditions exist then equations (2.11) and (2.12) can be combined and the Weber number is defined as in equation (2.13) (Shinnar, 1960).

$$We = \frac{\rho(\varepsilon d)^{2/3} d}{\sigma} \qquad (2.13)$$

In a dispersion the maximum stable droplet size (d_{max}) occurs when the forces are balanced i.e.

$$\frac{\rho(\varepsilon d_{\max})^{2/3} d_{\max}}{\sigma} = const \qquad (2.14)$$

Energy dissipation in a stirred tank is given by (Rushton, 1950):

$$\varepsilon = kN^3 D^2 \qquad (2.15)$$

where k is a constant, N is the rotational speed of the stirrer (s^{-1}) and D is the impeller diameter (m). Therefore, from equations (2.14 and 2.15), d_{max} can be expressed as (Shinnar, 1960):

$$d_{\max} = C\left(\frac{\sigma}{\rho_c}\right) N^{-6/5} D^{-4/5} \propto \varepsilon^{-0.4} \qquad (2.16)$$

or

$$d_{\max} = const.D.We_T^{-0.6} \qquad (2.17)$$

where We_T is the impeller Weber number.

For the case where $d \ll \eta$ then viscosity effects dominate (Hinze, 1955; Bourne and Baldyga, 1994) and breakage is caused by viscous shear effects. The Weber number is

therefore the ratio of viscous shear energy to the surface energy and according to Taylor's theory (Taylor, 1934)

$$We_{crit} = \mu_c \left(\frac{\partial u}{\partial r} \right) \left(\frac{d}{\sigma} \right) = f\left(\frac{\mu_d}{\mu_c} \right) \tag{2.18}$$

Shinnar (1960) applied the theory of local isotropic turbulence:

$$\left(\frac{\partial u}{\partial r} \right)^2 = \frac{2\varepsilon}{15\nu_c} \tag{2.19}$$

and derived the following relationship for d_{max}:

$$d_{\max} = const.\sigma\mu_c^{-1}\nu_c^{0.5}\varepsilon^{-0.5} f\left(\frac{\mu_d}{\mu_c} \right) \tag{2.20}$$

As can be seen, the dependence of drop size on energy dissipation is different for break-up due to the effects of dynamic pressure fluctuations and viscous shear.

2.2.3.3 Droplet Coalescence Mechanism

If two droplets in a dispersion come into contact then coalescence can result. The requirements for coalescence are that the adhesion energy (E_a), which acts to hold the drops together, is greater than the energy acting to break the droplet. In the case of $d>>\eta$, the

energy acting to break the droplet is the kinetic energy of turbulence, and adhesion energy is defined by Shinnar (1960) as:

$$E_a = A(h_o)d \tag{2.21}$$

where h_o is the inter-facial film thickness between the drops and $A(h_o)$ is an integral function of the attractive force between two drops, which can be taken as a constant for high values of d/h_o. As kinetic energy increases with droplet size more that adhesion energy, there exists a minimum droplet size (d_{min}) at which droplets will be stable. At this diameter the turbulence energy and adhesion energy are balanced, therefore:

$$\frac{E_t}{E_a} = \frac{C\rho_c u^2(d_{\min}).d^3_{\min}}{A(h_o).d_{\min}} = const \tag{2.22}$$

Assuming local isotropy, it can be derived that:

$$d_{\min} = const.\rho_c^{-3/8}\varepsilon^{-1/4} \tag{2.23}$$

In the case where $d << \eta$, the minimum drop size exists when the viscous shear force and the adhesion force (F) are balanced (Sprow, 1967a):

$$\frac{\mu_c\left(\frac{\partial u}{\partial r}\right).d^2_{\min}}{F} = const \tag{2.24}$$

Therefore, assuming local isotropy d_{min} is given by.

$$d_{\min} = F^{1/2}\mu_c^{-1/2}\nu_c^{-1/4}\varepsilon^{-1/4} \tag{2.25}$$

In most liquid-liquid dispersion processes, breakage and coalescence occur simultaneously and a point is reached at which the droplet size distribution stabilises and does not change with time. Stable distributions can be of one of two forms, depending on the energy dissipation rate in the system. As d_{max} decreases faster with energy dissipation than d_{min} there reaches a critical point beyond which d_{min} is greater than d_{max} (Shinnar, 1960). One type of stable distribution occurs when the energy dissipation is below the critical value, where droplets are too small to break and too large to overcome the turbulence energy and coalesce. All droplets are therefore individually stable and this is termed turbulence stabilised dispersion. The other type of stable drop size distribution occurs when the energy dissipation rate is above the critical value, in which case d_{min} is greater than d_{max} therefore droplets will coalesce up to the point where d_{max} is exceeded and then break. This cycle is continually repeated, resulting in a high degree of inter-droplet mixing. Both of these flow regimes have been observed experimentally (Shinnar, 1960; Church and Shinnar, 1961).

2.2.4 Techniques for Droplet Size Measurement

In order to study drop size it is important to establish a reliable measurement technique capable of determining the size of droplets as they exist in the system. Great care must be

taken in doing this as drop size can be easily influenced by changes in system conditions. There are generally two types of techniques that have been developed for measuring droplet size in liquid-liquid dispersions – (i) photograpic techniques and (ii) droplet stabilisation techniques, although some other methods are reported.

2.2.4.1 Photographic Techniques

There are various ways in which photography can be performed and it can be done from either inside or outside of the vessel. Chen and Middleman (1967) took photographs using an external light source and camera by illuminating a plane through the centre of the tank and taking picture perpendicular to the plane. A similar method was also used by Calabrese et al (1986a,b) and Wang and Calabrese (1986). Such techniques are good because they are non-intrusive but require transparent vessels and cannot be used for dispersions with a high phase fraction. Photographs can be taken directly from inside the vessel directly using a submerged photographic probe, which can be used with either an external or internal light source. Brown and Pitt (1970, 1972) used such a probe, but it had to be used in a non-transparent vessel with only a small window allocated for light transmittance from an external source. A similar method has also successfully been applied to transparent vessel by Mlynek and Resnick (1972) and Pacek et al (1993, 1994a,b). This technique, however, is limited by the fact that photographs can only be taken in the vicinity of the vessel wall due to the need for an external light source. Pacek and Nienow (1995), therefore, modified the technique by incorporating a submerged light transmitter, thereby eliminating the need for a transparent vessel and allowing measurements to be made at any location in the system. This is similar to the method used

previously by Okufi et al (1990) and provided pictures of excellent quality, which could be used to identify drops in high hold-up dispersions and could also identify phenomena such as phase inversion and air bubbles or droplets within drops. In summary, photographic techniques are good in that they allow direct and rapid measurements of the droplets in the system but each method suffers from certain drawbacks, such as the requirement for transparent vessels, the insertion of probes into the flow field, limitations to the range of suitable phase fractions or poor quality images being produced.

2.2.4.2 Droplet Stabilisation Techniques

Droplet stabilisation techniques involve stabilising the droplets from coalescence thereby allowing the distribution to remain unchanged, even under conditions of no agitation. This can be carried out in a number of ways. Shinnar (1960) and Church and Shinnar (1961) used a hot wax to form the dispersed phase which when cooled solidified and the DSD was maintained even if agitation was stopped. McCoy and Madden (1964, 1969) developed an encapsulation technique whereby a monomer was dissolved in the dispersed phase and a second reactant was added to the system at the point of measurement. Droplets were almost instantly encapsulated in a polymer film thereby stabilising them from coalescence. This technique was further developed by Mlyneck and Resnick (1972) who developed a sampling trap into which a small volume of the liquid-liquid medium was drawn and brought into contact with the secondary reactant. This method allowed a sample of stablised drops to be collected at any point in the vessel, allowing local DSDs to be determined. Another method is that of Konno et al (1982) and Zerfa and Brooks (1996) who withdrew samples and stabilised them with colloid solution prior to analysis. In each

of these stabilisation techniques the stablised droplets obtained must then to analysed to determine the size distribution. Droplet stabilisation methods have the advantage of being feasible with any type of vessel and generally require only a simple experimental set-up. Experimental procedure is more time consuming than with photography, though, and care must be taken not to disturb the drops during sampling.

2.2.4.3 Other Techniques

Droplets can also be measured using the capillary method of Verhoff et al (1977) in which drops are passed through a capillary. As they do so they are stretched due to the narrowness of the tube and the length of the deformed drop, which is measured using a light transmission technique, determines its volume. The light transmission technique was also shown to be capable of measuring the concentration of a dye within drops and so could be used to study levels of intermixing between drops. The capillary method cannot however be used to measure drops smaller than the diameter of the capillary tube and has also been shown to be unreliable at determining DSDs that contain large drops (Pacek and Nienow, 1995).

Another technique that has emerged involves using a submerged probe that incorporates a signal transmitter and receiver, where the signal used is influenced by the presence and size of a drop. Various signal types have been shown to be suitable, for example electrical current (Sprow, 1967b), acoustic waves (Smith, 1974) and light (Weinstein and Treybal, 1973). A similar method is the laser diffraction technique of Chatzi et al (1991a,b) in which a stream from the stirred vessel was continually pumped

through a measurement cell and the DSD was determined by laser diffraction. This method was shown to be more sensitive to detecting small drops than photographic techniques indicating suitability for fine dispersions.

Each of the techniques described above have their own advantages and drawbacks and the best technique to use is very often dependent on the specific application to which it is being applied.

2.2.5 Experimental Investigations into Drop Size

2.2.5.1 Effect of System Parameters on Drop Size

Many researchers have studied drop size in liquid-liquid dispersions and a wide range of liquids, vessel sizes and configurations, phase fractions and physical properties have been investigated. Droplets in such dispersions tend to be of a size larger than the micro-scale of turbulence and processes are normally breakage dominated, therefore equations of the form (2.21) for d_{max} generally apply.

It is, however, more common to describe drop size distributions in terms of a mean droplet diameter. For such a purpose the Sauter mean diameter (d_{32}) is defined as:

$$d_{32} = \frac{\sum n_i d_i^3}{\sum n_i d_i^2} \tag{2.26}$$

where n_i and d_i are the number and mean diameter of droplets in size intrval i. d_{32} has been shown to be directly proportional to d_{max} (Van Heuven and Beek, 1971; Brown and Pitt, 1972; Zerfa and Brooks, 1996) therefore equation (2.21) can be re-written as:

$$d_{32} = const.D.We_T^{-0.6} \tag{2.27}$$

Chen and Middleman (1967) investigated the drop size distribution of 14 dispersed phase liquids in 6 stirred tanks with 5 different impellers at a number of stirrer speeds and found that eqn (2.27) correlated the data well, with a constant of 0.053 providing the best fit. This was also in good agreement with the work of Sprow (1967b), who reported a value of 0.052, and the later work of Chatzi et al (1991a) who reported a value of 0.046 for a system in which they investigated the effect of stirrer speed and surface tension (stabiliser concentration).

The effect of phase fraction has also been studied and it has been found that droplet size increases as phase fraction increases (Van Heuven and Beek, 1971; Calabrese et al., 1986b; Brown and Pitt, 1970; Mlynek and Resnick, 1972; Zerfa and Brooks, 1996; Lee and Tasakorn, 1979). This observation has been attributed to two factors – (i) damping of the turbulence and (ii) increased droplet coalescence. In each of the investigations into the effect of the phase fraction on the Sauter mean diameter, the relationship between the two parameters was reported to be linear, therefore, the expression for mean drop size becomes:

$$d_{32} = c_1.(1 + c_2\varphi)D.We_T^{-0.6} \tag{2.28}$$

where Φ is the phase fraction. The constants (c_1 and c_2) vary, although not significantly, between researchers. This expression has also been shown by Konno et al (1977) to be capable of predicting droplet sizes in flow fields where eddy sizes are outside the inertial sub-range in which isotropic turbulence theory applies.

The above equation does not take account of the effect of liquid viscosity on droplet breakage as it is assumed that droplets are large enough for viscous effects to have only a negligible influence on the breakage process. However, if high viscosity fluids are being used in the system then this assumption may not be valid. The effect of dispersed phase viscosity has been studied by Calabrese et al (1986a,b) and Wang and Calabrese (1986) who proposed that eqn (2.28) would work well for low viscosity liquids and have derived the following expression for higher viscosity liquids:

$$\frac{d_{32}}{D} = 0.0053We^{-0.6}\left[1+0.91V_i^{0.84}\right]^{3/5} \tag{2.29}$$

where V_i is a viscosity number defined by:

$$V_i = \frac{\mu_d ND}{\sigma}\left(\frac{\rho_c}{\rho_d}\right)^{1/2} \tag{2.30}$$

where N is the rotational speed of the impeller (s^{-1}) and D is the impeller diameter (m).

2.2.5.2 Scale-Up Characteristics

Scale-up has been investigated by Okufi et al (1990), who studied drop size in three geometrically similar stirred tanks with a diameter ratio of 1:2:4. They found that average energy dissipation was a poor criterion for scale-up as in larger tanks the drop size was smaller. This may seem to disagree with the theory outlined above but can be explained by considering the variation of local energy dissipation in the system. At a constant average energy dissipation, the impeller tip speed is greater in larger tanks which will result in the highest value of local energy dissipation being greater. This will produce smaller drops in the impeller region and if the circulation time of drops through the bulk liquid is insufficient for coalescence to occur then a smaller mean drop size will be observed. On this basis it would be reasonable to assume that the maximum local energy dissipation, and not the average value, governs the size of droplets. This view is reinforced by the work Okufi et al (1990) who reported constant drop size with impeller tip speed.

2.2.5.3 Summary of Experimental Work

In summary it can be concluded that drop size in agitated systems is influenced by a number of factors such as system size and geometry, agitation intensity, energy dissipation, fluid physical properties (density, viscosity, inter-facial tension) of both phases, phase fraction and presence of stabilisers. As yet, there is not one correlation that accounts for all of these factors and most are generally confined to one system. Therefore, significant effort is still required in this area to gain a broader understanding of drop behaviour and to classify it in terms of the parameters listed above.

2.2.6 Modeling of Dynamic Droplet Behaviour

The time evolution of a population of droplets, with respect to drop size and size distribution, is dependent on the droplet breakage and coalescence rates as well as the rate at which droplets are entering and leaving the system. This can be expressed mathematically by the population balance equation (PBE), in which, for each droplet size that exists, the individual rate processes are described by a given function (Valentas and Amundson, 1966). The effects of droplets entering and leaving the system are easily accounted for by a simple mass balance but the effects of breakage and coalescence rates are more complicated. The breakage function generally consists of a term for breakage frequency and a term to describe the number and distribution of daughter droplets formed while coalescence is described in terms of collision frequency and coalescence efficiency. Many researchers have worked on population balance modeling and a vast literature in available on this topic. Only a brief summary is given here and a more comprehensive review is available elsewhere (Ramkrishna, 1985).

In most practical situations, no analytical solution to the full PBE exists due to the large number of possible breakage and coalescence events that can occur. Therefore, expressions for the breakage and coalescence functions must be developed from empirically derived correlations and mechanistic models in combination with experimental data and basic assumptions. Zeltin and Talvarides (1972) developed a model for droplet motion, based on random movement and the macro-scale circulation pattern, where breakage and coalescence were functions of position and must be determined from experimental data. Their model assumed that coalescence could result after a collision between droplets and the newly formed drop had a certain probability to break again.

Also, all droplets above d_{max} that entered the impeller region had a breakage probability of 100%. Coulolaglou and Talvarides (1977) assumed the vessel to behave as a homogeneous flow field and solved the PBE by introducing theoretical expressions based, on mechanistic models, for the breakage and coalescence functions. The model fitted experimental data very well and this approach was later extended by Tsouris and Talvarides (1994). An attempt to further improve accuracy was carried out by Nambier et al (1994) who incorporated a two-zone model that distinguished between the impeller and circulation regions.

Attempts have also been made to introduce simplifications to the PBE in order to make a solution computationally less time consuming. Laso et al (1987a) assumed breakage to be a first order process (breakage of one drop into two equally sized smaller drops) and coalescence to be second order (coalescence only occurs between two drops of the same size) and discretised the distribution into bins where the mean diameter of a bin was twice the diameter of the previous one. They found that their simplifications maintained the accuracy of the full PBE but significantly reduced computational effort. This model has been used to study the effects of system parameters on breakage and coalescence frequencies (Laso et al., 1987b). Hounslow et al (1988) and Hounslow (1990) simplified the population balance equation for growth and aggregation of crystals by transforming the partial differential integral equations into ordinary differential equations and applying a discretisation similar to that of Laso et al (1987a). This again reduced computational effort while maintaining accuracy.

The discretisation of the size range is also important. Laso et al (1987a,b) and Hounslow et al (1988) used a discretisation where droplets in each bin class were twice the

volume of those in the previous bin. The accuracy of this model would be reduced, though, if applied to a broad size distributions as bins at the large end of the range would contain a very broad range of sizes. An alternative approach is that of Lister et al (1995) who applied an adjustable discretisation where the volume of bin i could be half of that of bin i+2 or i+3 etc. This reduced bin size and improved accuracy but employing discretisations of this type must be balanced against the increased computational effort.

The population balance model, in one form or another, has been applied over a wide range of systems by a number of researchers who have introduced a variety of modifications, either to improve accuracy or to simplify the equations. There is no universally applicable solution and so the best model to use will often depend on the particular system as well as the accuracy required.

2.2.7 Summary

The ability to control droplet behaviour is crucial to suspension polymerisation processes as the droplet size distribution of the dispersed monomer phase determines the particle size distribution of the polymer product. There already exists an extensive literature on the control of droplet size in stirred tanks but only few investigations of this type have been conducted in OBCs. Research in this area has therefore been extended as part of the present work with emphasis being placed on the effect of operating parameters and scale-up.

2.3 Suspension Polymerisation

2.3.1 Introduction

2.3.1.1 Polymerisation Processes

Polymerisation processes can generally be classified into four catagories: bulk, solution, emulsion and suspension (Kumar and Gupta, 1978; Bisenberger and Sebastian, 1983). Each type of process has specific advantages and disadvantages and the best process to use depends on the product that is being manufactured. The main differences between each of these processes are outlined below:

Bulk polymerisation:

This process is carried out using monomer alone and yields a product of high purity in the form of a monomer-polymer syrup, which can then be molded into various shapes, for example sheets and rods.

Solution Polymerisation:

This process involves using a solvent for monomer and polymer and yields a product in the form of a solution of the polymer, which then has direct applications for example as a coating or adhesive.

Emulsion Polymerisation:

In this process the monomer is dispersed in an aqueous phase that contains dissolved initiator and yields a product in the form of a aqueous emulsion of very

fine polymer particles. Typical applications of such a product are paints and adhesives.

Suspension polymerisation

In the process of suspension polymerisation, one or more water insoluble monomers containing dissolved initiator is dispersed in an aqueous medium as droplets, which then polymerise to form solid polymer particles (Dawkins, 1989). Strong fluid agitation is required in order to create and maintain the dispersion throughout the duration of the reaction. Stabilising agents (colloids and surfactants) are also used to stabilise the suspended drops and inhibit coalescence. This type of process yields a product in the form of polymer particles and is used for the manufacture of a variety of polymer products for example polystyrene, polyvinylchloride and polymethylmethacrylate. The reaction may also be carried out as mass suspension polymerisation, which is a two-stage process (Yuan et al., 1991). First, bulk polymerisation is used until the solution reaches a certain viscosity and then this viscous liquid is dispersed in a aqueous phase and the polymerisation is completed in suspension.

2.3.1.2 Types of Suspension Polymerisation

There are two types of suspension polymerisation reaction depending on the properties of the monomer and polymer involved (Munzer et al., 1977):

1) Beads suspension polymerisation:

In this process the polymer is soluble in its monomer. Therefore as polymerisation proceeds within a droplet the viscosity of the droplet increases and the reaction passed through a "sticky" stage which increases the tendency for drops to coalesce with each other. As conversion of the monomer approaches 100% the drops become solid polymer spheres and are then in the form of the final product. Examples are polymerisation of styrene, methylmethacrylate, acrylate and vinylacetate.

2) Powder suspension polymerisation:

In this process the polymer is not dissolved by its monomer. As polymerisation proceeds the polymer is precipitated within each droplet resulting in irregular shaped particles being produced. Examples are polymerisation of vinylchloride, high-acrylonitrile and fluoroethylenes.

2.3.1.3 Stabilisers

The role of stabilisers is crucial in suspension polymerisation processes. Many different types of stabiliser have been tried and there exists an extensive patent literature relating to this topic. Stabilisers used in suspension polymerisation can generally be classified into three catagories (Munzer et al., 1977; Yuan et al., 1991).

1. Water-soluble polymers (natural polymers, modified natural polymers and synthetic polymers)
2. Water-insoluble inorganic powders (metal salts)

3. Mixed stabilisers (inorganic powders with surfactants or organic polymers with inorganic powders)

Each type of stabiliser has advantages and disadvantages and the best stabiliser(s) to use is dependent on the polymeristion process being carried out.

2.3.1.4 Advantages and Disadvantages of Suspension Polymerisation

The advantages and disadvantages of suspension polymerisation, in comparison to the other polymerisation processes (bulk, solution and emulsion), are (Yuan et al., 1991;Vivaldo-Lima et al., 1997):

Advantages:

- Good mixing characteristics due to low viscosity
- Effective temperature control
- Good heat transfer from aqueous to dispersed phase due to the high surface area to volume ratio of the drops
- Low separation cost (compared to emulsion)
- High product purity (compared to emulsion)
- Product in the useful form of polymer beads

Disadvantages:

- Lower productivity for the same reactor volume (compared with bulk)

- Waste water problems
- Fouling of surfaces in contact with the dispersion
- No continuous process available commercially yet

2.3.1.5 Factors Affecting Product Quality

In the manufacture of polymers by suspension polymerisation it is desirable to be able to control the physical and chemical properties of the final product. There are a number of factors that can affect the quality of the product and these can be divided in to two catagories (Vivaldo-Lima et al., 1997): (i) chemistry factors and (ii) physical factors.

The chemistry factors involved are the rates at which the various reactions, that occur in the system, proceed. These rates are influenced by factors such as temperature, viscosity and initiator concentration and determine product specification such as molecular weight distribution, residual initiator content and unreacted monomer content.

Physical factors influence the behaviour of the liquid-liquid dispersion and can be further divided into three categories (Brooks, 1990; Yuan et al., 1991): (i) Geometric factors (size and shape of reactor and agitator), (ii) Operating parameters (operational mode: batch or continuous, reaction time, agitation intensity, temperature, monomer phase fraction and type and concentration of stabilisers used) and (iii) Physical properties (interfacial tension, density and viscosity). Such factors determine the droplet size

distribution of the dispersed phase and hence the particle size distribution of the final product.

A substantial research effort has already been devoted to understanding effect the various factors discussed above and has been reviewed by a number of authors (Munzer et al., 1977; Dawkins, 1989; Brooks, 1990; Yuan et al., 1991; Arshady, 1992; Pla, 1995; Horak, 1996; Vivaldo-Lima et al., 1997). It is recognised, however, that no model can successfully describe all aspects of a suspension polymerisation system therefore significant effort in this area is still required (Vivaldo-Lima et al., 1997).

2.3.2 Reaction Kinetics

The mechanism of reaction in suspension polymerisation is similar to that of bulk and solution polymerisations. Results of early kinetic studies, using MMA and styrene, indicate that the reaction occurs as bulk polymerisation in each monomer droplet and that the rate of reaction is not influenced by the size of the drop (Munzer et al., 1977). Suspension polymerisation is therefore considered to be analogous to many small, water-cooled bulk polymerisations being carried out simultaneously and so the molecular weight distribution is dependent on the same factors as in the bulk process (Baillagou and Soong, 1985a,b; Billingham, 1989).

2.3.2.1 Kinetic mechanism

The reaction is initiated by increasing the temperature to the reaction temperature, at which point the initiator breaks down to form free radicals and monomer to polymer conversion commences. The kinetic mechanism of free radical polymerisation is as follows (Louie et al, 1985) :

1) Initiation

Upon reaching the activation temperature, an initiator molecule breaks to form two free radicals:

$$I \Rightarrow 2\,R\bullet$$

2) Propagation

A free radical then interacts with a monomer molecule producing a polymer one monomer unit in length:

$$R\bullet + M \Rightarrow P_1\bullet$$

The free radical polymer molecule can then interact with another monomer molecule and so the chain lengthens:

$$P_n\bullet + M \Rightarrow P_{n+1}\bullet$$

3) Chain Transfer

The free radical status of the chain can be transferred to a monomer molecule producing a dead polymer molecule as well as the new free radical:

$$P_n\bullet + M \Rightarrow D_n + P_1\bullet$$

Chain transfer can also be to a solvent molecule if present:

$$P_n\bullet + S \Rightarrow D_n + P_1\bullet$$

4) Termination

Termination occurs when two free radical polymer chains interact and can occur either as disproportionation:

$$P_m\bullet + P_n\bullet \Rightarrow D_m + D_n$$

or as combination:

$$P_m\bullet + P_n\bullet \Rightarrow D_{m+n}$$

2.3.2.2 Factors affecting chain length

The chain length and hence molecular weight distribution is governed by the rate at which each of the kinetic processes outlined above proceed at. These rates are sensitive to temperature and fluid properties and so control of reaction conditions is crucial to achieving desired product specification. For example, an increase in temperature affects initiation more than termination which can lead to thermal runaway and dead ending (low monomer conversion due to initiator burn-out). Another problem encountered in polymerisation (especially with MMA) is the Trommsdorff (or gel) effect (Tromsdorff, 1974). This occurs due to the increase in the viscosity of the monomer-polymer solution, which inhibits the diffusion of polymer molecules and hence reduces the termination rate. Subsequently, the solidification stage of the reaction can occur before either monomer or initiator are completely consumed. It is therefore desirable to be able to predict the effect of conditions within the reactor on the molecular weight distribution and models have been developed for this purpose (Baillagou and Soong, 1985b; Billingham, 1989).

2.3.3 Suspension Polymerisation Reactors

2.3.3.1 Reactor Requirements

The two crucial features of suspension polymerisation reactors are the ability to maintain the monomer in suspension and to control the temperature of the contents (Beckmann, 1973). It is for this reason that the most reactors employ a vessel with some kind of mechanical agitation and a jacket to control temperature. Polymerisation reactors should

also have a minimum internal surface area in order to limit the effects of fouling. It is desirable to control the particle size of the final product and produce beads of specific physical and chemical properties therefore, the ability to control the mixing characteristics is also important. The various types of reactor found in the literature are discussed in the following sub-sections.

2.3.3.2 Stirred Tank Reactor

The stirred tank was first applied to free radical suspension polymerisation by Hoffman and Delbruch (1909) and has since become the most widely used device for suspension polymerisation processes in the areas of both manufacturing and research. The advantages of stirred tank reactors are that they are simple in both design and construction, exhibit good mixing and temperature uniformity and there already exists a wealth of knowledge relating to the various characteristics of such devices (Yuan et al., 1991; Holland and Chapman, 1966; McDonough, 1992). However, such devices also suffer from the drawback that broad size distributions are often produced due to the difference in mixing intensity between the impeller and circulation regions and the variation of droplet circulation times in the reactor (Horak, 1996). Therefore, a number of other techniques have been developed in order to try to improve particle size control.

2.3.3.3 Stirred Tank Reactor with Draft Tube

The conventional stirred tank reactor was modified by Tanaka and Ozumi (1985) to incorporate a draft tube running vertically through the centre of the tank. The impeller was positioned within this tube and drove the circulation of liquid down through the tube and back up around the outside of the tube. The principle of this design was the improvement of circulation time characteristics that would be achieved under such conditions. The effects of draft tube length, impeller location and impeller speed on particle size distribution were investigated and it was found that, under the appropriate conditions, narrower PSDs could be produced than are achievable in stirred tank reactors. This was a promising result but the inclusion of the draft tube led to greater fouling which significantly restricts the potential of this device for industrial scale production of polymers by suspension polymerisation.

2.3.3.4 Loop Reactor

The loop reactor was initially developed by Tanaka and O'Shima (1988) as an alternative to the stirred tank as a reactor for suspension polymerisation of styrene. This device consisted of a series of pipes arranged in a rectangular loop joined by elbows with an impeller placed in one section, which drove the flow of liquid around the loop. In such a device, drop breakage would occur in the vicinity of the impeller and coalescence would occur in the recirculation section. The principle of the loop reactor is that the residence time distribution of droplets in the loop should be narrower that that in the circulation zone of a stirred tank, therefore, a narrower distribution of drop sizes should be obtained.

Conventionally, one impeller has been used in this device but some advantages of using two impellers have been reported (Tanaka et al., 1996).

One drawback of the loop reactor is the disturbance of the flow field due to elbows and so the circular loop reactor was developed in order to overcome this problem (Tanaka and Hosogai, 1990). This design has since been used to investigate further the effects of operating parameters such as impeller speed and geometry, phase fraction, stabiliser concentration and fluid physical properties (Hosogai and Tanaka, 1992a,b). Although this device appears to have potential, scale-up studies would be required to establish the suitability of the loop reactor for industrial scale production.

2.3.3.5 Stirred Tank with Pre-Mixer

One way to overcome the poor droplet size control obtainable in stirred tank reactor is to pre-disperse the monomer in the aqueous phase, using a more reliable and accurate dispersion technique, before transferring the dispersion to a stirred tank for reaction. Two methods for pre-mixing have been reported in the literature. Kamiyama et al (1993) used a system where the organic and aqueous phases were fed independently and simultaneously to a high speed mill, which created a fine dispersion. The dispersion was then passed to a stirred tank reactor where suspension polymerisation was carried out. This method was shown to be capable of generating very fine particles (1 - 10μm) of highly uniform morphology. Another method is that of Omi et al (1994) and Omi (1996) who produced droplets of narrow size distribution, by passing the monomer liquid through a porous glass

membrane into the aqueous phase, before transferring the dispersion to a stirred tank reactor.

2.3.3.6 Oscillatory Baffled Reactor

Bench scale OBRs have been used for both suspension polymerisation of MMA (Ni et al., 1999) and the inverse phase suspension polymerisation of acrylamide (Ni et al., 2000). Both investigations showed that suspension polymerisation could successfully be carried out indicating that the oscillatory baffled reactor is a suitable device for such processes.

2.3.3.7 Other Techniques

In addition to the techniques mentioned above, various other methods have emerged in the literature. For example, a method reported to generating small, uniformly sized particles was the aerosol technique of Panagiotou and Levendis (1991), in which monomer was sprayed into a thermal reactor via an atomizer. The fine drops produced were then polymerised to form polymer particles. PMMA particles have been produced by suspending the monomer in a gel, which prevented coalescence of the drops, and then allowing the reaction to take place (Polacco et al., 1994). This method eliminated the need for adding suspending agents but suffered from the drawback of poorer temperature control, although temperature profiles were to be satisfactory. Ultrasound has also been employed in the production of polymers by suspension polymerisation. This technique can

be used to control the droplet size distribution of a liquid-liquid dispersion and hence the particle size distribution of the polymer produced (Blondeau et al., 1995).

2.3.4 Controlling Particle Size Distribution

2.3.4.1 Introduction

Before polymerisation of the monomer commences, the liquid monomer exists as a population of droplets dispersed throughout the aqueous phase. These droplets are subject to the dynamic processes of breakage and coalescence as described in section 2.2. As polymerisation proceeds, the viscosity of the droplets increases which changes the nature of the interaction processes. During the "sticky" stage (30 - 70 % conversion) droplet breakage is prevented by the high dispersed phase viscosity, which increases the adhesive force of the droplets. Coalescence is prevented to some extent, but not entirely, by the addition of stabilisers, therefore there is a tendency for the size of drops in the suspension to increase throughout this period of the reaction. As conversion approaches 100% the droplets become virtually solid, therefore neither breakage or coalescence can occur, and the size distribution is that of the final product. The time evolution of the droplet population, and hence the final particle size distribution are influenced by factors such as the intensity of agitation applied, the monomer phase fraction, the concentration of stabilisers and the physical properties of the fluids involved.

2.3.4.1 Effect of Mixing Intensity

In a stirred tank reactor the mixing intensity is governed by the agitator speed as well as the impeller and vessel geometry. The effect of these criteria on the mean particle size and particle size distribution has been studied by a number of researchers and various correlations are reported. Hopff et al (1964) were the first to study the effects of mixing intensity on the mean particle size and from their work they reported that the following dependence of mean particle size on stirrer speed existed:

$$d_p \propto N^{-1.5} \tag{2.27}$$

where N was is the rotational speed of the impeller (s^{-1})

Later work by Langner et al (1979) investigated the effect of stirrer speed and impeller type on the particle size produced in suspension polymerisation of vinyl acetate and styrene. They reported the following correlations:

$$d_p \propto N^{-15} \quad \text{(Polyvinylacetate)} \tag{2.28}$$

$$d_p \propto N^{-3.3} \quad \text{(Polystyrene, N < 300rpm)} \tag{2.29}$$

$$d_p \propto N^{-0.3} \quad \text{(Polystyrene, N > 450rpm)} \tag{2.30}$$

It can be seen from the correlations that particle size was reduced by increasing stirrer speed. The dependence of polyvinylacetate particle size on the stirrer speed was close to that reported by Hopff et al (1964) but polystyrene showed a quite different characteristic. The polystyrene data were well correlated (although by different expressions) for high and low stirrer speeds but the exponent of the stirrer speed was observed to change over the intermediate range of $300 < N < 450$. This indicates that the formation of particles in suspension polymerisation is strongly dependent on the polymerisation system as well as the agitation rate. The impeller type and size was also found to have a significant effect on the particle size. This is not surprising as impeller geometry has a strong influence on the flow patterns and shear rates in the vessel, which in turn govern the behaviour of the dispersion.

Mean particle size in suspension polymerisation of styrene has since been further invesitgated. Leng and Quarderer (1982) found that, in an unbaffled vessel, particle size varied with the stirrer speed to the power of –1.5 over a range of impeller types, phase fractions and stabiliser concentrations. With the inclusion of baffles however, a similar trend to that of Langner et al (1979) was observed i.e. dependence of particle size on stirrer speed was lower at higher stirrer speeds. The correlations reported are given below:

$$d_p \propto N^{-1.5} \qquad (\mathrm{N} < 300\mathrm{rpm}) \tag{2.31}$$

$$d_p \propto N^{-0.8} \qquad (\mathrm{N} > 300\mathrm{rpm}) \tag{2.32}$$

Similar results were also reported by Schroder and Bernhard (1982) who investigated the effect of impeller speed and geometry on the resulting particle size. They observed that higher energy dissipation resulted in a narrower size distribution and a smaller mean particle size. They reported the following correlations for mean particle size for the operating range $\varepsilon < 1.4$ W/kg.

$$d_p \propto \varepsilon^{-0.42} \quad \text{(6-blade turbine)} \tag{2.33}$$

$$d_p \propto N^{-0.58} \quad \text{(Impeller stirrer)} \tag{2.34}$$

$$d_p \propto N^{-0.85} \quad \text{(Three stage intermig stirrer)} \tag{2.35}$$

In the range of $\varepsilon > 1.4$ W/kg, the dependence of particle size on energy dissipation was observed to decrease but has not been quantified in their work. The effect of impeller geometry was that high shear rate impellers resulted in the production of smaller particles, which is in good agreement with the results of a study later carried out by Aspostolidou and Stamatopudis (1990).

Erbay et al (1992) carried out a comprehensive investigation into a number of factors that influence the particle size distribution in suspension polymerisation of styrene. The application a regression model to their data yielded the equation:

$$d_p \propto N^{-1.11} D^{-0.8} \tag{2.36}$$

A correlation for the effect of stirrer speed on mean particle size for the suspension polymerisation of MMA is given by Kaflas et al (1993a,b) as:

$$d_p \propto N^{-1.4} \tag{2.37}$$

which is in reasonably good agreement with some of the other, previously reported work for other polymerisation systems.

Contrary to most other findings, an increase in particle size with stirrer speed has also been reported under certain conditions (Ahmed, 1984; Tanaka et al., 1987; Aspostolidou and Stamatopudis, 1990). Tanaka et al (1987) observed this to occur at high stirrer speeds where air was entrained at the liquid surface and resulted in the inclusion of bubble in the polymer particles. Increased particle size with increased stirrer speed has also been observed in case where stabiliser concentration was low, under which conditions it can be attributed to a combination of higher collision frequencies and poor coalescence in inhibition (Ahmed, 1984; Aspostolidou and Stamatopudis, 1990)

The effect of agitation rate on particle size has also been studied in some other types of reactor. In the square loop reactor, particle size showed a similar dependence on stirrer speed as the drop size and was correlated by the following equation (Tanaka and O' Shima, 1988).

$$d_p \propto N^{-1.2} \tag{2.38}$$

In the circular loop reactor, the dependence of particle size on the stirrer speed was reported as (Tanaka and Hosogai, 1990):

$$d_p \propto N^{-0.6} \qquad (\text{N} < 30\text{rad/s}) \tag{2.39}$$

$$d_p \propto N^{0.3} \qquad (\text{N} > 30\ \text{rad/s}) \tag{3.30}$$

The increase in particle size with impeller speed at high impeller speeds was attributed to high coalescence rates in the latter stages of the reaction and was considered a characteristic of this device.

In an oscillatory baffled reactor, the effect of varying the oscillatory velocity at a fixed baffle geometry was investigated by Ni et al (1999). It was found that the mean particle size PMMA varied with oscillatory velocity to the power of -1.2 and hence with energy dissipation to the power of -0.4.

2.3.4.2 Effect of Stabiliser concentration

The stabiliser concentration is a critical aspect of suspension polymerisation processes and has been the subject of research of a number of investigators (Hopff et al., 1964; Konno et al., 1982; Aspostolidou and Stamadopudis, 1990; Erbay et al., 1992; Kaflas et al., 1993a,b). It has been found that increasing the stabiliser concentration results in a decrease in the

particle size of the polymer produced and this has been attributed to three factors (Hopff et al., 1964; Davidson and Witenhafer, 1980; Konno et al., 1982; Deslandes, 1987):

(i) An increase in stabiliser concentration leads to an increase in aqueous phase viscosity, which hinders the coalescence of the dispersed drops.

(ii) An increase in the stabiliser concentration reduces the interfacial tension between the two phases thereby allowing the monomer to be dispersed more easily into smaller droplets.

(iii) Increasing the stabiliser concentration increases the thickness of the coalescence-inhibiting protective film surrounding the droplets.

2.3.4.3 Effect monomer of phase fraction

In order to maximise the productivity of suspension polymerisation reactors it is desirable to operate with as high a monomer phase fraction as possible whilst having enough aqueous medium to occupy the space between monomer droplets and maintain the stability of the dispersion. Typical monomer phase fractions are in the range 0.25 – 0.5 for industrial scale suspension polymerisation (Munzer et al., 1977) although fractions as low as 0.01 (Aspostolidou and Stamatopudis, 1990) are reported in experimental investigations.

The effect of monomer phase fraction on the resulting mean particle size has been studied for various suspension polymerisation systems, in both stirred tank and loop reactors covering phase fractions in the range 0.01 – 0.5 (Konno et al., 1982; Aspostolidou and Stamatopudis, 1990; Tanaka and Hosogai, 1990). The general trend is that higher

monomer phase fractions result in the production of larger polymer particles and this can be attributed to the existence of higher coalescence frequencies due to the greater number of droplets in the system. In the work of Konno et al (1982), however, a relatively high stabiliser concentration was used and no effect of the monomer phase fraction on the mean particle size was detected.

2.3.5 Evolution of Droplet Population During Reaction

Early researchers investigating particle formation in suspension polymerisation assumed that the droplet size distribution at the onset of reaction remained unchanged throughout the process and therefore determined the final particle size distribution (Hopff et al., 1964). Later investigations have however shown that this is not the case and that the drop size distribution can vary throughout the course of the reaction.

Langner et al (1979) have reported mean droplet and particle size data for suspension polymerisation of vinylacetate and styrene in stirred tanks over a range of stirrer speeds and impeller geometries. The final particle size was typically 50% greater that the mean droplet size of the steady state liquid-liquid dispersion than existed prior to the reaction. This indicates that a significant level of drop coalescence occurred during the reaction and can be attributed to the fact that dispersed phase viscosity increases with conversion.

Transient droplet behaviour has been studied in stirred tanks over a range of system geometries, stirrer speeds, monomer phase fractions and stabiliser concentrations (Konno et

al., 1982; Tanaka and Izumi, 1985). The effect of increasing the stirrer speed was to reduce the growth rate of droplets during the transient period of the reaction thereby resulting in the production of smaller particles (Tanaka and Izumi, 1985). The inclusion of a draft tube in the tank, however, altered this characteristic. Under such conditions, transient features were similar to the conventional stirred tank at high agitation rate but if a low stirrer speed was used, droplets showed no increase in size during the reaction (Tanaka and Izumi, 1985). This indicates that an improved circulation pattern can significantly reduce droplet coalescence during the reaction. The effect of monomer phase fraction and stabiliser concentration was studied by Konno et al (1982). They found that stabiliser concentration had no effect on the drop size distribution below 30% conversion but significantly affected the behaviour of droplets during the middle and late stages of the reaction, resulting in anything from unchanging to fast growing drops being observed. Using a higher monomer phase fraction resulted a higher particle growth rate and hence in larger particles being produced. An interesting feature of this study is that bimodal distributions were observed in all cases except that in which a very high stabiliser concentration was used. Bimodal distributions were evident from an early stage when the phase fraction was high but did not appear until later in the reaction at lower phase fractions and were attributed to the formation of a peak at high drop size due to coalescence.

Investigations into transient droplet behaviour have also been conducted in loop reactors. In the square loop reactor it was observed that mean droplet size remained constant throughout the reaction under each of the conditions tested (Tanaka and O' Shima, 1990), which is similar to the results reported at low agitation rate in the stirred tank with draft tube. The circular loop reactor, on the other hand, behaved more like the conventional stirred tank reactor, with an increase in droplet size during the reaction being

observed (Tanaka and Hosogai, 1990). However, further investigation into the behaviour of droplets in the circular loop reactor showed that it was possible to achieve characteristics similar to that of the square loop reactor if operating at a low power input or high stabiliser concentration.

Ni et al (1999) studied transient droplet behaviour during suspension polymerisation of MMA in an oscillatory baffled reactor over a range of mixing intensities for a fixed reactor geometry. Their data showed that the drop size distribution broadened considerable during the reaction with a threefold increase in mean drop size being observed.

In summary, it can be concluded that transient behaviour of the drop size distribution during the course of a suspension polymerisation reaction is influenced by a number of process conditions including reaction system, type and geometry of reactor, agitation rate, monomer phase fraction and stabiliser concentration. The process tends to be coalescence dominated and increases in drop size of up to four times have been observed.

2.3.6 Summary

In suspension polymerisation processes the particle size distribution achieved is dependent on many factors and can therefore be difficult to predict and control accurately. As a result of this, many techniques have been developed in order to improve the control of particle size. One such technique was the application of a bench scale OBR to suspension

polymerisation of MMA, in which it was observed that a good degree of control over the mean particle size could be achieved by varying in the oscillation frequency and amplitude. Scale-up studies are required, though, to determine if the same level of control can be achieved in the large scale production of polymers by suspension polymerisation in an OBR and that is the aim of the present investigation.

3 EXPERIMENTAL APPARATUS AND FACILITIES

Two experimental rigs were used in this project, a Perspex OBC with an internal diameter of 380mm and a stainless steel OBR of 213mm diameter, each of which are described in turn in the following sub-sections.

3.1 The Perspex OBC

The Perspex OBC is shown schematically in Figure 3.1 and consisted of a Perspex column of 380mm internal diameter, 2.04 m in height and with a wall thickness of 10mm with a operational capacity of around 200 l. Fluid agitation was provided by oscillating a baffle assembly consisting of two annular polypropylene baffles connected by three M16 screwed rods. Baffles of 10mm thickness and with a free area of either 20 %, 25 % or 31 % were available and the baffle spacing could be adjusted by moving the baffles along the rods into any required position. Oscillations were provided by means of a 5.5 kW motor via a linkage mechanism as shown. The vertical shaft of the linkage mechanism was guided by linear bearings as these provide excellent linear motion with very little vibration. The oscillation frequency was controlled by a frequency inverter and could be varied from 0 – 1 Hz. The oscillation amplitude was determined by the position at which the connecting rod joined the rotating arm on the motor and could be varied from 60 – 200 mm in increments of 20 mm. This rig was used for the flow visualisation and oil-water dispersion experiments, as described in Chapters 4 and 5.

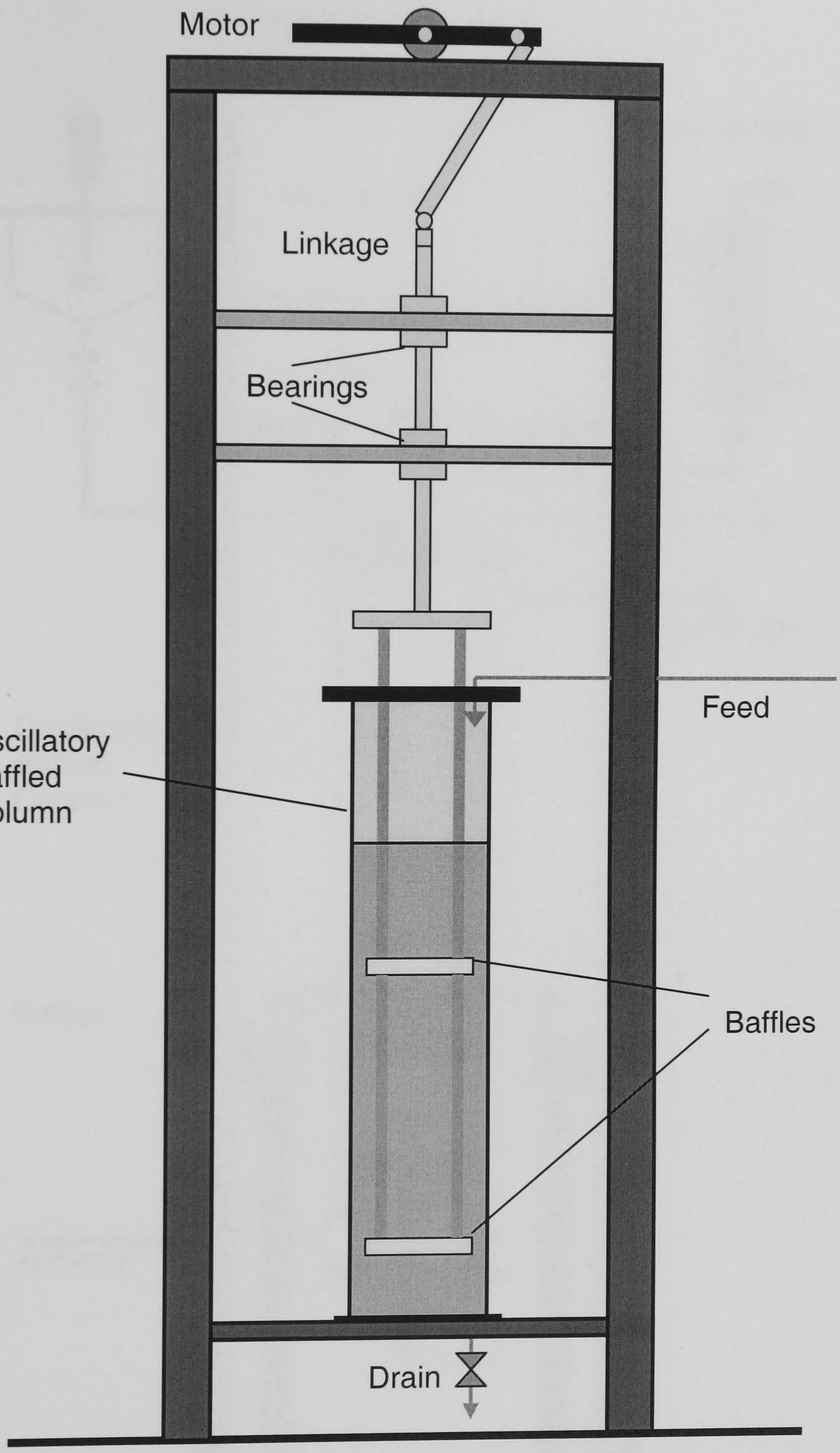

Figure 3.1: The Perspex Oscillatory Baffled Column

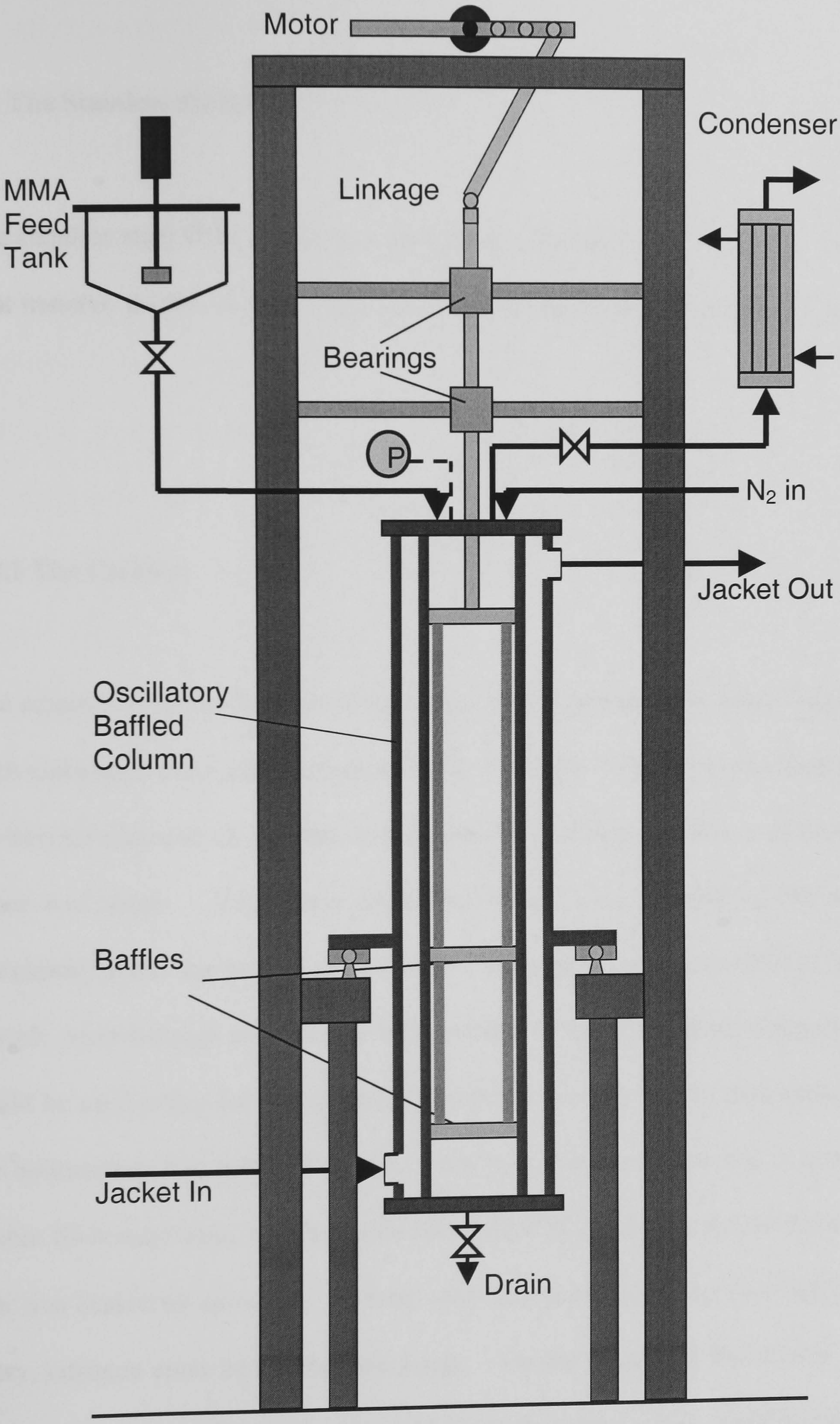

Figure 3.2: Stainless Steel OBC

3.2 The Stainless Steel OBC

The stainless steel OBC is shown schematically in Figure 3.2. This rig was used for the heat transfer, droplet size, and polymerisation experiments, as described in Chapters 6 – 9.

3.2.1 The Column

The reaction vessel comprised of two concentric stainless steel tubes flanged together at each end to provide a jacketed column 1.5m in height. The inner tube and outer tube had an internal diameter of 213mm and 273mm respectively and the wall thickness of both tubes was 4mm. Two ports (inlet and outlet) were located on the outer tube for circulating water for heating or cooling. There were also a number of 2mm diameter sample ports through to the inner tube located at various heights along the column that could be used either for withdrawing samples or for placing thermocouples. The lid of the reactor had five holes of various sizes in it. In the centre was a hole containing a 30mm ID bronze bush, which guided the oscillating shaft as it moved through the lid and this was sealed by an o-ring. There were also ports for outlet to condenser, monomer entry, nitrogen entry and a pressure gauge. On the bottom of the column was a 12 mm thick stainless steel plate with a tapped hole in the centre which could be fitted with either

a drain valve or a plug. Both the lid and bottom plate were fixed in position with bolts and the connections were sealed with PTFE gaskets.

3.2.2 The Baffle Oscillation Mechanism

Fluid agitation was achieved by oscillating two annular baffles connected together by three smooth, stainless steel rods. The baffle assembly was supported from a stainless steel disc which moved up and down in the upper region of the column. This disc had holes in it to allow liquid material to flow through during charging and was oscillated by a 5.5kW motor via a linkage mechanism. As with the Perspex rig, the vertical shaft was guided by linear bearings. The oscillation frequency could be varied between 0 and 2 Hz using a frequency inverter and the amplitude was determined by the position at which the connecting rod joined the rotating arm on the motor and could be varied from 50 to 100 mm in increments of 12.5 mm. Nine baffle assemblies were available which allowed baffle spacings of 263, 315, or 368 mm (corresponding to 1.25, 1.5 and 1.75 times the column internal diameter respectively) and baffle free areas of 20, 25 and 30 % to be used in any combination.

3.2.3 The Heating/Cooling System

The jacket on the column could be fed with either cold water from mains or hot water from an immersion tank, which could be thermostatically controlled at a specific

temperature between room temperature and 80°C (see Figure 3.3). When applying heating, the water was circulated through the jacket and then back to the hot water tank.

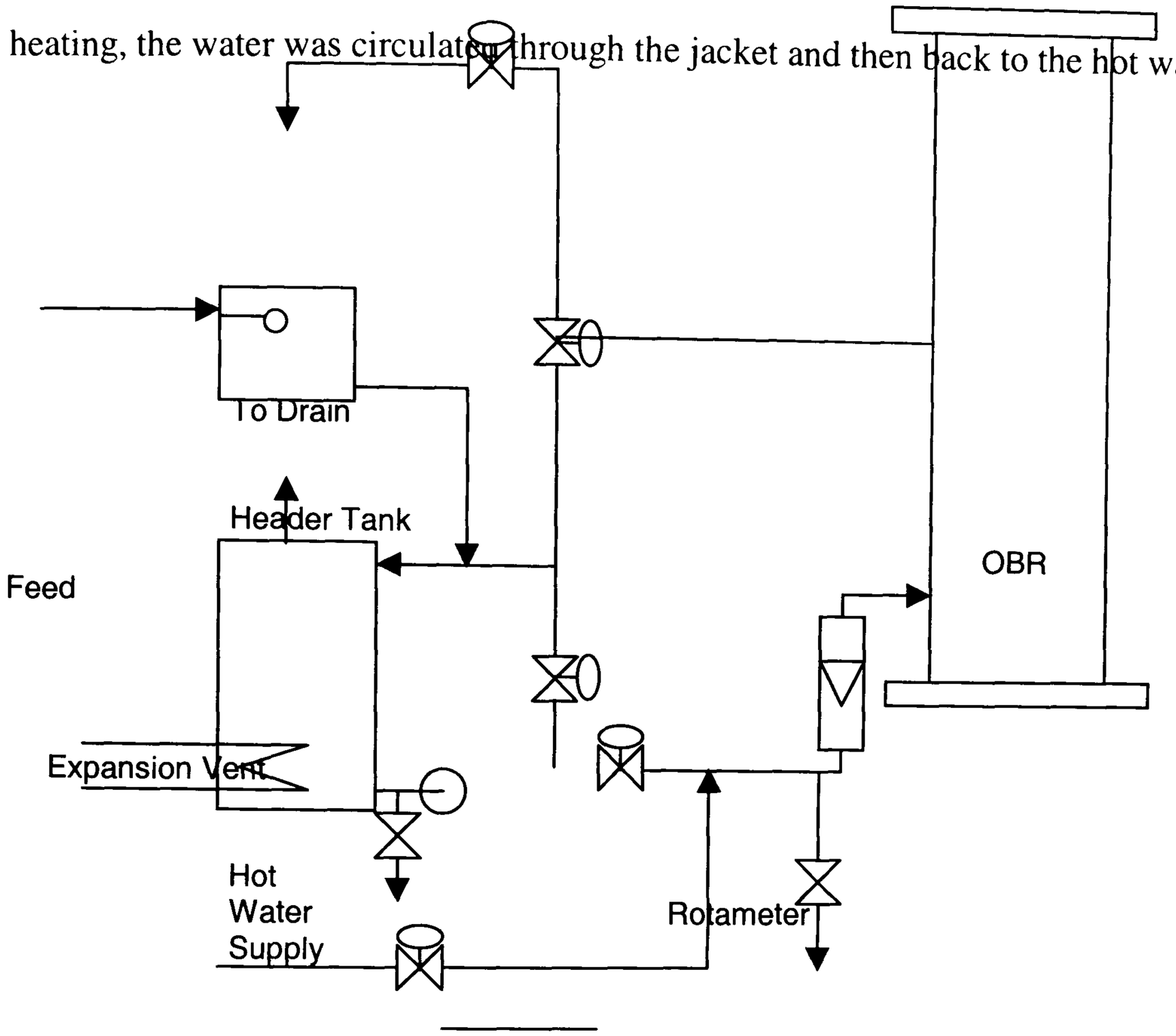

Figure 3.3: Heating Cooling System

When applying cooling, the water passed through the jacket then to a drain. During cooling the hot water was diverted through a bypass loop back to the immersion tank. The system could be changed from heating to cooling and vice versa by changing the position of the control valves which operated as fully open or fully shut only. The flowrate of water through the jacket could be controlled by valve on the inlet stream and

the was shown by a rotameter downstream of this valve. The maximum flowrates obtainable were 40 l/min for cooling water and 18 l/min for hot water.

3.2.4 Data Acquisition System

Thermocouples were located in the jacket inlet and outlet streams and could also be inserted into the reactor at various points via the ports on the wall. The signal from each of the thermocouples (up to a maximum of 8) was relayed to a signal amplifier and then to a computer via a data acquisition card. All data was logged, using DAS wizard acquisition software, into Microsoft excel columns, from which, the temperature profile for a reaction could be graphed and displayed.

4 FLOW VISUALISATION

4.1 Introduction

The mixing efficiency of any liquid mixing device is dependent on the fluid mechanical conditions in the system. Mechanical agitation results in the bulk motion of fluid in the form of eddies, which propagate through the fluid and interact with each other thereby reducing non-uniformities in the system. For the purpose of establishing design and scale-up rules for mixing equipment, it is desirable to have a knowledge of the fluid mechanical conditions that exist in a particular system. Such knowledge can be gained by flow visualisation, which involves adding small tracer particles to the fluid and observing their trajectories under conditions of fluid agitation. This method provides a good, qualitative understanding of mixing characteristics and has therefore been used in this investigation to study the flow patterns in the Perspex OBC.

4.2 Experimental Facilities and Procedures

Two pieces of metal sheet were fastened to one side of the framework of the Perspex OBC with a narrow vertical gap between them. An 800W spot lamp was positioned behind the plates and the light was concentrated through the slot thereby projecting a sheet of light of 30 mm wide by 1.3 m high through the centre of the column. The water was seeded with conifer pollen powder of an average size of 100 μm. The density of the pollen particle when wet is very close to that of water, ensuring that in each experiment there is no settling

of the tracer particles and that the particles follow the flow faithfully. By positioning a camera perpendicular to the plane and darkening the laboratory, photographs could be taken that captured 2D images of the flow patterns. In total, over 200 35 mm photographs were taken covering oscillation frequencies of 0.25 – 1 Hz, oscillation amplitudes of 100 – 180 mm, baffle free areas of 20, 25 and 31% and baffle spacings of 500, 600 and 800 mm.

4.3 Results and Discussion

4.3.1 Effect of Oscillation Frequency and Amplitude

Flow visualisation photographs of the OBC operating at various oscillation frequencies and amplitudes are shown in Figures 4.1 and 4.2 respectively. These were selected from a large number of photographs taken as a general representation of what was observed. In all cases the orifice diameter and the baffle spacing were kept constant. It can be seen from the photographs that eddies were formed behind the moving baffles under each of the conditions tested, similar to those observed in a 50 mm diameter OBC (Gough et al, 1997). This is an important result as it demonstrates that efficient eddy mixing can easily be achieved in an OBC of this scale. The effect of the oscillation frequency on such flow patterns (Figure 4.1) suggests that an increase of the oscillation frequency, while keeping the oscillation amplitude constant, resulted in an increase in the intensity of the mixing, as indicated by the chaotic particle trajectories shown in the photographs. Similar features were also observed for the oscillation amplitudes at a constant frequency (Figure 4.2). These results are expected as an increase of either the frequency or amplitude leads to an increase in the oscillatory velocity, thereby producing faster moving and more energetic

eddies, which in turn leads to better mixing. It also appears that at higher oscillation amplitudes the eddies formed were larger and occupied a greater percentage of the inter-baffled cavity, and such a trend was less noticeable for the higher oscillation frequencies. This implies that the oscillation amplitude could be the governing factor in determining the length to which a vortex propagates through the fluid.

4.3.2 Effect of Orifice Diameter

The orifice diameter is a key geometric parameter and thus has a significant influence on the fluid mechanics. It is therefore important to identify a feasible range of orifice diameters over which good mixing can be achieved.

In order to examine the effect of the orifice diameter on the flow patterns in the OBC, three orifice areas of 20, 25 and 31 % of the cross-sectional area, corresponding to an orifice diameter of 170, 190 and 210 mm respectively, were investigated while keeping all other parameters constant. Typical results are shown in Figure 4.3 from which it is evident that there were strong eddy motions within the baffled region for all the three baffle diameters tested. This indicates that all three of the constriction ratios tested in this study are suitable for use in oscillatory baffled tubes. It also appears that the eddy activities at α = 31% were less intensive than those at either α = 25% or 20% and there were occasional zones lacking of the chaotic particle movements. On the whole, however, this is what is expected as reducing the orifice diameter increases the velocity at which the fluid passes through the orifice and hence increases the intensity of the eddy mixing achieved.

4.3.3 Effect of Baffle Spacing

An appropriate baffle spacing creates an optimal environment for eddies to propagate within each baffled cavity. If the spacing is too small there will be insufficient room for the eddies to develop and if too large the eddies will diminish within the baffled cavity, resulting in stagnant regions within the column. In bench scale OBCs, the optimal baffle spacing reported is between 1.5 and 2 times the column diameter (Brunold et al., 1989; Ni and Gao, 1996a, Zhang et al., 1996; Ni et al., 1998a). To find out if such spacings would be applicable to the larger scale OBC, three baffle spacings of 500, 600 and 800 mm, corresponding to 1.25, 1.5 and 2.0 times the column diameter respectively, were tested for various oscillation amplitudes as shown in Figures 4.4, 4.5 and 4.6. It is observed that when operating with a low oscillation amplitude of 100 mm the eddies covered the entire baffled cavity when the spacing was low (Figure 4.4A) and substantial stagnant regions were observed at the higher baffle spacing of 800 mm (Figure 4.4C). With an increase of the oscillation amplitude the development of eddies encompassed the whole region even at a baffle spacing as high as two times the column diameter. This indicates that the baffle spacing and the oscillation amplitude are closely related. In order to assess this relationship a further set of experiments was carried out to physically measure the extent to which eddies occupied fixed baffled cavities at different oscillation amplitudes. This procedure involved marking the starting and finishing points of eddies as they propagated along the column. These measurements are summarised in Tables 4.1, 4.2 and 4.3 for baffled cavities of 500, 600 and 800 mm respectively, in which the length to which an eddy propagates along the column, L_e, is compared with the oscillation amplitude, x_o. The empty boxes in tables indicate conditions under which no measurements could be made due to the practical limitations of the rig. It can be seen from Tables 4.1-4.3 that with the

higher oscillation amplitudes the eddies propagated further along the column. In order to optimise the mixing capability of an OBC, the length of eddy propagation should be close or equal to the baffle spacing employed. It is evident form the results reported here that the ratio of the oscillation amplitude to the length of the eddy propagation (x_o/L_e) was always in the range of 0.15 – 0.3, therefore the optimum ratio of the oscillation amplitude to the baffle spacing should also lie within this range. This is in good agreement with that reported by Gough et al (1997), who, from their flow visualisation study in a 50 mm diameter OBC, suggested that the oscillation amplitude should be about one quarter of the baffle spacing. This is encouraging news as it suggests that the rule of determining the optimum baffle spacing could linearly be extended to larger columns with little modifications.

4.4 Conclusions

Flow visualisation observations are presented in this chapter, from which it has been shown that good eddy mixing can easily be achieved in an OBC of this scale. The intensity of this eddy mixing is controlled by the oscillation frequency and amplitude as well as the baffle orifice diameter due to the variations in fluid velocity induced by changing these parameters. Eddy propagation is governed by the oscillation amplitude and an amplitude equal to approximately one quarter of the baffle spacing has been identified as optimum, which is similar to findings in a smaller scale device.

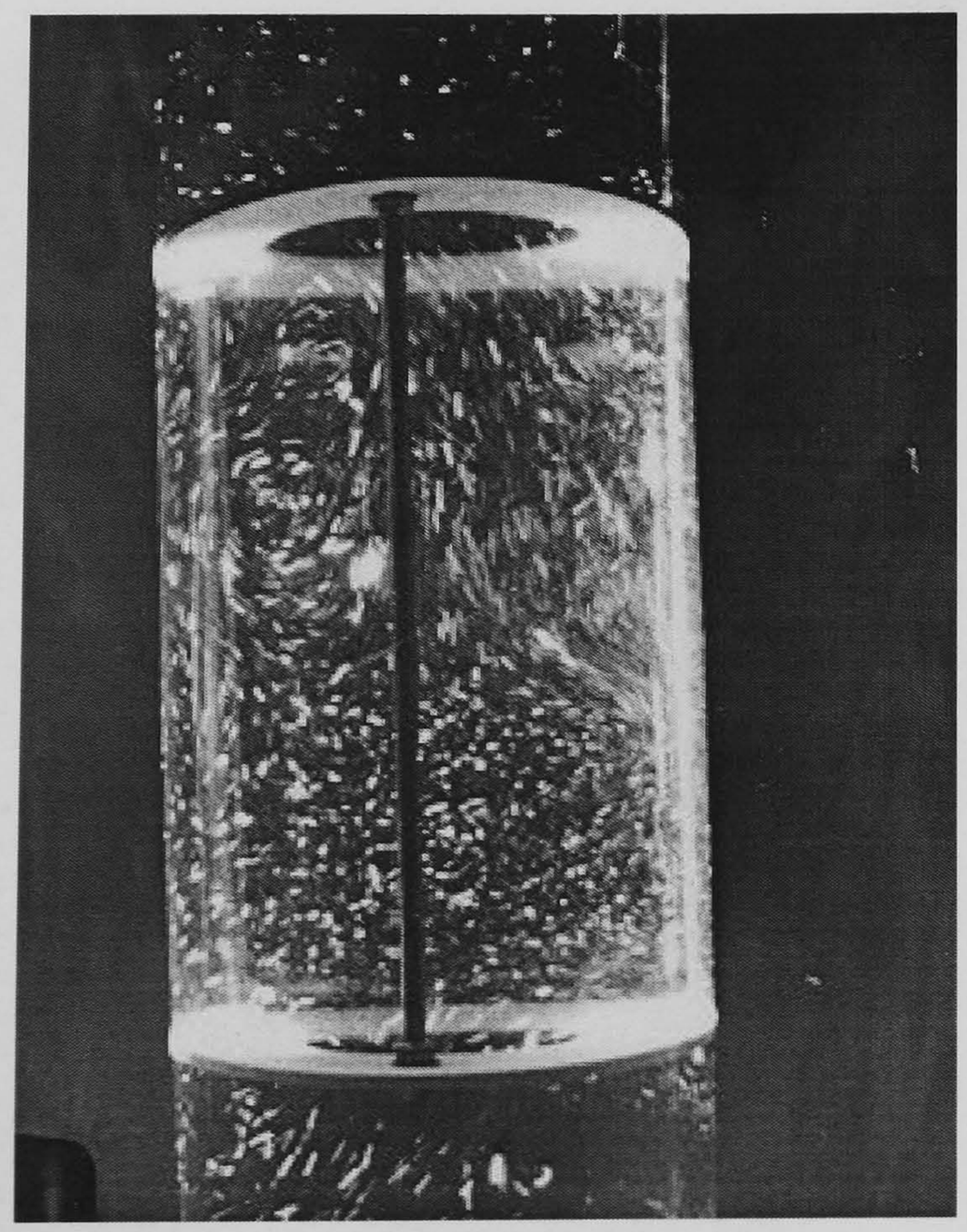

(A)

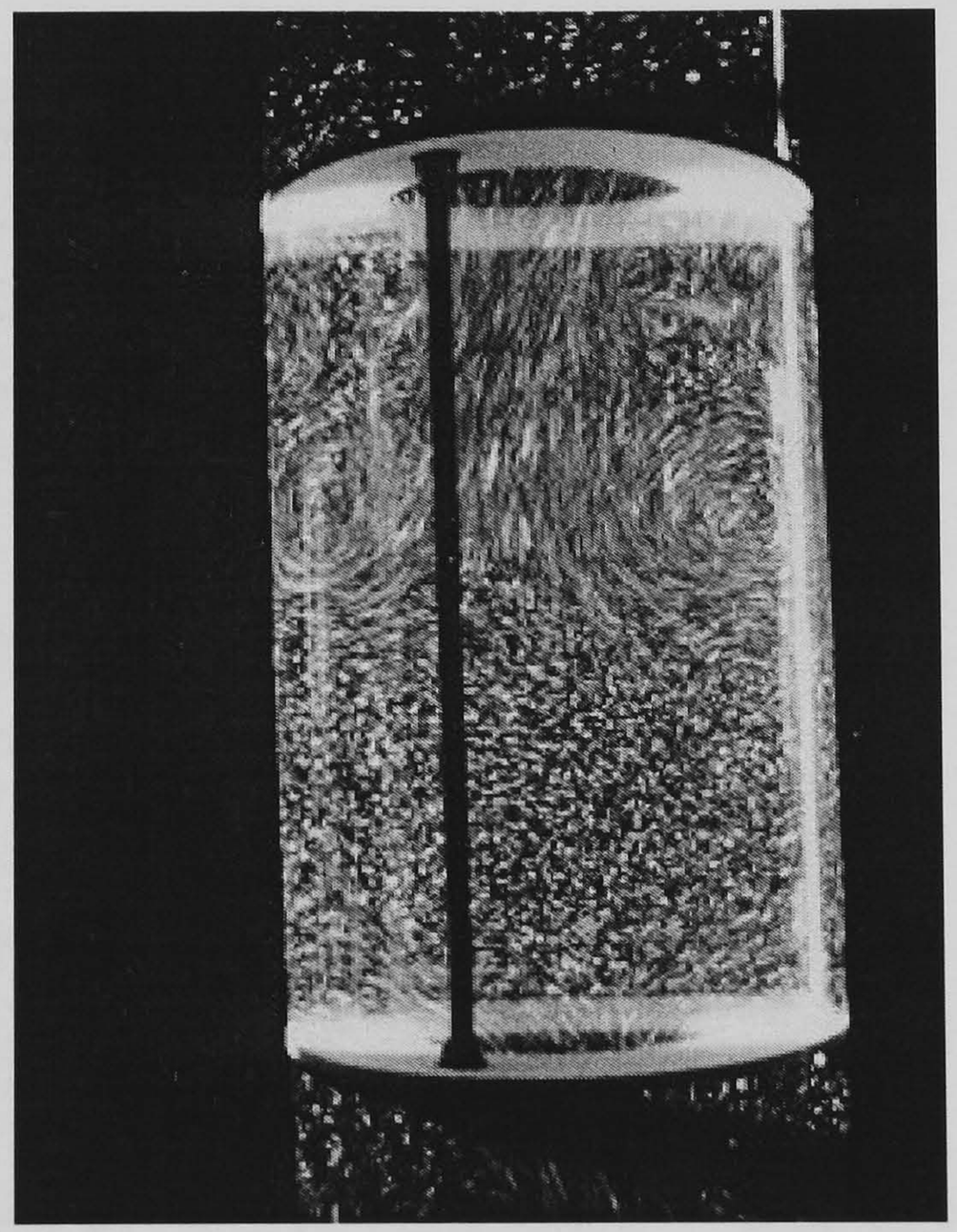

(B)

(C)

Figure 4.1: Effect of oscillation frequency on flow patterns (A) 0.25 Hz, (B) 0.5 Hz, (C) 0.75 Hz, (x_o = 100 mm, α = 25%, L = 600 mm)

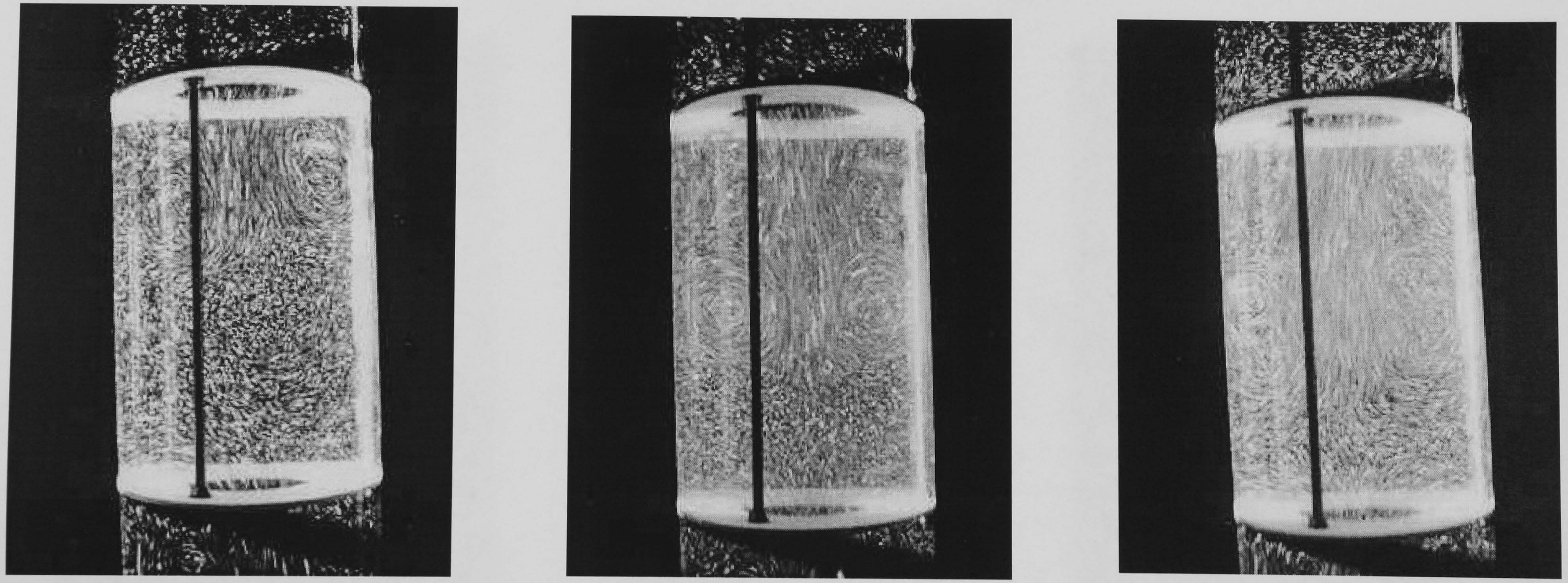

(A) (B) (C)

Figure 4.2: Effect of oscillation amplitude on flow patterns (A) 100 mm, (B) 140 mm, (C) 180 mm, (f = 0.5 Hz, α = 25 %, L = 600 mm)

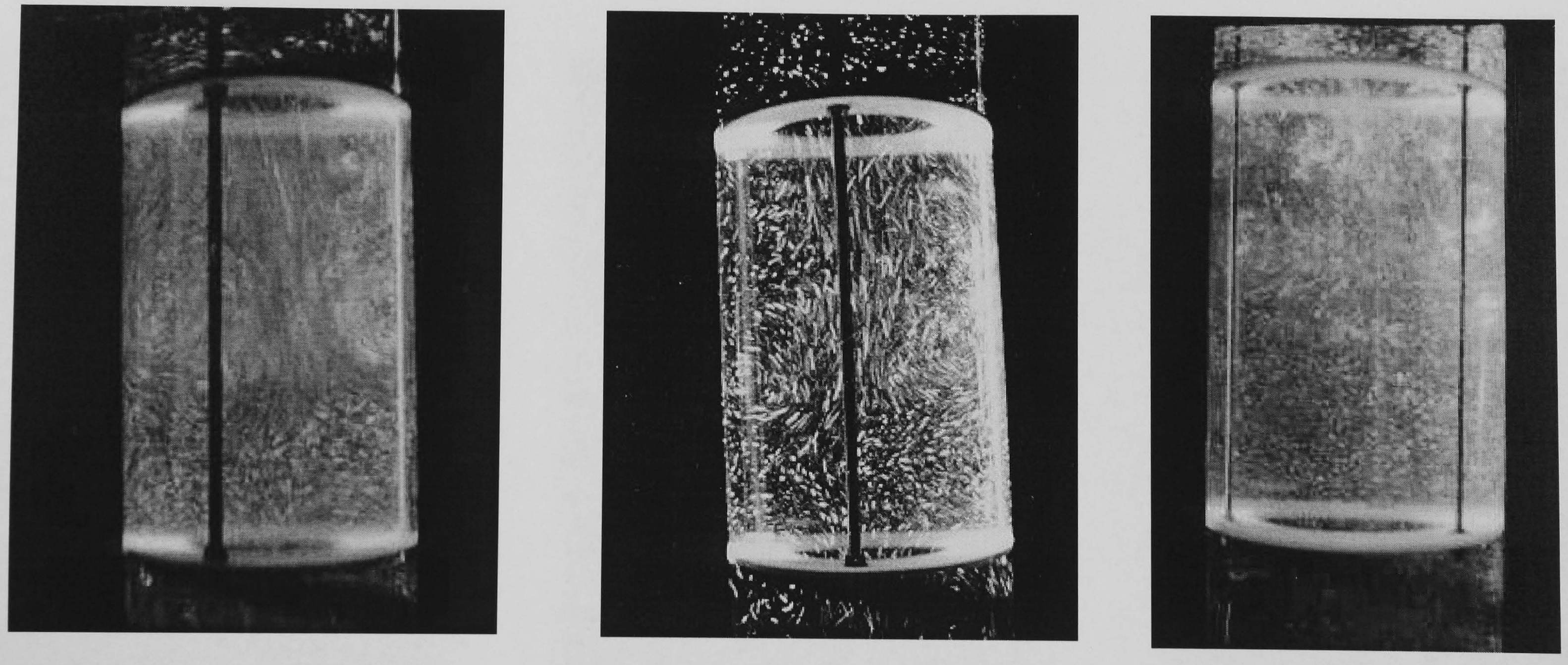

(A) (B) (C)

Figure 4.3: Effect of baffle free area on flow patterns (A) $\alpha = 20\%$, (B) $\alpha = 25\%$, (C) $\alpha = 31\%$ (f = 0.25 Hz, x_o = 140 mm, L = 600 mm)

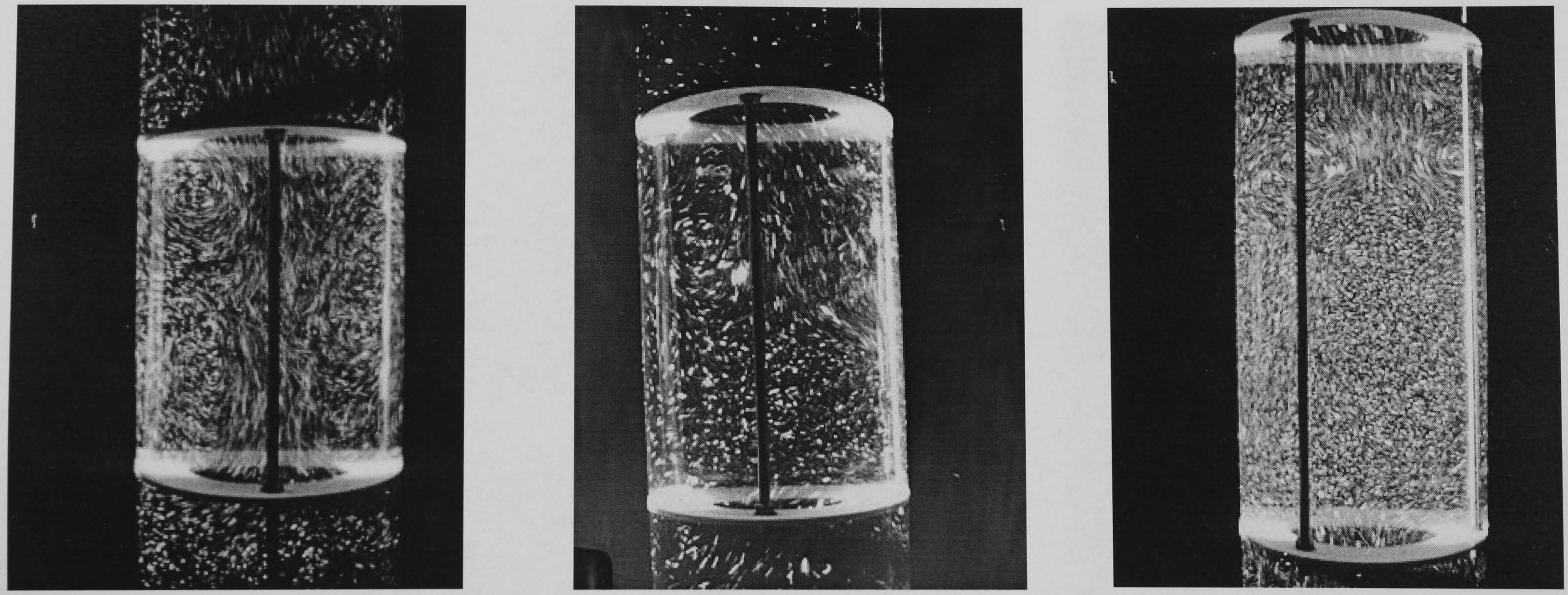

(A) (B) (C)

Figure 4.4: Effect of baffle spacing on flow patterns (A) L = 500 mm, (B) L = 600 mm, (C) L = 800 mm (f = 0.25 Hz, x_o = 100 mm, α = 25%)

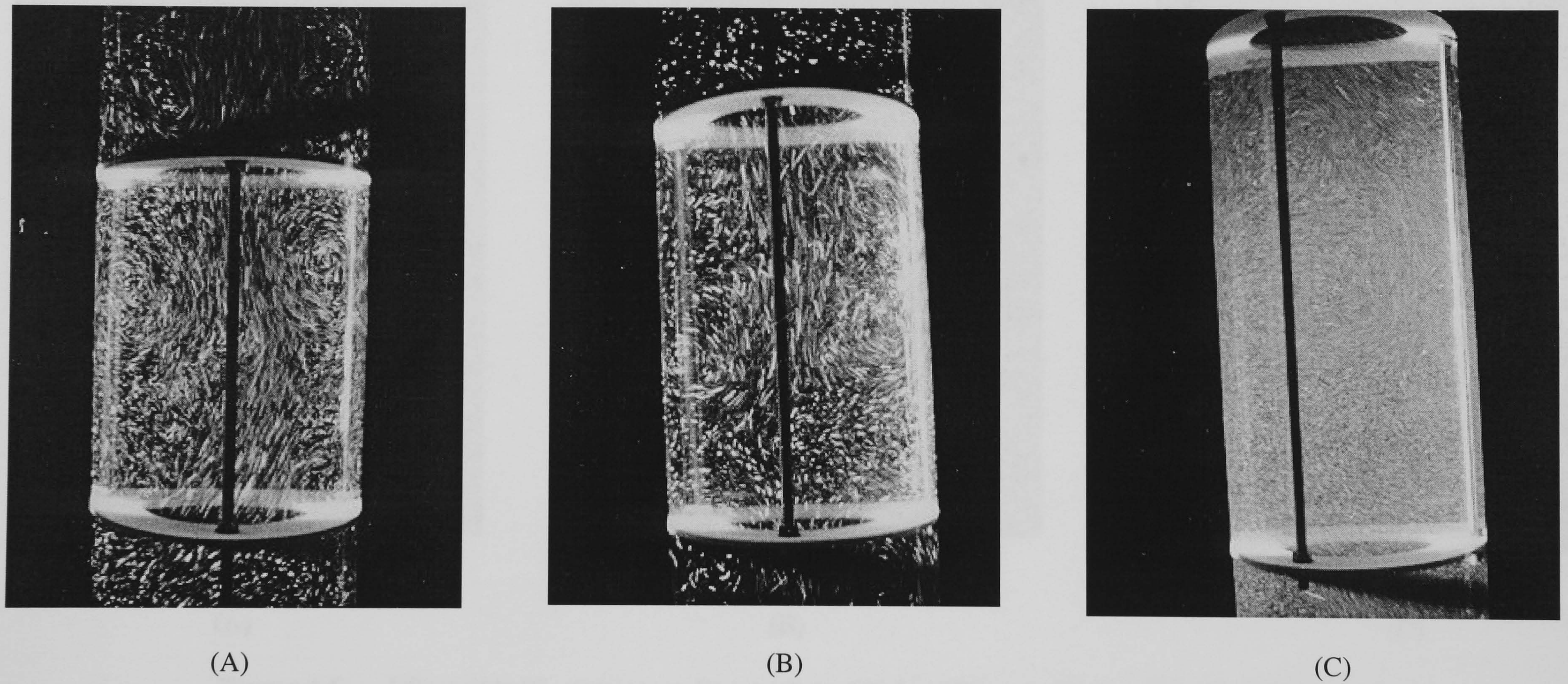

(A) (B) (C)

Figure 4.5: Effect of baffle spacing on flow patterns (A) L = 500 mm, (B) L = 600 mm, (C) L = 800 mm (f = 0.25 Hz, x_o = 140 mm, α = 25%)

(A) (B) (C)

Figure 4.6: Effect of baffle spacing on flow patterns (A) L = 500 mm, (B) L = 600 mm, (C) L = 800 mm (f = 0.25 Hz, x_o = 180 mm, α = 25%)

Table 4.1: Effect of oscillation frequency and amplitude on the length to which eddies propagate through the baffled cavity (baffle spacing = 800 mm)

Baffle free area (%)	Oscillation frequency (Hz)	Oscillation Amplitude (mm)					
		100		140		180	
		L_e (mm)	x_o/L_e	L_e (mm)	x_o/L_e	L_e (mm)	x_o/L_e
31	0.25	415	0.24	600	0.23	630	0.29
	0.5	415	0.24	600	0.23	680	0.26
	0.75	420	0.24	600	0.23	-	-
	1.0	420	0.24	-	-	-	-
25	0.25	630	0.16	700	0.20	800	0.23
	0.5	570	0.18	660	0.21	800	0.23
	0.75	570	0.18	590	0.24	-	-
20	0.25	550	0.18	700	0.20	800	0.23
	0.5	600	0.17	725	0.19	800	0.23
	0.75	600	0.17	-	-	-	-

Table 4.2: Effect of oscillation frequency and amplitude on the length to which eddies propagate through the baffled cavity (baffle spacing = 600 mm)

Baffle free area (%)	Oscillation frequency (Hz)	Oscillation Amplitude (mm)					
		100		140		180	
		L_e (mm)	x_o/L_e	L_e (mm)	x_o/L_e	L_e (mm)	x_o/L_e
31	0.25	420	0.24	470	0.30	600	0.30
	0.5	420	0.24	480	0.29	600	0.30
	0.75	440	0.23	480	0.29	-	-
	1.0	450	0.22	-	-	-	-
25	0.25	470	0.21	600	0.23	600	0.30
	0.5	530	0.19	600	0.23	600	0.30
	0.75	540	0.19	-	-	-	-
20	0.25	500	0.20	600	0.23	600	0.30
	0.5	510	0.20	600	0.23	600	0.30
	0.75	520	0.19	-	0.23	-	-

Table 4.3: Effect of oscillation frequency and amplitude on the length to which eddies propagate through the baffled cavity (baffle spacing = 500 mm)

Baffle free area (%)	Oscillation frequency (Hz)	Oscillation Amplitude (mm)					
		100		140		180	
		L_e (mm)	x_o/L_e	L_e (mm)	x_o/L_e	L_e (mm)	x_o/L_e
31	0.25	420	0.24	460	0.30	500	0.36
	0.5	440	0.23	480	0.29	500	0.36
	0.75	440	0.23	490	0.29	-	-
	1.0	450	0.22	-	-	-	-
25	0.25	500	0.20	500	0.28	500	0.36
	0.5	500	0.20	500	0.28	500	0.36
	0.75	500	0.20	-	-	-	-
20	0.25	500	0.20	500	0.28	500	0.36
	0.5	500	0.20	500	0.28	500	0.36
	0.75	500	0.20	-	-	-	-

5 OIL-WATER DISPERSION

5.1 Introduction

The ability to completely disperse one immiscible liquid into another is essential to the process of suspension polymerisation. Complete dispersion occurs when the mixing intensity is high enough that no stratification exists between the two phases and the dispersed phase exists entirely as droplets in the continuous phase. If OBRs are to be used for suspension polymerisation then complete dispersion of monomer in the aqueous phase must be readily achievable. This has already been demonstrated on a bench scale OBC (Zhang et al., 1996) but as yet no work has been reported in larger devices. In this chapter, the resulting effects of varying operating conditions and baffle geometry on the characteristics of oil-water dispersion in the Perspex OBC are reported.

5.2 Experimental Facilities and Procedures

The Perspex OBC was used in all oil-water dispersion experiments. The oil phase used was silicone oil of a density of 920 kgm^{-3} and a viscosity of 5 mPa.s, and the aqueous phase was mains supply water. This is the same materials as that used by Zhang et al (1996) in a 50 mm diameter OBC, therefore a comparison can be made between the two systems. The interfacial tension between the oil and water phases was measured using mutually saturated samples on a Torsion Balance, and was found to be 0.0205 Nm^{-1} at 21 ^{o}C.

Each experiment started by firstly adding the required amounts of water and the silicone oil to the column allowing the contents to settle until a clear interface was stabilized. The total operational volume, which depended on the baffle spacing applied, was 159 l, 170 l and 193 l respectively for the baffle spacings of 500, 600 and 800 mm so that the liquid surface was always of the same height above the highest baffle.

A sampling point situated on the base of the column, as shown in Figure 5.1, was used to collect oil-water samples as this is the point in the column where the oil fraction is the lowest. The sampling procedure involved collecting an oil-water sample (approx 100ml) in a measuring cylinder, allowing the oil and water layers to separate and then recording the volume fractions of oil and water in the sample. A relative fraction of oil has been defined as:

$$f_r = \frac{f_{sample}}{f_{overall}} \tag{5.1}$$

where f_r is the relative fraction, f_{sample} the oil fraction in the sample (%) and $f_{overall}$ the overall oil fraction initially used in the system (%). f_r thus represents the degree of oil-water dispersion achieved in this pilot OBC. Therefore, f_r = 1 refers to a uniform dispersion between oil and water as the oil fraction in samples equals that in the initial set-up in the column. f_r = 0, on the other hand, indicates that no oil trace was found in the sample and that the oil and water remain in separate layers with little or no mixing between the two phases. In addition, such a definition also allows comparisons to be made between experiments in which different overall oil fraction are used.

The effects of oscillation time, oscillation frequency, oscillation amplitudes, baffle spacing, orifice diameter and phase fraction were investigated in this study.

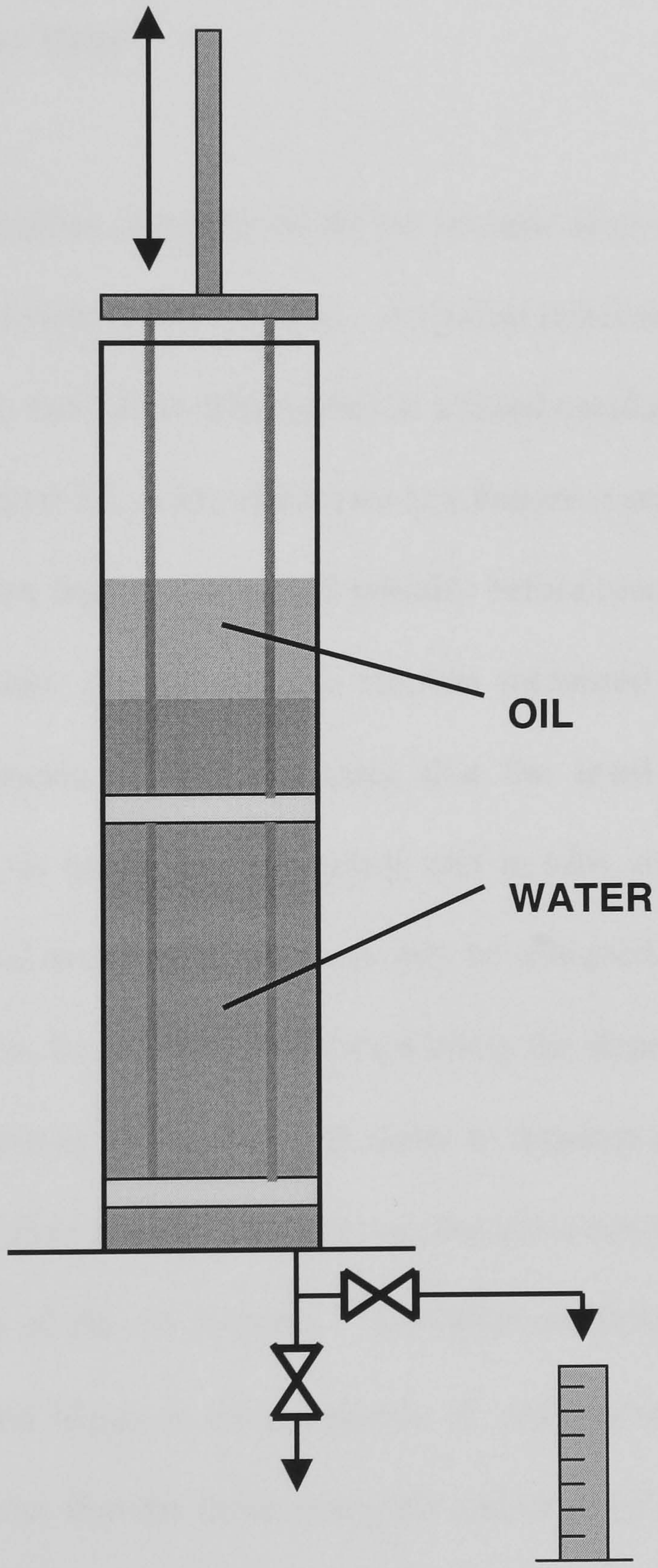

Figure 5.1: Location of sampling point

5.3 Results and Discussion

Raw data from the oil-water dispersion experiments are listed in Appendix 1

5.3.1 Effect of Oscillation Time

When oscillation of the baffles commenced the oil became dispersed in the water and the level of dispersion (i.e. f_r) increased with time. A typical dynamic response of the relative fraction, for four different oscillation frequencies at a fixed oscillation amplitude and baffle geometry, is shown is Figure 5.2, from which two key features can be extracted. Firstly, as time proceeded the relative fraction increased initially before reaching a steady state, after which it remained constant, and the relative fraction measured at this steady state was higher at higher frequencies. This indicates that the level of oil-water dispersion achievable is dependent on oscillation frequency, and in turn, on the oscillatory velocity ($x_o f$), and that a uniform oil-water dispersion can only be achieved if the oscillatory velocity is high enough. This can be explained by considering the dependence of the dispersion process on fluid mechanics in the system. In order to disperse the oil into the water, the velocity of bulk fluid motion generated by the oscillations must be sufficient to overcome the terminal rise velocity of the oil droplets. At higher oscillatory velocities, the fluid is moving more quickly and hence is more capable of transporting the oil throughout the system. It is also the case that the more energetic eddies generated at higher frequencies break the oil into smaller droplets, which are easier to transport. The second notable feature in Figure 5.2 is that the rate of the rising of the relative fraction was greater at higher frequencies (oscillatory velocities) than at lower ones. This is a result of the more

rapid generation of eddies in the system. Another interesting point is that the steady state at each of the oscillatory velocities (frequencies) was achieved in the first two to three minutes of the operation, reflecting the efficiency of the chaotic mixing established within the OBC. Therefore, all of the steady state data presented in the remaining part of this chapter refers to a sampling time of 10 minutes.

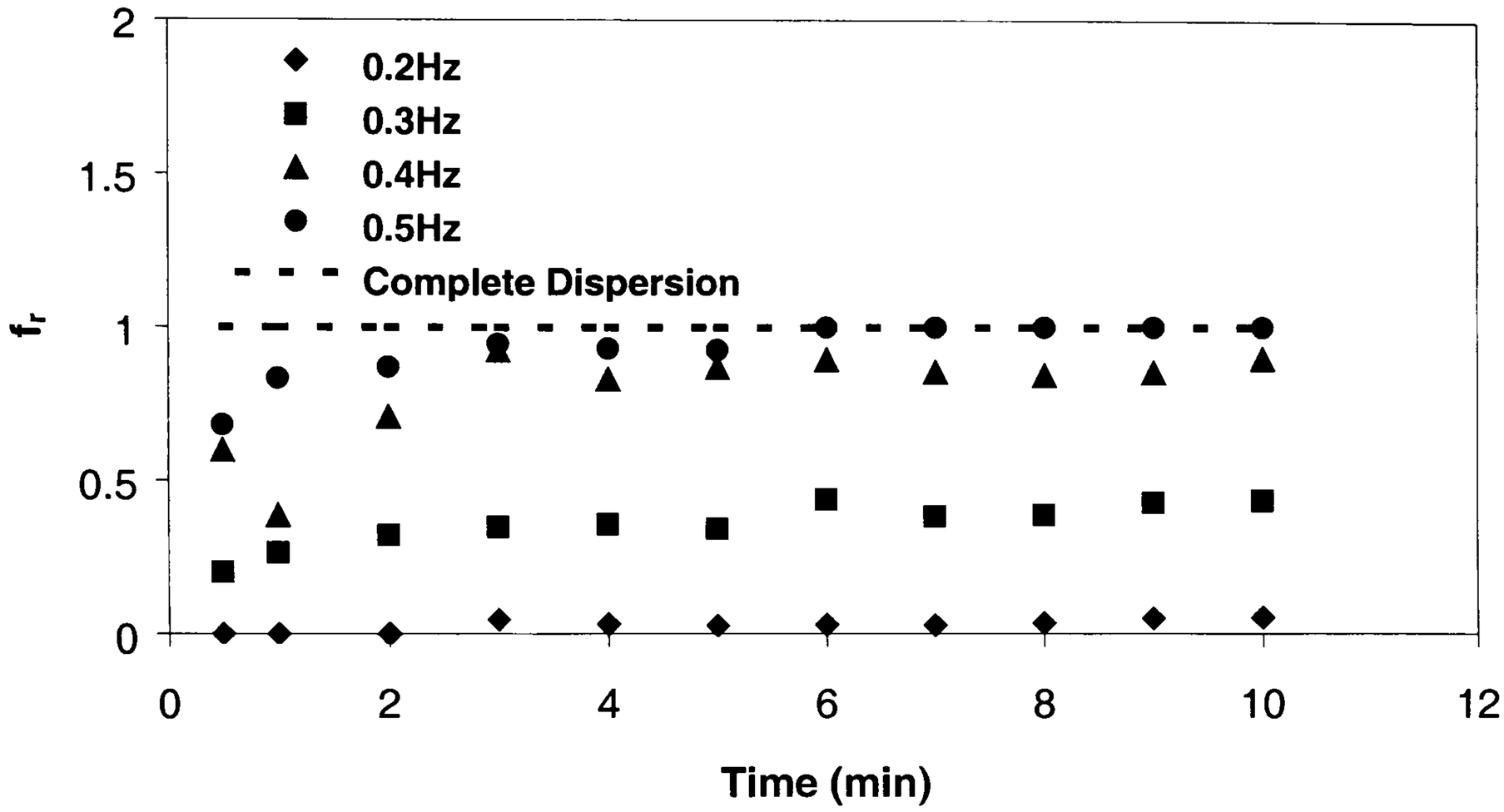

Figure 5.2: Effect of time and oscillation frequency on level of oil-water dispersion achieved (x_o = 140 mm, α = 31%, L = 600 mm)

5.3.2 Effect of Operating Conditions on the Degree of Oil-Water Dispersion

Figure 5.3 shows the effect of the oscillatory velocity ($x_o f$) on the relative fraction for variations in both oscillation frequency and amplitude. It is evident that the relative fraction increases in an almost linear fashion with $x_o f$ before levelling off when complete dispersion is achieved. This indicates that the degree of dispersion that can be achieved in

the OBC is proportional to the oscillatory velocity. Similar results at different baffle free areas and baffle spacings are shown in Figures 5.4 and 5.5 respectively from which it can be seen that the near linear dependence of f_r on $x_o f$ is again observed at each of the baffle geomerties tested. Also, Figure 5.4 shows that higher relative fractions are obtained with the lower baffle free areas. This can again be related to fluid mechanics as a smaller orifice results in a greater fluid velocity (for a given oscillatory velocity) in the orifice, greater eddie velocities and hence more effective dispersion of the oil. The baffle spacing, on the other hand, does not have much effect on the relative fraction. This is due to the fact that while baffle spacing governs the extent to which eddies can propagate through the fluid, it has only as small effect on fluid velocity or mixing intensity. Therefore, only very high or very low values of baffle spacing (probably outwith the feasible operating range) would be expected to show any significant effect on oil-water dispersion in the system..

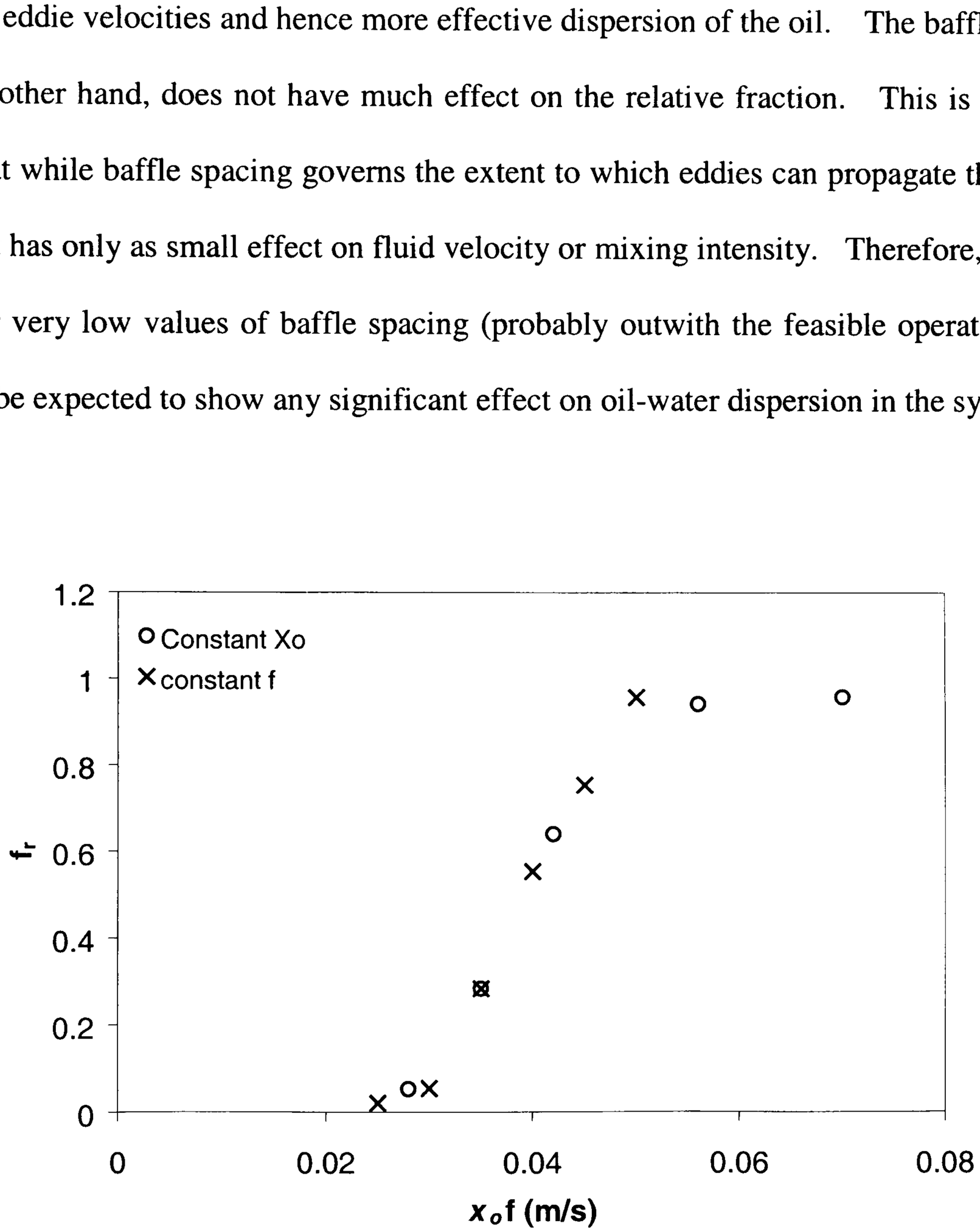

Figure 5.3: Effect of oscillatory velocity on f_r (α=31%, L=600mm)

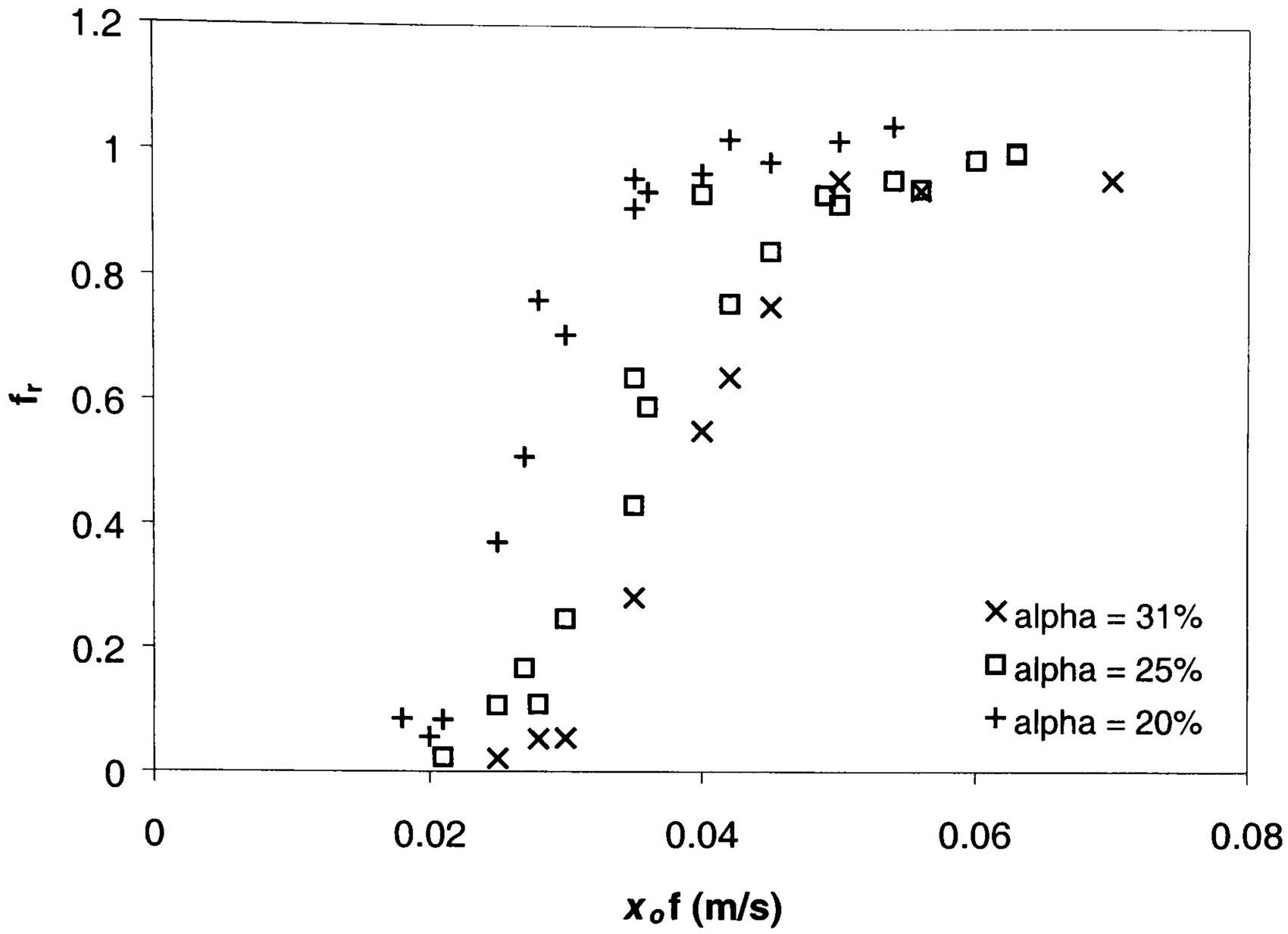

Figure 5.4: Effect of oscillatory velocity and α on f_r (L=600mm)

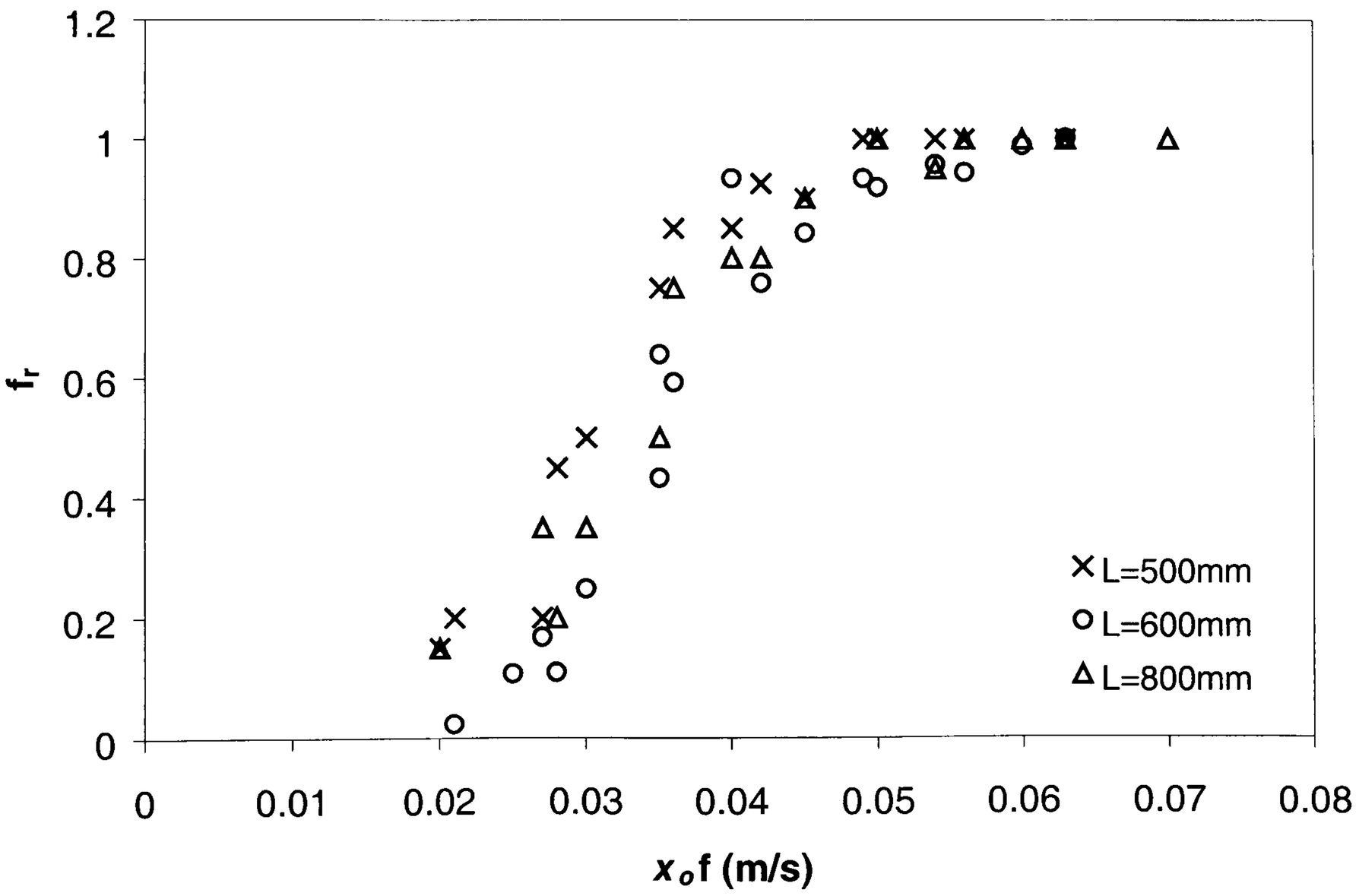

Figure 5.5: Effect of oscillatory velocity and baffle spacing on f_r (α=25%)

5.3.3 Minimum Frequency for Complete Dispersion

5.3.3.1 Definition

For liquid-liquid dispersion studies in stirred tanks the concept of a minimum agitation speed, at which a complete dispersion is achieved, has been used as the indicator for assessing the state of dispersion for different systems (Van Heuven and Beek, 1971; Skelland and Lee, 1978; Skelland and Seksaria, 1978; Skelland and Ramsay, 1987; Skelland and Kanel, 1990; Armenante and Huang, 1992). By applying the same principle to liquid-liquid dispersion in an OBC, the minimum agitation speed is replaced by a minimum oscillation frequency (Zhang et al., 1996). This frequency is of course dependent on the oscillation amplitude and the baffle geometry as well as the fluid physical properties. For the purpose of this study the minimum frequency for complete dispersion was defined as the lowest frequency at which the relative fraction at steady state was observed to be over 95%. Although complete dispersion, defined in this way, is in fact actually uniform dispersion, it has been shown that there is not a great difference (typically 8%) between the minimum agitation speed for complete dispersion and uniform dispersion in a stirred tank (Skelland and Lee, 1978). If it is assumed that this is also the case for the minimum oscillation frequency in an OBC, then a direct comparison between results from the present study and those previously reported in a 50mm OBC (Zhang et al., 1996), using the visualisation method, can be made with reasonable accuracy.

5.3.3.2 Effect of Amplitude and Baffle Geometry on f_{min}

The minimum frequency for complete dispersion was obtained for a numbers of oscillation amplitudes at various orifice diameters and baffle spacings and the results are plotted in Figures 5.6 and 5.7 respectively. The general trend for both figures is that the minimum oscillation frequency decreased as the oscillation amplitude increased and this can be related to the fluid mechanics in the OBC. It has already been shown that the degree of dispersion of the oil is related to the oscillatory velocity. Therefore, the effect of an increase in amplitude can be balanced by using a lower frequency, and vice versa, in order to achieve the same fluid mechanical conditions. From Figure 5.6 it can be seen that when a smaller baffle free area is used, the minimum frequency for complete dispersion is reduced. This is for the same reason as described in section 5.3.2 with respect to fluid mechanics. It is also evident from Figure 5.6 that the effect of the orifice diameter on the minimum oscillation frequency was greater at the lower oscillation amplitudes than at higher ones. At the oscillation amplitude of 100 mm, for example, the minimum oscillation frequency decreased from 0.7 – 0.5 Hz as the orifice diameter decreased, while at the higher amplitude of 180mm a lesser difference in the minimum oscillation frequency is observed. It is likely that this is linked to the fact that the increase in the power input due to an increase in the oscillation amplitude is far greater than that of a decrease in the orifice diameter, which is evident from the energy dissipation equation (2.5), where the power index for the oscillation amplitude is 3, while that for the baffle free area term is 2. Therefore, as the oscillation amplitude is increased, the effect of orifice diameter on the minimum oscillation frequency for complete oil-water dispersion is reduced.

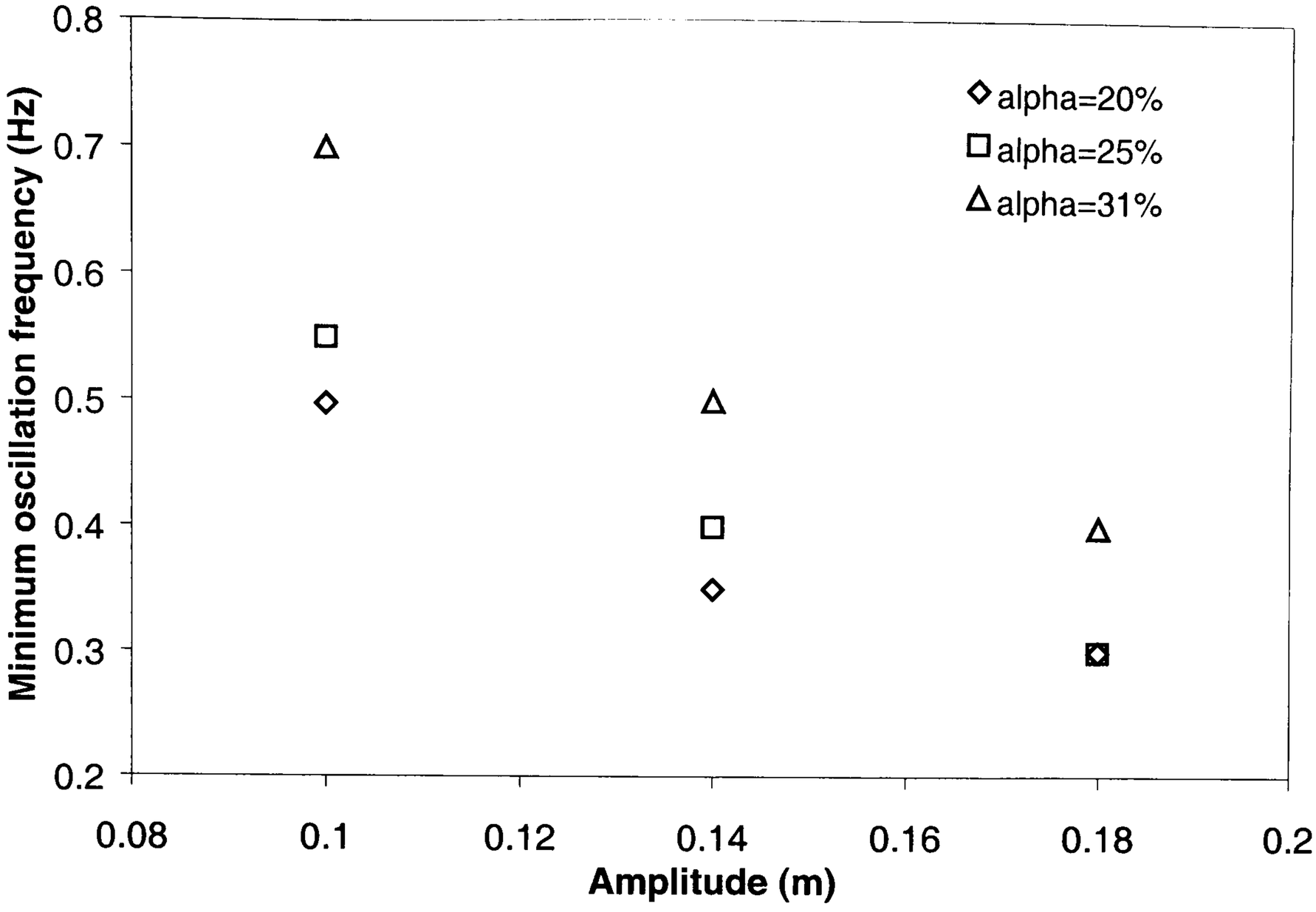

Figure 5.6: Effect of amplitude and α on f_{min} (L=600mm)

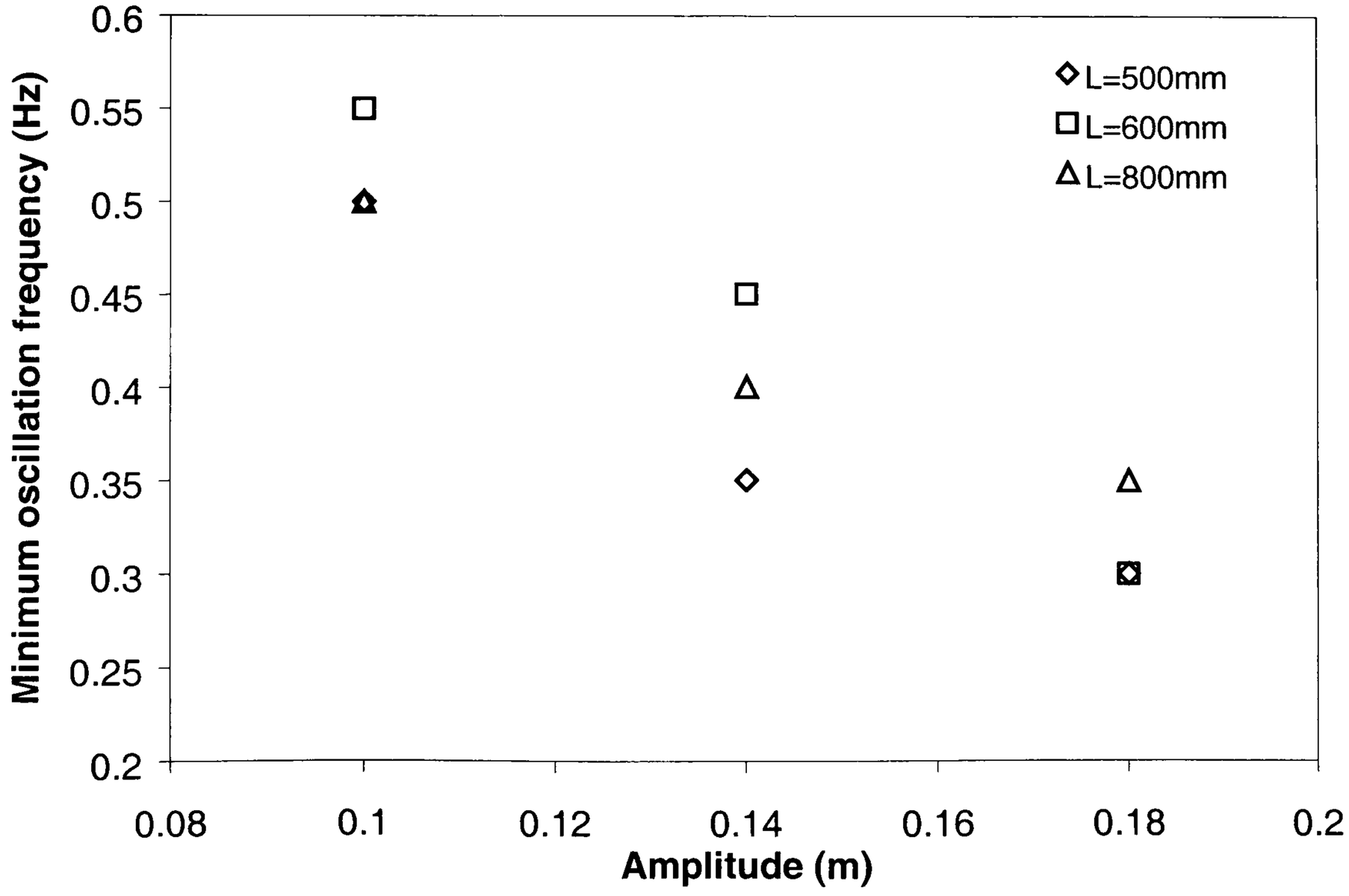

Figure 5.7: Effect of amplitude and L on f_{min} (α=25%)

The relationship of the minimum oscillation frequency and the baffle spacing is shown in Figure 5.7. It is again observed that the minimum frequency for complete dispersion decreases as the oscillation amplitude increases. It is also evident that the data collected at different spacings are close together, which suggests that the effect of the baffle spacing on the minimum oscillation frequency is weak. Again this can be related to fluid mechanics as discussed in section 5.3.2.

The results shown in Figures 5.6 and 5.7 are in general agreement with what has been observed in a bench scale OBC (Zhang et al., 1996) although the oscillation amplitudes used on the bench scale were an order of magnitude lower than that in the present OBC and, consequently, the oscillation frequencies were, an order of magnitude greater.

5.3.3.3 Effect of Oil Phase Fraction

The effect of the overall oil fraction on the minimum oscillation frequency was also investigated and four oil fractions of 10%, 20%, 30% and 36% (v/v) were examined. Figure 5.8 shows some typical results of these experiments, which indicate that the oil fraction had a negligible effect on the minimum oscillation frequency. This is again consistent with the previous findings of Zhang et al (1996) and can be attributed to the fact that there was not much difference between the physical properties of the two phases.

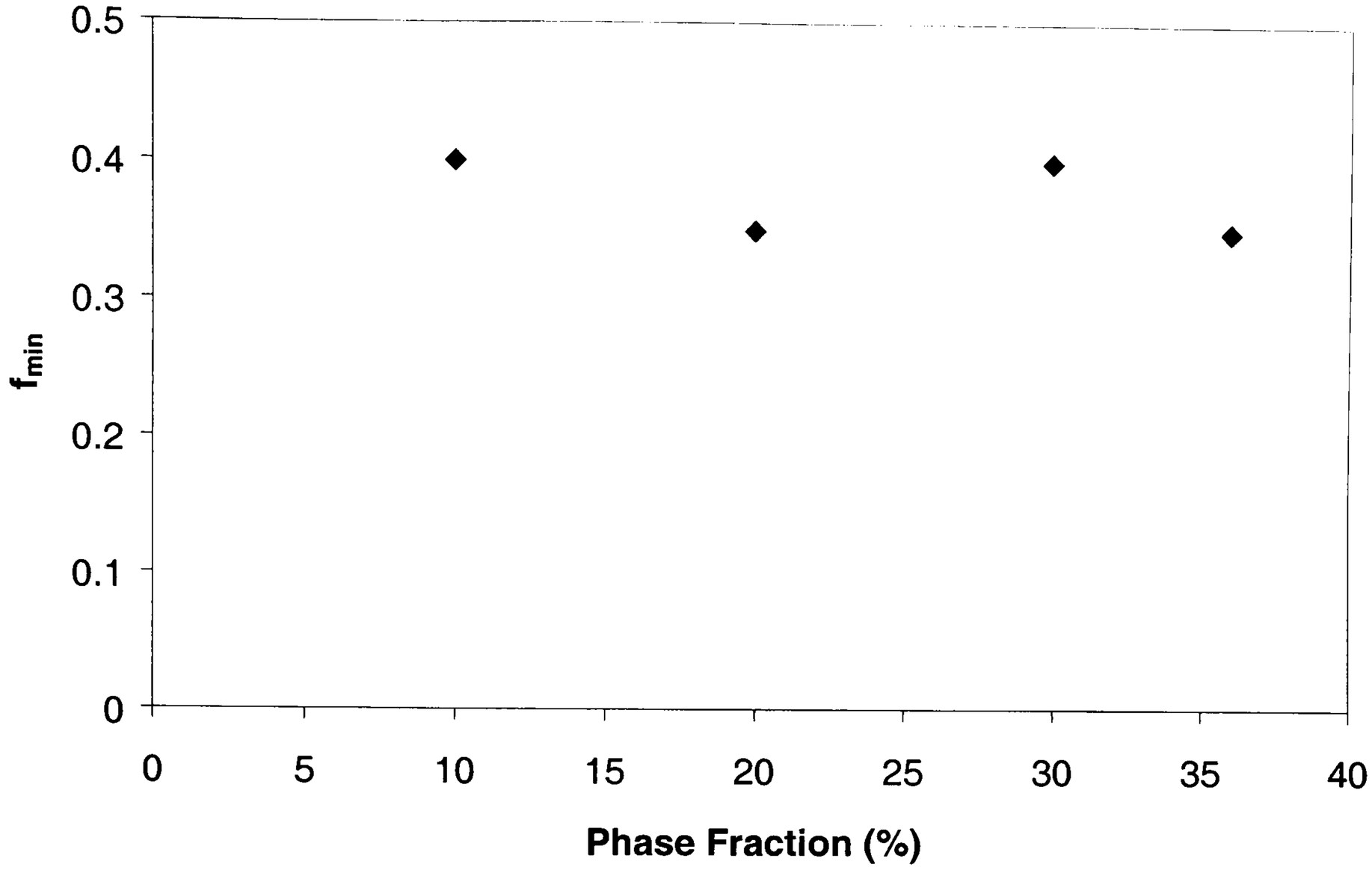

Figure 5.8: Effect of oil phase fraction on f_{min} (x_o=140mm, α=25%, L=600mm)

5.3.4 Effect of Energy Dissipation

The effect of energy dissipation (evaluated from eqations 2.4 and 2.5) on the relative fraction is shown in Figure 5.9. It can be seen that as the energy dissipation is increased, the relative fraction also increases. This is expected as higher energy dissipation means higher mixing intensity as a result of more rapid eddy motion in the system. It can also be seen that an energy dissipation of about 0.5W/kg is required in order to achieve complete dispersion and so, on conclusion, the OBC should always be operated at an energy dissipation above this threshold value when carrying out any liquid-liquid dispersion process.

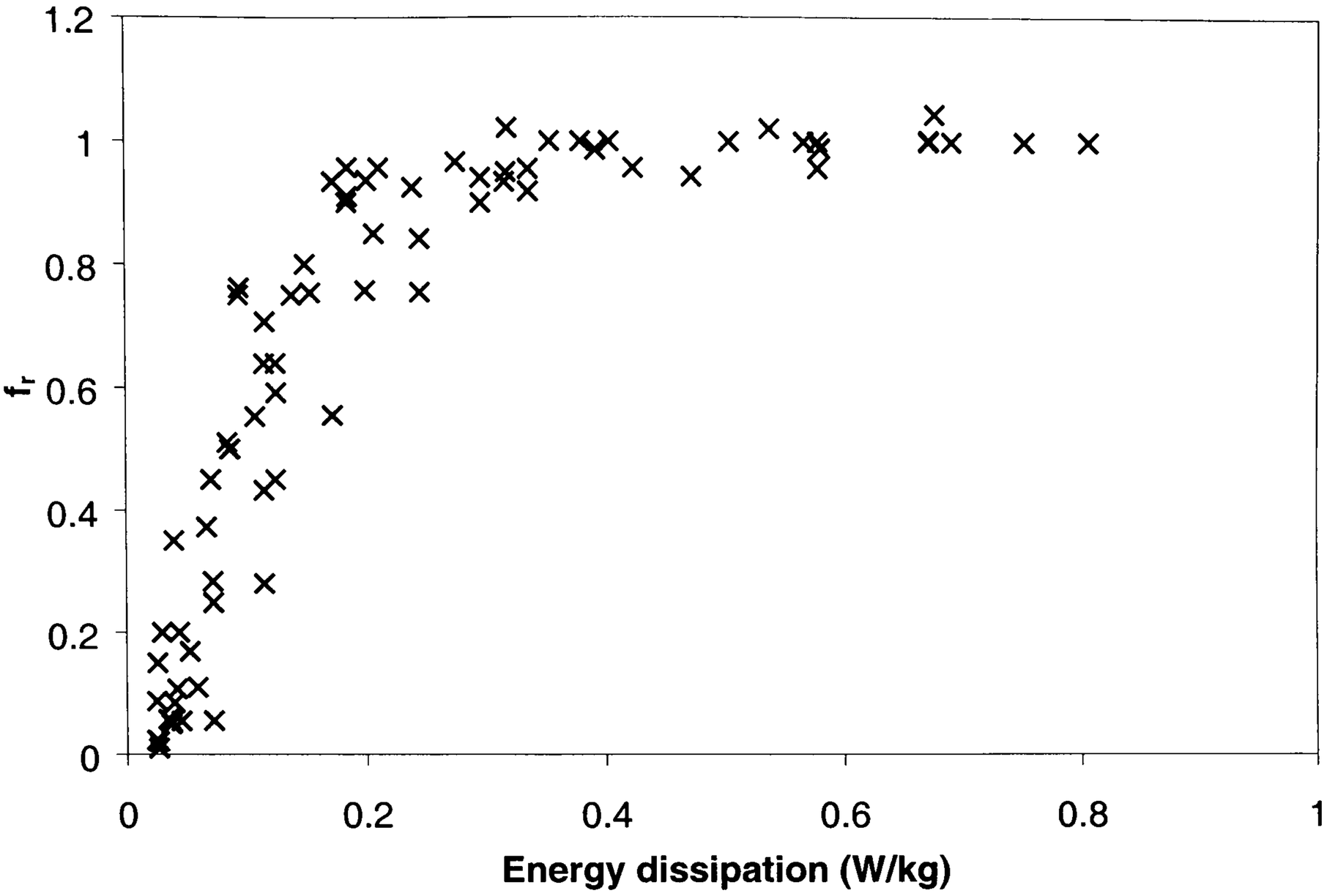

Figure 5.9: Effect of energy dissipation on f_r

5.3.5 Scale-up

5.3.5.1 Effect of Scale-Up on Minimum Energy Dissipation

The energy dissipation required to achieved complete dispersion, compared with that in a bench scale (50 mm diameter), is shown in Figure 5.10 for different baffle free areas. In both devices, the baffle spacing was 1.5 times the column diameter and the ratio of oscillation amplitude to baffle spacing was 0.16. It can be seen that the energy dissipation required is lowest at a baffle free area of about 25% in both cases, which indicates that this is the optimum orifice size to use. It can also be seen that the energy dissipation rate

required is different in the two OBCs, indicating that energy dissipation can not be used as a scale-up criteria for determining the point of complete dispersion in OBCs.

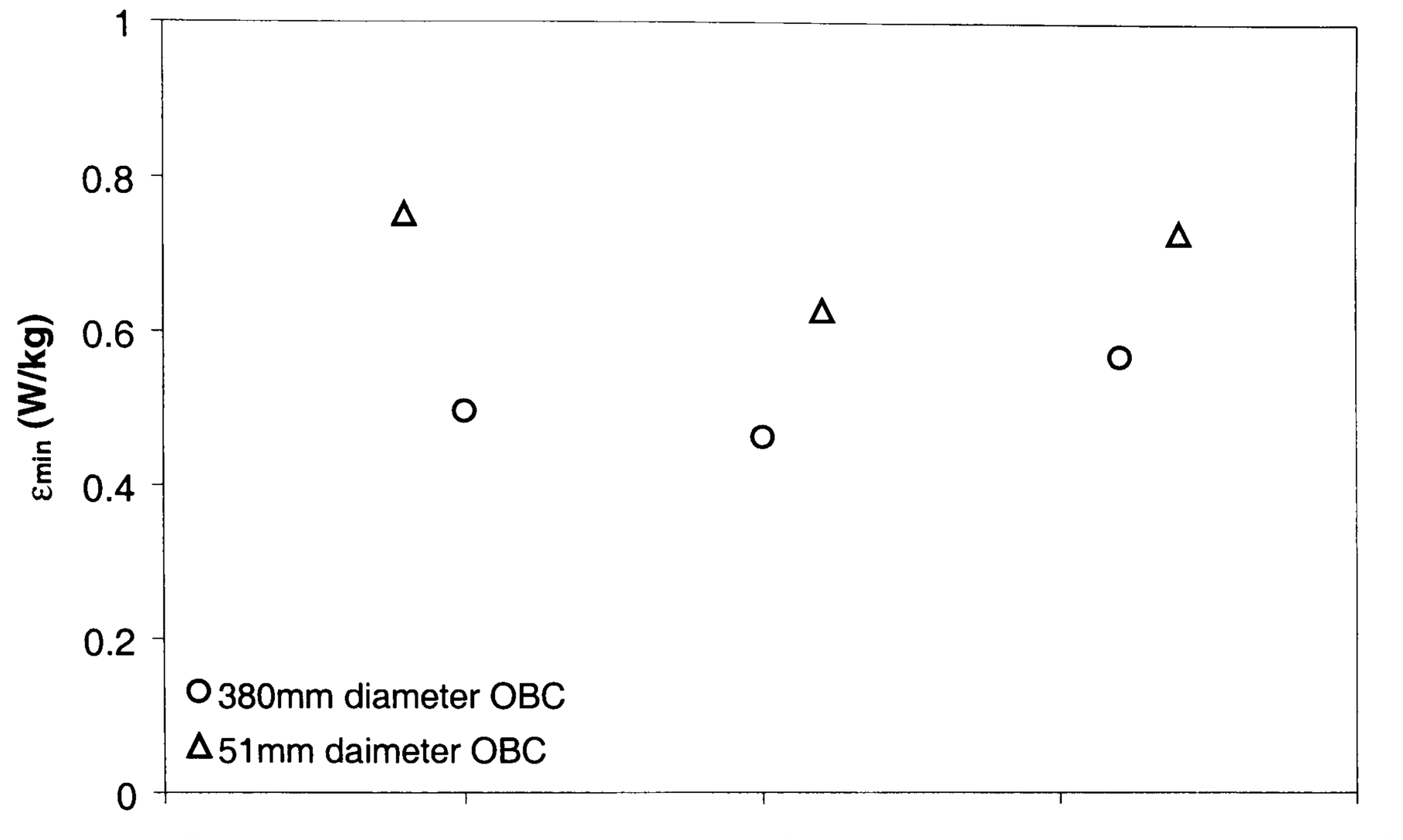

Figure 5.10: Minimum energy dissipation for complete dispersion

This can be explained by considering the relationship between energy dissipation and oscillatory velocity. Energy dissipation in an OBC can be evaluated from equations (2.4) and (2.5).

$$\varepsilon = \frac{P}{\rho V} \tag{2.4}$$

$$\frac{P}{V} = \frac{2\rho N}{3\pi C_D^2}\left(\frac{1-\alpha^2}{\alpha^2}\right)x_o^3\omega^3 \tag{2.5}$$

Also, the baffle spacing and oscillation amplitude can be expressed in terms of column diameter, as shown in equations (5.2) and (5.3).

$$L = \frac{1}{N} = K_1 D \tag{5.2}$$

$$x_o = K_2 D \tag{5.3}$$

Therefore, for a given liquid-liquid system (i.e. constant density):

$$\varepsilon \propto \frac{K_2^3}{K_1}\left(\frac{1-\alpha^2}{\alpha^2}\right) D^2 f^3 \tag{5.4}$$

or, for a particular geometric configuration (i.e. K_1, K_2 and α are constant):

$$\varepsilon \propto D^2 f^3 \tag{5.5}$$

Therefore, for columns of diameter D_1 and D_2 operating at the same energy dissipation rate:

$$D_1^2 f_1^3 = D_2^2 f_2^3 \tag{5.6}$$

which can be rearranged to:

$$f_2 = \left(\frac{D_1}{D_2}\right)^{2/3} f_1 \tag{5.7}$$

Also, if geometric similarity is maintained:

$$x_{o_2} = \left(\frac{D_2}{D_1} \right) x_{o_1} \tag{5.8}$$

Therefore, from equations (5.7) and (5.8):

$$(x_o f)_2 = \left(\frac{D_2}{D_1} \right)^{1/3} (x_o f)_1 \tag{5.9}$$

It is evident from equation (5.9) that as the column diameter increases, the oscillatory velocity increases as well, which would result in more effective dispersion of the oil.

5.3.5.2 Effect of Scale-Up on Minimum Oscillatory Velocity

The minimum oscillatory velocity required for complete dispersion is plotted in Figure 5.11 for both the 50mm diameter column and the380mm diameter column. It can be seen that a lower oscillatory velocity is required in the smaller diameter column, indicating that oscillatory velocity is also a poor scale-up criteria. This is related to the fact that, to achieve complete dispersion, the velocity of the fluid in the system must be able to overcome the settling velocity of the oil droplets, which depends on droplet size (by equation 5.10, i.e. Stoke's law) and hence on energy dissipation rate (as outlined in chapter 2.2.2). Therefore, the result of operating two columns of different diameter at the same

oscillatory velocity, would be more effective dispersion of oil in the smaller column due to the presence of smaller drops, which exist as a result of the higher energy dissipation rate.

$$u_t \propto d_{drop} \tag{5.10}$$

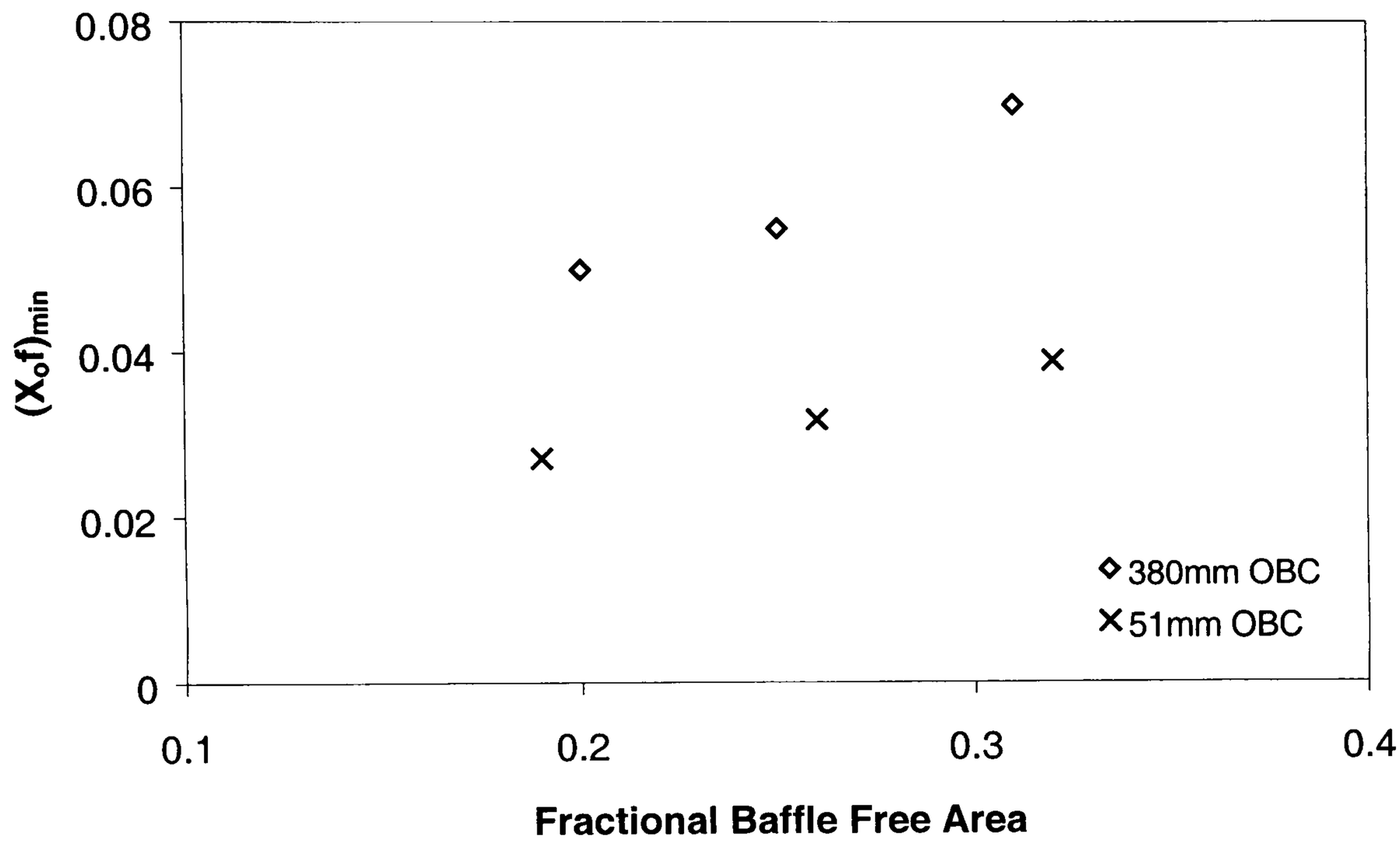

Figure 5.11: Minimum oscillation frequency for complete dispersion

5.3.5.3 Scale-Up Correlation

As neither energy dissipation or oscillatory velocity can be used on its own as a reliable scale-up criteria for liquid-liquid dispersion in an OBC, a rule must be established that takes the influence of both of these factors into account. In light of these findings a scale-up relationship is derived below based on the assumption that the governing factor for

achieving complete dispersion is that the terminal settling velocity of the oil has to be balanced by the velocity of bulk fluid movement.

Combining equation (5.10) with the theory outlined in section 2.2.2 and equation (5.4), it is evident that the terminal settling velocity of an oil droplet can be expressed as:

$$u_t \propto \varepsilon^a \propto \left[\frac{K_2^3}{K_1}\left(\frac{1-\alpha^2}{\alpha^2}\right)D^2 f^3\right]^a \tag{5.11}$$

where the power index a is determined by the droplet breakage and coalescence rates and can vary from –0.25 to –0.5.

Also, the maximum velocity of the fluid moving in the system is proportional to the oscillatory velocity and inversely proportional to the baffle free area. Therefore, the requirement for complete dispersion is given by:

$$\frac{K_2 D f_{\min}}{\alpha} = k\left[\frac{K_2^3}{K_1}\left(\frac{1-\alpha^2}{\alpha^2}\right)D^2 f_{\min}^3\right]^a \quad (-0.5 \le a \le -0.25) \tag{5.12}$$

which can be rearranged into:

$$f_{\min} = \frac{k^{1/(1-3a)}}{K_1^{a/(1-3a)} K_2}\left[\left(\frac{1-\alpha^2}{\alpha^2}\right)^a \alpha\right]^{1/(1-3a)} D^{(2a-1)/(1-3a)} \quad (-0.5 \le a \le -0.25) \tag{5.13}$$

For a given liquid-liquid system, of constant physical properties, it is reasonable to assume that a, in the above equations is a constant. Therefore, for a given geometrical configuration, equation (5.13) can be expressed as:

$$f_{\min} = KD^{b} \quad (-0.86 \leq b \leq -0.8) \tag{5.14}$$

Applying this relationship to the experimental data plotted in Figures 5.10 and 5.11, the required value for the exponent b was found to vary from –0.75 to –0.78 (depending on baffle free area) as shown in Figure 5.12. This is slightly outwith the range that is expected form equation (5.14) and returns a value of a of –0.86, which is considerably outwith the range predicted by equation (5.12). This apparent discrepancy between predicted and experimental results can be attributed to the fact that a different experimental technique was used to obtain the data in each of the columns. Complete dispersion, as determined by the sampling technique used in the present work, is in fact *uniform* dispersion, which is a different condition form the state of *complete* dispersion, as determined by the visualisation method used by Zhang et al (1996) in the 50mm diameter OBC. The two conditions are related however and it has been shown that, for a stirred tank, the minimum stirrer speed for uniform dispersion is typically 8% greater than the minimum stirrer speed for complete dispersion (Skelland and Lee, 1978). If this relationship is also assumed to exist in OBCs then the error induced by the difference in experimental techniques can be compensated for by increasing the f_{min} data from the 50mm diameter OBC by 8%. Figure 5.13 shows a plot of the corrected data, from which the typical values of b and a are –0.8 and –0.5 respectively, which are within the ranges expected from equation (5.12) and (5.14).

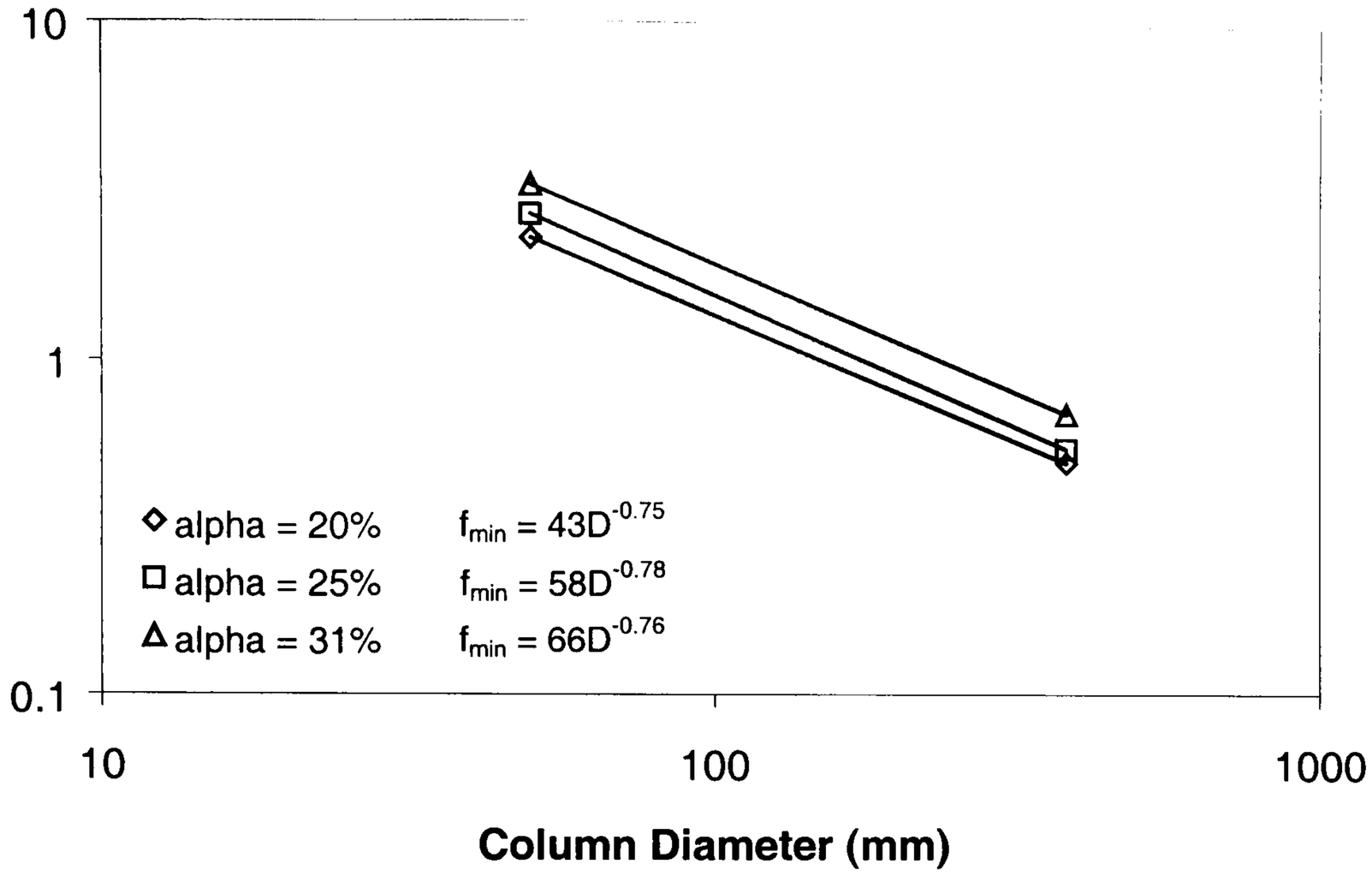

Figure 5.12: Effect of column diameter on f_{min}

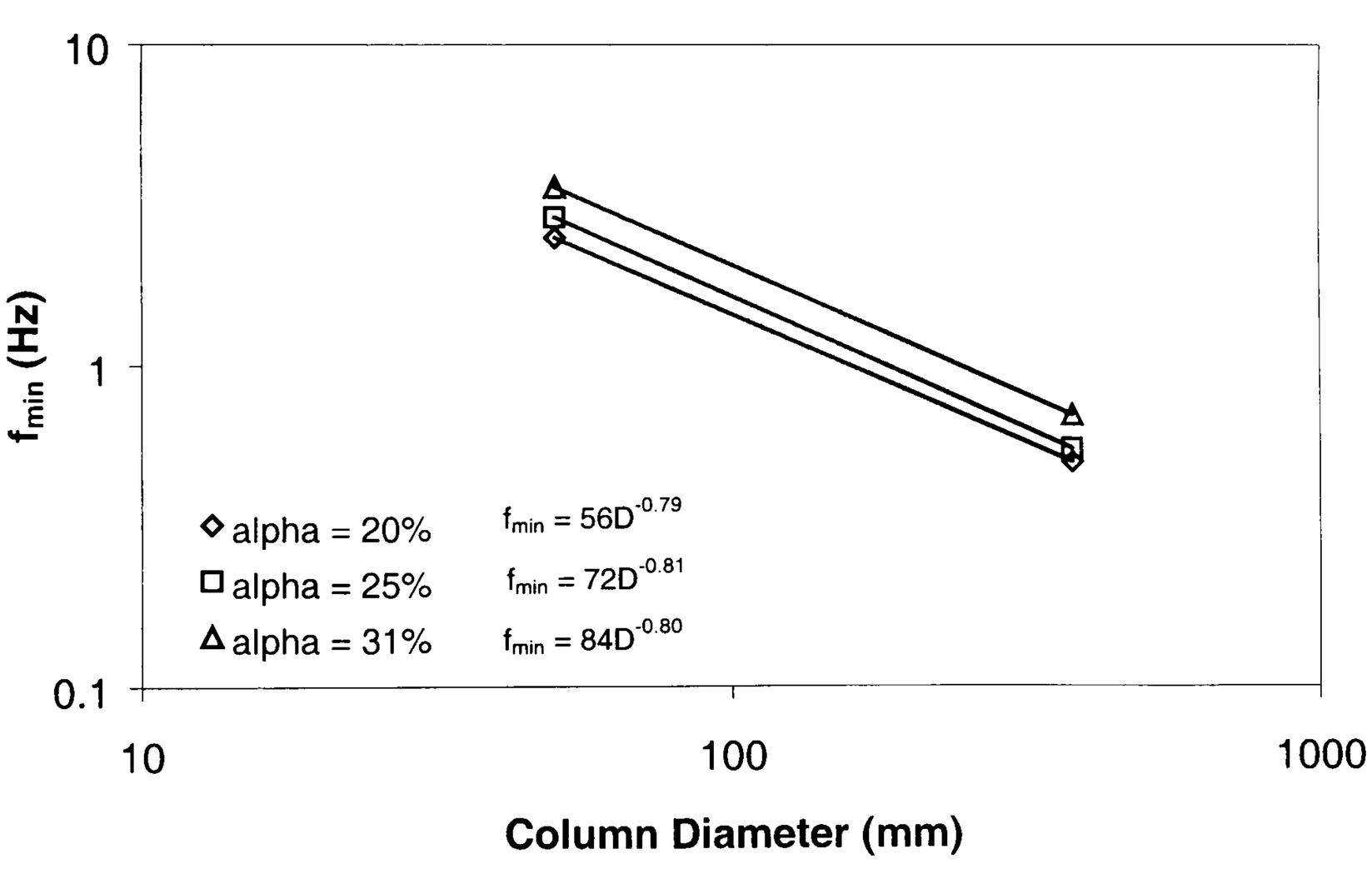

Figure 5.13: Effect of column diameter on f_{min}

(data corrected for experimental technique)

By taking b = -0.8 (a = -0.5) and substituting the appropriate geometrical expressions for K_1 and K_2, equation (5.13) can be re-written as:

$$f_{\min} = K^{0.4}\left(\frac{D}{x_o}\right)\left(\frac{L}{D}\right)^{0.2}\left[\left(\frac{1-\alpha^2}{\alpha^2}\right)^{-0.5}\alpha\right]^{0.4} D^{-0.8} \qquad (5.15)$$

and from the experimental data collected in this study and that reported by Zhang (1997) in a 50mm OBC, the best fit correlation was found to be:

$$f_{\min} = 0.18\left(\frac{D}{x_o}\right)\left(\frac{L}{D}\right)^{0.2}\left[\left(\frac{1-\alpha^2}{\alpha^2}\right)^{-0.5}\alpha\right]^{0.4} D^{-0.8} \qquad (5.16)$$

which, as can be seen from Figure 5.13, provides a reasonably good fit to all of the experimental data obtained from both the 50 mm diameter OBC (x_o = 11.8mm, α = 20 –30 %, L = 45 – 90 mm) and the 380 mm diameter OBC (x_o = 100 – 180 mm, α = 20 – 30%, L = 500 – 600 mm).

The relationship in equation (5.16) is also in reasonably good agreement with that reported in equation (2.9) for stirred tanks, in which the minimum stirrer speed for complete liquid-liquid dispersion to vary with impeller diameter to power of -0.71. Dispersion characteristics can therefore be said to be similar in both types of device.

$$N_{\min} = C\left(\frac{T}{D}\right)^{\alpha} \frac{g^{0.42}\Delta\rho^{0.42}\mu_m^{0.08}\sigma^{0.04}\Phi^{0.05}}{D^{0.71}\rho_m^{0.54}} \qquad (2.9)$$

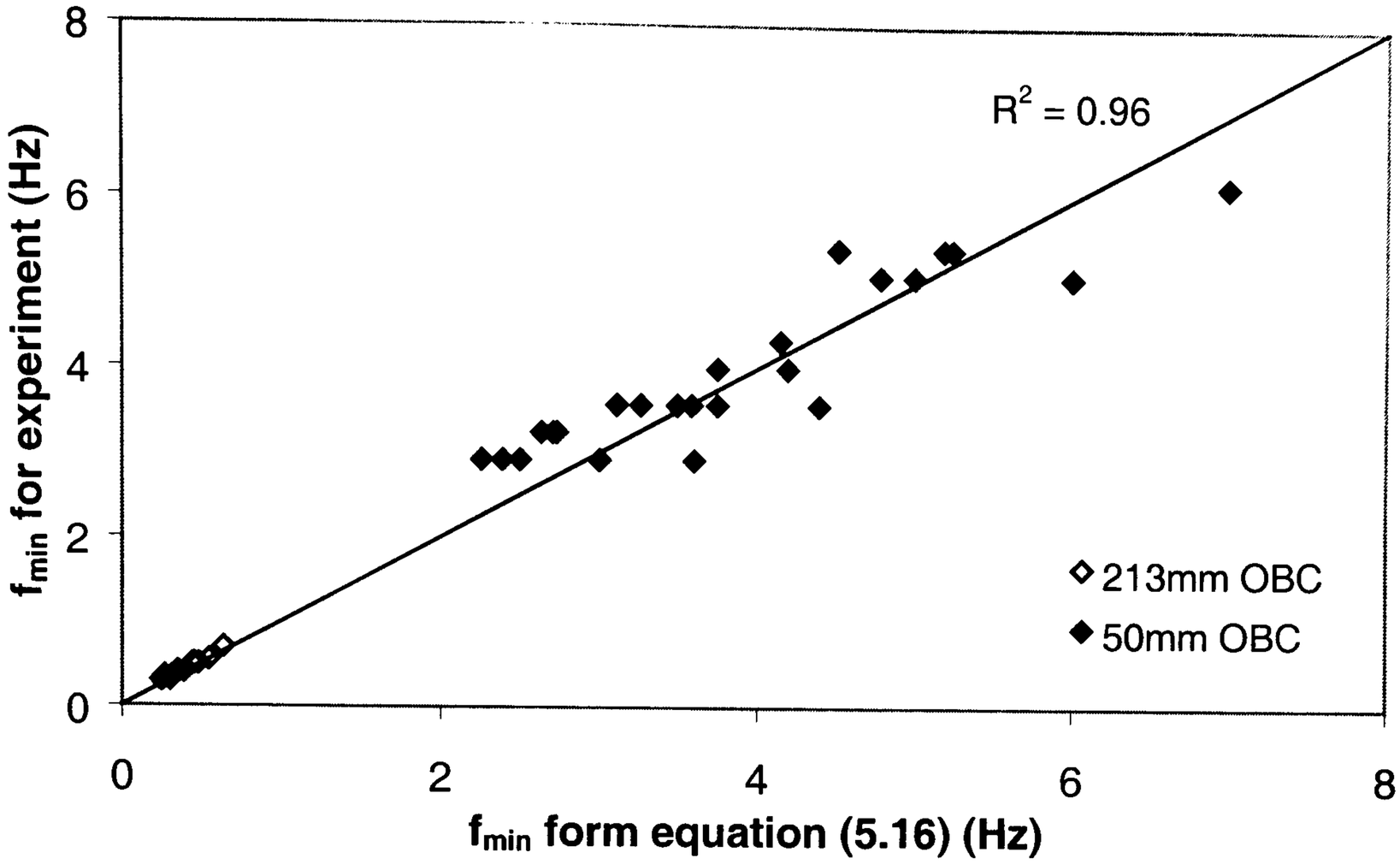

Figure 5.13: Comparison of correlation with experimental data

5.4 Conclusions

Results of an oil-water dispersion study in an OBC of 380mm in diameter were reported in this chapter. It was found that that the degree of oil-water dispersion in the OBC increases linearly with the oscillatory velocity until a complete dispersion is achieved and the rate of such an increase was greater for smaller orifice diameters than for larger ones while the effect of baffle spacing was much lower. The minimum oscillation frequency for complete dispersion has been determined over a range of amplitudes and baffle geometries and it was observed this frequency was lower for higher oscillation amplitudes and lower orifice diameters and independent of baffle spacing. These results can be explained in terms of fluid mechanics and mixing intensity as using a higher frequency or amplitude or a lower orifice diameter results in the generation of faster moving eddies which disperse the oil

more effectively, while varying the baffle spacing has little effect on the overall mixing intensity. The effect of energy dissipation was also studied and it was found that there exists a threshold value of about 0.5 W/kg above which complete dispersion is achieved.

Results from this investigation were compare with those reported from a similar study in a 50mm diameter oscillatory baffled column. It was observed that neither energy dissipation nor oscillatory velocity provide reliable criteria for scale up and so a scale-up relationship was derived that takes into account the effect of both of these factors. This relationship provides a reasonably good fit to the experimental data and also agrees well with a previously reported correlation for liquid-liquid dispersion in stirred tanks.

6 HEAT TRANSFER

6.1 Introduction

In the process of suspension polymerisation it is crucial to closely control the temperature of the reactor contents in order to achieve the correct reaction conditions. This involves removing large quantities of heat form the reactor as the reaction is highly exothermic (ΔH_R = -55.5 kJ/mol (Brandrup et al., 1999)). Heat transfer in bench scale OBCs has been studied previously and indicates that good heat transfer rates are easily achievable (Ni et al., 1997). In this chapter, heat transfer data from the current device are reported and compared with that reported for a bench scale OBC and stirred tanks.

6.2 Experimental Facilities and Procedures

The stainless steel OBC was used for the heat transfer experiments. Thermocouples were positioned at two points along the height of the column (one in between the two baffles and one below the lowest baffle), each with the tip situated at the column centre, and were also located on the jacket inlet and outlet streams. All thermocouples were calibrated against a standard thermometer using a water bath, both before and after the study.

Experiments were performed to determine both tube side and shell side correlations. To determine the shell side correlation, the heat transfer rates were determined at differeent shell side flowrates while maintaining tube side conditions constant. To determine the

tube side correlation, the column was charged with 25 l of a two phase liquid-liquid medium and the effect of varying the oscillatory velocity, on the heat transfer rate, was determined for a given shell side flowrate. Details of the liquid-liquid recipe used, which was based on a confidential formulation supplied by Ineos Acrylics Ltd, are given below:

Organic Phase:

Methylmethacrylate:	9 kg

Aqueous Phase:

Distilled Water:	16 kg
Colloid:	0.38 kg
5% w/w Surfactant 1:	2.1 g
Surfactant 2	0.42 g
Ammonia solution	8.6g

The absence of initiator ensures that no reaction occurs during these experiments and does not affect the heat transfer properties of the medium.

6.3 Results and discussion

6.3.1 Heat Loss from the System

The heat loss form the system by natural convection was determined by first heating the reactor contents to a uniform temperature of 50°C, then continually monitoring the

temperature at two locations in the column under conditions of no oscillation and no shell side flow rate over a period of 30 minutes. The results are shown in Figure 4.1, which shows that the temperature remains approximately constant. Heat losses can therefore be assumed to be negligible and hence are not taken into consideration in the remaining part of this study.

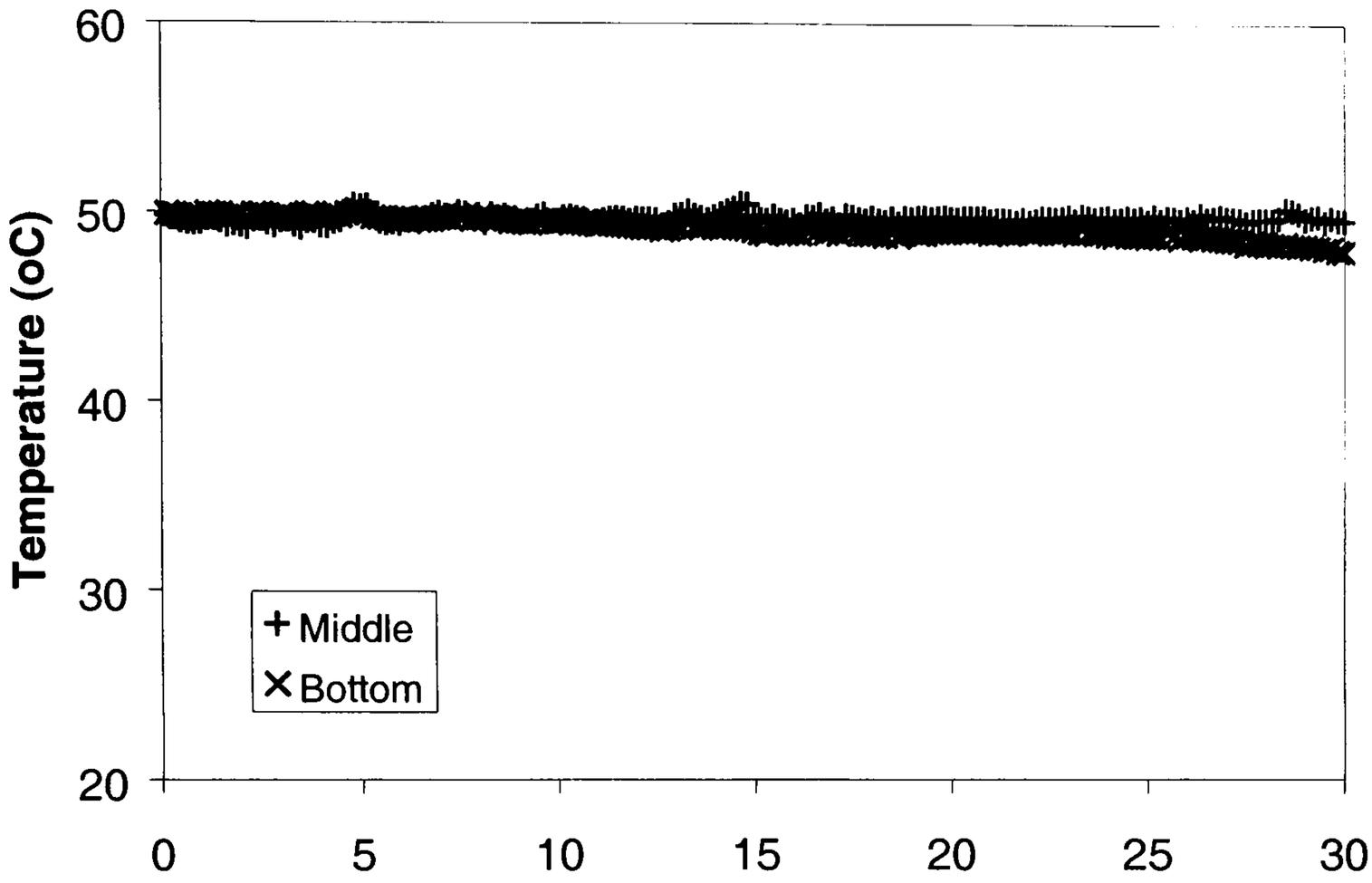

Figure 6.1: Temperature drop due to heat loss by natural convection

6.3.1 Temperature Uniformity

The effect of cooling without and with oscillation is shown in Figures 6.2 and 6.3 repectively. It can be seen that without oscillation, liquid in the lower part of the reactor is cooled quicker as a result of the cooling water entering the jacket at the bottom.

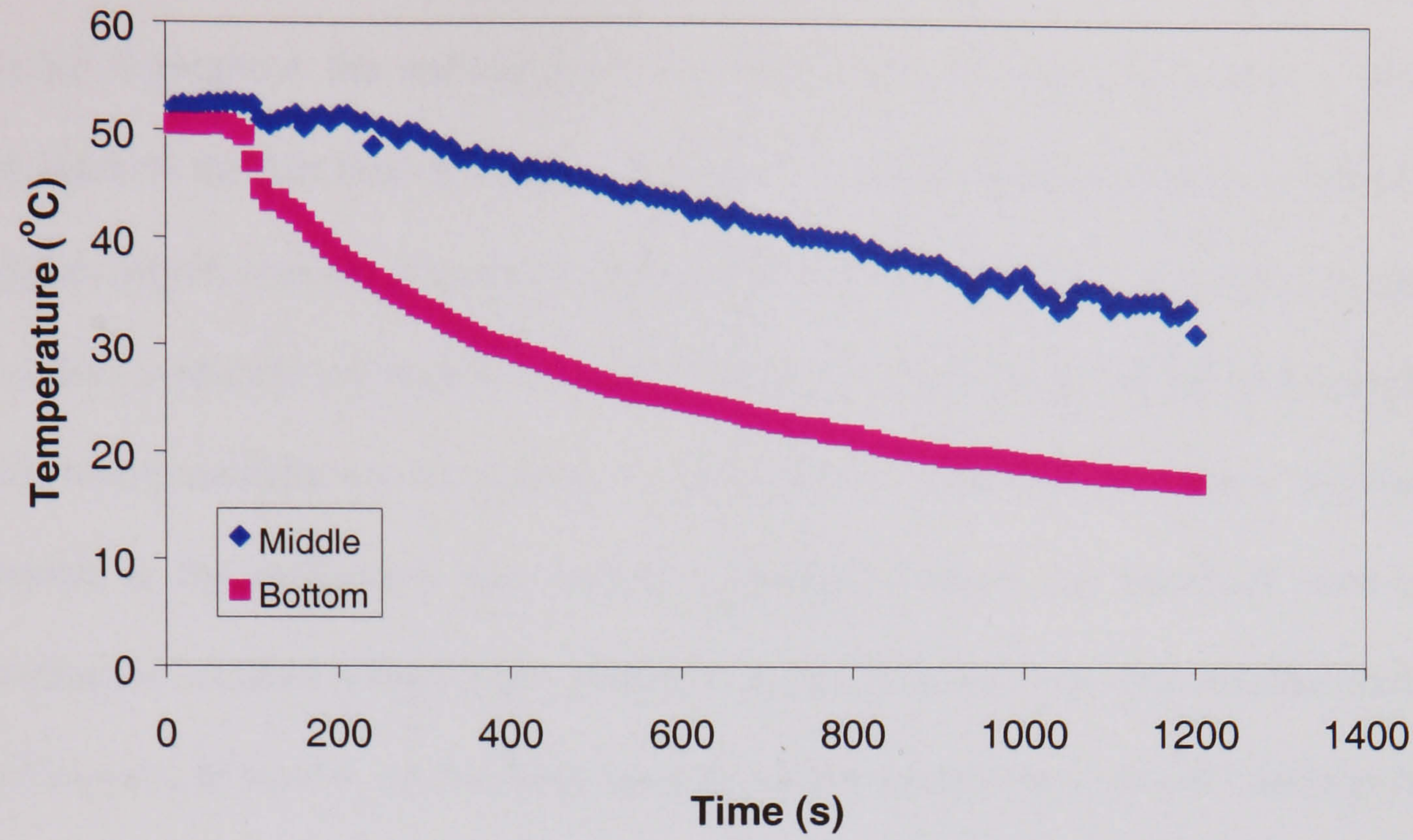

Figure 6.2: Temperature profile without oscillation

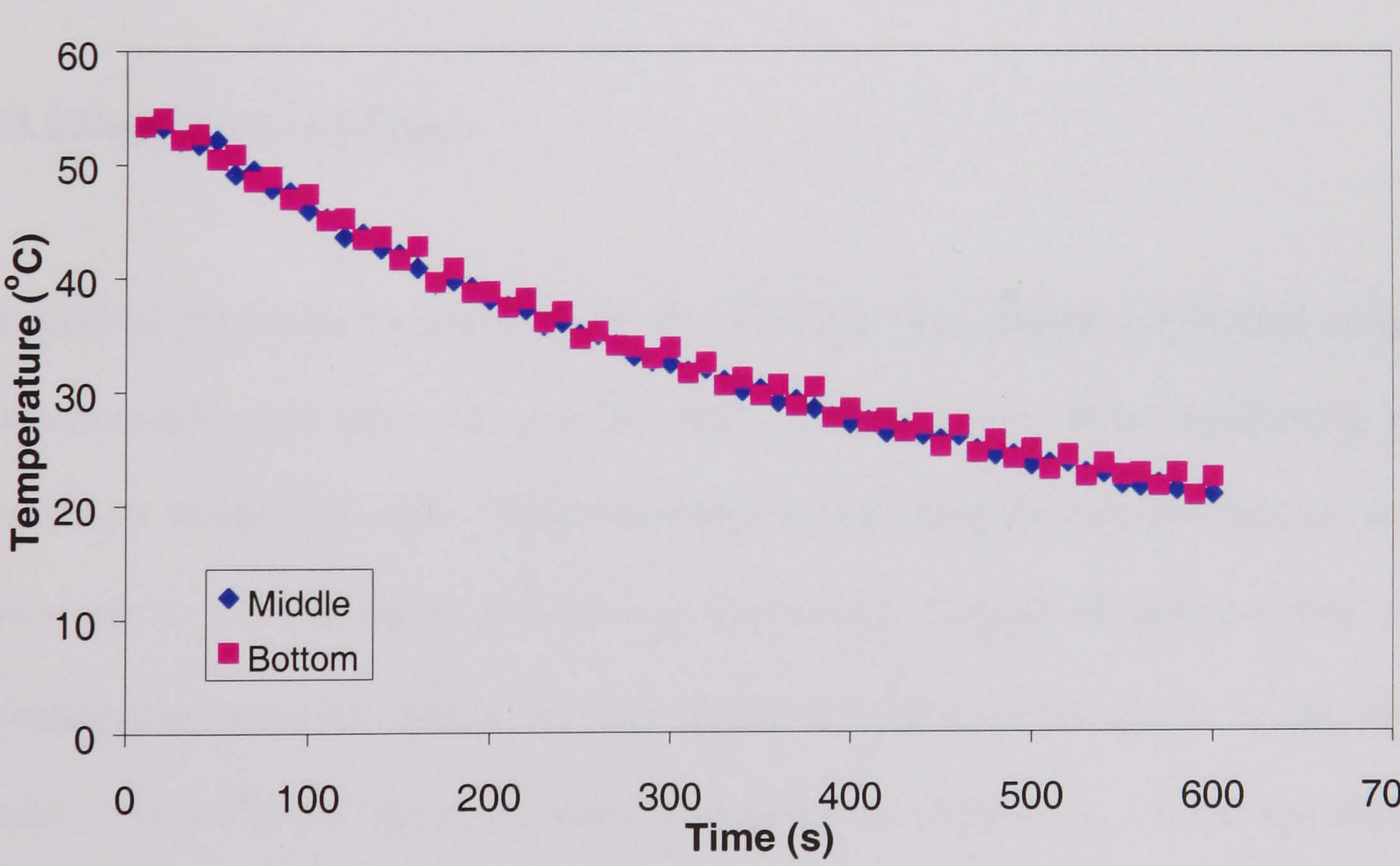

Figure 6.3: Temperature profile with oscillation

(f = 1Hz, x_o = 75mm, α = 25%, L = 315mm)

In contrast to this, however, the temperature profiles remain uniform along the length of the reactor throughout the cooling cycle when oscillating baffles are used. This can be attributed to the fact that the eddies generated by the oscillations provide a well mixed flow regime, which ensures that temperature uniformity throughout the column is maintained. It is also evident from Figures 4.1 and 4.2 that the contents are cooled more quickly in the case where oscillations are present. This result is expected as without oscillation, heat transfer is by conduction and natural convection which are relatively slow processes resulting in shallow temperature gradients at the wall and low heat transfer rates. With oscillations, however, the resulting eddy mixing present in the system convects heat away from the walls much more rapidly resulting in steeper temperature gradients and improved heat transfer.

4.3.2 Shell Side Correlation

In order to determine a correlation for the shell side heat transfer coefficient, temperature measurements were taken for varying shell side conditions while maintaining constant conditions on the tube side. This was done by modifying the experimental set-up so that hot water at a temperature of 50°C was continually pumped through the tube side at a constant flowrate, while cold water was passed through the shell side at 10, 20, 30 and 40 l/min. No baffles or oscillation were used in these experiments. Time was allowed for steady state to be reached and the temperature was recorded at both the tube and shell side inlet and outlet. The experimental data is listed in Appendix 2.1.

The rate of heat transfer (Q) in such a continuous system is defined by:

$$Q = m_c C_{pc}(T_{c_{in}} - T_{c_{out}}) = m_h C_{ph}(T_{h_{out}} - T_{h_{in}}) = UA\Delta T_m \quad (6.1)$$

where: m_c = mass flowrate of cooling water (kg s^{-1})

C_{pc} = specific heat capacity of cooling water (J kg^{-1} K^{-1})

Tc_{in} = jacket inlet temperature (K)

Tc_{out} = Jacket outlet temperature (K)

m_h = mass flowrate on tube side (kg s^{-1})

C_{ph} = specific heat capacity of water on tube side (J kg^{-1} K^{-1})

Th_{in} = Tube side inlet temperature (K)

Th_{out} = tube side outlet temperature (K)

U = overall heat transfer coefficient (W m^{-2} K^{-1})

A = heat transfer area (m^2)

ΔT_m = log mean temperature difference

The overall heat transfer coefficient (U) is related to the individual heat transfer coefficients by:

$$\frac{1}{U} = \frac{1}{h_t} + \frac{d}{d_s}\frac{1}{h_s} + \frac{d}{2}\frac{\ln\left(\frac{d_s}{d}\right)}{k_t} \quad (6.2)$$

where h_t is the tube side heat transfer coefficient (W m^{-2} K^{-1}), h_s is the shell side heat transfer coefficient (W m^{-2} K^{-1}), k_t is the thermal conductivity of the tube material (16 W m^{-1} K^{-1} for stainless steel) and d and d_s are, respectively, the inner and outer diameter of the

inner tube (m). As the tube side conditions are maintained constant it can be assumed that the tube side coefficient is a constant for all experiments and hence eqn (6.2) can be expressed as:

$$\frac{1}{U} = \frac{d}{d_s}\frac{1}{h_s} + const \tag{6.3}$$

It is normal to relate the shell side coefficient to the shell side Reynolds number by an equation of the form:

$$h_s = a\,\mathrm{Re}_s^b \tag{6.4}$$

where

$$\mathrm{Re}_s = \frac{uD_m}{\nu} \tag{6.5}$$

and D_m is the hydraulic mean diameter of the flow area. The power index b in equation (6.4)varies from 0.45 (for laminar) to 0.8 (for turbulent) (Perry and Green, 1994). For each of the shell side flowrates tested in this work the shell side Reynolds number was below 2000 indicating that the flow was laminar and so constant, b, in eqn (6.4) was fixed at 0.45.

Therefore, equation (6.3) can be re-written as:

$$\frac{1}{U} = k\left(\frac{d}{d_s}\frac{1}{\mathrm{Re}_s^{0.45}}\right) + const \tag{6.6}$$

Overall heat transfer coefficients were obtained from eqn (6.1) for each of the shell side flowrates tested and by plotting 1/U vs 1/Re^0.45 (see Figure 6.4), a best fit correlation for h_s was established as:

$$h_s = 40\,\mathrm{Re}_s^{0.45} \tag{6.7}$$

which allows the shell side coefficient to be determined for any given shell side flowrate.

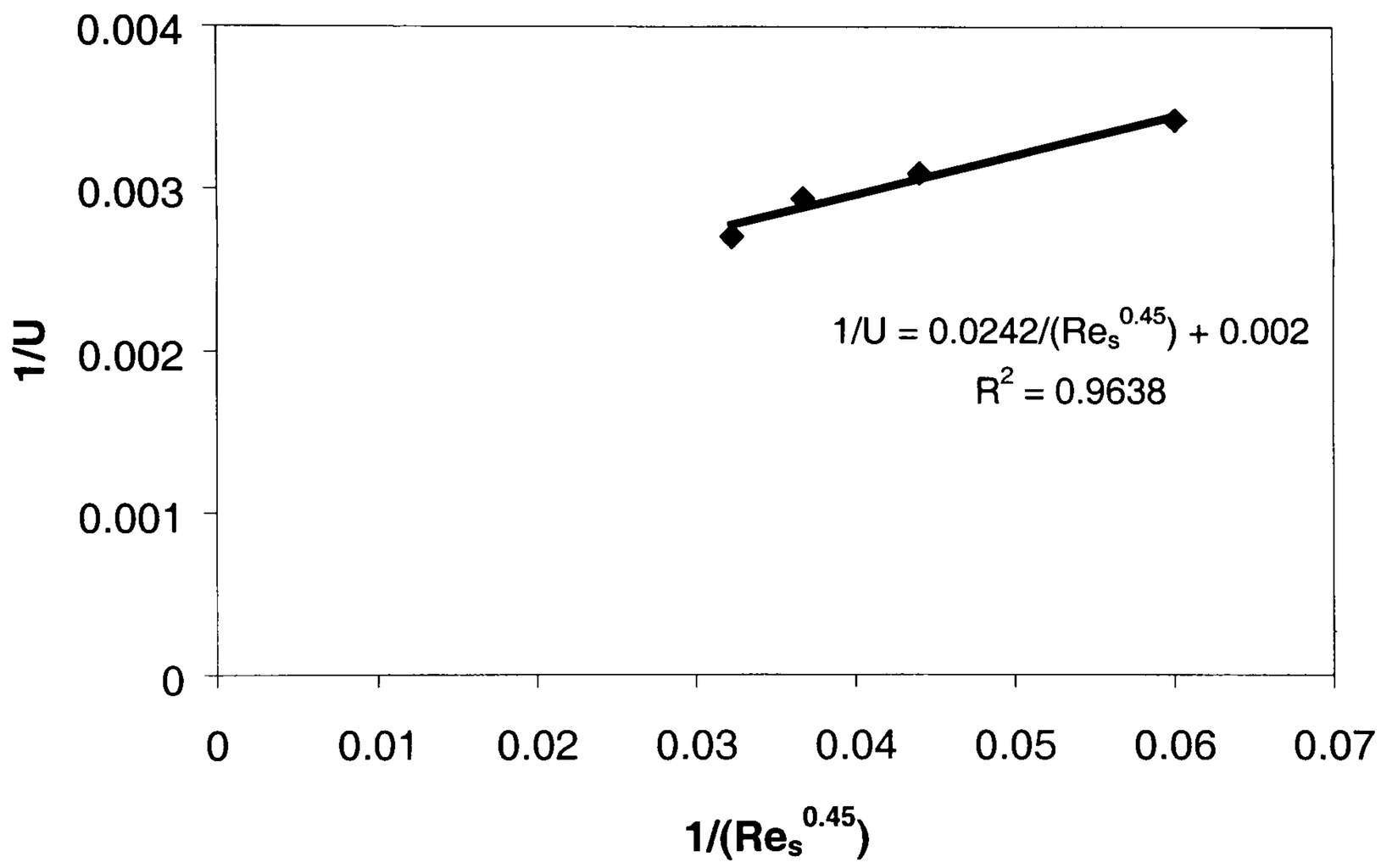

Figure 6.4: Correlation between 1/U and $1/(Re_s^{0.45})$

6.3.3 Tube side correlation

A number of experiments were performed to determine the effect of oscillation conditions on the tube side heat transfer coefficient. These experiments were performed by initially heating the reactor contents to 50°C and then apply cooling water at a constant flowrate of 30 l/min for 5 minutes. During this period, the temperature of the jacket inlet and outlet streams, as well as that of the column contents, was recorded continuously. Oscillation frequencies of 0.6 – 2.0 Hz and oscillation amplitudes of 50 – 100 mm were tested, for a fixed baffle geometry of α = 25% and L = 315mm, and the raw experimental data from these experiments are listed in Appendix 2.2.

In a batch system such as the one used here, the heat transfer rate is given by:

$$Q = m_c C_{pc}(T_{c_{in}} - T_{c_{out}}) = MC_p\left(-\frac{dT}{dt}\right) = UA\Delta T_m \qquad (6.8)$$

where M , C_p and T are the mass (kg), specific heat capacity (J kg^{-1} K^{-1}) and temperature (K) of the column contents respectively, t is time (s) and ΔT_m is the log mean temperarure difference (K). Equation (6.7) can be rearranged by eliminating T_{out} to give:

$$t = \frac{M}{m_c}\frac{C_p}{C_{pc}}\frac{K_1}{K_1 - 1}\ln\left(\frac{T_i - T_{c_{in}}}{T - T_{c_{in}}}\right) \qquad (6.9)$$

where T_i is the initial temperature of the column contents and K_1 is defined by

$$K_1 = \exp\left(\frac{UA}{m_c C_{pc}}\right) \tag{6.10}$$

Therefore, for any given set of oscillatory conditions the overall heat transfer coefficient can be established from eqns (6.9) and (6.10) and the tube side heat transfer coefficient can then be calculated from eqns (6.2) and (6.7). Details of calculated values are listed in Appendix 2.3. The effects of the oscillation frequency and amplitude on the tube side heat transfer coefficient are shown in Figure 6.5, from which it can be seen that heat transfer rates are higher at higher oscillation frequencies and amplitudes. This result is expected as increasing the frequency or amplitude results in an increase in mixing intensity thereby increasing the rate of forced convection in the system.

For the purpose of comparison with other researchers, tube side Nusselt numbers have been determined from:

$$Nu_t = \frac{h_t d}{k} \tag{6.11}$$

and these have been correlated with the oscillatory Reynolds number and Prandtl number (see Figure 6.6) to yield the relationship in equation (6.12).

$$Nu_t = 0.06\,\mathrm{Re}_0^{0.68}\,\mathrm{Pr}^{0.33} \tag{6.12}$$

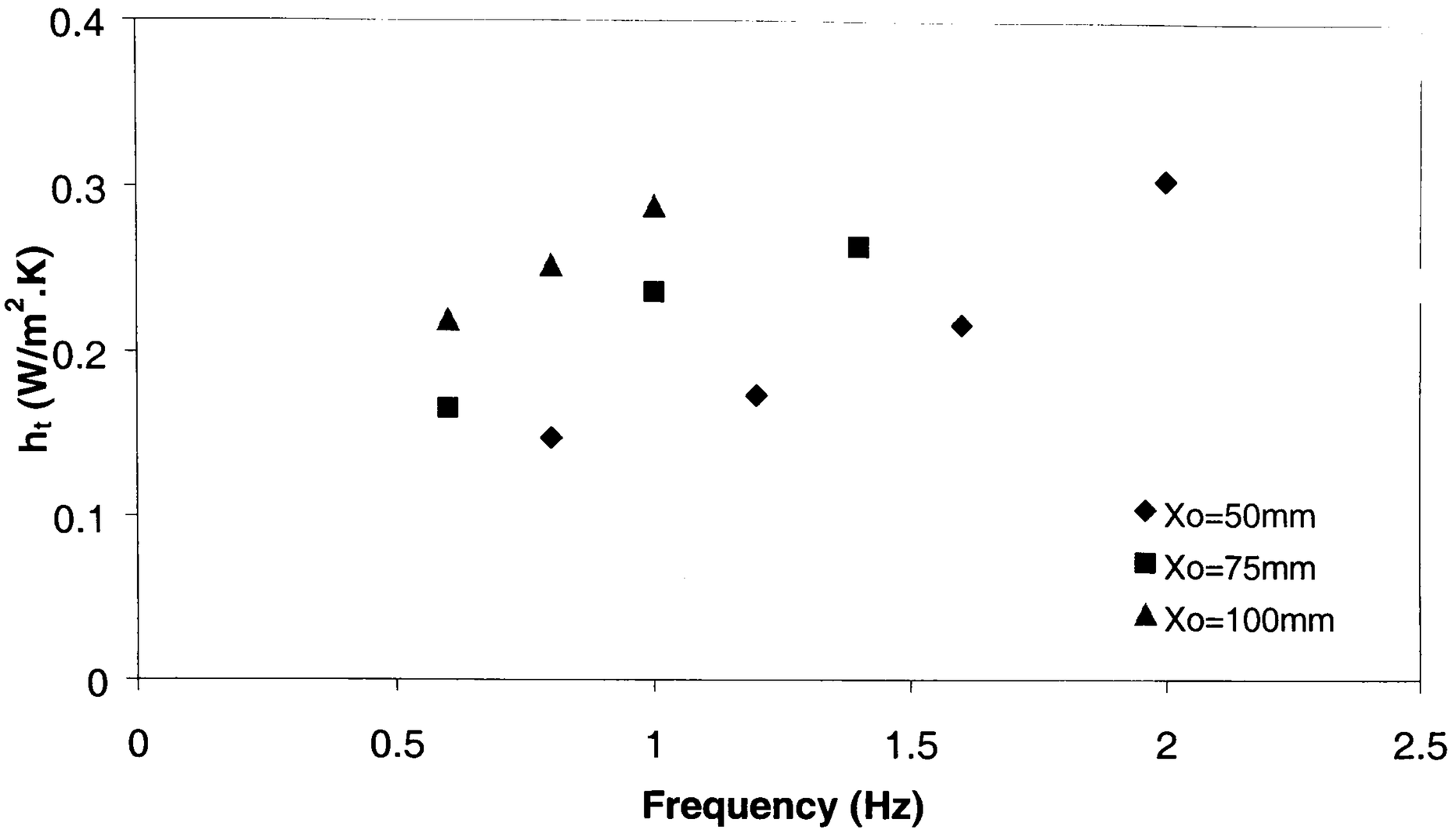

Figure 6.5: Effect of frequency and amplitude on tube side heat transfer coefficient

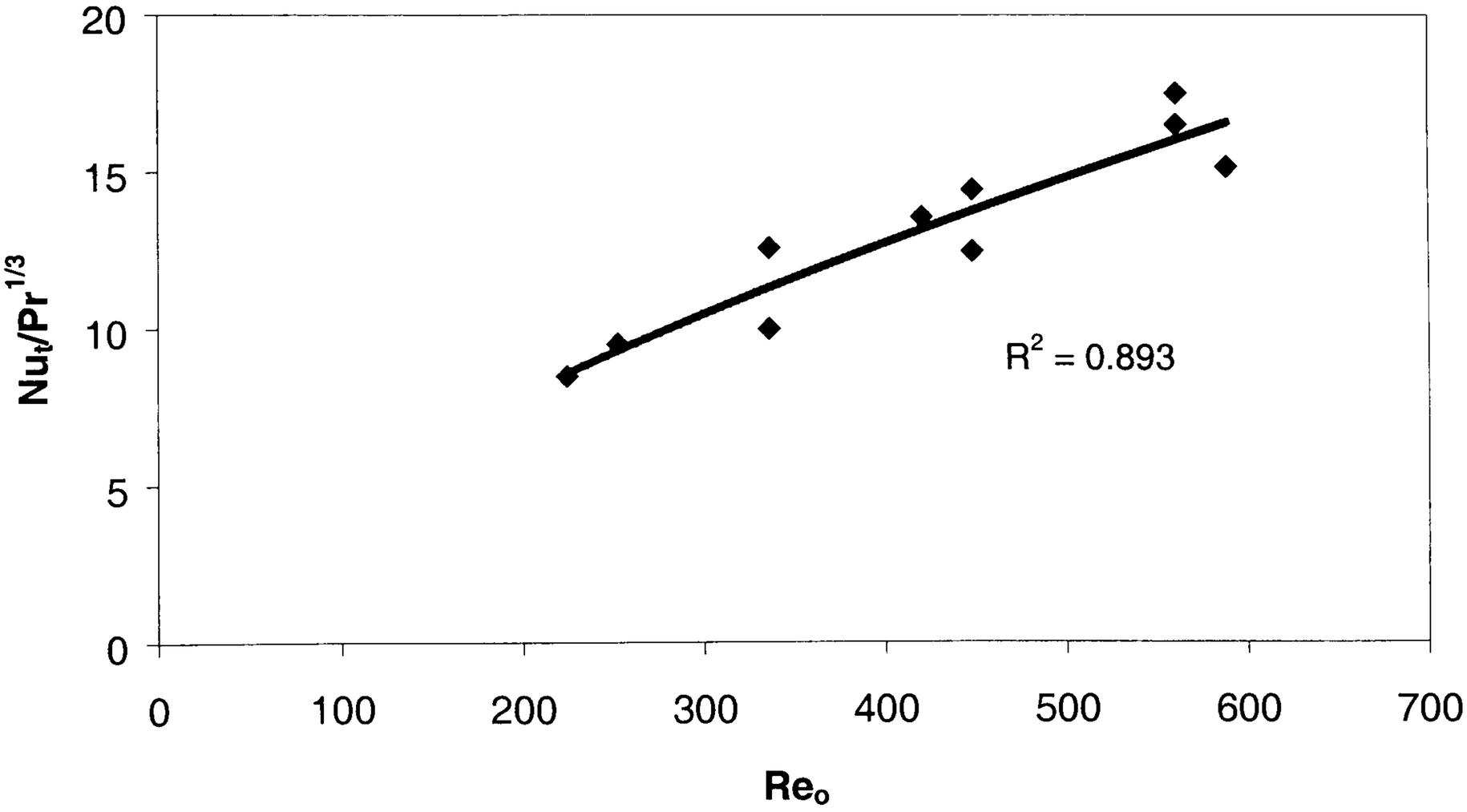

Figure 6.6: Heat transfer correlation

The correlation for heat transfer in a 50mm OBC, which used an oil as the tube side fluid, is given in equation (6.13) (Ni et al., 1997). On comparison of equations (6.12) and (6.13) it can be seen that the Nusselt number in both devices varies with oscillatory Reynolds number to a similar power index, which indicates that the nature of the relationship between the heat transfer coefficient does not vary with column size. It is also evident from equations (6.12) and (6.13) that lower Nusselt numbers are predicted, for a given oscillatory Reynolds number, in the larger device. This can be attributed to the fact that the two studies used different liquids therefore the variation in the constant is a result of the difference in the fluid physical properties between the two systems.

$$Nu_t = 0.474\,\mathrm{Re}_o^{0.562}\,\mathrm{Pr}^{0.33} \qquad (6.13)$$

A correlation has also been reported by Mackley and Stonestreet (1995), for heat transfer in a continuous oscillatory baffled tube, as:

$$Nu_t = 0.0035\,\mathrm{Re}_n^{1.3}\,\mathrm{Pr}^{1/3} + 0.3\frac{\mathrm{Re}_o^{2.2}}{\left(\mathrm{Re}_n + 800\right)^{1.25}} \qquad (6.14)$$

This correlation is quite different to the one reported here indicating that the operational mode of an oscillatory baffled device has an effect on the heat transfer characteristics.

For heat transfer in stirred tanks the tank Nusselt number is related to the impeller Reynold's (Re_{ST}) number by (Howard, 1977):

$$Nu_t = 0.73\,\mathrm{Re}_{ST}^{0.65}\,\mathrm{Pr}^{0.33}\left(\frac{\mu}{\mu_w}\right)^{0.24} \tag{6.15}$$

This correlation is close to both the correlation obtained in this work and that of Ni et al (1997), which indicates that heat transfer capabilities in batch OBCs and stirred tanks do not differ substantially.

6.3.4 Scale-Up

Heat transfer studies in OBCs of 50 mm and 213 mm diameter have yielded equations in the form of eqn (6.16) to describe the heat transfer characteristics,

$$Nu_t = C\,\mathrm{Re}_0^a\,\mathrm{Pr}^{0.33} \qquad (0.562 \le \mathrm{a} \le 0.68) \tag{6.16}$$

where C is a constant for a particular system. Equation (6.16) can be rearranged to:

$$h_t = Ck^{1.33}\left(2\pi\rho\right)^a C_p^{0.33}\,\mu^{(0.33-a)}\,D^{(a-1)}\left(x_o f\right)^a \tag{6.17}$$

As heat transfer in OBCs is forced convection driven, the heat transfer coefficient will be dependent predominantly on viscosity, oscillatory velocity and column diameter. Therefore, the effect of scale-up on the heat transfer coefficient can be written as:

$$h_t \propto \left(x_o f\right)^a D^{(a-1)}\mu^{(0.33-a)} \tag{6.18}$$

This expression was used to correlate the data from the present study and that obtained in the 50 mm OBC (Zhang, 1997). The best fit relationship was found to be:

$$h_t = 0.24(x_o f)^{0.65} D^{-0.35} \mu^{-0.32} \tag{6.19}$$

which, as can be seen from Figure 6.7, provides a reasonable fit to the experimental data.

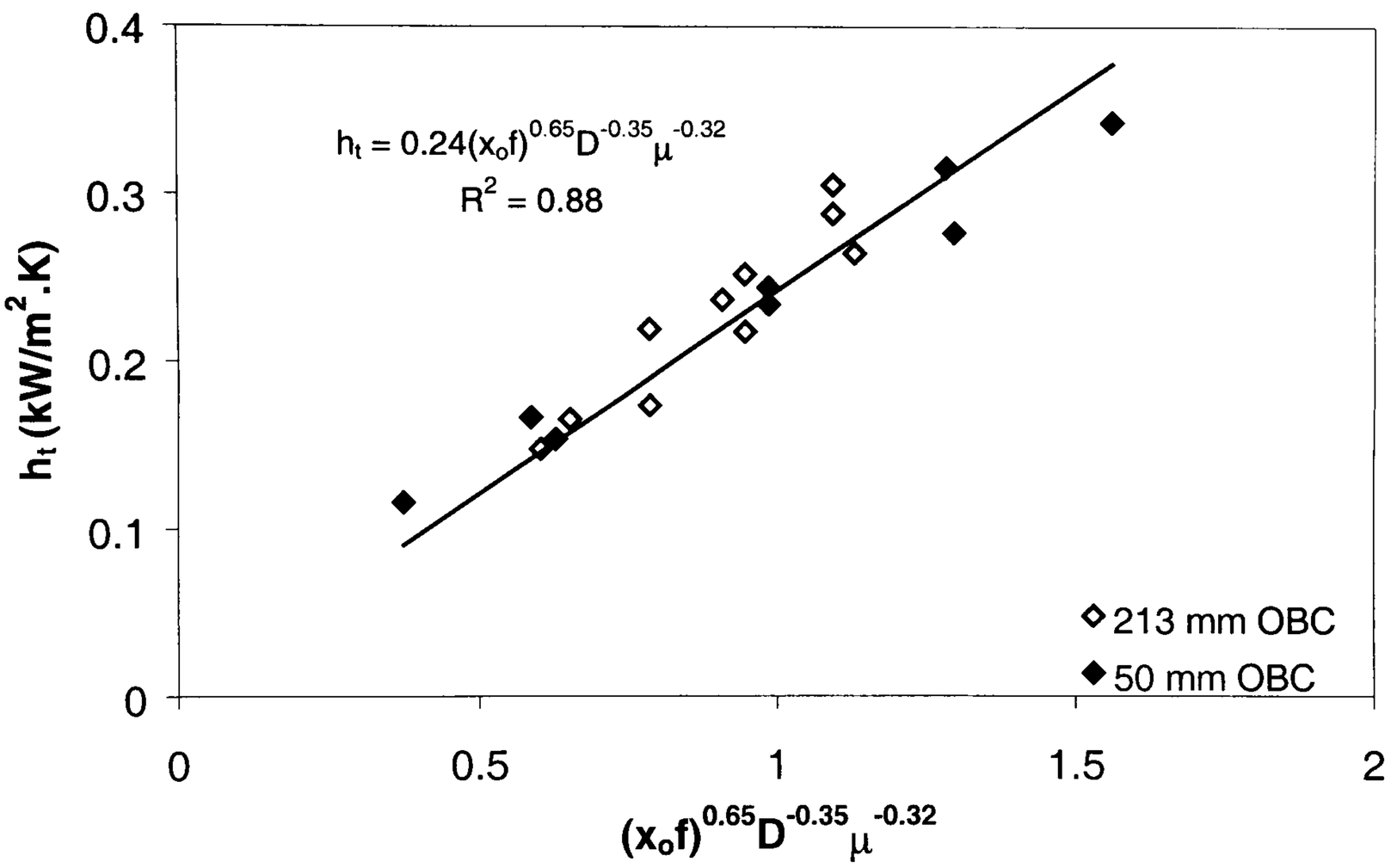

Figure 6.7: Scale-up correlation for heat transfer coefficient

6.4 Conclusions

Experimental heat transfer data in an OBR of 213 mm in diameter have been reported in this chapter. It was observed that temperature uniformity along the column was

maintained when oscillating baffles were present inside the column. It was also observed that the column contents could be cooled more quickly in the presence of baffles and oscillation than without, which was due to improved heat transfer characteristics as a results of forced convection induced by mechanical agitation. The effect of varying the oscillatory Reynolds number was studied from which it was found that increases in oscillation frequency or amplitude result in an increase in the heat transfer rate. A correlation has been established that relates the tube side Nusselt number to the oscillatory Reynolds number, which compares well with those reported in the literature for a smaller scale OBC and stirred tanks. The effect of column diameter on the heat transfer characteristics has also been studied and a scale-up correlation has been established that relates the tube side heat transfer coefficient to the column diameter, oscillatory velocity and fluid viscosity.

7 DROPLET SIZE DISTRIBUTION

7.1 Introduction

In the process of suspension polymerisation, the droplet size distribution of the dispersed monomer phase governs the particle size distribution of the final polymer product produced. Therefore, the ability to control this droplet size distribution (DSD) is crucial so that the polymer being manufactured complies with the product specification.

The droplet size distribution is determined by the dynamic processes of droplet breakage and coalescence which occur simultaneously in the system, as described in chapter 2. For any given system, a steady state will eventually be reached and the DSD that is obtained depends on agitation intensity and the geometry of the vessel used. Design and scale–up criteria for DSD in stirred tanks are based on semi-empirical correlations, a number of which are already reported in the literature. To date, few studies of this type have been conducted in OBCs, relating mean drop size to the energy dissipation in the system. In this chapter, results of a droplet study are reported. The work was carried out in the 213mm diameter OBC, using MMA as the dispersed phase and covering a range of operating parameters and baffle geometries.

7.2 Experimental Facilities and Procedures

7.2.1 Materials and Methods

In each of the DSD experiments the stainless steel OBR was charged with the same liquid-liquid recipe as that used in the heat transfer experiments. Experiments to determine drop size distribution were performed over a range of operating conditions covering oscillation frequencies of 0.4 – 2.0Hz, oscillation amplitudes of 50 – 100mm, baffle free areas of 20, 25 and 30% and baffle spacings of 263, 315 and 368mm.

7.2.2 Droplet Measurement Technique

Droplets size distributions were determined using a droplet stabilisation method that involved collecting samples from the oscillatory baffled column and placing them under a microscope for analysis.

7.2.2.1 Sampling and Stabilisation

Sampling points were located at three points along the height of the column that allowed a sample column contents to be drained out. Sample ports consisted of a 2mm internal diameter tube fitted with a ball valve. For the results to be reliable, it was important that the drops were disturbed as little as possible by the sampling procedure and that they remained stable after sampling. By nature, the samples of droplets withdrawn from the

column were not stable and coalescence of the drops could be seen to occur by viewing the sample under a microscope. The following procedure was therefore developed in order to stabilise the collected drops.

A small volume of the column contents was drained from one of the sample ports into a 100ml beaker containing a solution of 10ml of 50% w/w colloid solution and 10ml of 1% w/w of sodium dodecyl sulphate (SDS) solution. When the drops entered the beaker they were immediately surrounded by the colloid thereby preventing coalescence from occurring. The SDS is a surfactant and helped the stabilised drops to separate out thereby preventing clustering. A small amount of the sample was then transferred to a glass slide and covered, allowing images to be taken under a microscope, where the drops were observed to remain stable, even for periods of up to one hour. It should be pointed out that the volume of drops in each sample would differ.

7.2.2.2 Image Analysis

The images from the microscope were relayed to a computer via a video camera and a digitising board. Aquitas Image Analysis (IA) software from DDL (Dynamic Data Links) was used to view the images from the microscope which were then saved in bitmap form for analysis. A typical droplet image is shown in Figure 7.1. The Aquitas IA software was used to count and measure the diameter of all the drops in each image. The data was then exported to a spreadsheet in Microsoft Excel, which was used to produce droplet size distribution plots. From the DSD, the Sauter mean droplet diameter was determined from equation (2.26)

$$d_{32} = \frac{\sum n_i d_i^3}{\sum n_i d_i^2} \tag{2.26}$$

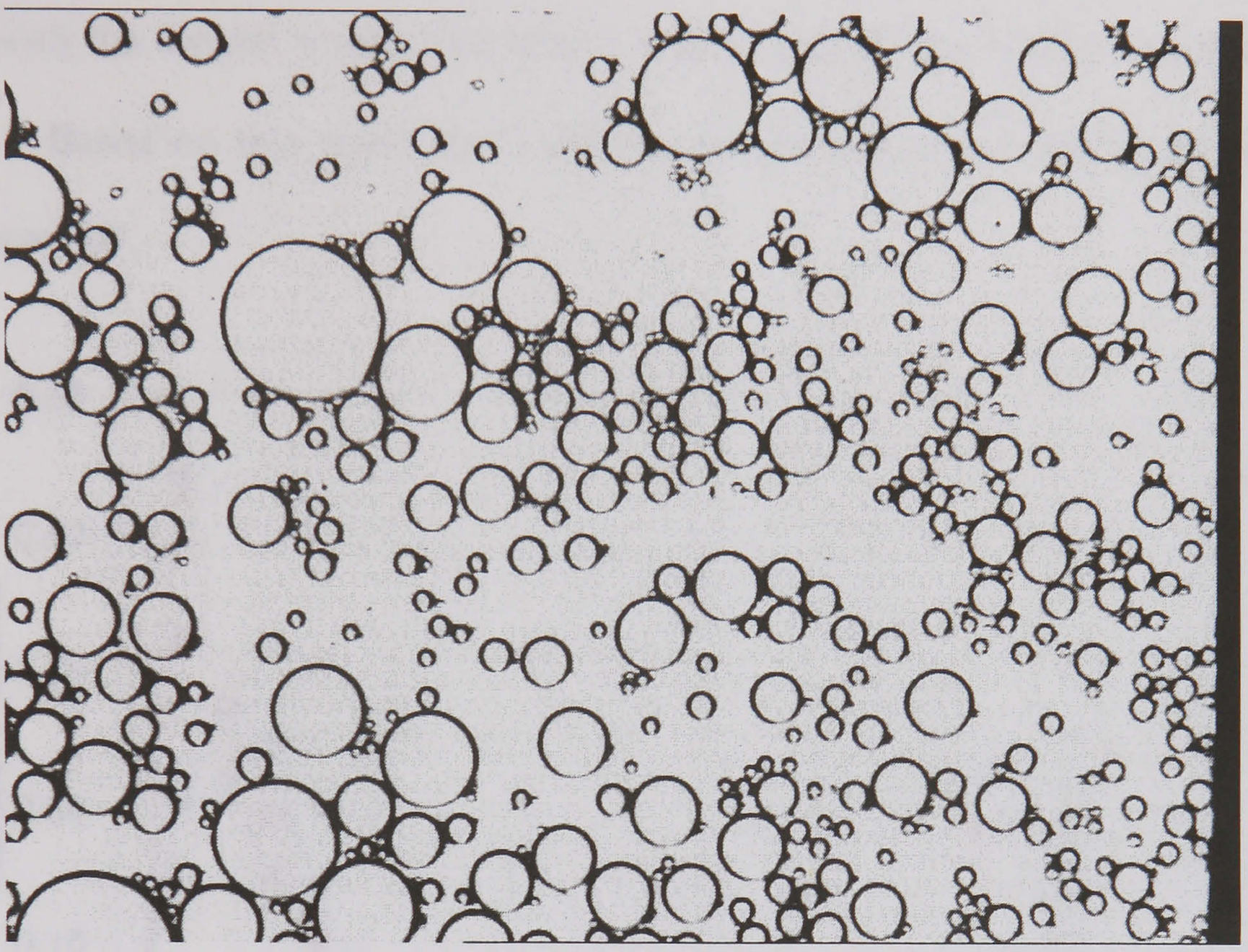

Figure 7.1: Typical droplet image

7.3 Results and Discussion

Droplet size distribution data from the droplet study are listed in Appendix 3.

7.3.1 Droplet Number

In order to minimise the sampling and analysis time, it was important to establish how many droplets were required to produce a reliable distribution. To do this, analysis was

performed on an increasing number of images in order to determine the minimum number of droplets at which the size distribution remained unaffected. The results of this test are shown in Figure 7.2 It can be seen that for a droplet number of below 300 distributions changed with the droplet number but above 300 drops the distributions are more or less constant. Based on this result the minimum number of drops used in all subsequent analysis was 500.

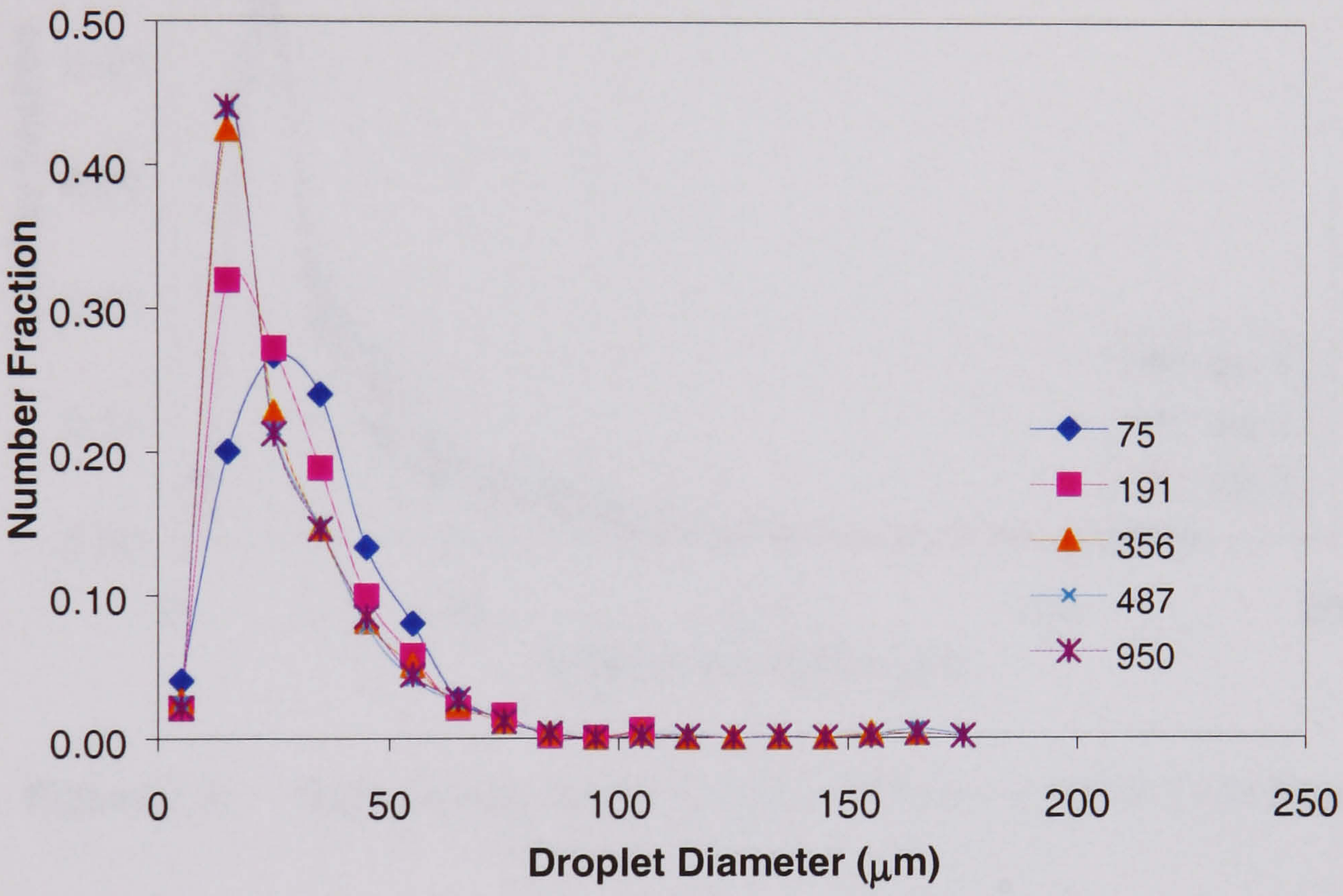

Figure 7.2: Effect of droplet number on drop size distribution

7.3.2 Repeatability

Repeatability tests were performed to determine the consistency of the results. This was done by performing the same experiment on three different days and comparing the droplet size distribution plots obtained. The droplet size distributions and mean droplet diameters are shown in Figure 7.3 and Table 7.1 respectively, from which it can be seen that there is

good agreement between the results obtained on the three different days. This level of consistency indicates that the repeatability is of a high degree and provides confidence in the results obtained.

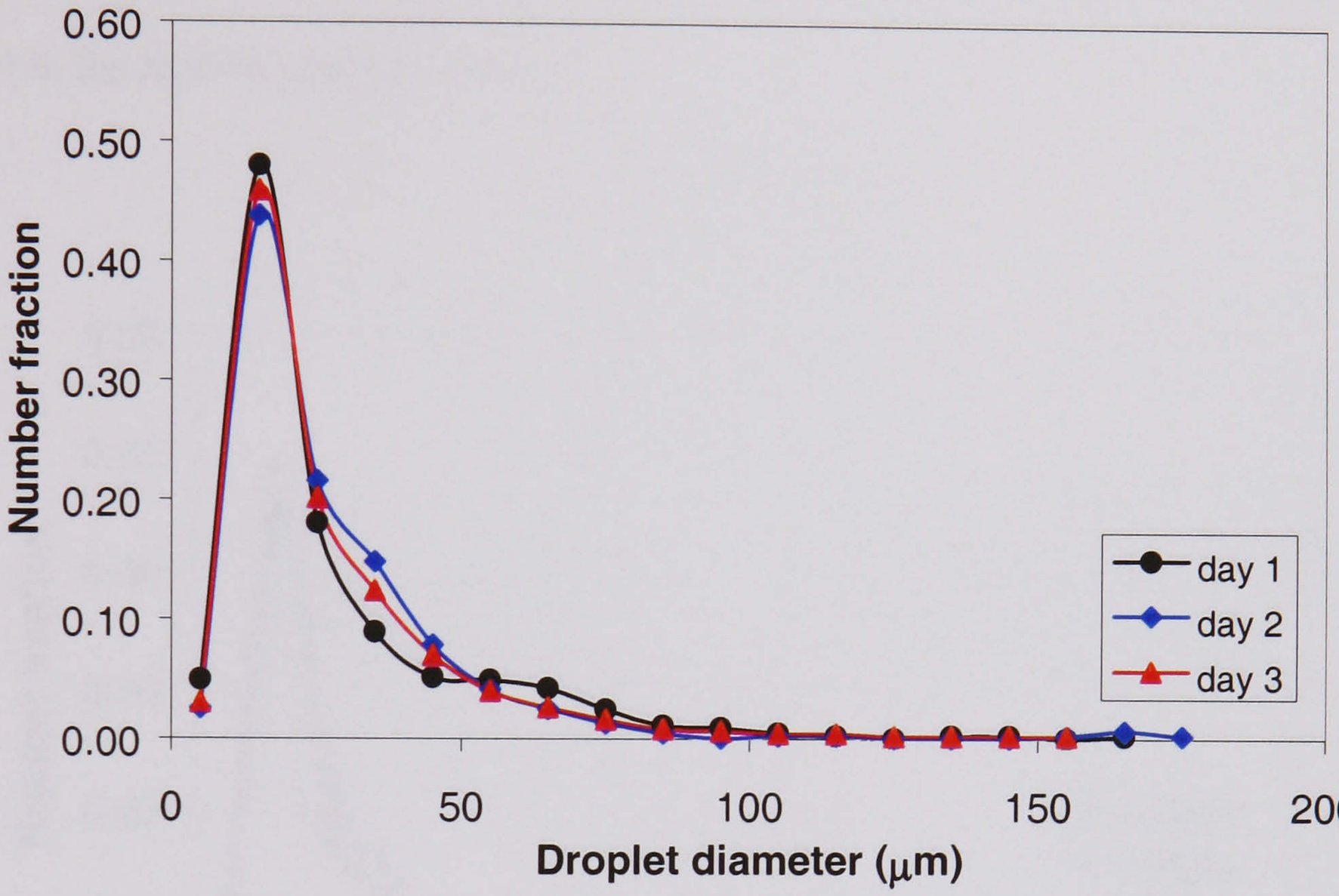

Figure 7.3: Repeatability test (f=1.0Hz, x_o=75mm, α=25%, L=315mm)

Table 7.1: Sauter mean droplet diameters obtained from repeatability test

Time of experiment	**Day 1**	**Day 2**	**Day 3**
d_{32} (μm)	74.3	75.1	78.3

7.3.3 Uniformity

The variation of drop size distribution in the system with respect to position was studied by comparing drop size distributions obtained from three different locations in the column. The three sampling points of top, middle and bottom refer to a position above the top

baffle, in between the two baffles and below the lower baffle respectively. The results are presented in Figure 7.4 and Table 7.2 shows the variation of mean drop size with position. It can be seen that the droplet size distribution and mean drop size is reasonably uniform along the height of the column ensuring that a sample taken from any port will be representative of the entire system. Therefore, in all remaining experiments, only samples taken from the middle port were used.

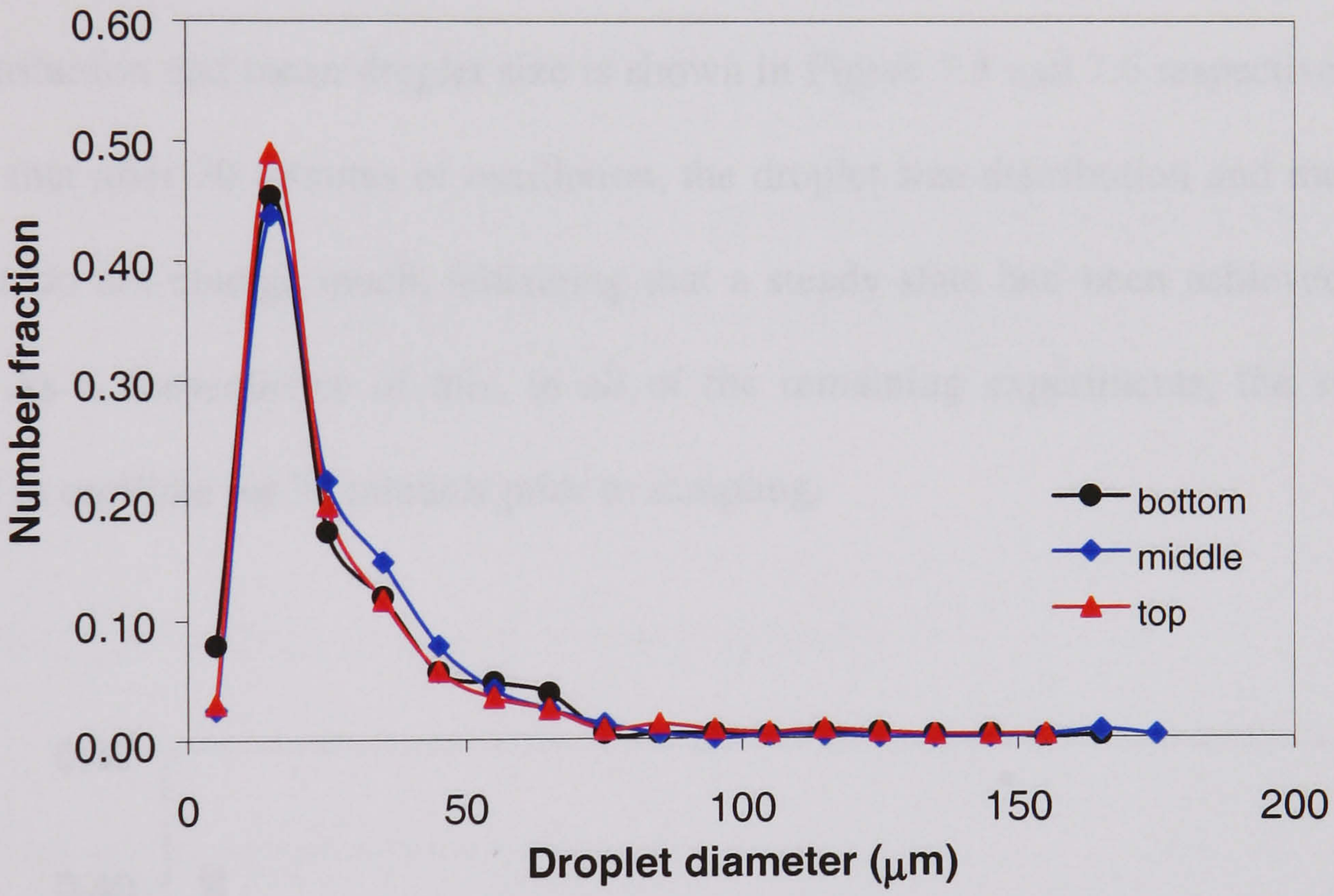

Figure 7.4: Effect of sample location on drop size distribution

(f=1.0Hz, x_o=75mm, α=25%, L=315mm)

Table 7.2: Effect of sample location on Sauter mean droplet diameter

Sample location	**Top**	**Middle**	**Bottom**
d_{32} (μm)	73.2	74.3	69.6

7.3.4 Effect of Oscillation Time

At the start of an experiment the MMA and bulk liquid are stratified in the system and the MMA becomes dispersed as droplets once oscillation commences. After a certain time has elapsed the droplet size distribution of the dispersed phase becomes stable with respect to time and a steady state is established. It is important to know the time required for the system to reach a steady state of droplet distribution and this was determined by measuring the DSD at 15 minute intervals for 1 hour. The effect of oscillation time on the droplet size distribution and mean droplet size is shown in Figure 7.5 and 7.6 respectively. It can be seen that after 30 minutes of oscillation, the droplet size distribution and mean droplet diameter do not change much, indicating that a steady state had been achieved after this time. As a consequence of this, in all of the remaining experiments, the system was allowed to oscillate for 30 minutes prior to sampling.

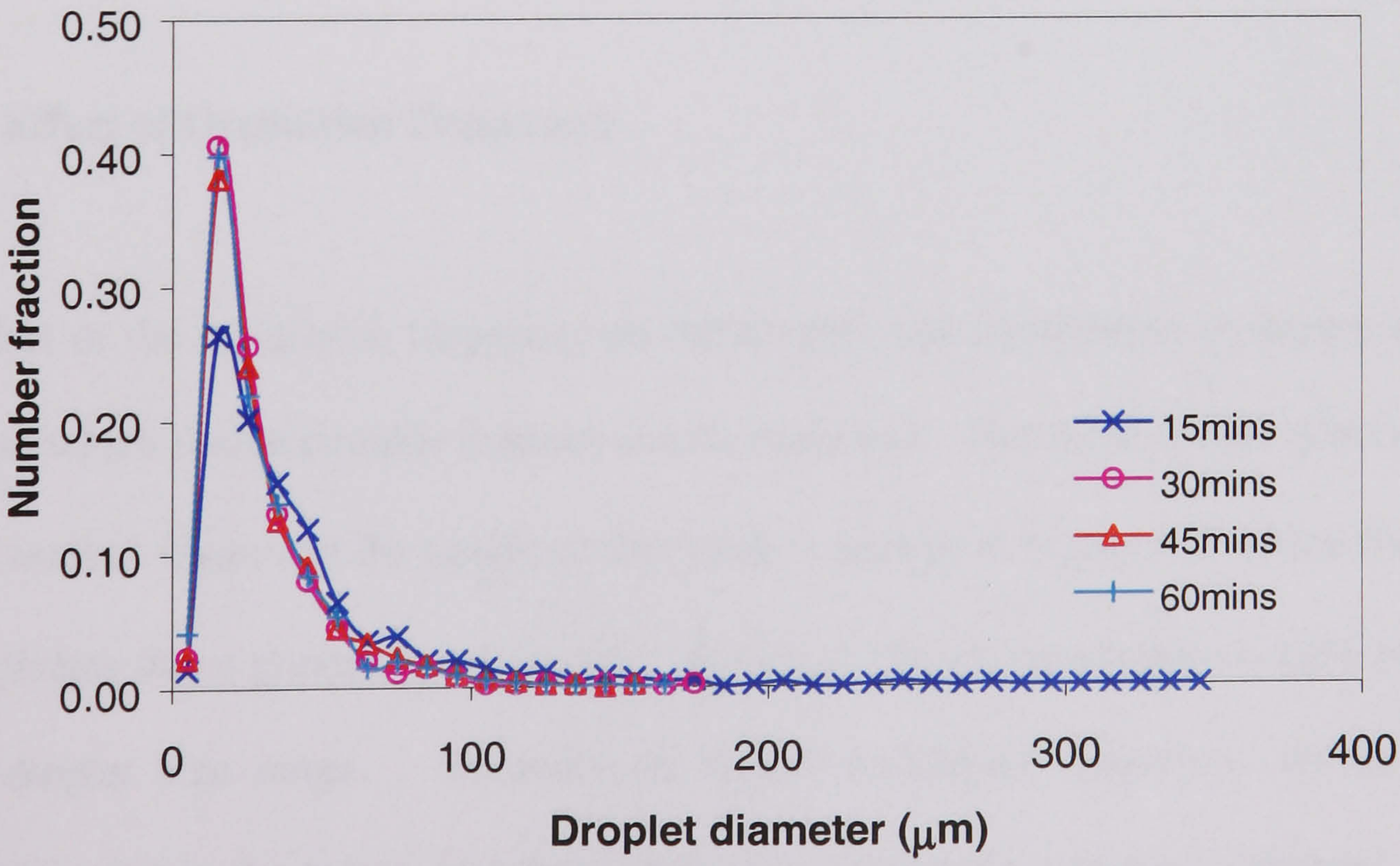

Figure 7.5: Effect of oscillation time on DSD (f=1.0Hz, x_o=75mm, α=20%, L=315mm)

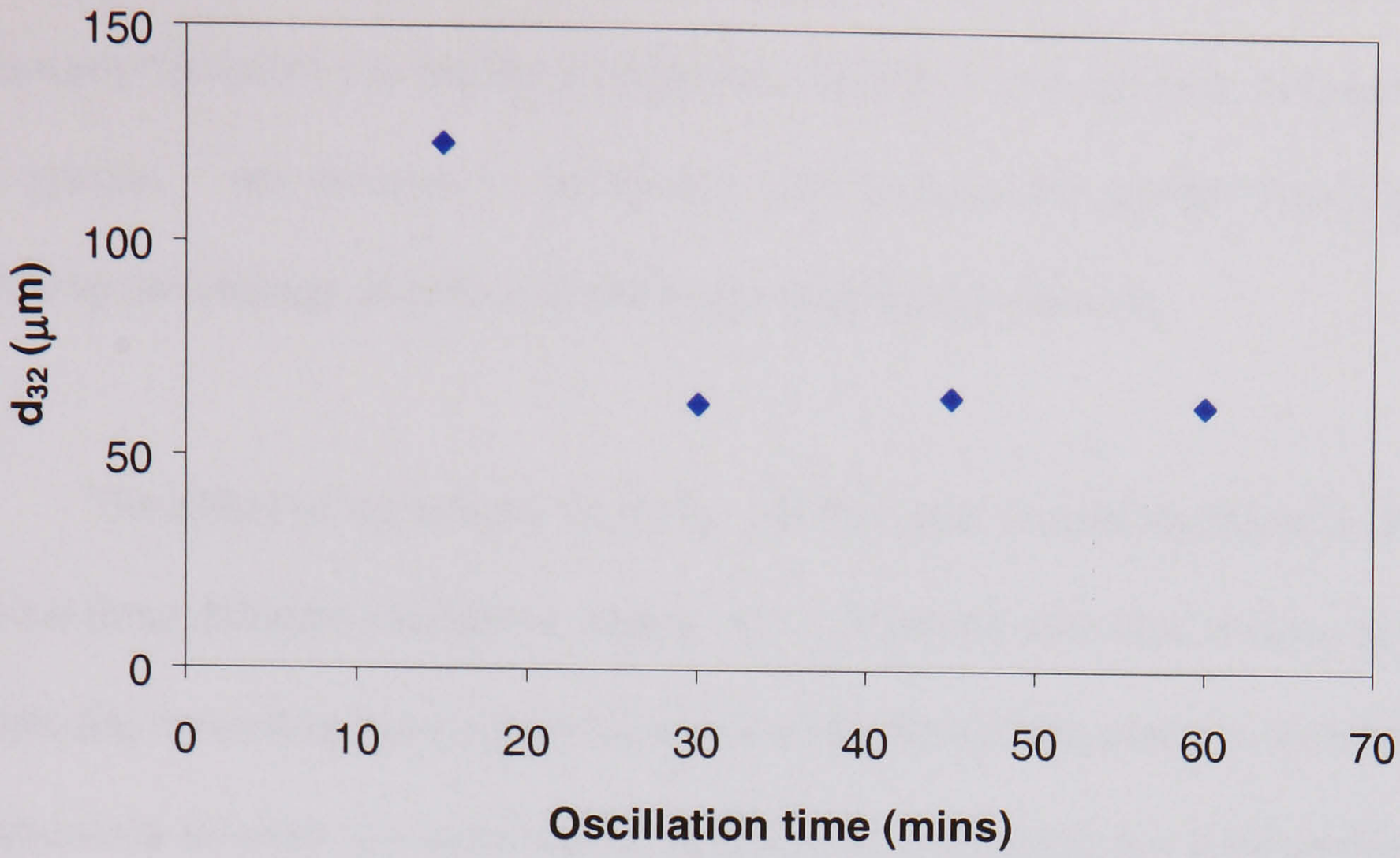

Figure 7.6: Effect of oscillation time on Suater mean droplet diameter (f=1.0Hz, x_o=75mm, α=20%, L=315mm)

7.3.5 Effect of Oscillation Frequency and Amplitude

7.3.5.1 Effect of Oscillation Frequency

The effect of the oscillation frequency on the droplet size distribution is shown in Figure 7.7, from which two noticeable features can be observed. Firstly, all of the plots exhibit a peak at around 15μm and the height of this peak is greater at higher oscillation frequency. This indicates that a greater fraction of the existing drops are concentrated at the lower end of the droplet size range. Secondly, at higher oscillation frequency, the tail of the distribution plot is shorter or, in other words, the distribution becomes narrower. These results are expected and can be explained by considering the relationship between the

oscillation frequency and the energy dissipation in the system. Increasing the oscillation frequency increases the energy dissipation and hence increases the turbulence intensity in the system. An increase in turbulence will increase the droplet breakage rate thereby reducing the average droplet size and narrowing the distribution.

The effect of oscillation frequency on the mean droplet diameter is shown in Figure 7.8 for three different oscillation amplitudes. It can be seen that at each of the amplitudes tested, the mean drop size is decreased as the oscillation frequency is increased and that the relationship between d_{32} and f can be represented by a power law relationship. The best fit value of the exponent was found to lie the range -0.97 to –1.11 (± 0.1) at each of the amplitudes, which is close to the value of –1.2 observed in a 50mm diameter OBC (Ni et al., 1998a), indicating that the dependence of drop size on frequency is similar in both devices.

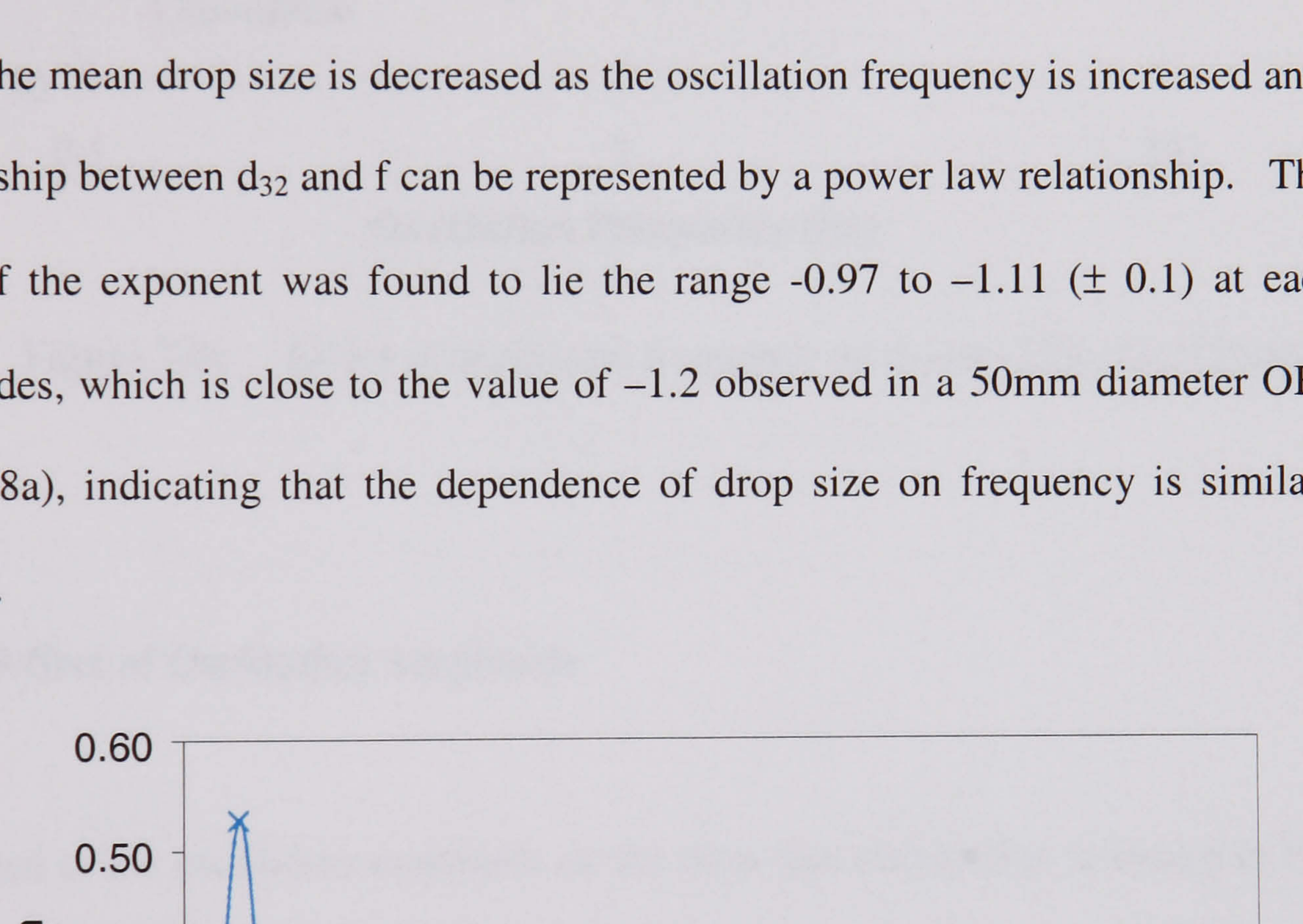

Figure 7.7: Effect of frequency on drop size distribution

(x_o=100mm, α=25%, L=315mm)

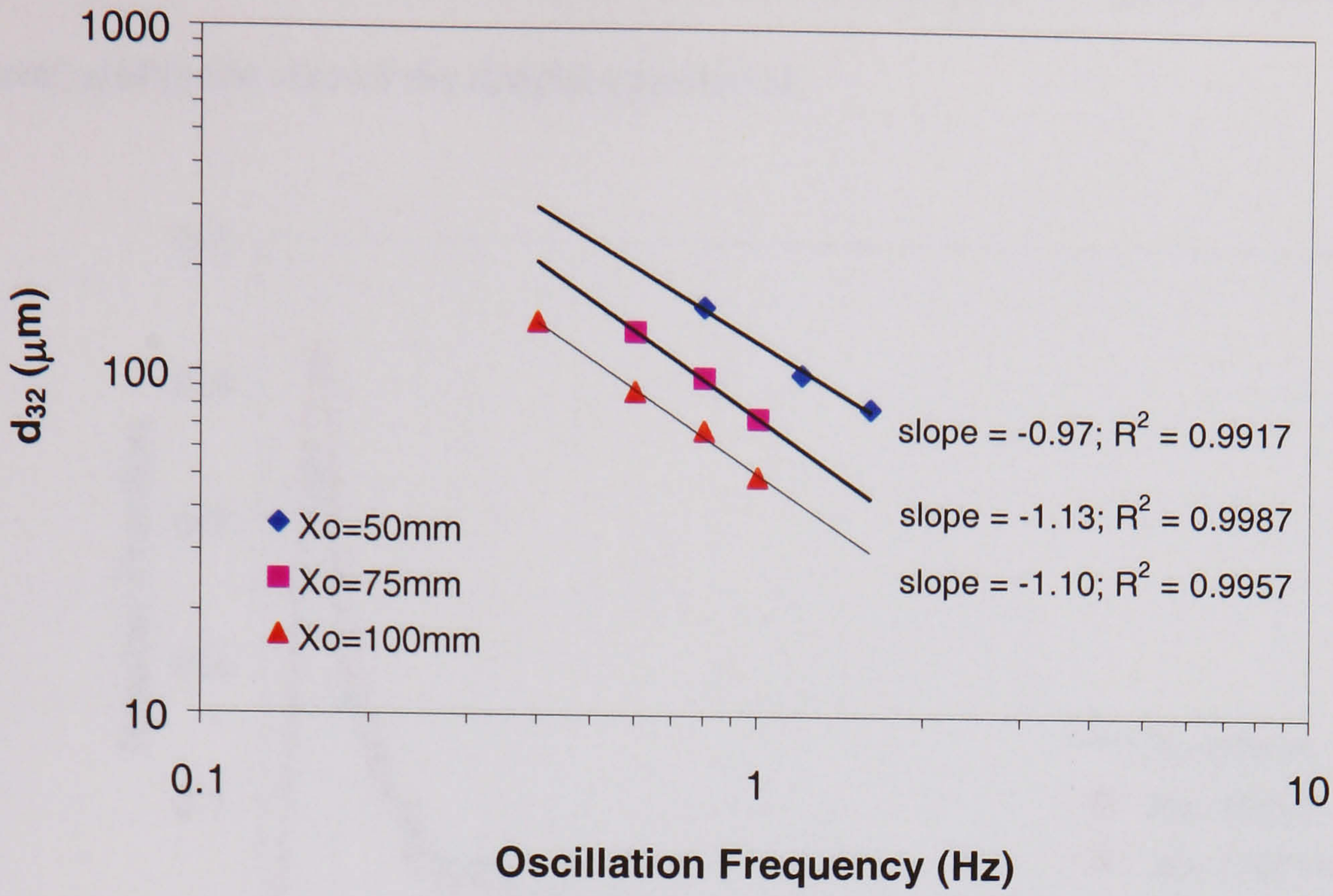

Figure 7.8: Effect of oscillation frequency on d_{32} (α=25%, L=315mm)

7.3.5.2 Effect of Oscillation Amplitude

The effect of the oscillation amplitude on the drop size distribution is shown in Figure 7.9. It can be seen that the oscillation amplitude has a similar effect on the DSD as the oscillation frequency. This can again be related to the energy dissipation in the system, which exhibits a similar dependence on both frequency and amplitude (see eqn 2.5).

The effect of oscillation amplitude on the mean droplet size is shown in Figure 7.10. It was found that mean droplet diameter varies with oscillation amplitude to a power of -1.2 (± 0.035). This indicates that drop size is slightly more dependent on the oscillation amplitude than the oscillation frequency. This could be due to the fact that, while both contribute equally to the mixing intensity, the amplitude governs the extent to which eddies

propagate throughout the baffled cavity and so may play a slightly more dominant role in determining the size of the droplets produced.

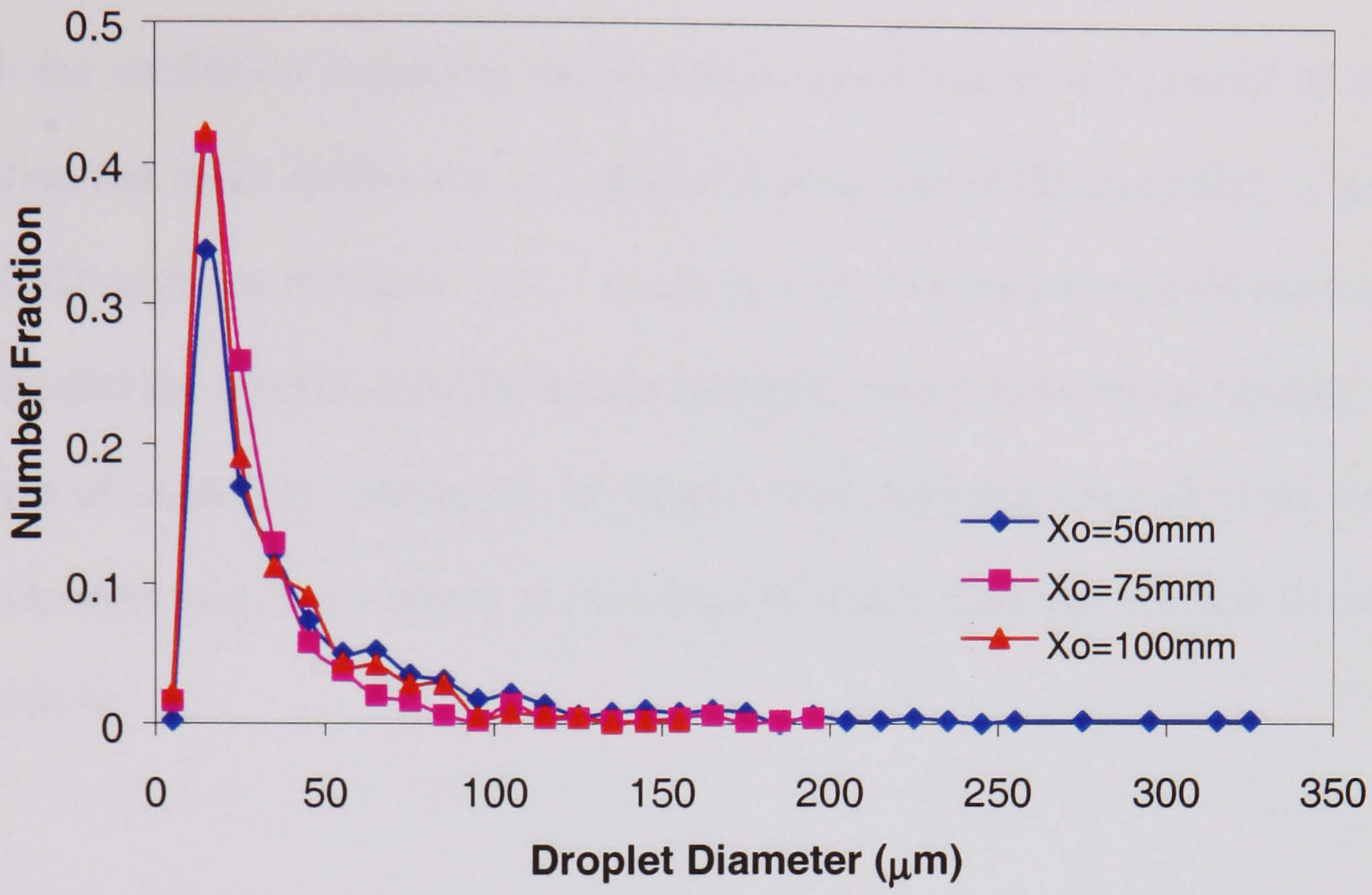

Figure 7.9: Effect of amplitude on drop size distribution (f=0.8Hz, α=25%, L=315mm)

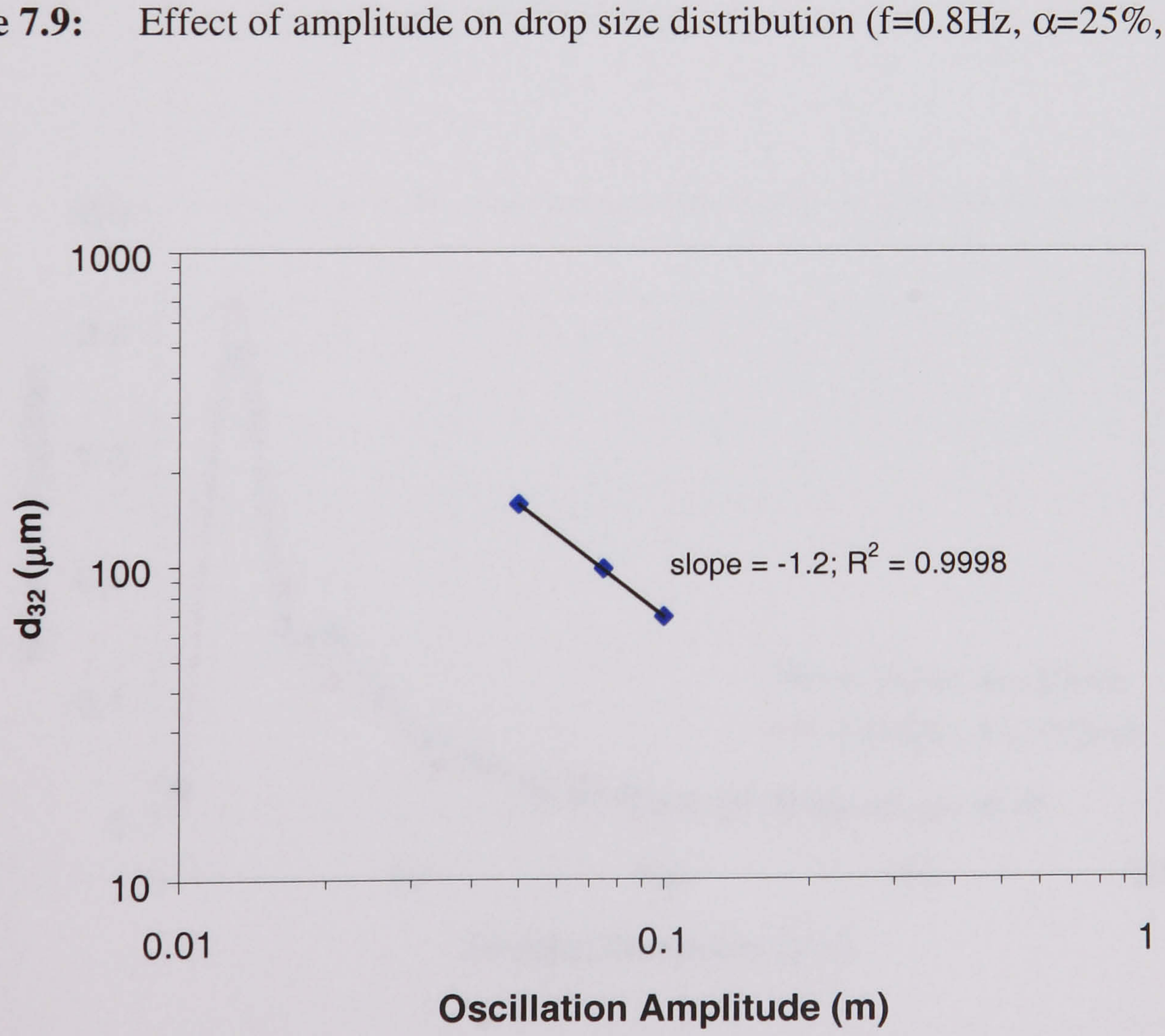

Figure 7.10: Effect of oscillation amplitude on d_{32} (f=0.8Hz, α=25%, L=315mm)

7.3.5.3 Effect of Oscillatory Velocity

As both the oscillation frequency and amplitude contribute to the control of drop size distribution and mean droplet size in a similar manner, the effect oscillatory velocity (x_of) on the DSD is shown in Figure 7.11. It can be seen that the two distributions are close, indicating that the droplet size distribution is indeed governed by the oscillatory velocity. The effect of oscillatory velocity on the Sauter mean diameter, over all of the oscillation frequencies and amplitudes tested, is illustrated in Figure 7.12 and the best fit power law correlation is:

$$d_{32} = 4.26(x_o f)^{-1.11} \qquad (7.1)$$

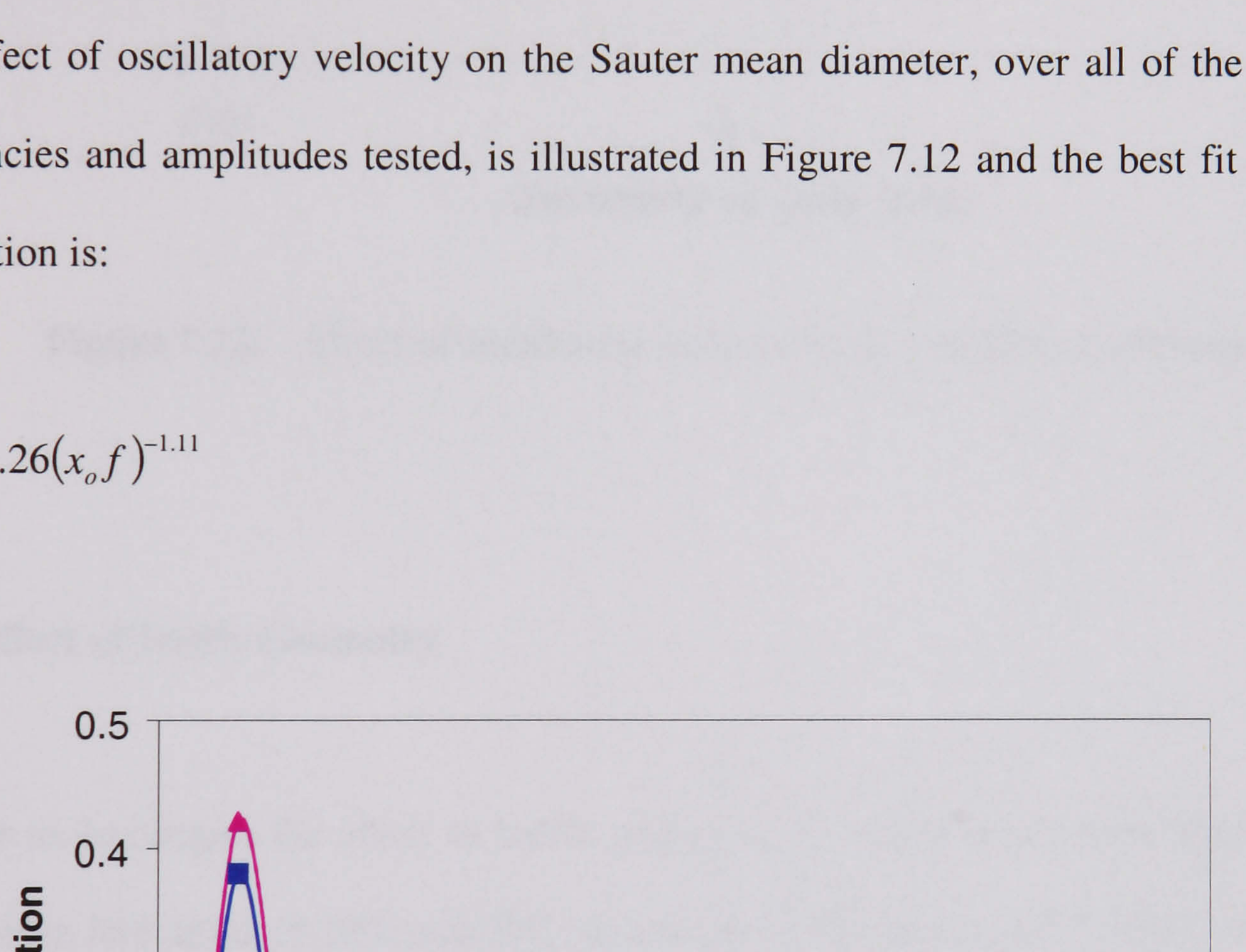

Figure 7.11: Effect of frequency and amplitude, at constant oscillatory velocity on drop size distribution (α=25%, L=315mm)

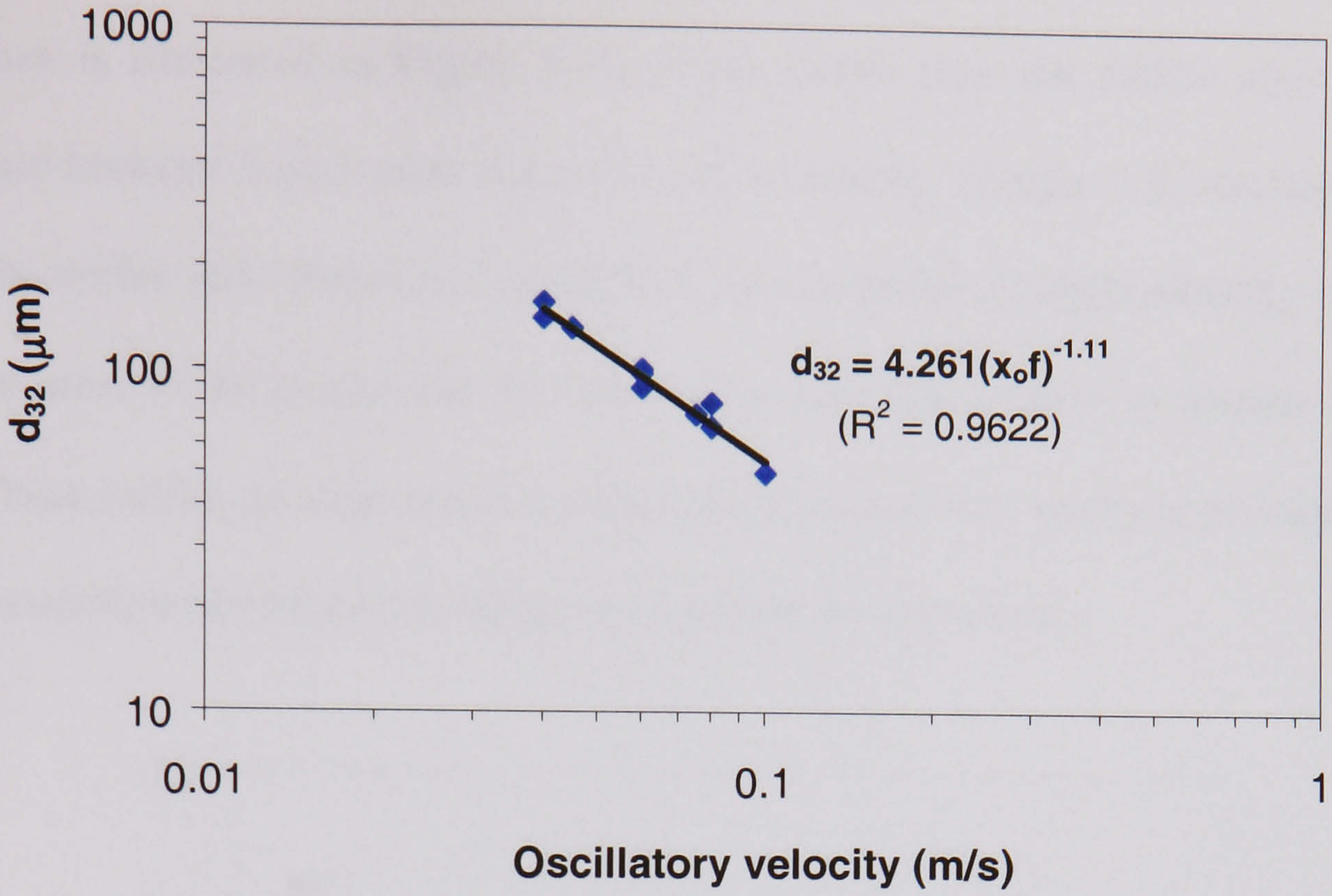

Figure 7.12: Effect of oscillatory velocity on d_{32} (α=25%, L=315mm)

7.3.6 Effect of Baffle Geometry

In order to investigate the effect of baffle geometry, the experiments were repeated at two more baffle free areas of 20% and 30%, at a fixed baffle spacing of 315mm, and a further two baffle spacings of 263mm ($1.25D_i$) and 368mm ($1.75D_i$), at a fixed baffle free area of 25%.

7.3.6.1 Effect of Baffle Free Area

The typical effect of baffle free area on the droplet size distribution is illustrated in Figure 7.13. It was generally observed that using a smaller baffle orifice results in the generation

of smaller drops and a narrower distribution (shorter tail). The resulting effect on mean droplet size is illustrated in Figure 7.14, which shows how the orifice size affects the relationship between Sauter mean diameter and oscillatory velocity. It was found that for each of the orifice sizes tested, d_{32} varied with $x_o f$ to a power of approximately –1.11 (with an typical error of ±0.2) and that the mean drop size was smaller at smaller baffle free areas. These results are expected as decreasing the orifice area results in an increase in the energy dissipation and hence the turbulence intensity in the system.

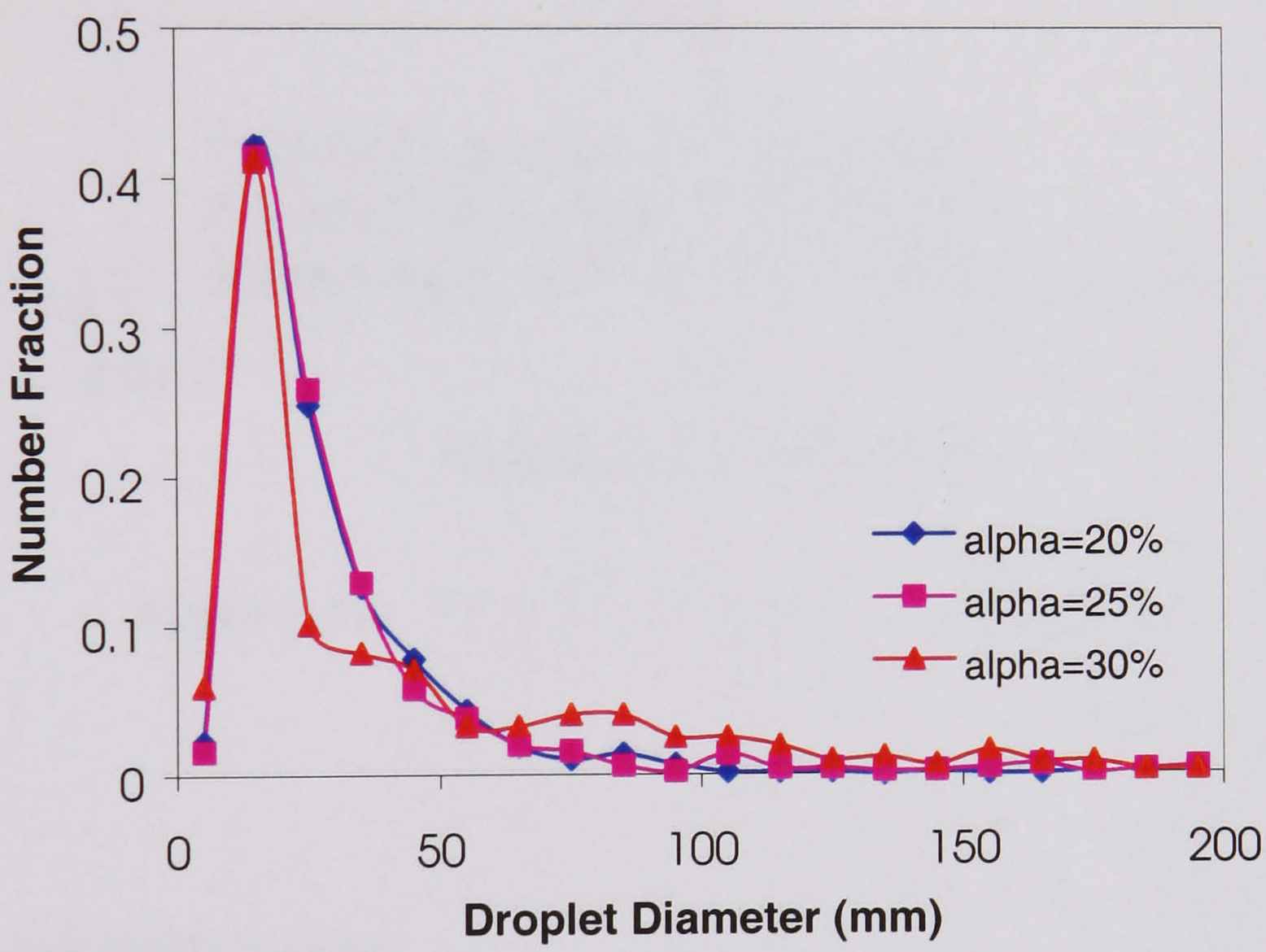

Figure 7.13: Effect of baffle free area on drop size distribution (f=1.0Hz, x_o=75mm, L=315mm)

It is also evident from Figures 7.13 and 7.14 that d_{32} is a much weaker function of baffle free area than of oscillatory velocity. This can be attributed to the individual contribution that these parameters make towards the energy dissipation in the system. As shown by equation (2.5), energy dissipation is dependent on baffle free area by the term $(1-\alpha^2)/\alpha^2$, which is much weaker than the oscillatory velocity term, $(x_o f)^3$. Also, the energy

dissipation increase is only 2.4 fold over the relatively short range (20 – 30 %) of baffle free areas tested and so the effect of orifice size on the drop size is difficult to determine accurately within the scope of experiments.

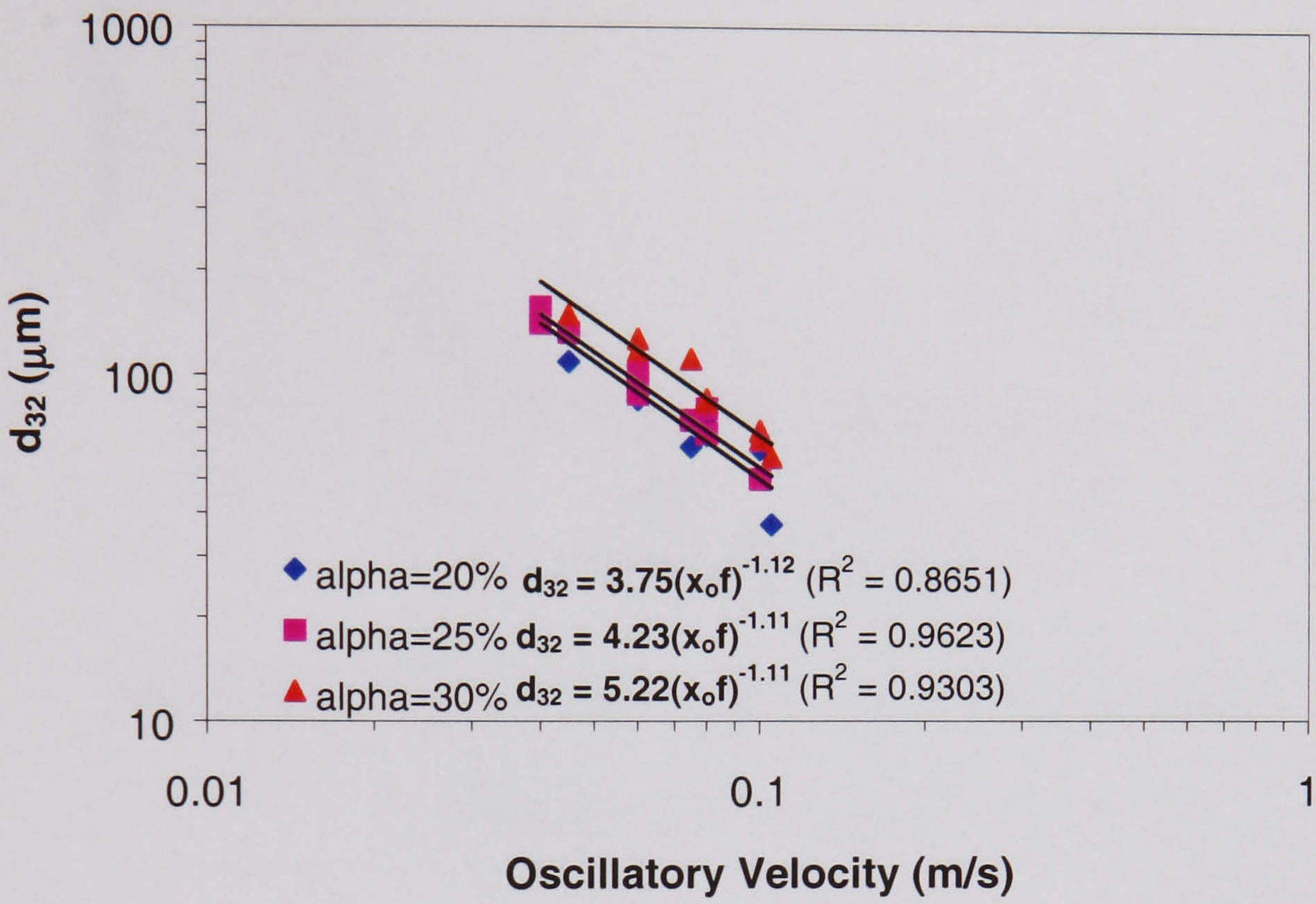

Figure 7.14: Effect of $x_o f$ and α on d_{32} (L=315mm)

7.3.6.2 Effect of Baffle Spacing

The effect of the baffle spacing on drop size distribution is illustrated in Figure 7.15. It can be seen that the baffle spacing has little influence on the DSD. This can be attributed to the fact that the energy dissipation has only a weak dependence on baffle spacing and it is unlikely that any significant effect could be observed over the range of baffle spacings tested. The effect of the baffle spacing on the Sauter mean diameter is illustrated in Figure 7.16 and d_{32} varied with $x_o f$ to a power of –1.11 (±0.25) for each of the baffle spacings tested, with similar constants.

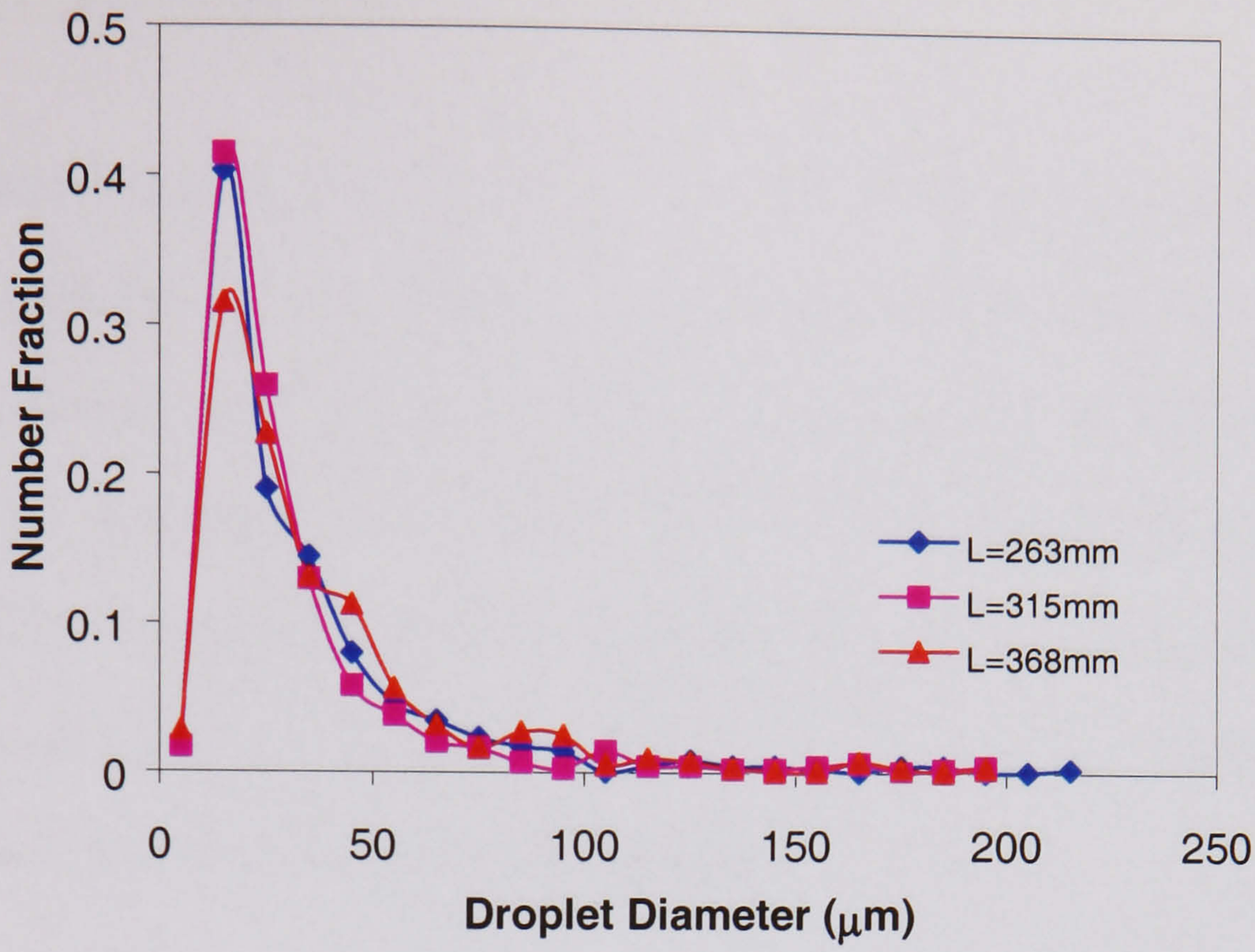

Figure 7.15: Effect of baffle spacing on drop size distribution

(f=1.0Hz, x_o=75mm, α=25%)

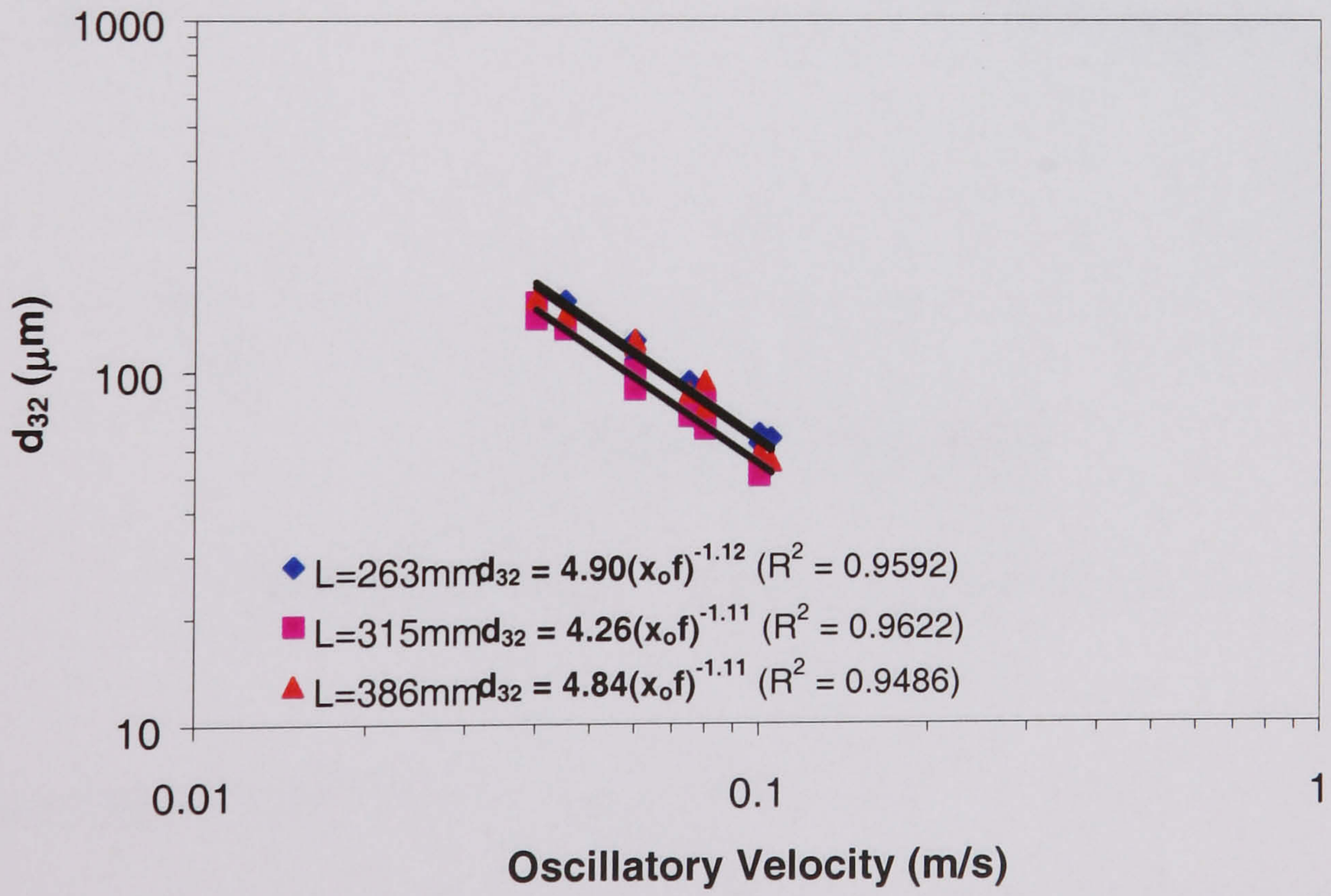

Figure 7.16: Effect of x_of and L on d_{32} (α=25%)

7.3.7 Effect of Energy Dissipation

All of the mean droplet size data collected, over the entire range of operating parameters and baffle geometries tested, are plotted against energy dissipation (as calculated by equations (2.4) and (2.5)) in Figure 7.17 and the best fit power law relationship is given by equation (7.2). The mean drop size varies with energy dissipation to the power of –0.35 (±0.04), which is between the values of -0.25 and -0.4 predicted by isotropic turbulence theory for coalescence only and breakage only systems respectively, indicating that it is likely that both mechanisms are present in the system.

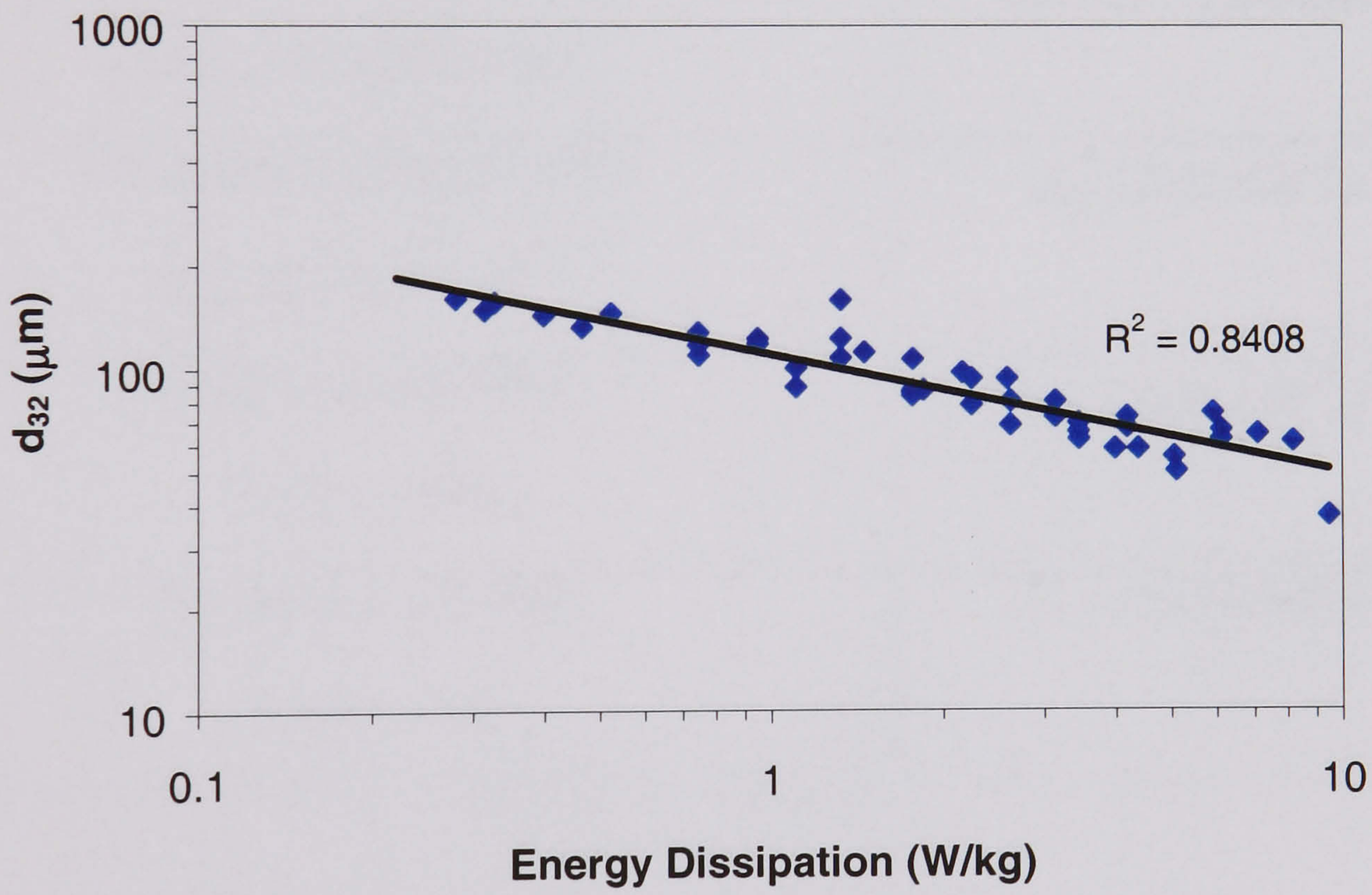

Figure 7.17: Effect of energy dissipation on d_{32}

$$d_{32} = 11(\pm 0.5) \times 10^{-5} \varepsilon^{-0.35(\pm 0.04)} \qquad (7.2)$$

A comparison of equation (7.2) with those obtained by other researcher in other liquid-liquid mixing devices is given in Table 7.3. It can be seen that in each of the

devices, the dependence of mean droplet on energy dissipation shows a similar exponent but the preceding constant varies for different systems. This indicates that while the mean drop size varies between systems, the nature of the relationship between the energy dissipation and d_{32} remains unchanged.

Table7.3: Comparison of correlation for d_{32} in different devices

Device and Reference	**Correlation for d_{32}**
Stirred Tank (Brown and Pitt, 1970; Van Heuven and Beek, 1971; Mlynek and Resnick, 1972; Lee and Tasakorn, 1979; Zerfa and Brooks, 1996)	$d_{32} = K\varepsilon^{-0.4}$ $3.87\times10^{-5} \le K \le 8.88\times10^{-5}$
Reciprocating Plate Column (Baird and Lane, 1973)	$d_{32} = 3.21\times10^{-5}\varepsilon^{-0.4}$
50mm Diameter OBR (Ni et al., 1998a)	$d_{32} = 6.80\times10^{-5}\varepsilon^{-0.4}$
213mm Diameter OBR (Present study)	$d_{32} = 11.0\times10^{-5}\varepsilon^{-0.35}$

7.4 Scale-Up Characteristics

One of the main objectives of this study was to establish a scale-up rule for drop size in an OBR. The data collected has therefore been compared with that collected by Ni et al (1998a) who investigated the same liquid-liquid system in a 50mm diameter OBC.

Ni et al (1998a) used a baffle geometry comprising of a baffle spacing of 1.5 times the tube diameter and a baffle free area of 20% and reported that the correlation in equation (7.3) provided the best fit to their data. Using the same geometrical configuration in the 213mm diameter OBC in this study yielded the relationship in equation (7.4). Good agreement can be seen between the power index in both equations indicating that the same trend exists between drop size and energy dissipation in the two columns. However, it can be seen that drop sizes are 3.75 times larger in the larger diameter column, indicating that oscillatory velocity is not a good scale-up criterion.

$$d_{32} = 0.99\times10^{-6}\left(x_o f\right)^{-1.2} \qquad \text{(50mm diameter OBR)} \qquad (7.3)$$

$$d_{32} = 3.75\times10^{-6}\left(x_o f\right)^{-1.11} \qquad \text{(213mm diameter OBR)} \qquad (7.4)$$

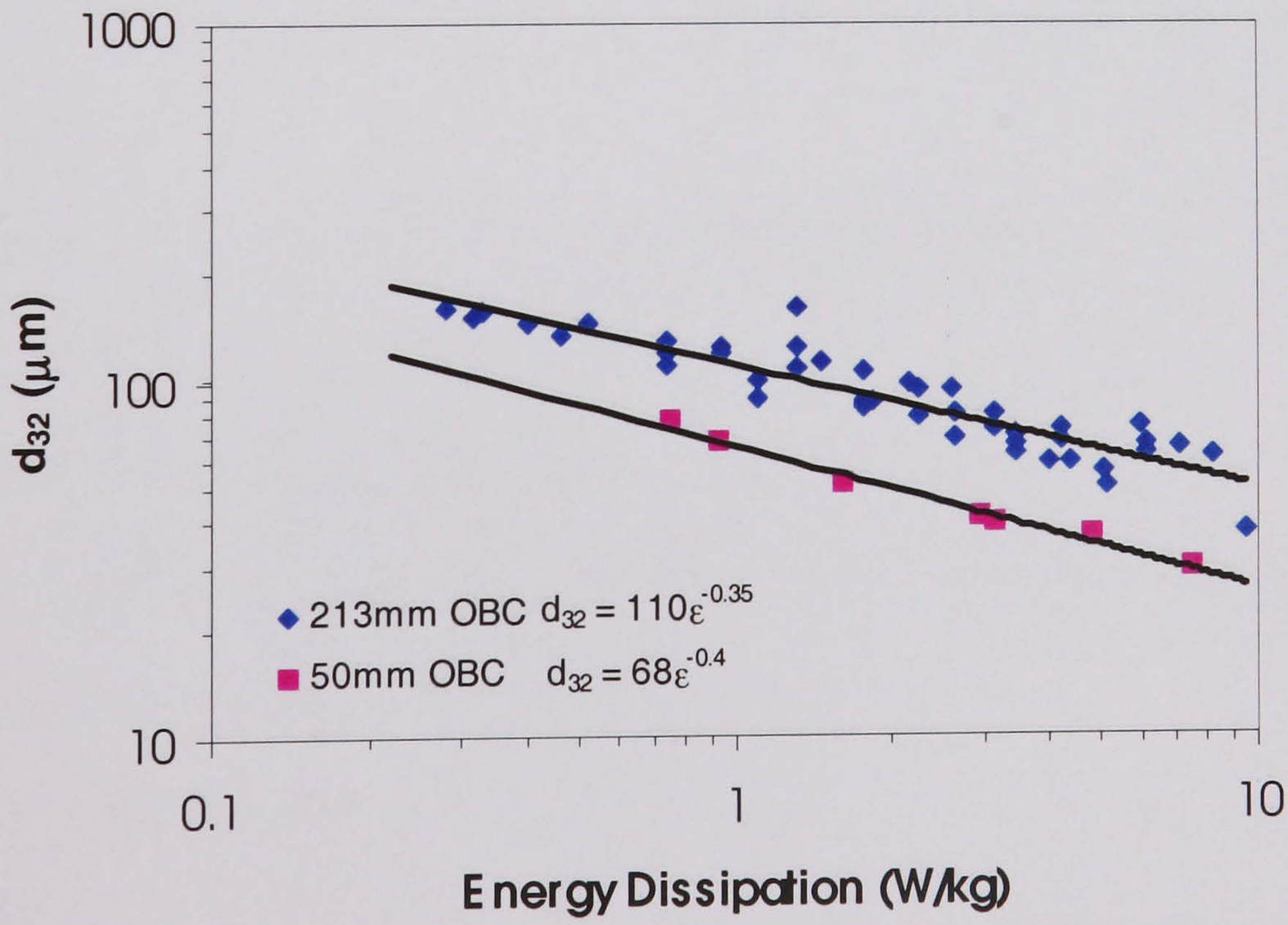

Figure 7.18: Comparison of the effect of energy dissipation on d_{32} in OBCs of 50mm and 213mm in diameter

This result can partly be explained in terms of energy dissipation. Using a larger diameter column means using a larger baffle spacing in order to maintain the ratio of baffle spacing to column diameter within a feasible operating range. Therefore a 4-fold increase in diameter typically results in a 4-fold decrease in energy dissipation, which would result in larger droplets being produced. However, the average energy dissipation in the system also proves to be an unsuitable scale-up criterion as can be seen from Table 7.3 and Figure 3.18, which shows the comparison between mean droplet size data collected over a range of energy dissipation in the two different columns.

The lower power index and the larger droplets observed for the larger diameter column indicate that coalescence was more significant. In order to gain an understanding of why this is, the influence of all scale-up factors must be considered. The following list highlights the major changes that occur in the system when scaling from small to large:

1 Higher oscillatory velocity for a given energy dissipation (for a fixed baffle geometry)

2 Higher oscillatory Reynolds number (due to larger diameter)

3 Larger circulation zone (baffle cavity)

4 Longer circulation time (due to lower frequency)

5 Lower baffle edge length ($\propto D$) per unit volume ($\propto D^3$) (i.e. the amount of sharp edge available for flow separation to occur over)

6 Larger primary eddies

The fact that the larger OBC is showing signs of higher coalescence suggests that Factors 3 and 4 are most significant i.e. the longer circulation period of the drops is

allowing coalescence to occur much more readily in the larger column. Therefore, while equations and models derived from isotropic turbulence theory provide satisfactory understanding of basic phenomena, they cannot be applied universally to all situations without modification.

Based on the experimental findings of this work and that reported by Ni et al (1998b), a scale-up correlation has been established as:

$$d_{32} = 2.25\times10^{-4} D^{0.4} \varepsilon^{-0.4} \qquad (7.4)$$

where D is the column diameter (m). This equations is however based on data obtained from only two columns of different diameter and so further study is required to verify the applicability of this relationship to devices of other diameters.

7.5 Conclusions

In this chapter, results from a droplet study in a 213mm diameter oscillatory baffled reactor are reported. Drop size distribution and mean drop size data were determined over a range of operating parameters and baffle geometries and have been compared with previous findings by other researchers.

Increasing the oscillation frequency or amplitude resulted in narrowing the drop size distribution and a reduction in mean drop size and this can be attributed to the increase

in energy dissipation experienced when operating at a higher oscillatory velocity. The mean drop size was found to vary in a similar manner with the oscillatory velocity to that reported in a smaller OBC, indicating the similarity in mixing characteristics between large and small scale devices. The baffle geometry was found only to have a weak, but noticeable, effect on drop size. A reduction in the baffle free area resulted in the generation of smaller drops, which can again be attributed to the effect of energy dissipation. Baffle spacing on the other hand had little effect on the drop size distribution and no real trend was evident.

Comparison with work reported by other researchers indicates that while drop size varies between devices, the dependence on energy dissipation does not change considerably. An investigation of scale-up characteristics for oscillatory baffled columns indicates that larger drops are produced in a larger diameter column; for a given energy dissipation. This is attributed to a combination of the longer circulation periods and the presence of less well defined fluid mechanics in columns of larger diameter. A scale-up correlation incorporating column diameter, is proposed for the system investigated but more experimental data, at different column diameters, is needed to verify this relationship.

8 BREAKAGE AND COALESCENCE MODELLING

8.1 Introduction

The evolution of the dispersed phase droplet size distribution in a liquid-liquid dispersion is governed by the droplet breakage and coalescence processes. The nature of these interactions is dependent on a number of parameters, such as mixing intensity, geometry of vessel and agitator, phase fraction, fluid physical properties, the presence of stabilisers, etc. Prediction of breakage and coalescence rates is therefore difficult and must be done by using a mathematical model with experimental data. Such an approach has been applied in this work. This chapter describes the development, evaluation and validation of a model for calculating droplet breakage and coalescence rates.

8.2 The Model

The model that is employed in this work is based on that originally developed by Saye (2001), within the C.O.B.R.A. group, for the evaluation of droplet breakage and coalescence rates from experimental drop size distributions. The model utilises an approach which is similar to that of the discretised population balance method by Laso et al. (1987), but in absence of any *a priori* assumption of functional form for breakage and coalescence rates. This itself is in contrast to the traditional approach. In the model, the conservation of volume is satisfied, and both breakage and

coalescence rates are the unknowns, and have to be evaluated from the experimental data.

8.2.1 General assumptions

For a liquid dispersion within the OBR, V_d is the total volume of the dispersed phase, which consists of a number of drops of various sizes. It is the number and sizes of all drops forming V_d that define a drop size distribution at any given time t. It is assumed that the conservation of volume can be applied as the effect of pressure variation in OBRs on the drop volume is negligible. There should be therefore no growth in drops, and coalescence of two drops of volumes, v_1 and v_2, will result in a droplet with a total volume of v_1+v_2. Similarly, the volumes of drops formed by breakage should equal to the volume of the initial mother drop.

Mixing is assumed to be efficient enough for droplets in V_d to be uniformly distributed in space. The enhanced and more uniform mixing provided by the OBR justifies the assumption faithfully. Consequently, the drop size distributions will not vary in space, but are a function of time. Furthermore, the variations of the DSDs with time are solely driven by the processes of breakage and coalescence. In other words, the model does not account for dispersion or transport of droplets, or any effect due to gravity.

8.2.2 Droplet Discretisation

The model uses a geometrical discretisation of the drop volume scale, similar to that reported by Hounslow *et al.* (1988). The characteristic volume of drops in any given class is $\sqrt{2}$ times the characteristic volume of the previous class, corresponding to a diameter ratio of $2^{1/6}$. Because of the $\sqrt{2}$ ratio, the characteristic volume of the classes doubles every second class. Figure 8.1 is the schematic diagram showing the discretisation of drop classes. Although any other ratio could have been used, we found that the $\sqrt{2}$ ratio is a sensible balance between generating fine enough drop bins from the experimental drop measurements and not requiring excessive CPU times.

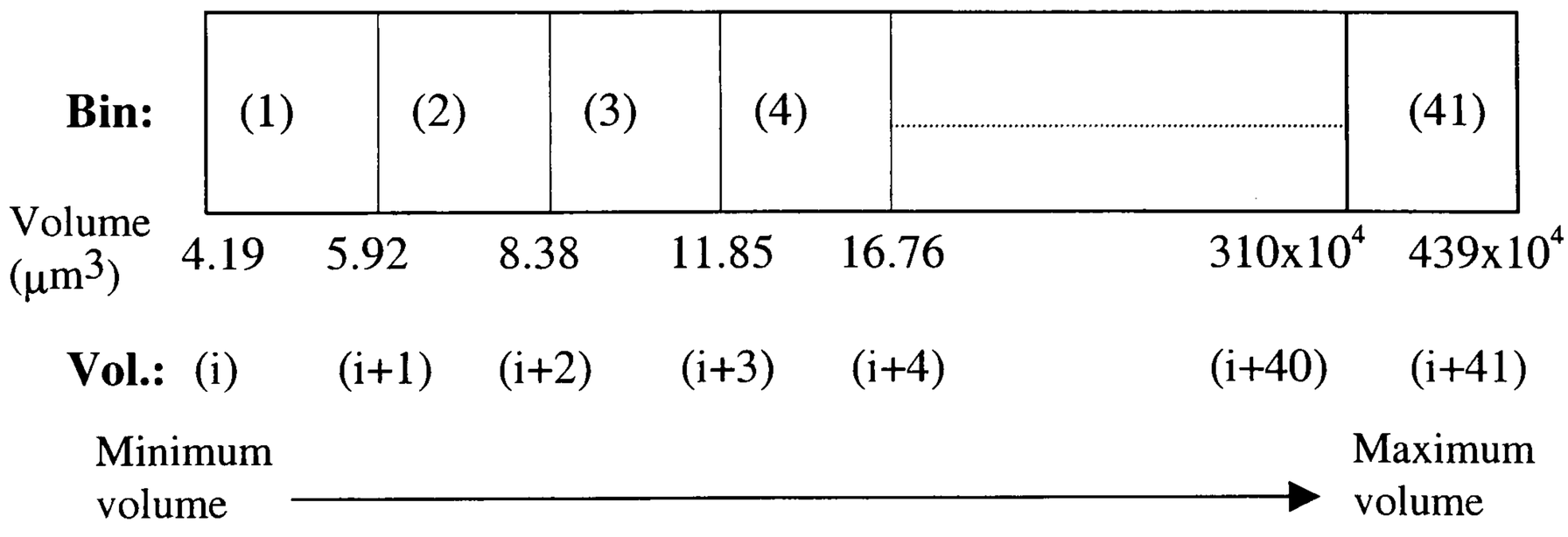

Figure 8.1: The discretised volume bins of droplets used in the model

8.2.3 The Continuity Equation of Volume Fraction

On the basis of the assumptions and the discretisation rule described above, the full continuity equation of drop distribution based on the discretised population balance equation can be simplified to:

$$\frac{\partial}{\partial t} f_i(t) = B_i^+(t) + B_i^-(t) + C_i^+(t) + C_i^-(t) \tag{8.1}$$

Where $B_i^+(t)$ and $B_i^-(t)$ are the birth and death rates of drops occurring in class i because of breakage, $C_i^+(t)$ and $C_i^-(t)$ are the birth and death rates in class i due to coalescence and $f_i(t)$ is the volume fraction of drops in class i of a distribution defined as:

$$f_i = \frac{\sum_k v_k n_{k,i}}{\sum_j \left(\sum_k v_k n_{k,j} \right)} \tag{8.2}$$

Where $n_{k,j}$ is the number of drops with volume v_k in any class j of the distribution.

For this the condition of $\sum_i f_i = 1$ is always valid.

8.2.3.1 Breakage Equations

In establishing the droplet breakage term, the binary breakage mechanism is adopted. Although other methods of droplet breakage have been reported (Tsouris & Tavlarides, 1994), this assumption allows simple relationships and less computational complexity. Under this assumption, a drop of volume, v, will break up into two equally sized drops of a volume, v/2. By the conservation of volume, the breakage of drops from a class *i* will result in a fraction of volume available in class *i* travelling two classes down to class (*i*-2). If g_i is the fraction of a drop volume leaving class *i* per unit of time, commonly known as the breakage rate then the class *i* undergoes a loss of volume of $g_i f_i V_d$ per unit of time, which is expressed in terms of volume fraction as:

$$\frac{\partial f_i}{\partial t} = -g_i f_i \tag{8.3}$$

Applying the conservation of volume, the same amount of volume allocated to class (*i*-2) is:

$$\frac{\partial f_{i-2}}{\partial t} = g_i f_i \tag{8.4}$$

Therefore:

$$B_i^-(t) = -g_i f_i(t) \tag{8.5}$$

$$B_i^+(t) = g_{i+2} f_{i+2}(t) \tag{8.6}$$

In a more concise manner, $\mathbf{g}$ is defined as a vector containing the breakage rates over all classes of the distribution. The breakage rates are assumed to be independent of time, and their dimension is the reciprocal of time (/s). As the rates are defined in terms of fractions of volume, their values are in between 0 and 1. Furthermore, in order to maintain the consistence of the breakage equation with the drop classes, no droplets with a volume less than a minimum volume in the distribution should be formed by breakage, for example, breakage is not permitted in the first two classes, consequently $g_1 = g_2 = 0$.

8.2.3.2 Coalescence Equations

Coalescence is a more complex phenomenon than breakage as it involves drops from various classes of a distribution. The general scheme would be a drop from a class i interacting with a drop from a class j, and the resulting coalesced drop moving into a suitably identified class k. In the model, only three types of drop interactions are considered in establishing the coalescence equations, and they are:

Type (a): coalescence of drops from the same class ($j=i$),

Type (b): coalescence of drops from two adjacent classes ($j=i\pm1$),

Type (c): coalescence of drops from classes one class apart ($j=i\pm2$).

In other words, a drop from any given class can interact with drops from five classes. It is assumed that coalescence always involves the same number of coalescing drops. This is necessary in order to identify the class into which the resulting coalesced drop falls. In the model, the coalescence is also a binary process, meaning that one given drop will coalesce with another drop. This is in line with the assumptions commonly reported in the literature regarding coalescence (Coulaloglou & Tavlarides, 1976, 1977; Tsouris & Tavlarides, 1994). When two drops are coalescing with volume v_i and v_j respectevely, the volume of the resulting drop is thus $v_i + v_j$. To fullly model the effect of drop coalescence, one needs to determine to which class k this total volume corresponds. This operation is made difficult by the choice of a geometric discretization of the volume range.

For the three interactions described above, one needs to identify the class k for each interaction. For example, for Type (a), $k = i+2$. For Types (b) and (c), the coalesced droplets do not fall into a single drop class, but two adjacent ones, i.e. classes $(j+1)$ and $(j+2)$, with $j>i$. In those cases, ratios are used to properly describe how the total volume is split between the two classes after coalescence. For Type (b), for instance, a fraction $k_{b,1}$ will be allocated to class (j+1), while a fraction $k_{b,2} = 1 - k_{b,1}$ to class (j+2). Likewise for Type (c), a fraction $k_{c,1}$ will be allocated to class (j+1), and a fraction $k_{c,2} = 1 - k_{c,1}$ to class (j+2). The values of $k_{b,1}$, $k_{b,2}$, $k_{c,1}$ and $k_{c,2}$ can be computed based on the assumption that droplet volumes are uniformly distributed in each class as: $k_{b,2} = \frac{1}{2\sqrt{2}}$, $k_{b,1} = 1 - \frac{1}{2\sqrt{2}}$, $k_{c,1} = \frac{3}{2} - \sqrt{2}$ and $k_{c,2} = \sqrt{2} - \frac{1}{2}$.

$\beta_{i,j}$ is the fraction of a drop volume in class i interacting with class j per unit of time, known as the coalescence rate. The class i thus undergoes a loss of volume $\beta_{i,j} f_i V_d$ expressed in terms of volume fraction as:

$$\left.\frac{\partial f_i}{\partial t}\right)_j = -\beta_{i,j} f_i \tag{8.7}$$

In a similar manner, the class j undergoes a loss of volume $\beta_{j,i} f_j V_d$ as

$$\left.\frac{\partial f_j}{\partial t}\right)_i = -\beta_{j,i} f_j \tag{8.8}$$

This will result in gains in both classes (j+1) and (j+2) respectively

$$\frac{\partial f_{j+1}}{\partial t} = k_{x,1}(\beta_{i,j} f_i + \beta_{j,i} f_j) \tag{8.9}$$

$$\frac{\partial f_{j+2}}{\partial t} = k_{x,2}(\beta_{i,j} f_i + \beta_{j,i} f_j) \tag{8.10}$$

where x stands for the type of interactions involved (x = 'b' or 'c'). In the particular case of Type (a), this results in a loss in class i as:

$$\left.\frac{\partial f_i}{\partial t}\right)_i = -\beta_{i,i} f_i - \beta_{i,i} f_i = -2\beta_{i,i} f_i \tag{8.11}$$

and a gain in class (i+2) being:

$$\left.\frac{\partial f_{i+2}}{\partial t}\right)_i = 2\beta_{i,i} f_i \tag{8.12}$$

Type (a) will generate a loss

$$C^-_{i,(a)} = \left.\frac{\partial f_i}{\partial t}\right)_{loss\,(a)} = -2\beta_{i,i} f_i \tag{8.13}$$

as well as a gain:

$$C^+_{i,(a)} = \left.\frac{\partial f_i}{\partial t}\right)_{gain\,(a)} = 2\beta_{i-2,i-2} f_{i-2} \tag{8.14}$$

Likewise Type (b) will induce a loss in class *i:*

$$C^-_{i,(b)} = \left.\frac{\partial f_i}{\partial t}\right)_{1oss\,(b)} = -\beta_{i,i-1} f_i - \beta_{i,i+1} f_i \tag{8.15}$$

as well as a gain:

$$C^+_{i,(b)} = \left.\frac{\partial f_i}{\partial t}\right)_{gain\,(b)} = k_{b,1}(\beta_{i-2,i-1} f_{i-2} + \beta_{i-1,i-2} f_{i-1}) \tag{8.16}$$

$$+ k_{b,2}(\beta_{i-3,i-2} f_{i-3} + \beta_{i-2,i-3} f_{i-2})$$

The loss for Type (c) in class i is

$$C^{-}_{i,(c)} = \frac{\partial f_i}{\partial t}\Bigg)_{loss\,(c)} = -\beta_{i,i-2} f_i - \beta_{i,i+2} f_i \tag{8.17}$$

and the gain is:

$$C^{+}_{i,(b)} = \frac{\partial f_i}{\partial t}\Bigg)_{gain(c)} = k_{c,1}(\beta_{i-3,i-1} f_{i-3} + \beta_{i-1,i-3} f_{i-1}) \tag{8.18}$$

$$+ k_{c,2}(\beta_{i-4,i-2} f_{i-4} + \beta_{i-2,i-4} f_{i-2})$$

The coalescence rates $\beta_{i,j}$ can then be gathered into a non-symmetrical matrix

$\boldsymbol{\beta}$. The total loss B^{-}_{i} undergone by class i is derived as the sum of the losses:

$$C^{-}_{i} = -\left(2\beta_{i,i} + \beta_{i,i-1} + \beta_{i,i+1} + \beta_{i,i-2} + \beta_{i,i+2}\right) f_i \tag{8.19}$$

It can be seen that five coefficients $\beta_{i,j}$ are needed at most in order to describe the effects of coalescence on class i, and this is the consequence of only three drop interactions being accounted for in the model. The overall coalescence rate in class i is

$$\beta_{i,total} = 2\beta_{i,i} + \beta_{i,i-1} + \beta_{i,i+1} + \beta_{i,i-2} + \beta_{i,i+2} \tag{8.20}$$

The three individual rates for each Type of interaction can also be computed as:

$$\beta_{Type(a),i} = 2\beta_{i,i} \tag{8.21}$$

$$\beta_{Type(b),i} = \beta_{i,i-1} + \beta_{i,i+1} \tag{8.22}$$

$$\beta_{Type(c),i} = \beta_{i,i-2} + \beta_{i,i+2} \tag{8.23}$$

All coalescence rates are considered to be independent of time, and their dimension is the reciprocal of time (/s). Because the rates are also defined in terms of fractions of volume, their values are too in between 0 and 1. Furthermore, there are also restrictions on coalescence, similar to the breakage, as coalescence in some of the drop classes would result in drops with the size, which is larger than a maximum volume in the distribution. These interactions include the first four and the last three drop classes. In these cases, only the interactions of drops that result drop volumes being less or equal to the maximum volume are considered in the model.

8.2.3.3 The Combined Model

By combining both the breakage and coalescence equations, a linear differential model is obtained as:

$$\frac{d}{dt}(\mathbf{f}) = (\mathbf{A})(\mathbf{f}) \tag{8.24}$$

where $\mathbf{f}$ stands for the vector consisting of the volume fractions f_i, and $\mathbf{A}$ a mass matrix that is derived from both vector $\mathbf{g}$ and matrix $\boldsymbol{\beta}$. The volume fractions in all the classes in eq. (24) are a function of time. To solve the linear differential equation, an initial condition is needed, which is a droplet size distribution at any given time from experiments.

By varying vector $\mathbf{g}$ and/or matrix $\boldsymbol{\beta}$, the solution of $\mathbf{f}$ can be modified so that it fits the experimental distributions $\mathbf{f}_{exp}$. An objective function can then be built, which utilises $\mathbf{g}$ and $\boldsymbol{\beta}$ as variables to compute the normal of the error vector $\left(\mathbf{f}-\mathbf{f}_{exp}\right)$. The error returned by the objective function is minimised by varying vector $\mathbf{g}$ and matrix $\boldsymbol{\beta}$. When global minima of the objective function are reached, $\mathbf{g}$ and $\boldsymbol{\beta}$ are then the breakage and coalescence rates that govern the evolution of the volume fractions $\mathbf{f}_{exp}$ with time. The model equations are solved using Matlab in the form of several code modules, the integration is carried out using Euler's method with a time step of 1 minute. It can be seen that the advantage of not pre-assume any functional form for breakage and coalscence rates in the model is achieved at the expense of minimizing a large number of parameters.

8.3 Experimental Facilities and Procedures

8.3.1 Experimental Set-Up

All DSD data used in the model were collected from the stainless steel OBR, which was operated with a fixed baffle geometry of $\alpha = 25\%$ and $L = 315mm$. Two liquid-liquid recipes were studied, the details of which are outlined in Table 8.1. MMA(1) is the same recipe as that used in the heat transfer droplet size distribution experiments. MMA(2), on the other hand, contains a large amount of surfactants, which significantly inhibits coalescence and allows the system to operate with breakage only. Droplet size distributions were obtained using the same sampling and analysis technique as outlined in Chapter 7.

Table 8.1: Specification of MMA Recipes

	MMA(1)	**MMA(2)**
Continuous Phase:		
Water	16 kg	16 kg
Colloid	0.38 kg	0.38 kg
Surfactant 1	2.1 g	21 g
Surfactant 2	0.42 g	0.42 g
Ammonia Solution	8.6 g	8.6 g
Dispersed Phase:		
MMA	9 kg	9 kg

8.3.2 Procedures

8.3.2.1 Breakage-Only Experiments

Experiments were performed to determine the breakage rates of droplets in a non-coalescing system. Recipe MMA(2) was used in these experiments and the DSD was measured every 10 minutes for a time period of 50 minutes. This procedure was carried out at frequnecies of 0.6, 1.0 and 1.4 Hz at an amplitude of 75 mm and at a further two amplitudes of 50 and 100 mm at a frequency of 1.0 Hz. The DSD data collected are listed in Appendix 3.2.

8.3.2.2 Experiments with Breakage and Coalescence

Table 8.2: Range of operating parameters studied in experiments to determine breakage and coalescence rates

x_o (mm)	Initial frequecny (Hz)	Final frequency (Hz)
75	1.4	0.6
75	1.4	0.8
75	1.4	1.0
50	2.0	0.8
100	1.0	0.8

Experiments using recipe MMA(1) were conducted to obtain DSD data from a system in which breakage and coalescence occurred. The system was initially agitated at an oscillatory velocity of 100 mm/s for 30 minutes, which allowed a stable dispersion to be achieved, and the drop size distribution was determined. This was followed by a step reduction in the oscillation frequency and DSDs were again measured in 10 minute intervals for 50 minutes. The range of operating conditions studied is outlined in Table 8.2 and the DSD data collected are listed in Appendix 3.2.

8.4 Results and Discussion

8.4.1 Breakage-Only Experiments

In the case of the breakage-only experiments, the high surfactant concentration of recipe MMA(2) effectively eliminates coalescence of droplets in the system. Under such conditions the model can be simplified by setting the coalescence rates to zero, i.e. $C_i^+(t)+C_i^-(t) = 0$. This simplified model was used to evaluate droplet breakage rates in the system under each of the conditions tested.

The effect of the oscillation frequency and amplitude on the droplet breakage rates are shown in Figures 8.2 and 8.3 respectively. Two significant features are exhibited by these graphs. Firstly, it can be seen that the droplet breakage rate is higher for larger droplet diameters. This is expected, as larger droplets are more likely to deform and break in a turbulently agitated system than smaller ones. Secondly, it is evident that breakage rates are higher at higher oscillation frequencies

and amplitudes. This is also expected as using a higher frequency or amplitude increases the energy dissipation in the system, which, in turn, results in a more turbulent flow field and a higher droplet breakage probability.

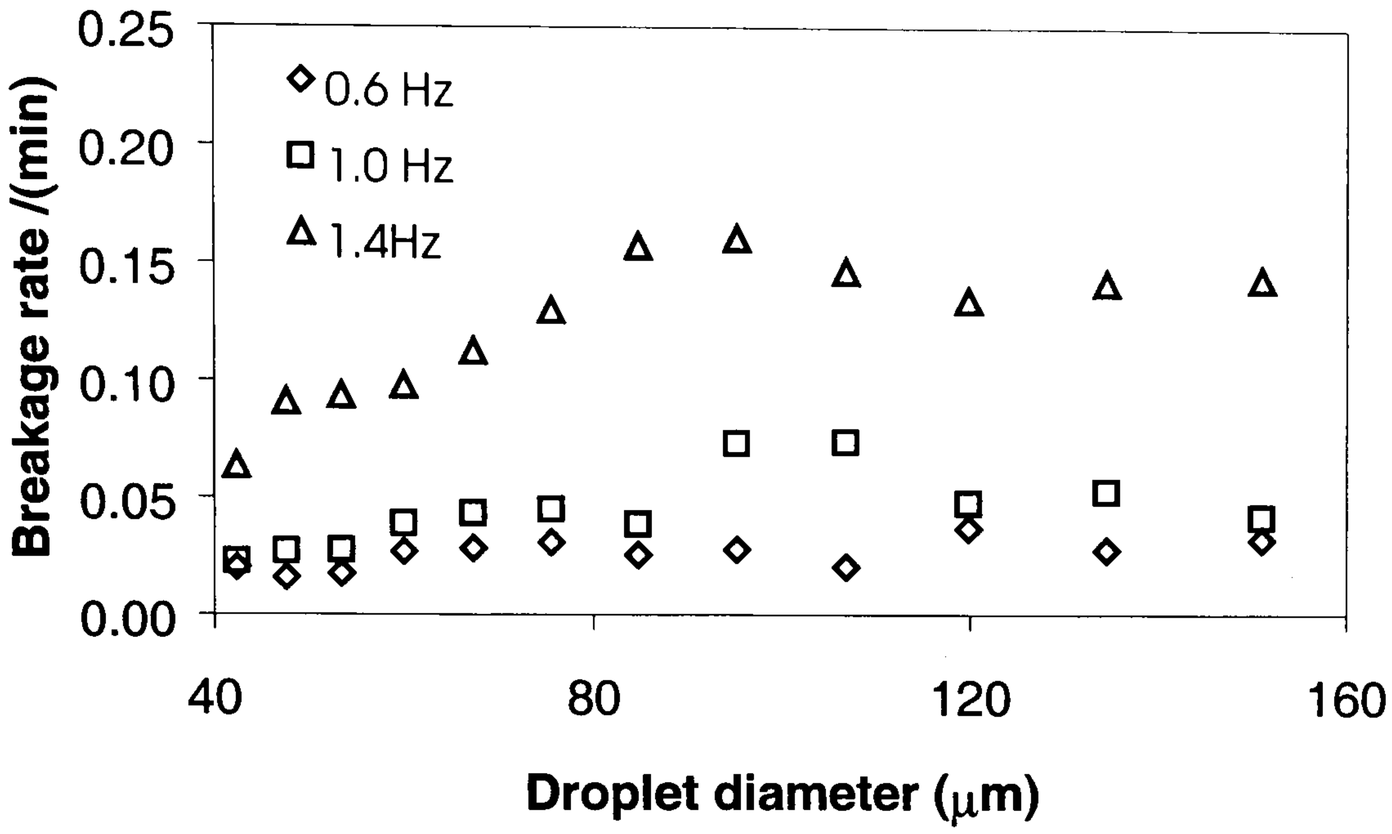

Figure 8.2: Effect of frequency on breakage rate (x_o = 75 mm)

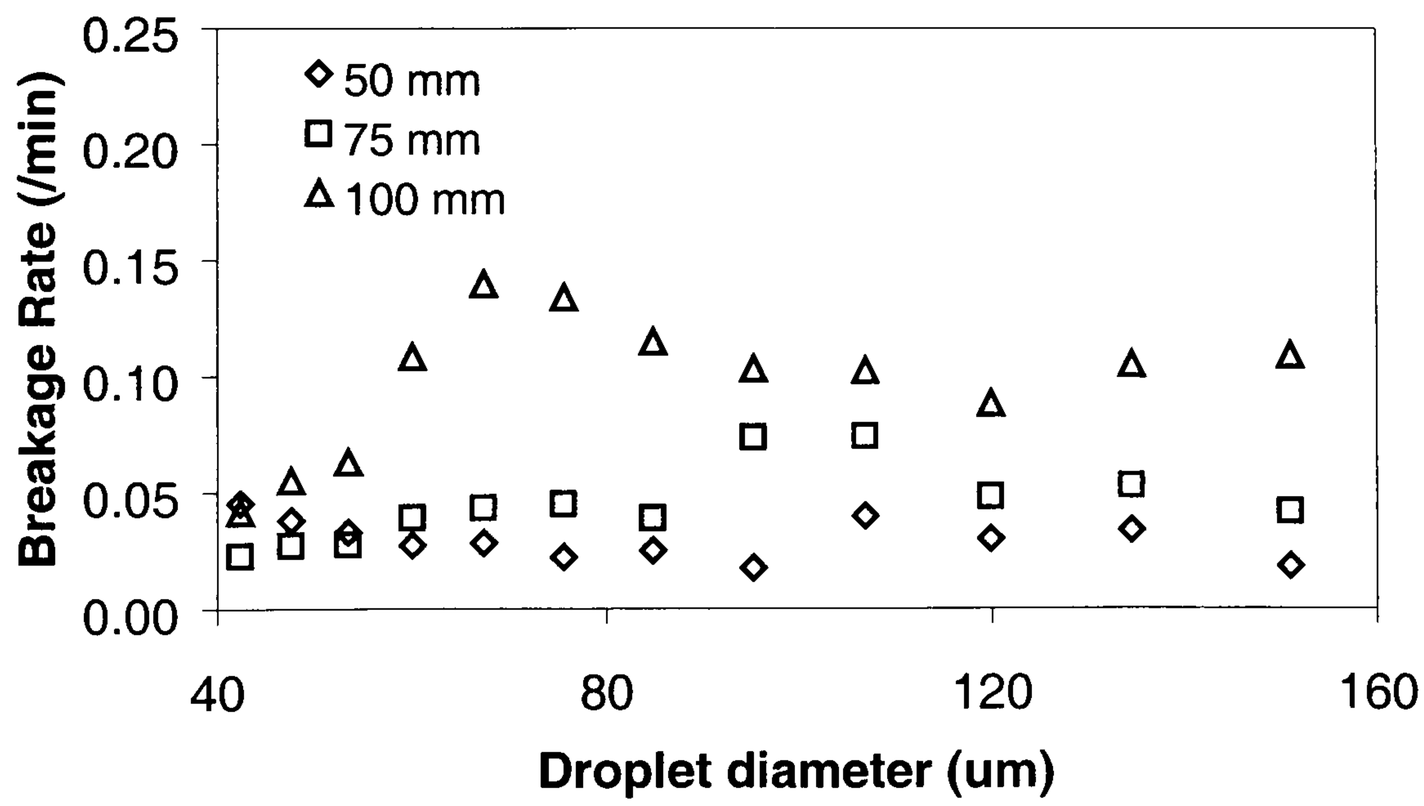

Figure 8.3: Effect of amplitude on breakage rate (f = 1.0Hz)

8.4.2 Experiments with Breakage and Coalescence

In the case where recipe MMA(1) was used, no simplifications were made to the PBE and the model, as described in section 8.2, was used to evaluate the breakage and coalescence rates. Figures 8.4 and 8.5 show respectively breakage and coalescence rates evaluated by the model over a range of operating parameters. It can be seen, from Figure 8.4, that varying the frequency had no identifiable effect on the calculated breakage rate with typical values of about 0.18 /s (accepting some scattering) being returned for each of the frequencies tested. This result could be due to the fact that the range of frequencies studied (0.6 – 1.0 Hz) may have been too narrow for the effect to be detected within the accuracy limits of the model. From Figure 8.5, it can be seen that the calculated coalescence rates vary significantly over the droplet size range under each of the conditions tested. Such variation is unlikely to be truly representative of what is physically happening in the system and is more likely to be a result of limitations of the model when dealing with the complex equations that describe the coalescence interactions. The scatter in the calculated breakage and coalescence rates is greater than in the case where the model was used for breakage only, indicating that accuracy is lost by increasing the number of parameters in the minimisation process. Generally it can be seen that the magnitude of the coalescence rates is larger than that of the breakage rate for the range of droplet sizes investigated. This implies that the coalescence mechanism plays a more dominant role in the formation of droplets in the OBR system and this can be attributed to the fact that the data used was collected after a step reduction in frequency. It is also evident, from the data plotted in Figure 8.6, that the percentages of the individual coalescence rates contribution to the overall are 24%, 39% and 37%

for the Type (a), (b) and (c) drop interaction respectively, which seems a reasonable result as there is no reason to assume any type to be dominant.

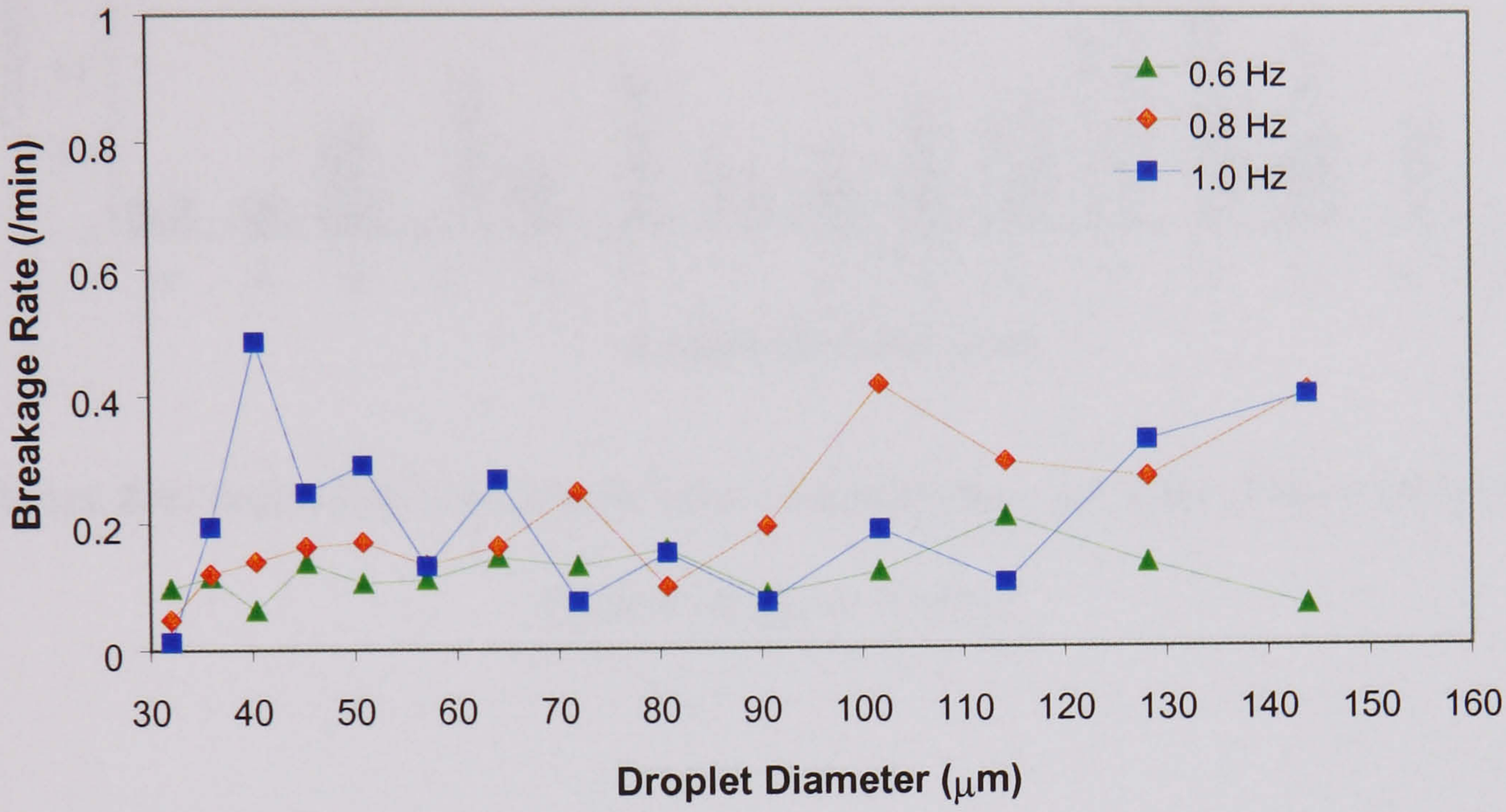

Figure 8.4: Effect of frequency on the evaluated breakage rate (x_o = 75 mm)

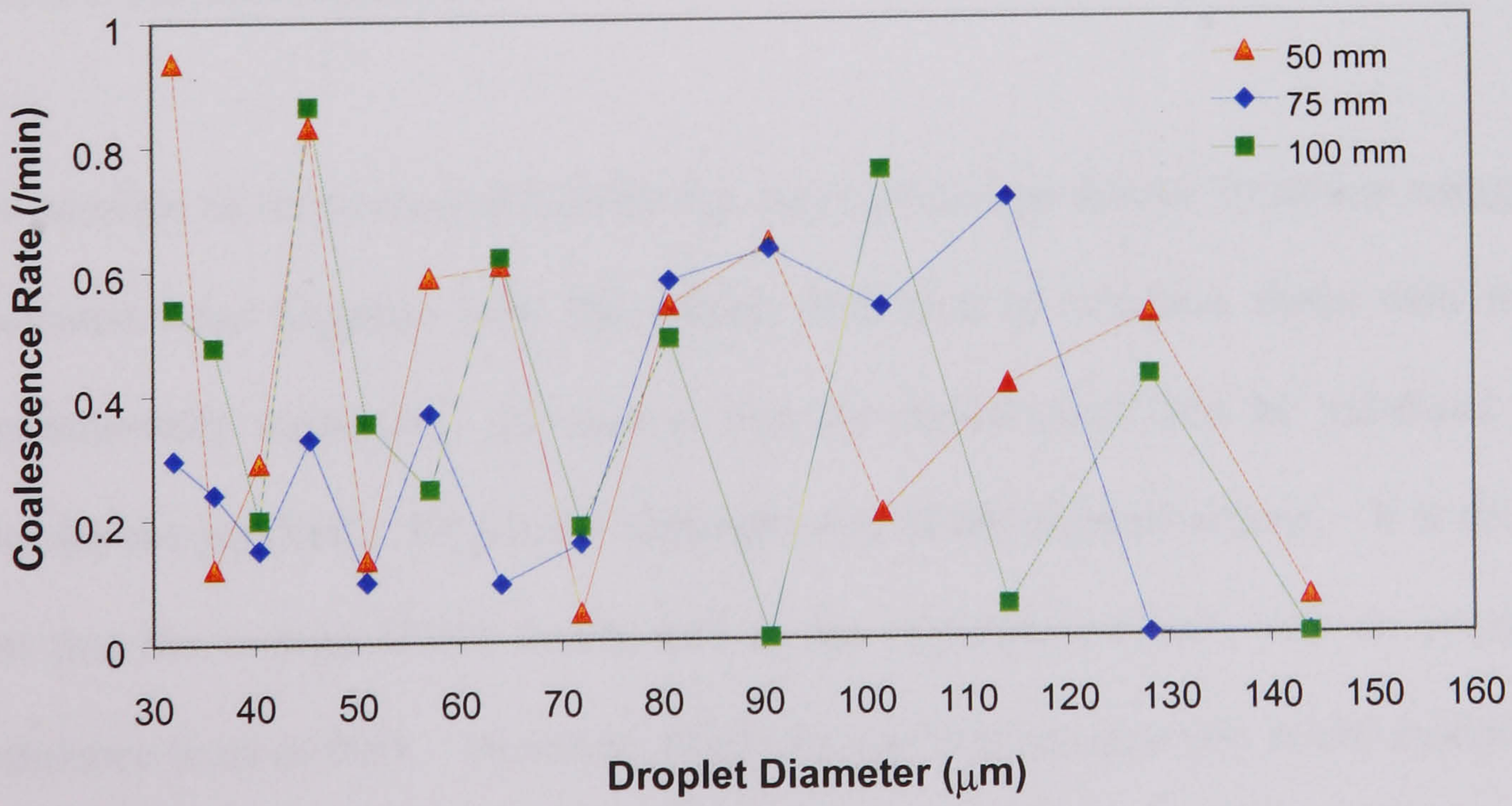

Figure 8.5: Effect of amplitude on coalescence rate (f = 0.8 Hz)

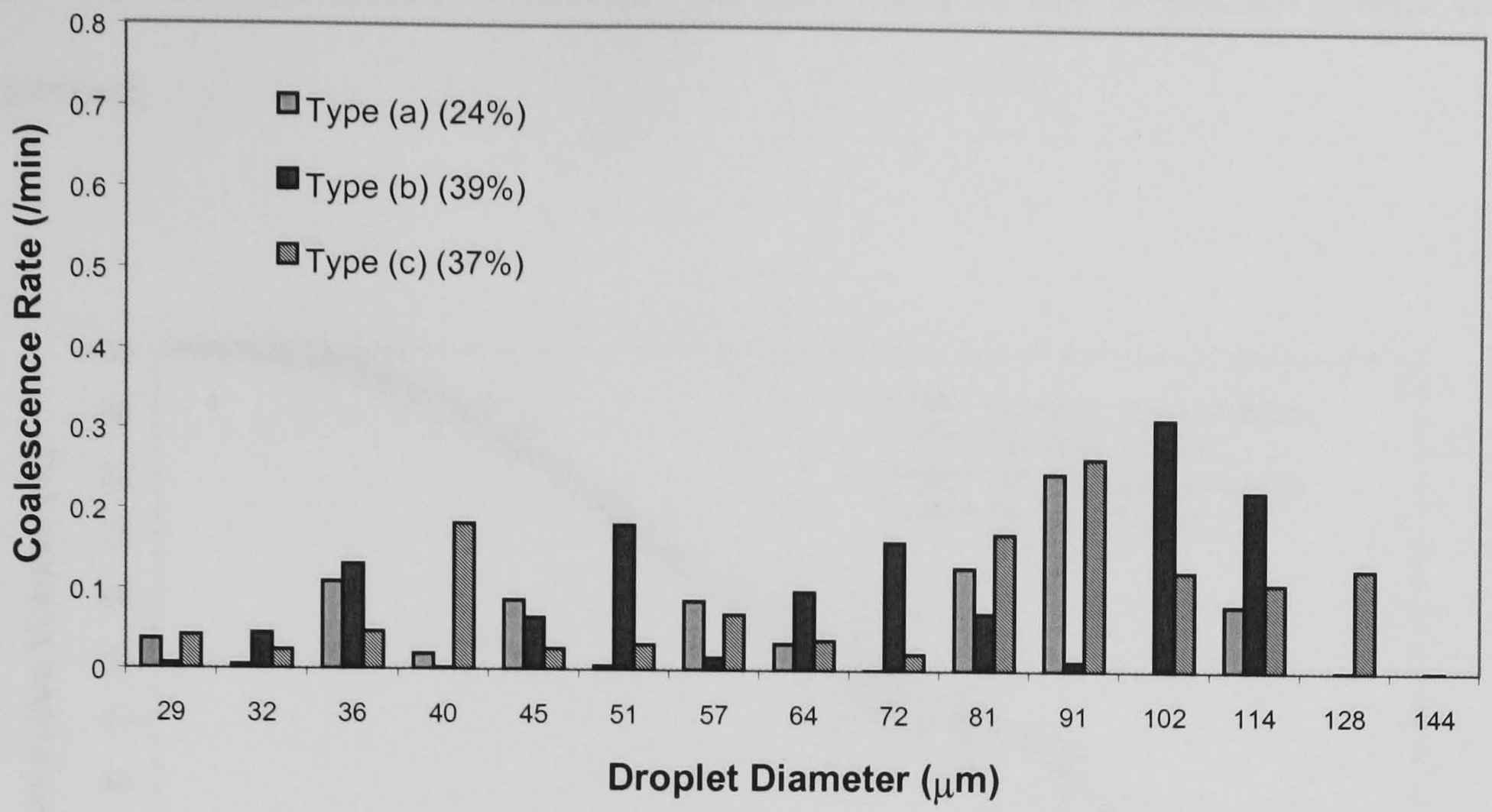

Figure 8.6: Individual coalescence rates evaluated for each type of drop interaction

(f = 0.8 Hz, x_o = 75 mm)

8.4.3 Model Validation and Robustness Test

8.4.3.1 DSD Reconstruction

It is possible to reconstruct the DSDs for every given operational condition using the calculated rates together with the model, and then to compare these with those experimentally measured. In such a way the model itself can be validated and assumptions justified. Figure 8.7 illustrates one of the reconstructions. It is clearly seen that the re-built DSDs match well to the experimental data with an averaged confidence level of 90%. However, from the constitutive equations of the model it is clear that the reliability of the breakage and coalescence rates is heavily relying upon the minimisation process, with effectively a matrix of close to 80 parameters being

minimised simultaneously. Therefore, the robustness of the model also needs to be examined.

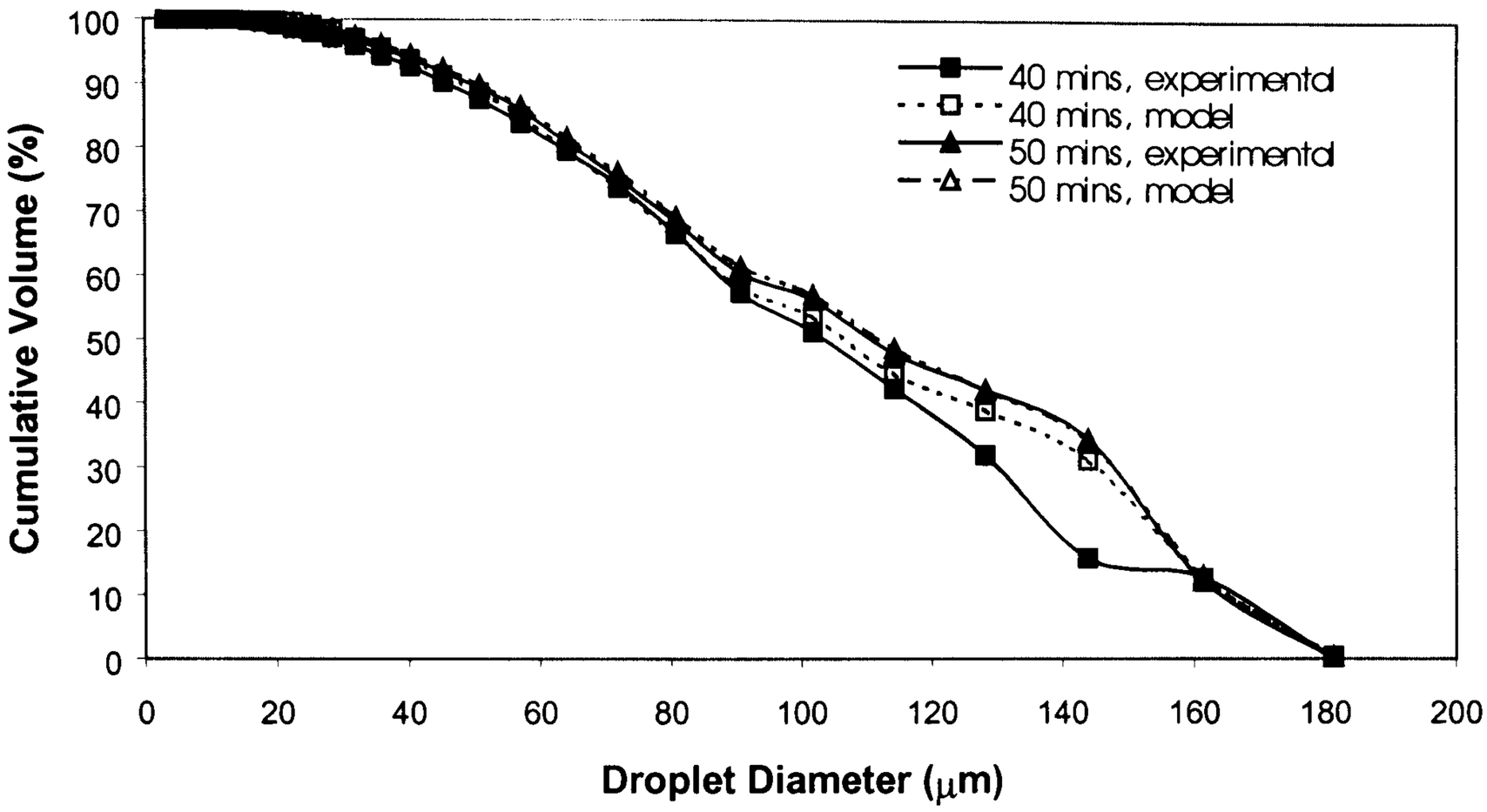

Figure 8.7: Comparison of DSDs between reconstructed and experimental measured (f = 0.6 Hz, x_o = 75 mm)

8.4.3.2 Robustness of the Model

The model was written in a Matlab programme, and there is a large number of parameters in the minimisation process (an average of between 70 and 80) to be minimised, as opposite to the traditional discretized population balance model by Laso et al. (1987) involving only a maximum of 10 variables. The aim of the minimisation carried out in our model is to achieve a global minimum for all the parameters, not local ones. In order to assess the reliability of the minimisation process, and in turn, the breakage and coalescence rates, we carried out a few simple exercises.

In the first test, user-defined breakage and coalescence rates, $\mathbf{g}$ and $\boldsymbol{\beta}$, were arbitrarily chosen, from which DSDs were generated for times from t=0 to t=100 with an interval of 10 minutes. The model was then applied to extract breakage and coalescence rates from these constructed DSDs. By comparing the extracted rates with the user-defined ones, the accuracy and the reliability of the model can be assessed. The tests are likely to depend on the number of sets of DSD curves being used as input to the model, therefore three numbers of DSD curves were chosen for the test. Test 1 employs two sets of DSD curves, corresponding to t=0 and t=10; Test 2 uses 6 sets, corresponding to t=0, 10, 20, 30, 40 and t=50; and Test 3 utilises 11 set, corresponding to t=0, 10, 20, 30, 40, 50, 60, 70, 80, 90 and t=100.

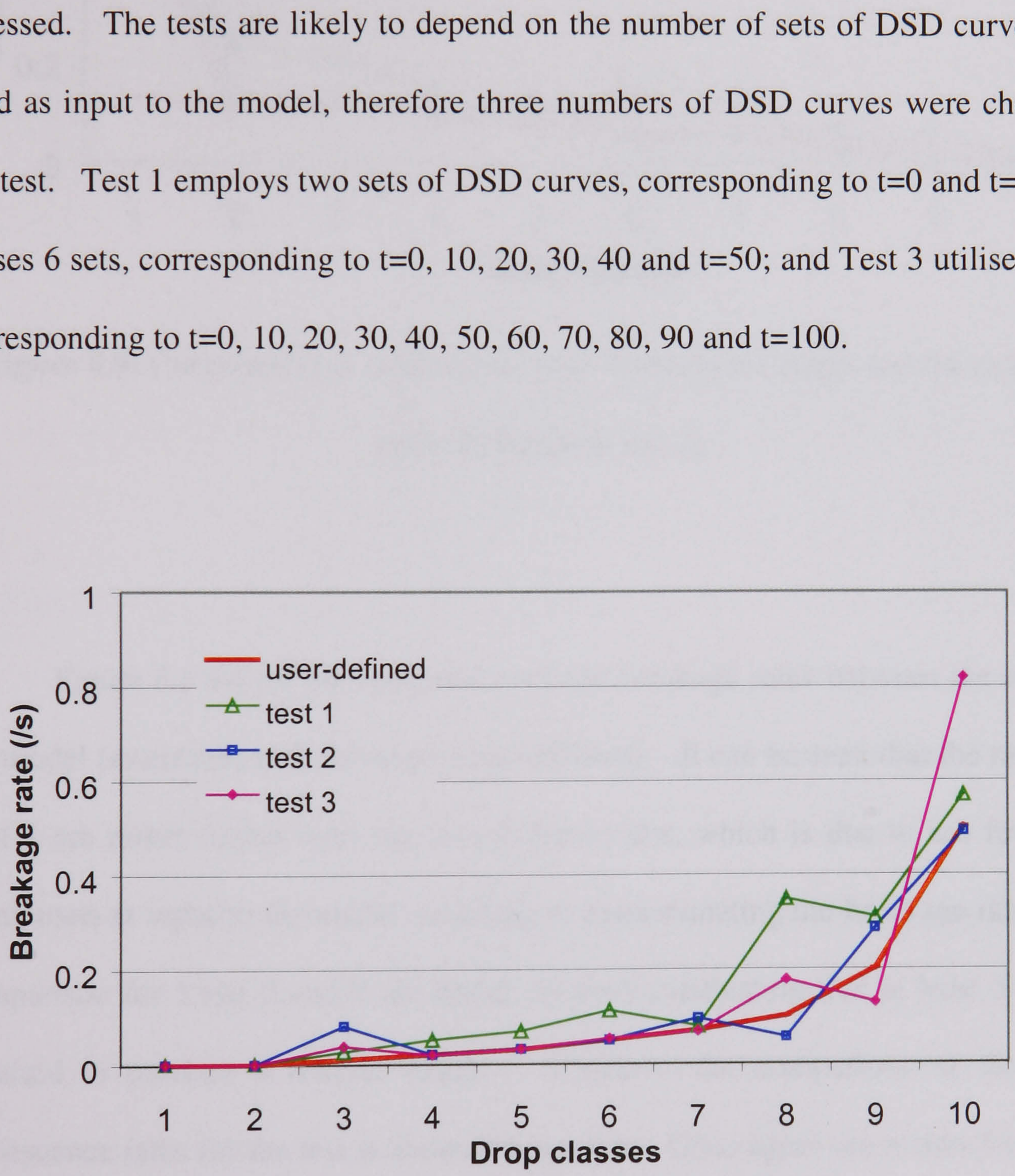

Figure 8.8: Comparison of breakage rate between the target and the extracted ones

(Robustness test 1)

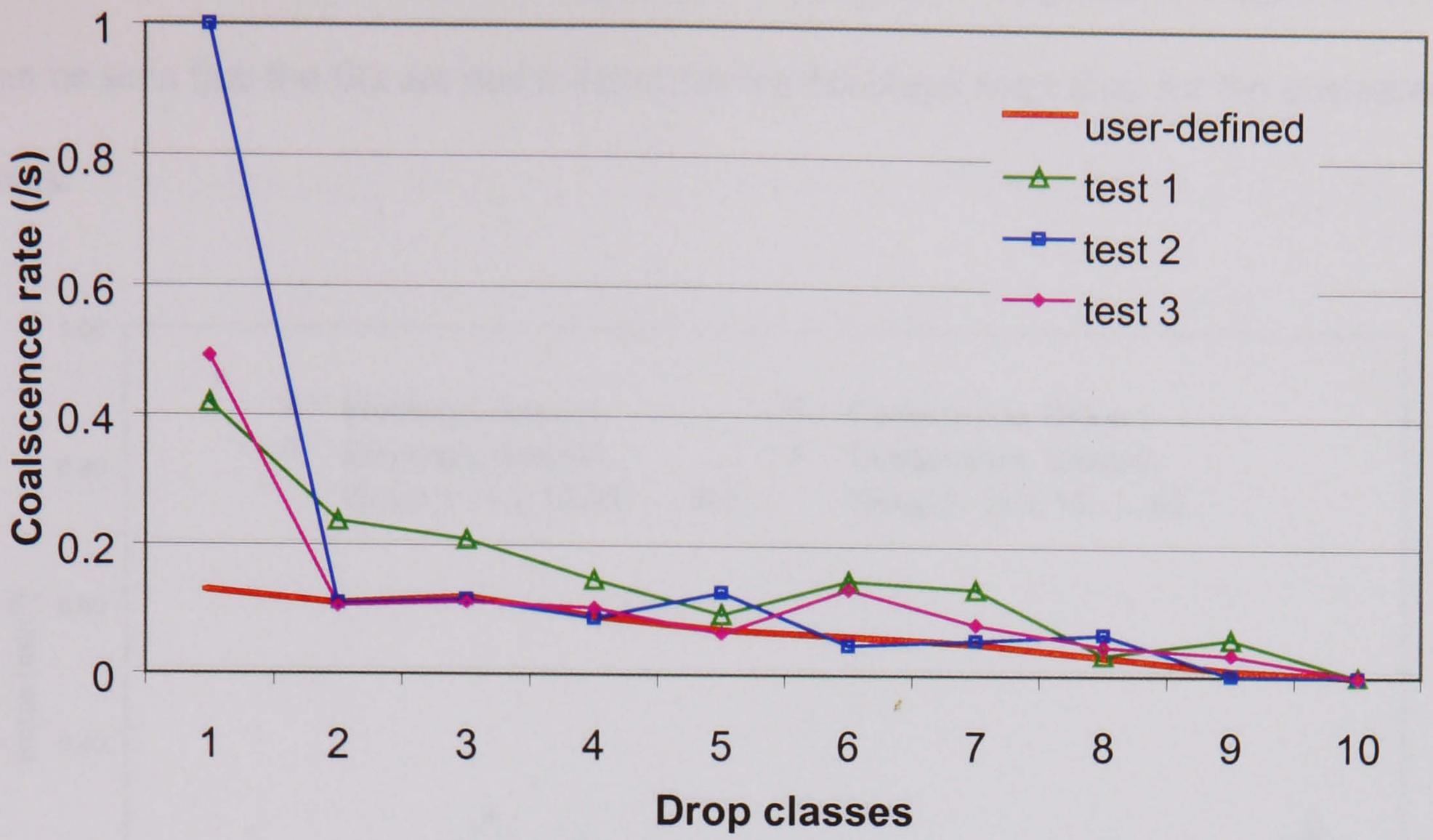

Figure 8.9: Comparison of coalescence rates between the target and the extracted ones (Robustness test 1)

Figure 8.8 shows the comparison of the breakage rates between the output of the model (extracted) and the target (user-defined). It can be seen that the rates from Test 1 are rather higher than the user-defined rates, which is due to too few DSDs being used as input to the model, resulting in overestimating the breakage rates. The comparison for Tests 2 and 3 are better, however, indicating that at least 5 DSDs a required to produce a reliable result. Similarly, the comparison of the overall coalescence rates for the test is shown Figure 8.9. Once again the results from Tests 2 and 3 gave a better fit than Test 1. The number of experimental data sets used in the model are usually either 5 or 6, which is within the range required.

Another test involves two groups of DSDs obtained at t=0, 10, 20, …, 100 minutes and at t= 5, 15, 25, …, 95 minutes respectively. The fits of both breakage

and coalescence rates for the two groups of DSDs are compared in Figure 8.10. It can be seen that the fits are much better for the breakage rates than for the coalescence rates.

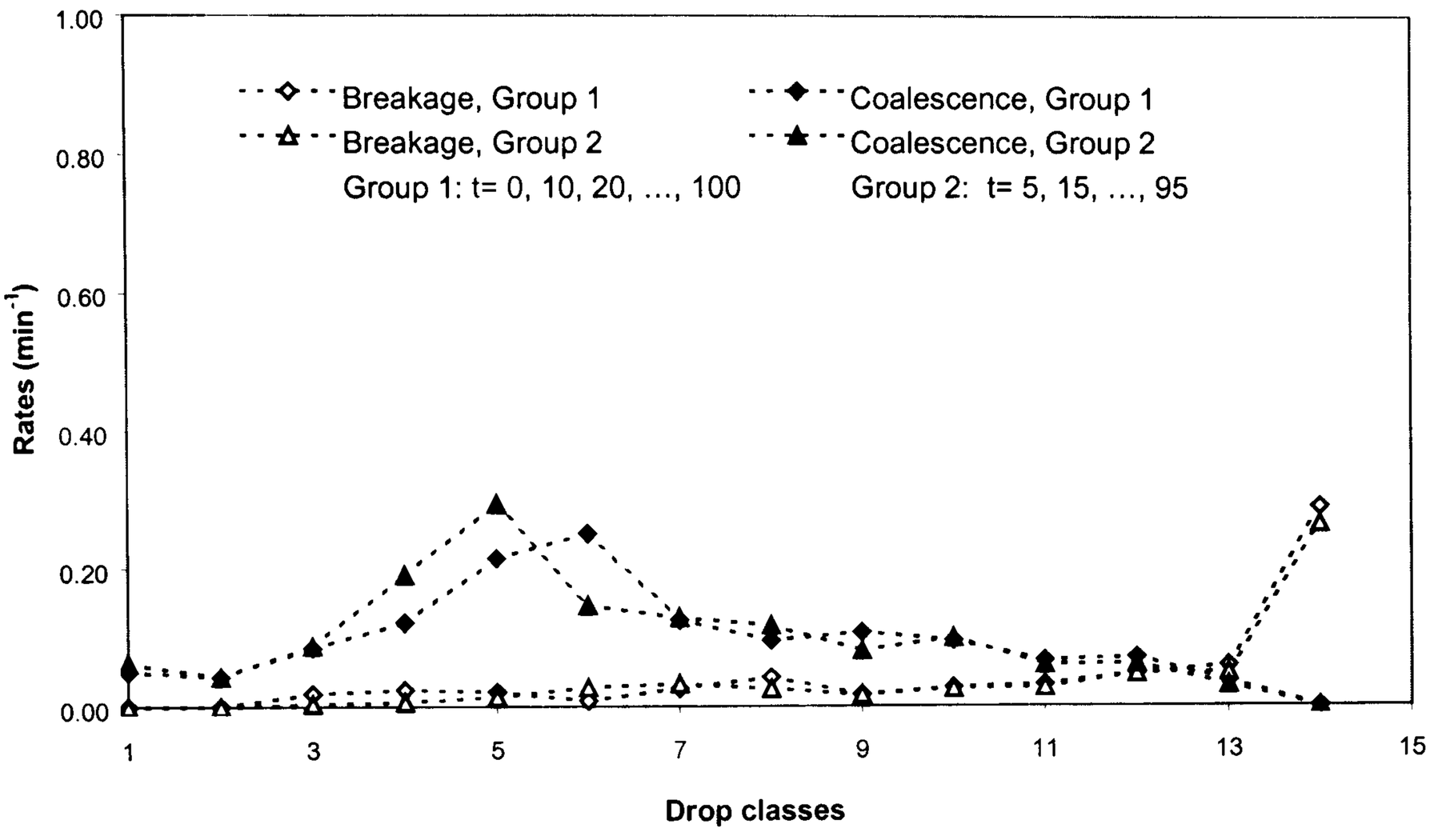

Figure 8.10: Comparison of breakage and coalescence rates (Robustness test 2)

In summary, the results from Figures 8.8 to 8.10 indicate that the model is fairly robust in evaluating the breakage and coalescence rates, though some levels of discrepancies exist between the target and re-evaluated rates. At this early stage of the model development these results are satisfactory but the key area for future development is the improvement of accuracy when dealing with experimental data.

8.4.4 Comparison of Scale-Up

Droplet size distributions have previously been studied in a bench scale 50-mm diameter OBR (Ni et al., 1998), and the data can be used in conjunction with the

model to evaluate the breakage and coalescence rates in the bench scale OBR. These can then be compared with that evaluated for the pilot OBR of 210 mm in diameter. Figures 8.11 and 8.12 show such comparison at similar oscillatory velocities for breakage and coalescence rate respectively. It can be seen that the rates of breakage and coalescence are of a same magnitude for both OBR systems. This indicates that the breakage and coalescence rates evaluated are independent of reactor sizes, or in other words, the scale-up in rates is approximately linear within the OBR systems.

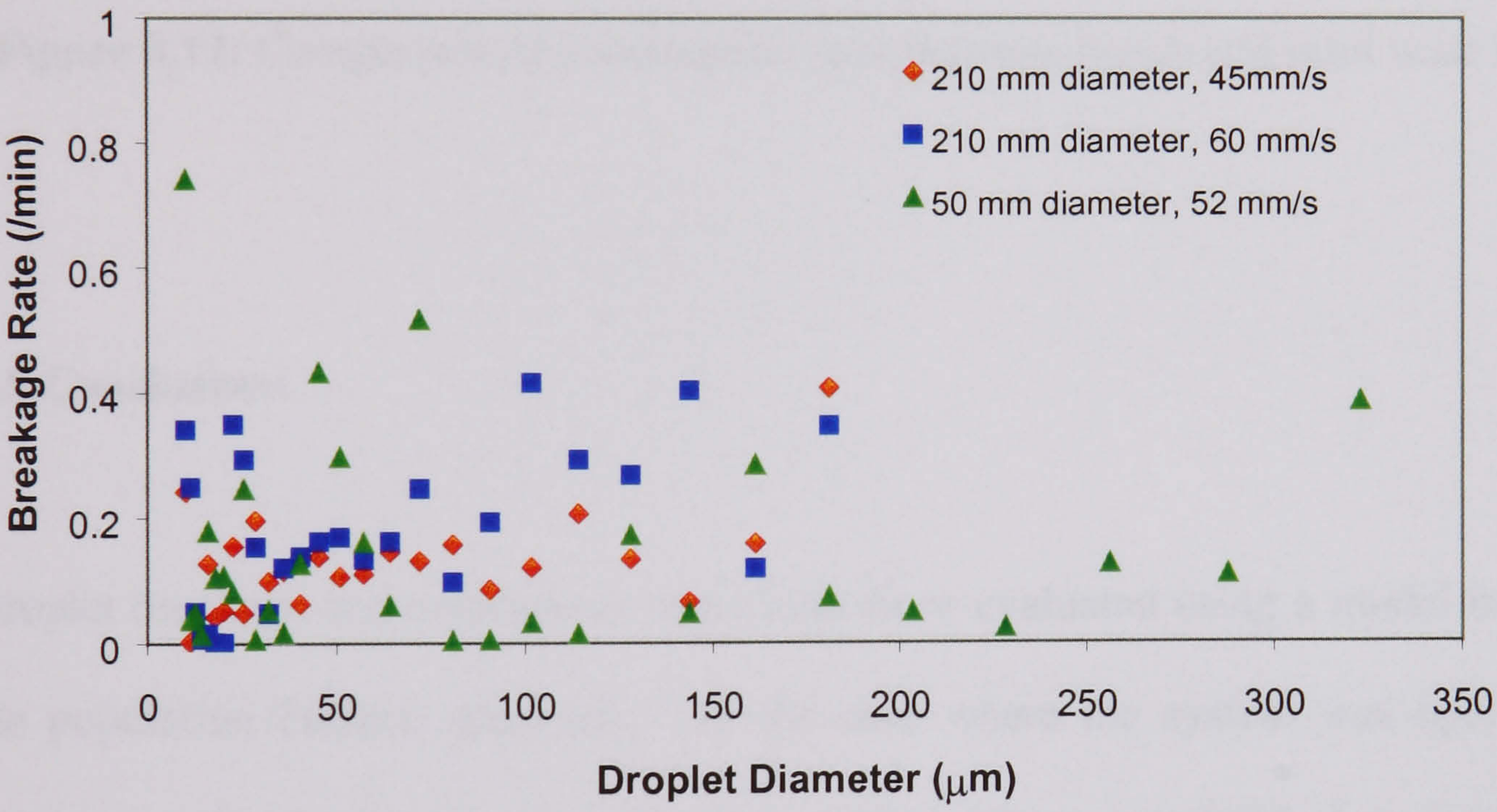

Figure 8.11: Comparison of breakage rates between bench and pilot scale OBRs

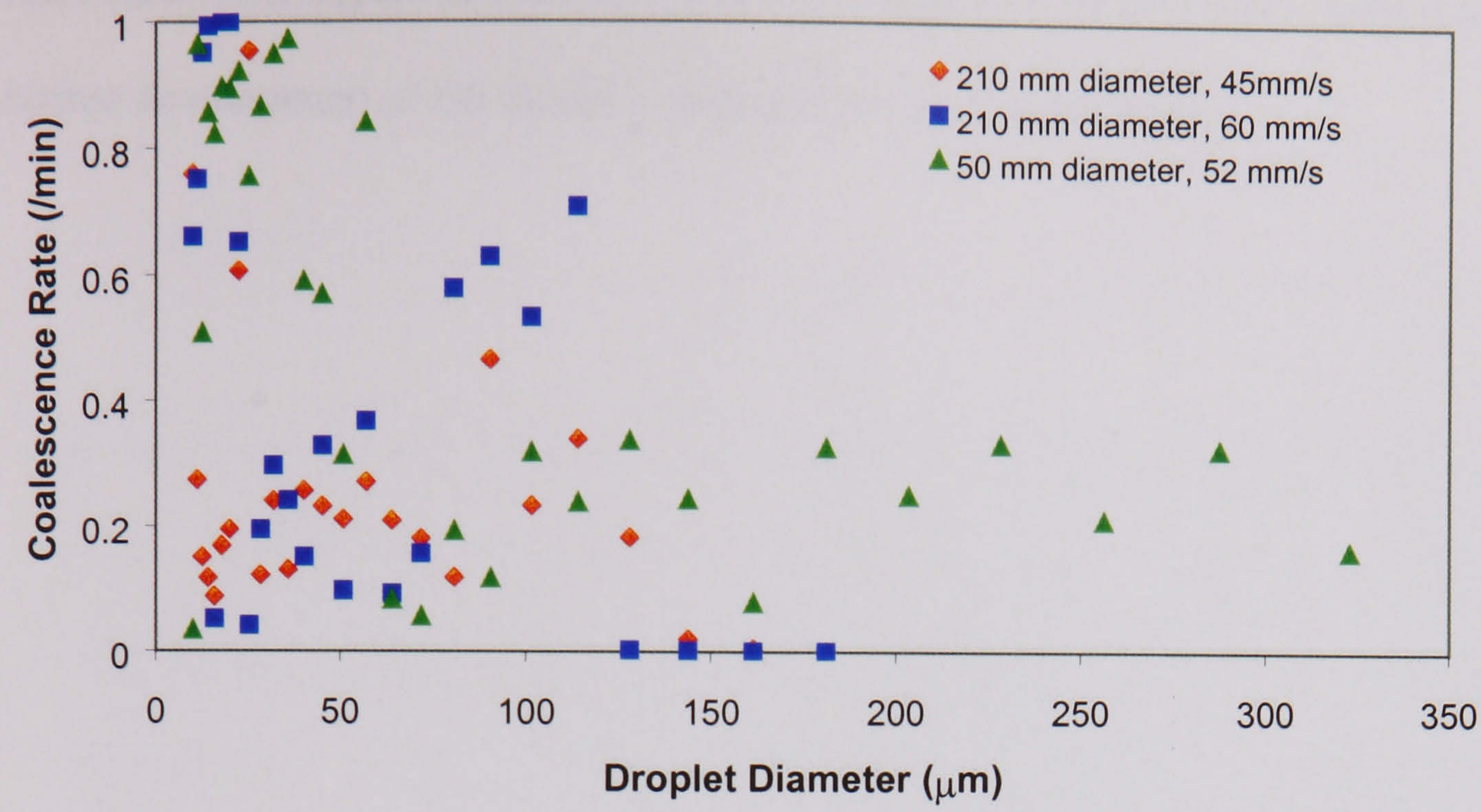

Figure 8.12: Comparison of coalescence rates between bench and pilot scale OBRs

8.5 Conclusions

Droplet breakage and coalescence rates have been evaluated using a model based on the population balance approach. In the case where the system was operated as breakage only, the breakage rates were calculated from a simplified version of the model and indicated that droplet breakage increased with increases in the oscillation frequency or amplitude. In the case where both breakage and coalescence were present coalescence rates were generally evaluated to be higher than breakage rates, which is expected due to the operational conditions of the system. Of the three types of coalescence interaction (a, b and c) considered by the model, neither was observed to be dominant, indicating a near equal probability a drop undergoing either of the interactions. On comparison with results obtained form data in a bench scale OBC, breakage and coalescence rates were observed not to be influenced by column size. The robustness of the model was examined and found to be satisfactory. The results

calculated from experimental data, however, showed a lot of scatter, indicating that further development of the model is required to improve accuracy.

9 SUSPENSION POLYMERISATION

9.1 Introduction

A model suspension polymerisation reaction of MMA was carried out to test the effect of operating conditions on the characteristics of the polymer produced. Various oscillation frequencies, oscillation amplitudes, baffle spacings and baffle free areas were used in the investigation.

9.2 Experimental Facilities and Procedures

9.2.1 Apparatus and Materials

The stainless steel oscillatory baffled reactor was used in all suspension polymerisation tests. The hole in the base of the column was fitted with a plug as there was concern that a valve may become blocked by build-up of polymer during the reaction. A thermocouple was located in the column, below the lowest baffle, as well as on the jacket inlet and outlet streams.

The reaction mixture consisted of an aqueous phase and an organic phase. The aqueous phase was the same as that used in the heat transfer and droplet size studies, details of which given in Chapter 6. The organic phase consisted of 9 kg of MMA plus 86 g of

initiator. All materials were supplied by Ineos Acrylics Ltd. Further to this, methylethylketone (MEK) was also required for washing the reactor to remove fouling.

9.2.2 Procedures

9.2.2.1 Reaction Procedure

The following experimental procedure was developed for the completion of a suspension polymerisation reaction:

1. Pre-mix MMA and initiator in feed tank for 30 mins
2. Add 14 kg of distilled water plus the colloid and surfactants to the reactor
3. Start nitrogen purge and cooling water to condenser
4. Heat aqueous phase to 60°C then start data logger
5. Drop organic phase followed by 2 l of distilled water, to flush
6. Heat reactor contents to the reaction temperature of 76°C
7. Close condenser valve, switch off N_2 and stop flow of hot water to jacket
8. Maintain reaction temperature of 76°C by manually adjusting the flowrate cooling water through the jacket.
9. Allow the temperature to rise during exotherm.
10. When reaction has finished, cool the reactor contents to 50°C and discharge into a collection tank

11. Stop data logger and save data, reopen condenser valve and collect two 1 l samples of the polymer slurry for analysis

12. Wash reactor with water at 60°C for 30 mins

13. Discharge water, fill the reactor with MEK and leave overnight

14. Apply nitrogen purge and wash the column with MEK, at its boiling point of 80°C, under agitation for 1 hr

15. Cool MEK to 30°C and discharge into drums

16. Wash the reactor with water, containing surfactant, under agitation for 30 mins at 60°C

17. Discharge the water and then rinse the column and baffles with tap water

9.2.2.2 Product Recovery

Once a reaction was complete, the PMMA particles had then to be recovered from the polymer slurry. The product recovery process is crucial to obtaining the product in the correct condition and was carried out in three stages:

1. Washing - This was carried out by filtering the slurry sample using a buchner funnel and vacuum flask arrangement while continually washing with water and stirring to remove any residual colloid. Resulting product was clean, damp particles with a typical moisture content of 10 – 15% (w/w).

2. Drying - After washing, PMMA particles were left in an oven at 60°C overnight to dry.

3 Sieving - Dry product was sieved through a 250 μm mesh to remove any oversize (mesh size was determined by the product specification supplied by Ineos Acrylics Ltd).

9.2.2.3 Analysis of Results

All PMMA samples were sent to Ineos Acrylics Ltd for analysis. Particle size distributions were obtained using a Coulter LS 230 laser particle size analyser. In addition, the molecular weight distribution (by gel permeation chromatography) and the residual initiator content of the polymer in each of the samples was also determined.

9.2.2.4 Range of Operating Conditions Studied

Suspension polymerisation reactions were carried out using a variety of operating parameters and baffle geometries. Three oscillation frequencies of 0.8, 1.0 and 1.2 Hz were each used in combination with three oscillation amplitudes of 50, 75, and 100mm at five different baffle geometries. The baffle geometries used were three baffle free areas of 20, 25 and 30 % at a baffle spacing of 315 mm ($1.5D_i$) plus a further two baffle spacings of

263 mm ($1.25D_i$) and 368 mm ($1.75D_i$) at a baffle free area of 25%. In total, therefore, 45 reactions were carried out.

9.3 Results and Discussion

9.3.1 Temperature Profile of Reaction

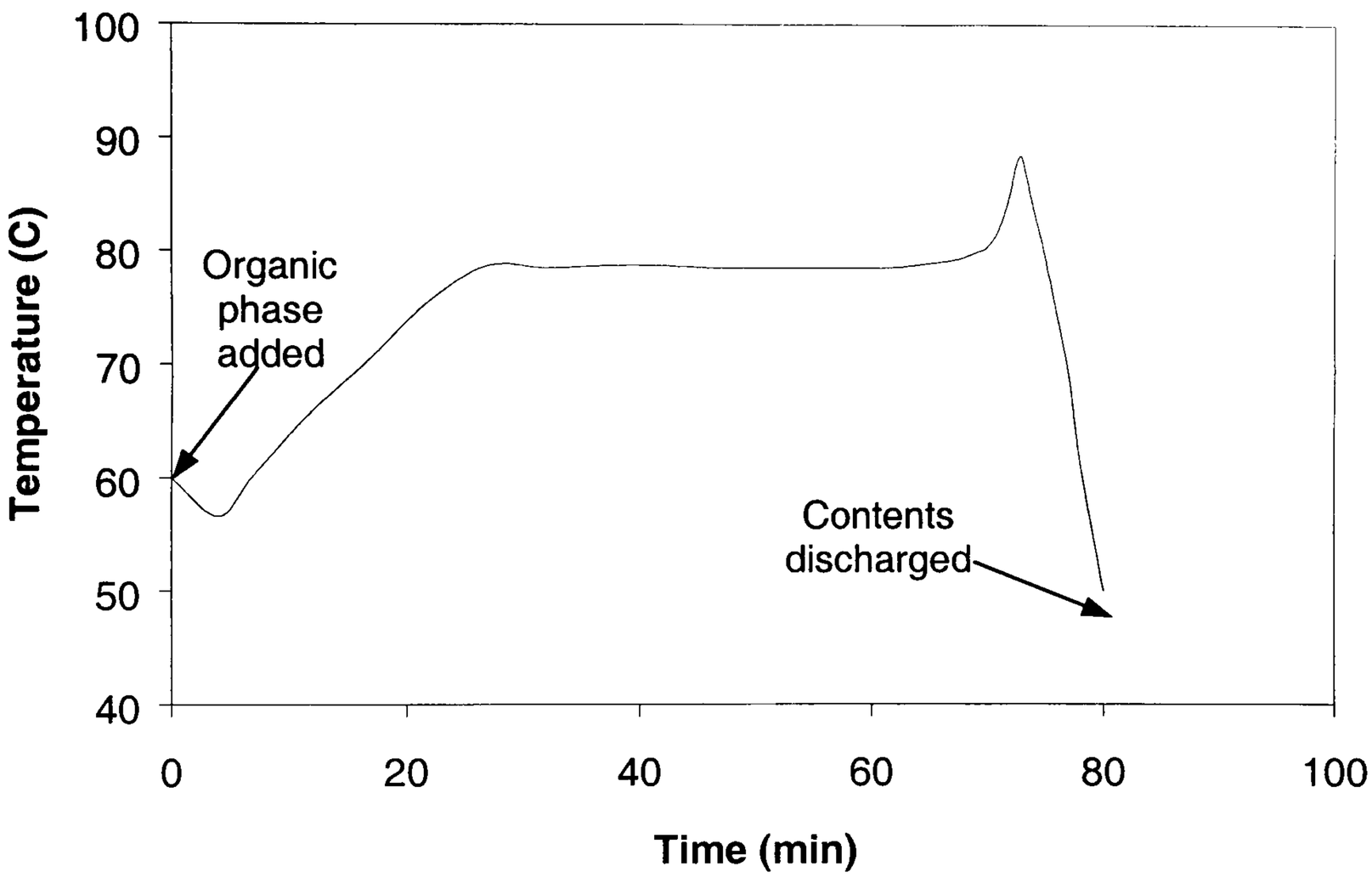

Figure 9.1: Reaction temperature profile (f=1.0Hz, x_o=75mm, α=25%, L=315mm)

As product quality is highly sensitive to reaction temperature it is crucial to obtain the correct temperature profile for the reaction. A typical temperature profile is shown in Figure 9.1, which shows how the temperature of the reactor contents changed between the point at which the organic phase was added and the point of discharge of the polymer product. It can be seen that once the reaction temperature was reached, it was maintained

for about 30 mins after which the temperature began to rise due to the highly exothermic stage that occurs at the end of a reaction. Upon completion of the reaction the temperature began to decrease again and the contents were cooled to the discharge temperature. The observed profile is of the desired shape and was easily achieved for each of the reactions carried out, indicating that temperature control was effective.

9.3.2 Oversize Fraction

The particle size distribution produced by any particular reaction depended on the operating conditions applied and as a result of this, oversize fractions varied from < 1% to > 50%. Clearly, a high oversize fraction indicates that a significant quantity of the product is being lost during sieving. Therefore, in the following analysis, results from the 20% of experiments that resulted in oversize fractions of > 20% are excluded.

9.3.3 Effect of Operating Parameters on Particle Size

Particle size distribution data are listed in Appendix 4.1

9.3.3.1 Effect of Oscillation Frequency

The effect of varying the oscillation frequency, at a fixed oscillation amplitude and baffle geometry, on the particle size distribution of the polymer is illustrated by Figure 9.2. It

can be seen that operating at a higher oscillation frequency results in smaller particles and a narrower particle size distribution being observed. This result is expected and can be explained by considering the relationship between the particle size distribution and the droplet size distribution of the dispersed phase prior to the reaction. As outlined in Chapter 7, smaller droplets are produced at higher oscillation frequencies. Therefore, upon polymerisation, smaller particles are also produced at higher oscillation frequencies.

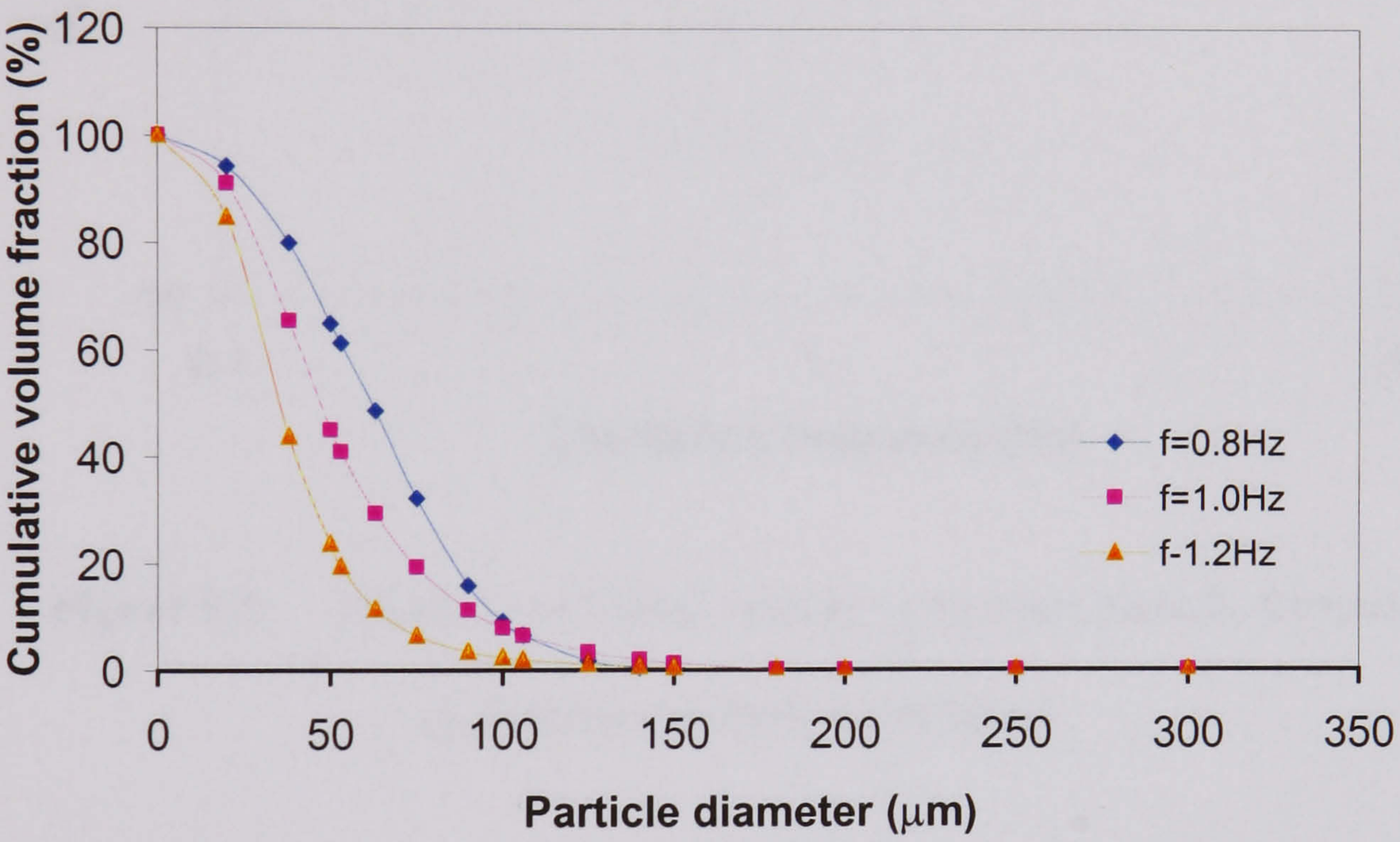

Figure 9.2: Effect of oscillation frequency on PSD (x_o=100mm, α=20%, L=315mm)

The PSD can be characterised by the mean particle size, $d_{v,0.5}$, which is the particle diameter at which the cumulative volume fraction is 50%. The effect of oscillation frequency on $d_{v,0.5}$ is shown in Figure 9.3, from which it can be seen that $d_{v,0.5}$ is dependent on oscillation frequency to the power –1.4. This dependence is slightly greater than that of the mean droplet diameter (d_{32}) on oscillation frequency and this is likely to be a result of the difference in conditions that exists between a reacting and non-reacting system. During a reaction the viscosity of the dispersed phase increases and there is a tendency for

droplets to coalesce without breakage. Therefore a reduction in energy dissipation (or frequency) would result in a greater increase in droplet size than would be expected than in the non-reaction case.

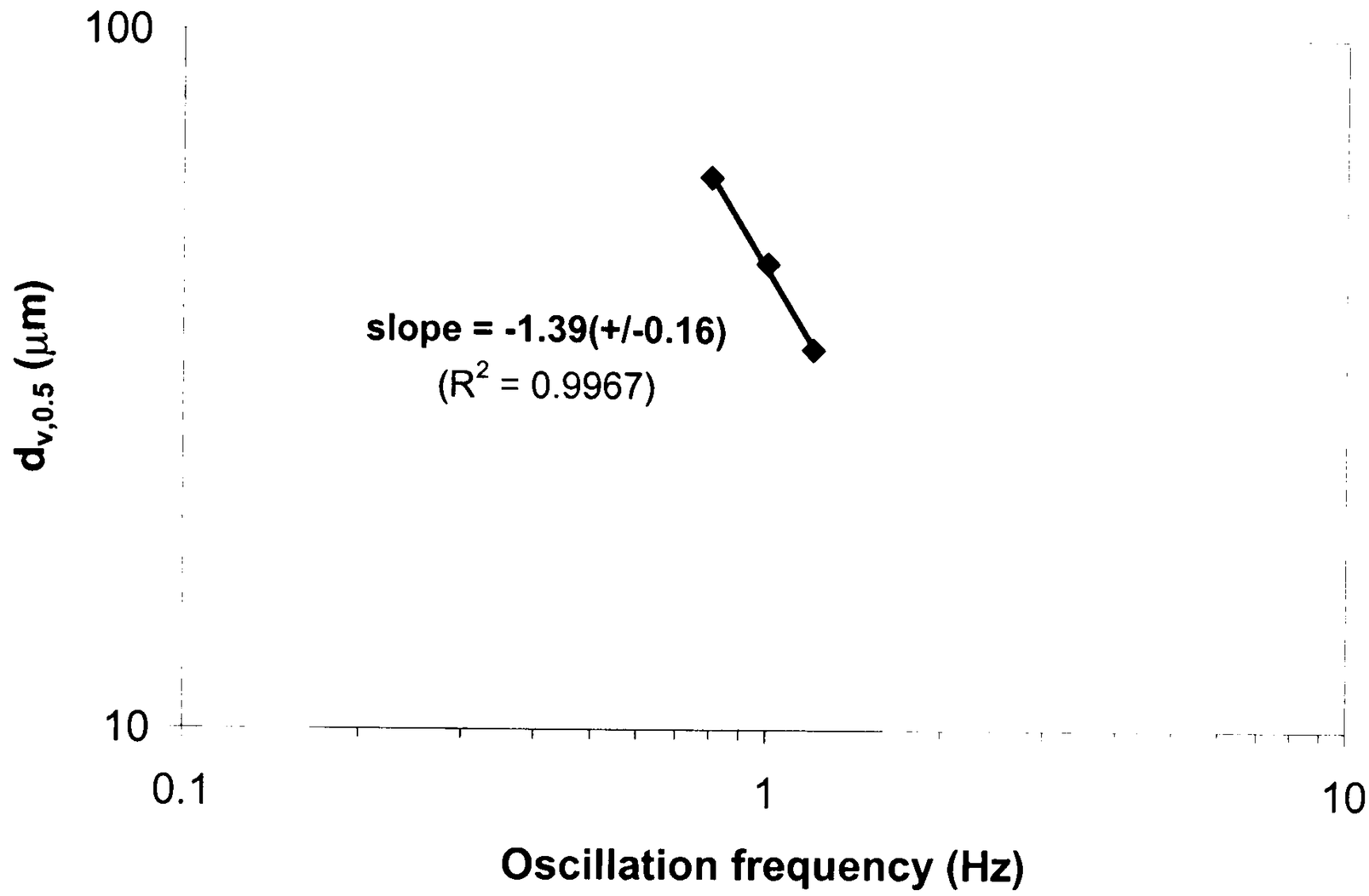

Figure 9.3: Effect of oscillation frequency on mean particle diameter

(x_o=100mm, α=20%, L=315mm)

9.3.3.2 Effect of Oscillation Amplitude

The effect of oscillation amplitude on the particle size distribution and the mean particle size is shown in Figures 9.4 and 9.5 respectively. It can be seen that the oscillation amplitude has a similar effect on particle size as the oscillation frequency, i.e. as the oscillation amplitude is increased, the particle size distribution becomes narrower and the mean particle size is reduced. This is expected as both oscillation frequency and amplitude contribute in a similar way to the energy dissipation in the system (see eqn 2.5).

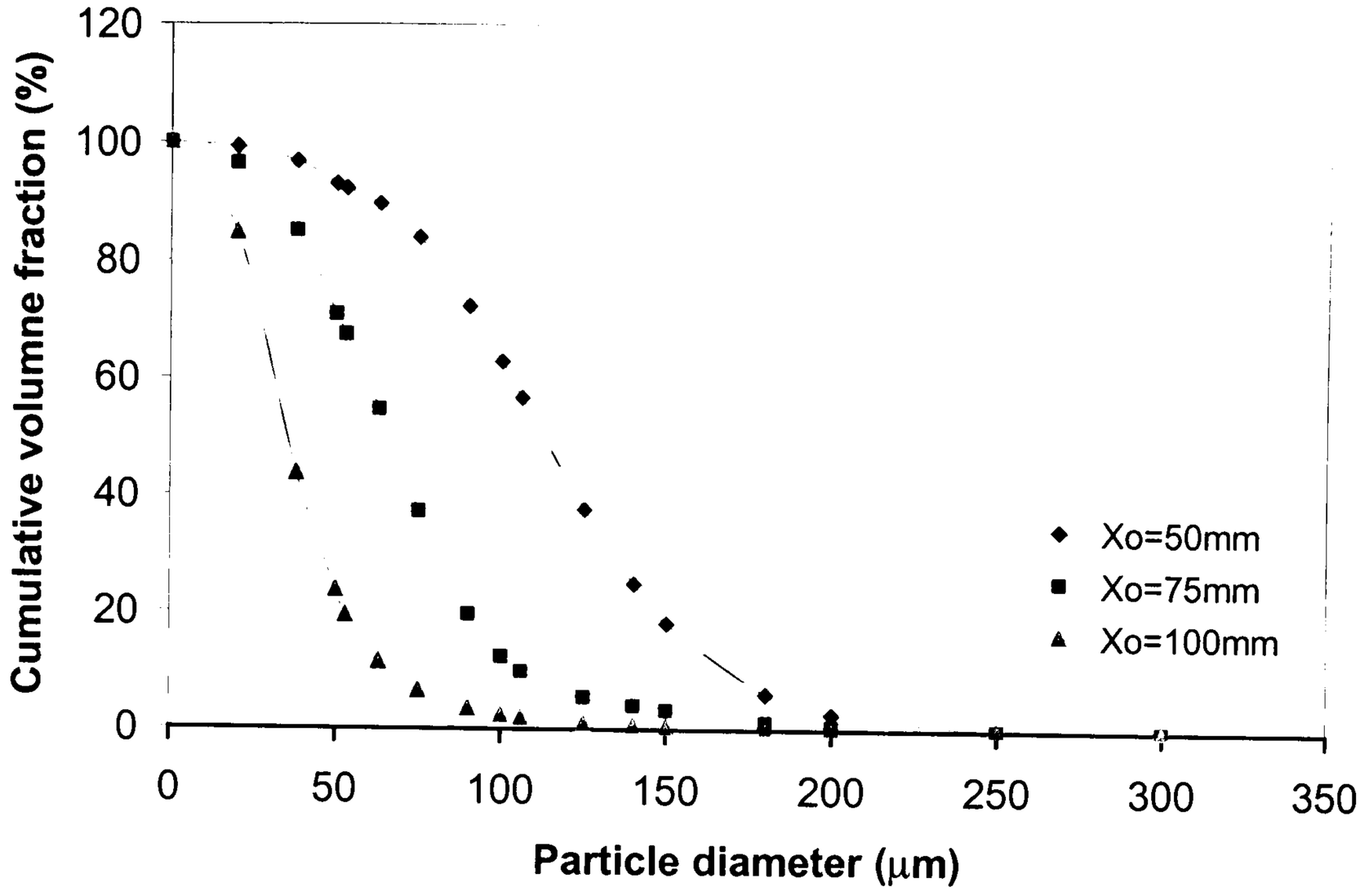

Figure 9.4: Effect of oscillation amplitude on PSD (f=1.2Hz, α=20%, L=315mm)

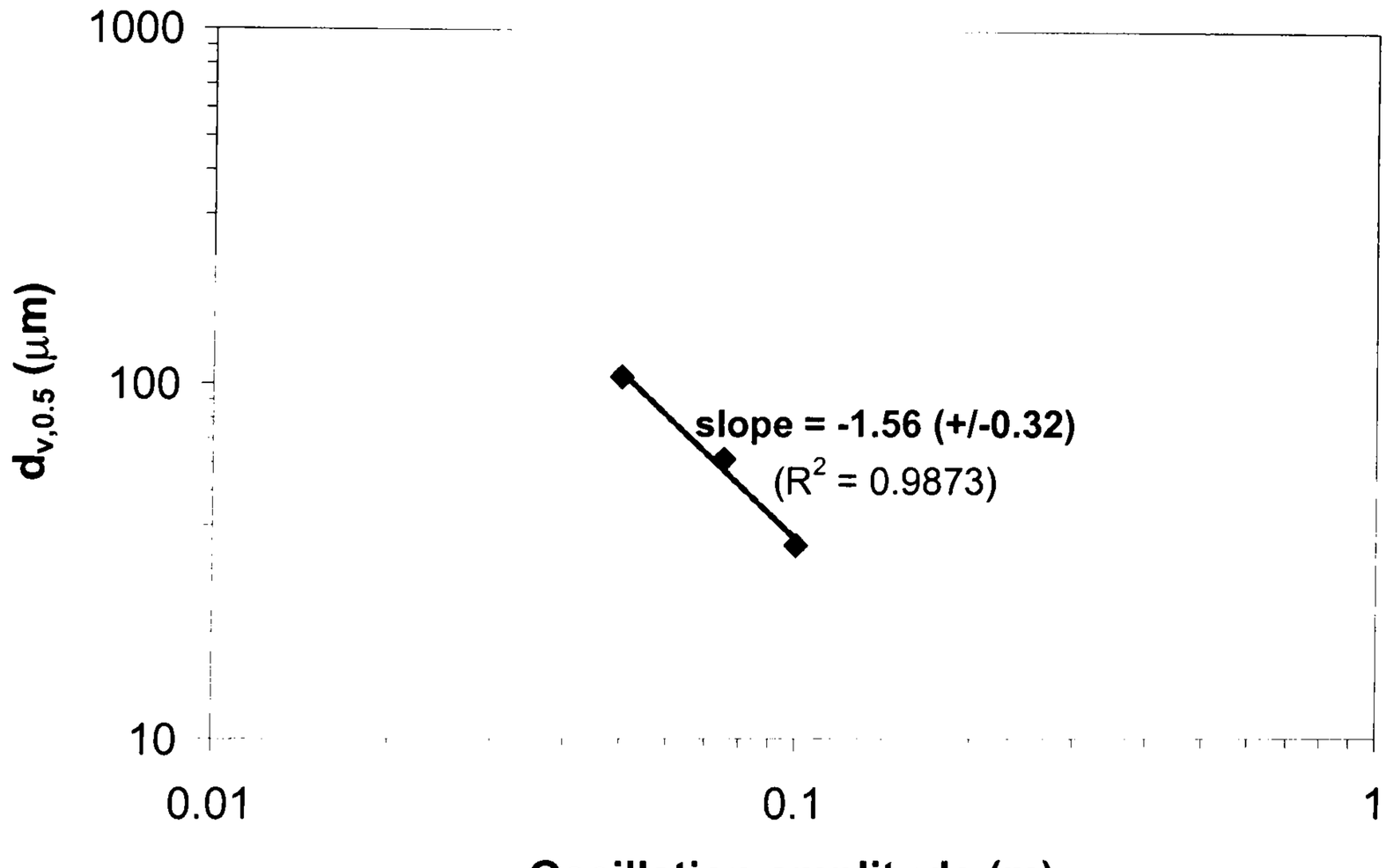

Figure 9.5: Effect of oscillation amplitude on mean particle diameter

(f=1.2Hz, α=20%, L=315mm)

9.3.3.3 Effect of Oscillatory Velocity

It is evident from Figures 9.3 and 9.5 that the mean particle size exhibits a similar dependence on both oscillation frequency and amplitude. The combined effect of the oscillatory velocity (x_of) on the mean particle size is shown in Figure 9.6 and the best fit correlation is given by equation (9.1).

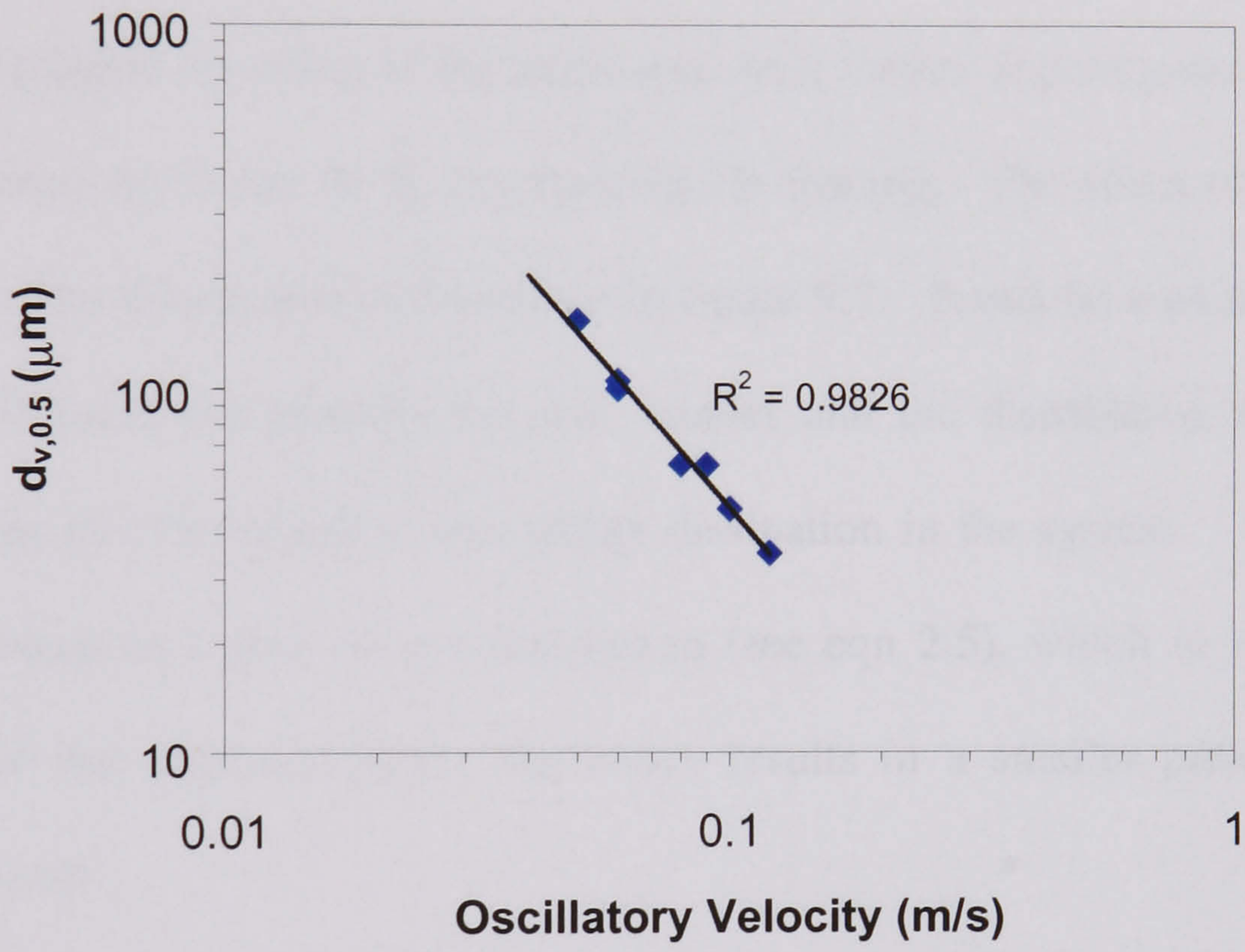

Figure 9.6: Effect of oscillatory velocity on mean particle size (α=20%, L=315mm)

$$d_{v,0.5} = 1.12\times10^{-6}\left(x_o f\right)^{-1.6} \tag{9.1}$$

It can be seen that equation (9.1) fits the data very well ($R^2 > 0.98$), which indicates that varying the oscillatory velocity provides a high degree of control over the particle size. It is also evident that the dependence of the mean particle size on the oscillatory velocity is

greater than that of the mean droplet size and this is due to the difference in physical properties between the two systems as explained in section 9.3.3.1.

9.3.4 Effect of Baffle Geometry

9.3.4.1 Effect of Baffle Free Area

In order to investigate the effect of the baffle free area, further experiments were performed at baffle free areas of 25 and 30 %, at a fixed baffle spacing. The effect of baffle free area on the particle size distribution is illustrated in figure 9.7. It can be seen that as the baffle free are is decreased the particles become smaller and the distribution narrows. This observation can also be related to the energy dissipation in the system. Using a smaller orifice area results in higher energy dissipation (see eqn 2.5), which in turn reduces the droplet size of the dispersed phase and hence results in a smaller particle size of the polymer produced.

The effect of the baffle free area on the relationship between mean particle size and oscillatory velocity is shown in Figure 9.8 and the equations providing the best fit to the data are given in equations 9.1, 9.2 and 9.3 for baffle free areas of 20%, 25% and 30% respectively. It is evident that the mean particle size is lower at lower orifice sizes and that the mean particle size varies with oscillatory velocity to approximately the same power index for each of the orifice diameters tested.

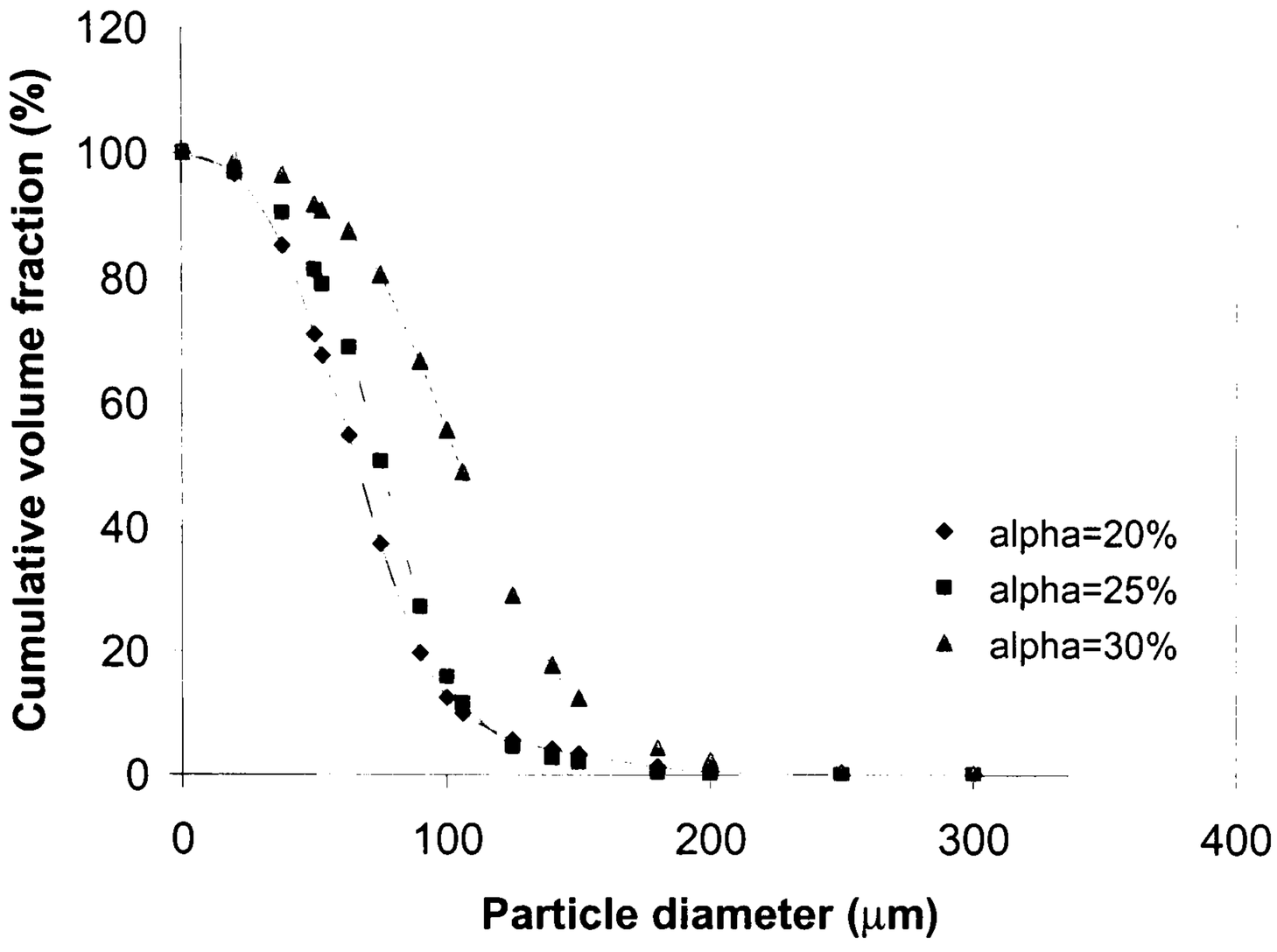

Figure 9.7: Effect of baffle free area on PSD (f=1.0Hz, x_o=100mm, L=315mm)

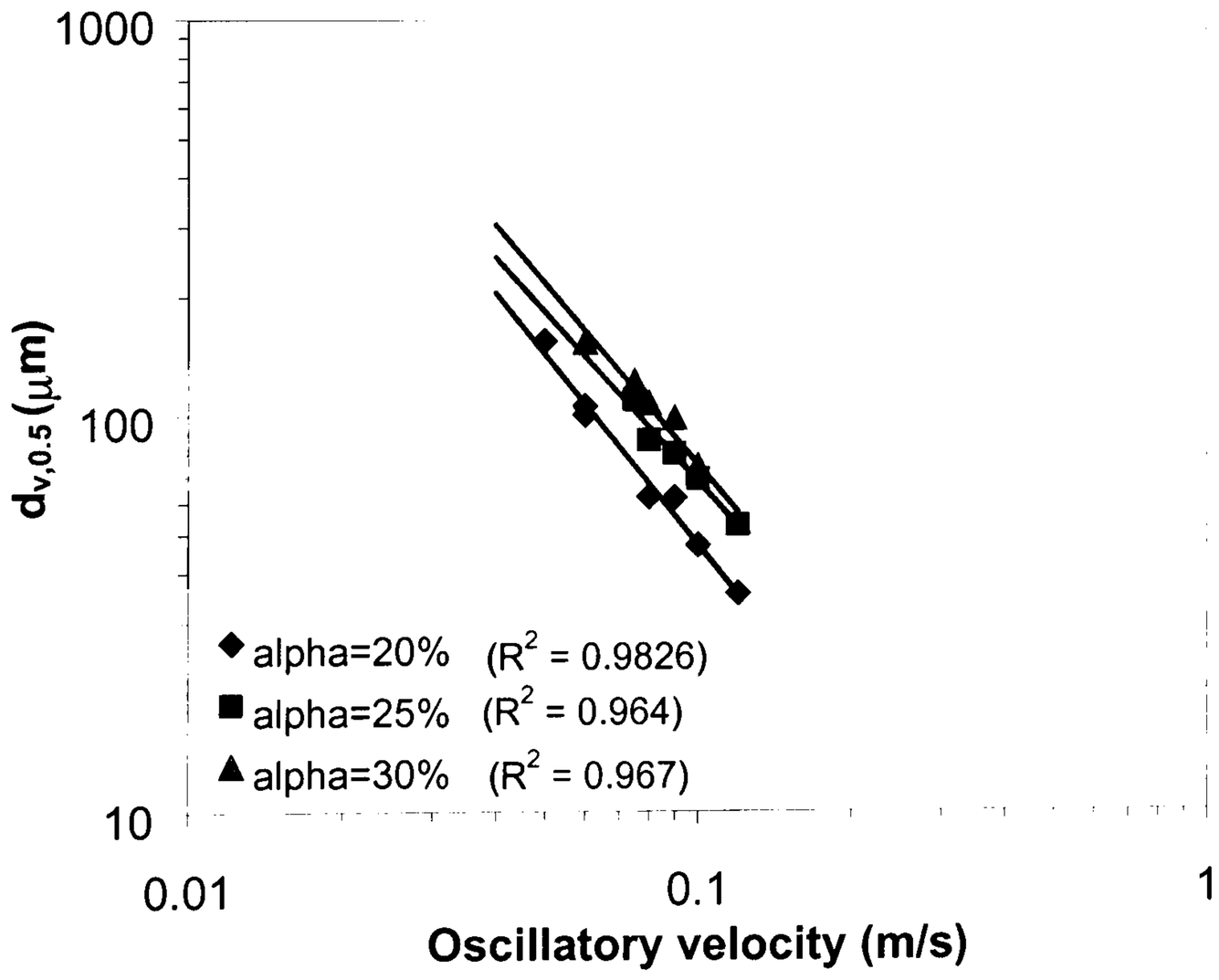

Figure 9.8: Effect of x_of and α on mean particle size (L=315mm)

$$d_{v,0.5} = 2.25\times10^{-6}\left(x_o f\right)^{-1.43} \tag{9.2}$$

$$d_{v,0.5} = 2.23\times10^{-6}\left(x_o f\right)^{-1.53} \tag{9.3}$$

9.3.4.2 Effect of Baffle Spacing

The effect of baffle spacing was investigated by performing experiments at a further two baffle spacings of 263mm and 368mm at a fixed baffle free area of 25%. Figure 9.9 shows the effect of varying the baffle spacing on the particle size distribution, from which it can be seen that the PSD does not change much and no clear trends are in evidence. This can again be explained in terms of energy dissipation as varying the baffle spacing has little effect on the energy dissipation in the system.

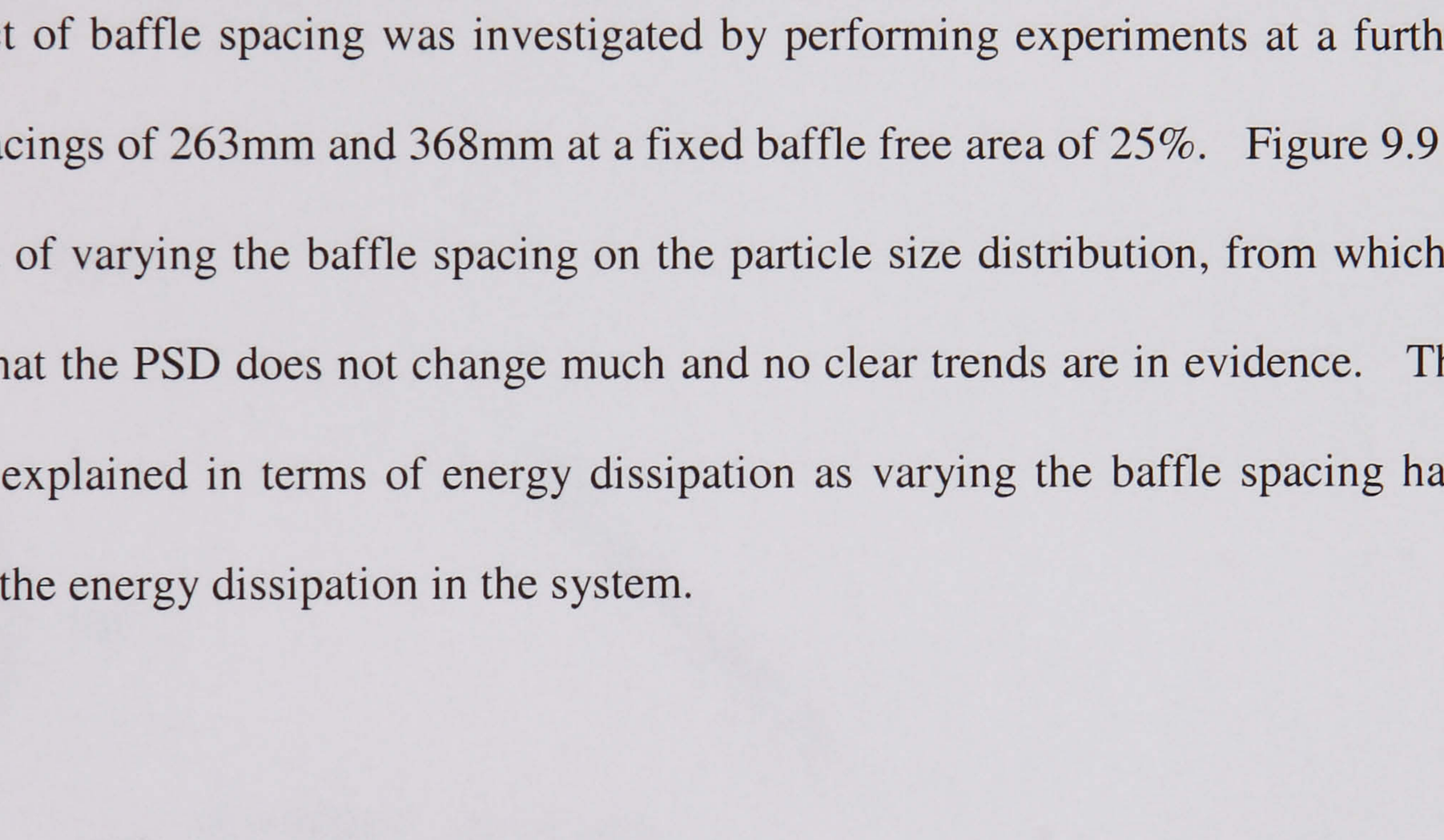

Figure 9.9: Effect of baffle spacing on PSD (f=1.0Hz, x_o=75mm, α=25%)

The effect that varying the baffle spacing has on the mean particle size is illustrated in Figure 9.10 and the best fit equations relating mean particle diameter to oscillatory velocity are given in equations 9.1, 9.4 and 9.5 for the three baffle spacings used. It can be seen that the mean particle size does not vary significantly with baffle spacing and that $d_{v,0.5}$ varies with oscillatory velocity to a power of –1.5 to –2.0 for each of the baffle spacings tested. This indicates that particle size is only a weak function of baffle spacing and this can be attributed to the weak dependence of energy dissipation on baffle spacing.

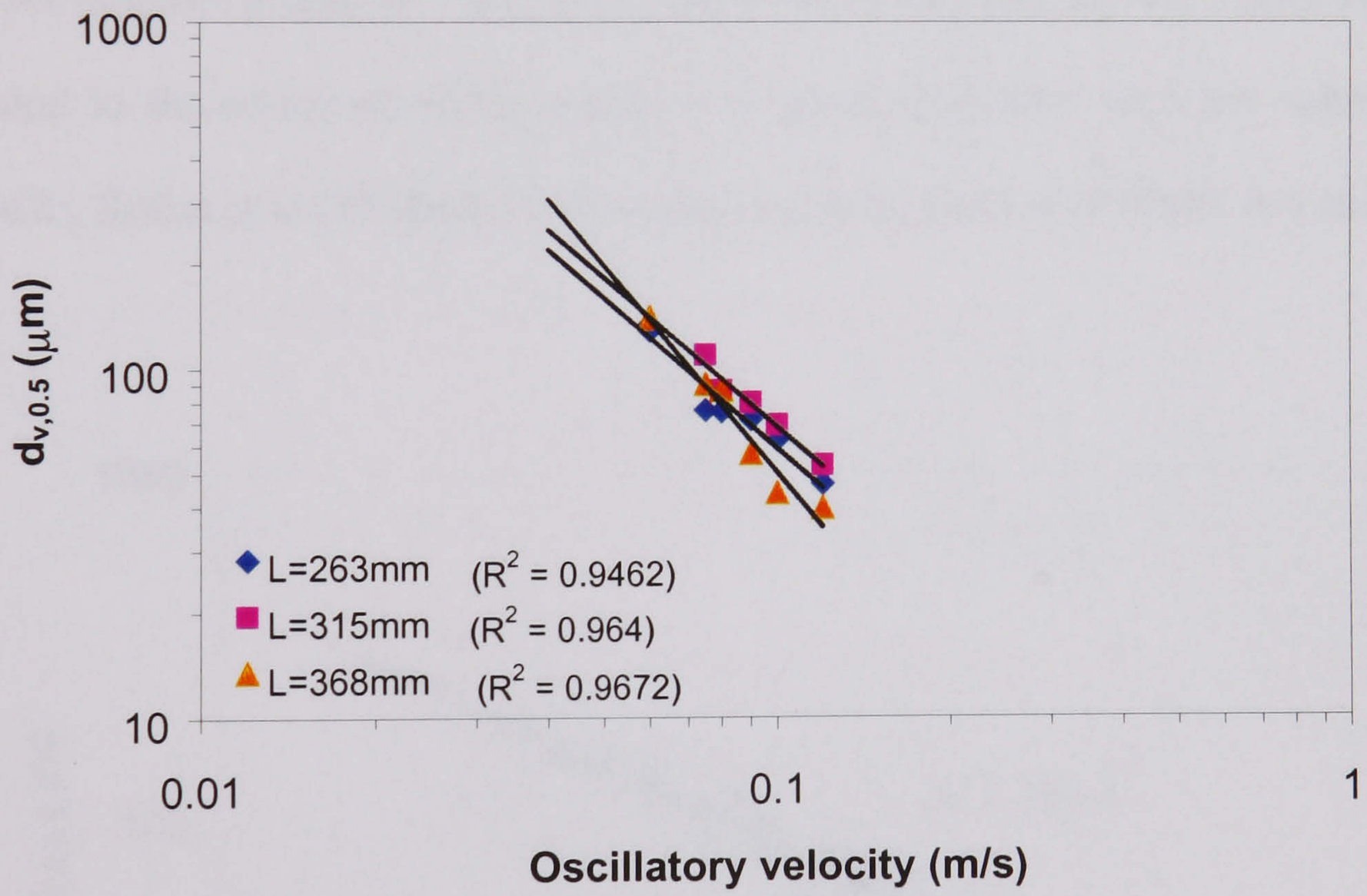

Figure 9.10: Effect of oscillatory velocity and baffle spacing on mean particle size (α=20%)

$$d_{v,0.5} = 2.16\times10^{-6}\left(x_o f\right)^{-1.44} \tag{9.4}$$

$$d_{v,0.5} = 0.53\times10^{-6}\left(x_o f\right)^{-2.0} \tag{9.5}$$

9.3.5 Effect of Energy Dissipation

The effect of the energy dissipation in the system, as calculated by equation (2.5), on the mean particle size is shown in Figure 9.11 and the best fit power law relationship is given by equation (9.6). It can be seen that equation 9.6 provides a reasonable good fit to the data, indicating that energy dissipation is the predominant factor in determining the particle size of the polymer produced. It is also evident that mean particle size varies with energy dissipation to the power of –0.51, which is in good agreement with the value of –0.47 reported by Kaflas et al (1993a,b) for suspension polymerisation of MMA in a stirred tank.

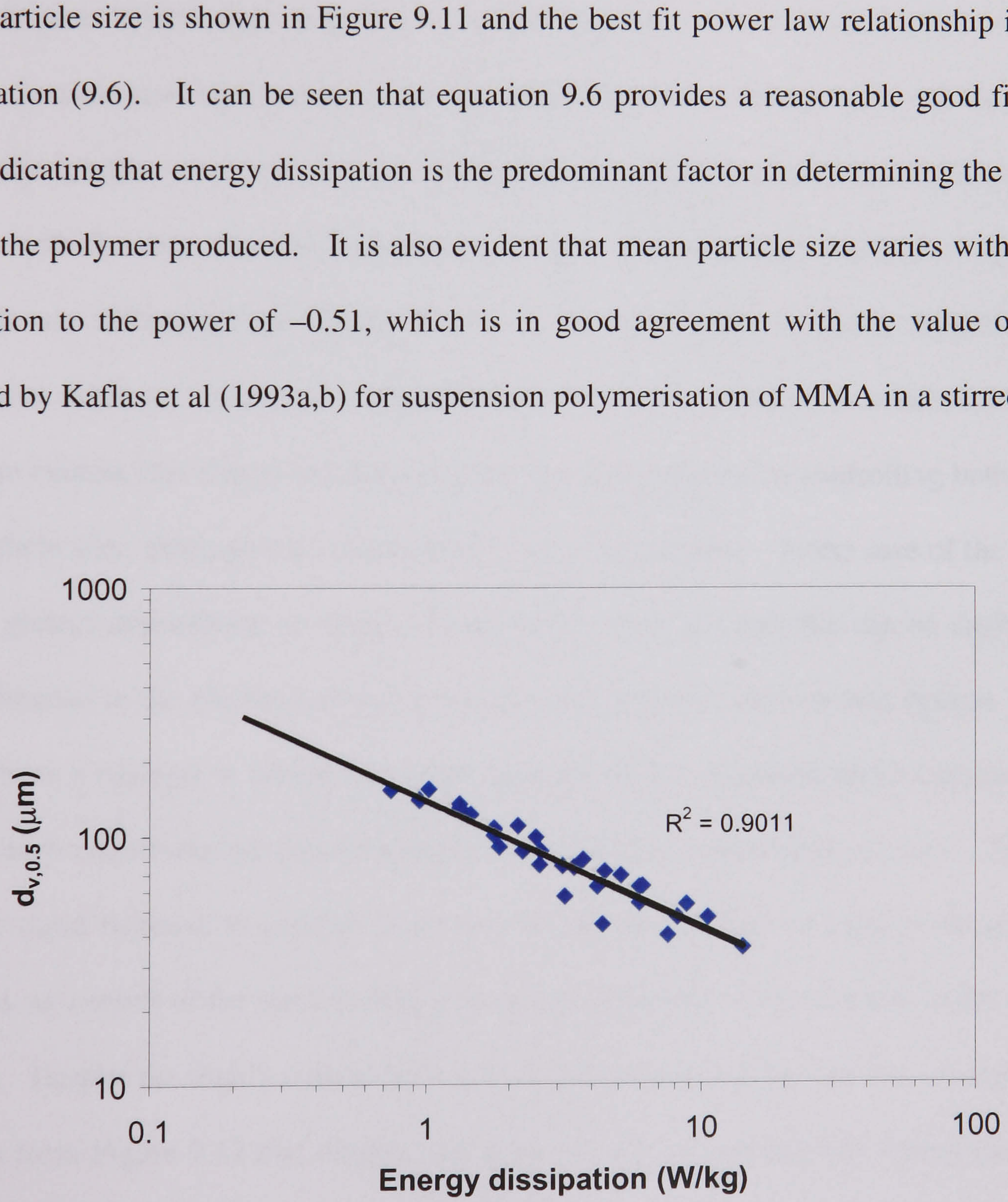

Figure 9.11: Effect of energy dissipation on mean particle size

$$d_{v,0.5} = 138.7(\pm 10) \times 10^{-6}\, \varepsilon^{-0.51(\pm 0.08)} \tag{9.6}$$

9.3.7 Comparison of Final Particle Size with Initial Drop Size

The particle size of the polymer product is determined by the way in which the dispersed phase droplets behave during the course of the reaction. It would therefore be expected that the particle size would be in some way dependent on the initial drop size that existed before the reaction commenced. On comparison of the particle size data reported in this chapter with the drop size data reported in Chapter 7, it is evident that both droplets and particles are influenced by similar factors. In both cases a strong dependence on oscillatory velocity is observed while the effect of system geometry is somewhat weaker. It is also evident that energy dissipation is the governing factor for controlling both droplet and particle size, although the relationship for each is different. In the case of the particle size, a greater dependence on energy dissipation is observed and this can be attributed to the difference in the physical nature between a reacting and non-reacting system. In the case where a reaction is taking place the viscosity of the dispersed phase increases with time, which effectively prevents breakage but still allows coalescence to occur. Therefore a more rapid increase in particle size than droplet size occurs as energy dissipation is reduced, as a result of the more readily coalescing behaviour of the droplets in the reacting system. Despite the highly coalescing nature of droplets during the reaction, though, it can be seen from Figure 9.12 that droplet size does not change significantly during the course of the reaction, over the range of conditions studied here. This can be attributed to the presence of stabilisers in the system which hinder the coalescence process significantly. It

is also evident from Figure 9.12, however, that at lower energy dissipation the graphs of mean drop size and mean particle size begin to diverge, indicating that coalescence is more significant under such conditions. This result indicates that a high level of mixing intensity as well as with the presence of stabilisers is required to prevent coalescence.

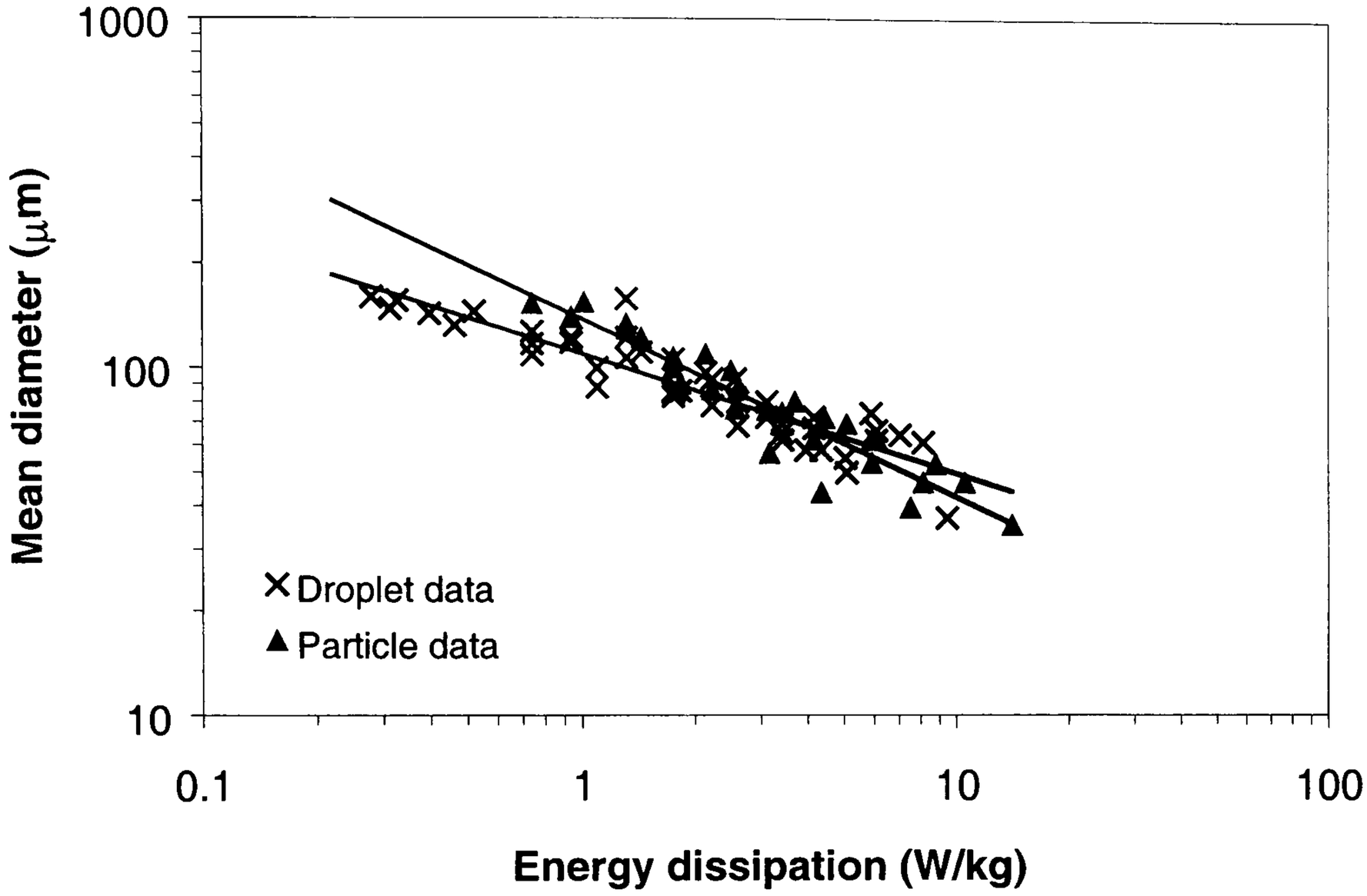

Figure 9.12: Comparison of mean droplet at particle sizes

9.3.8 Effect of Scale-Up on Particle Size

The primary objective of this project was to study the effects of scale-up on the characteristics suspension polymeristion. Particle size and droplet size results obtained have therefore been compared with those from the small scale OBR of Zhang (1997). The effect of energy dissipation on the mean drop size and the mean particle size in both devices is plotted in Figure 9.13 and the best fit correlations are summarised in Table 9.1. Also, correlations expressing the dependence of mean particle size on the mean drop size

are given by equations (9.6) and (9.7) for the 50mm diameter and 213mm diameter OBR respectively. It is evident that different transient droplet behaviour occurs in the two devices. In the small column, significant coalescence was reported to occur resulting in particles that were 3 times the size of the initial droplets. However, no such growth is observed in the larger column.

Table 9.1: Correlations for mean drop size and mean particle size in OBCs of 213mm and 50mm in diameter

Device	Droplet Correlation	Particle Correlation
50mm OBC	$d_{32} = 68\times10^{-6}\varepsilon^{-0.4}$	$d_{v,0.5} = 211\times10^{-6}\varepsilon^{-0.4}$
213mm OBC	$d_{32} = 110\times10^{-6}\varepsilon^{-0.35}$	$d_{v,0.5} = 138.7\times10^{-6}\varepsilon^{-0.51}$

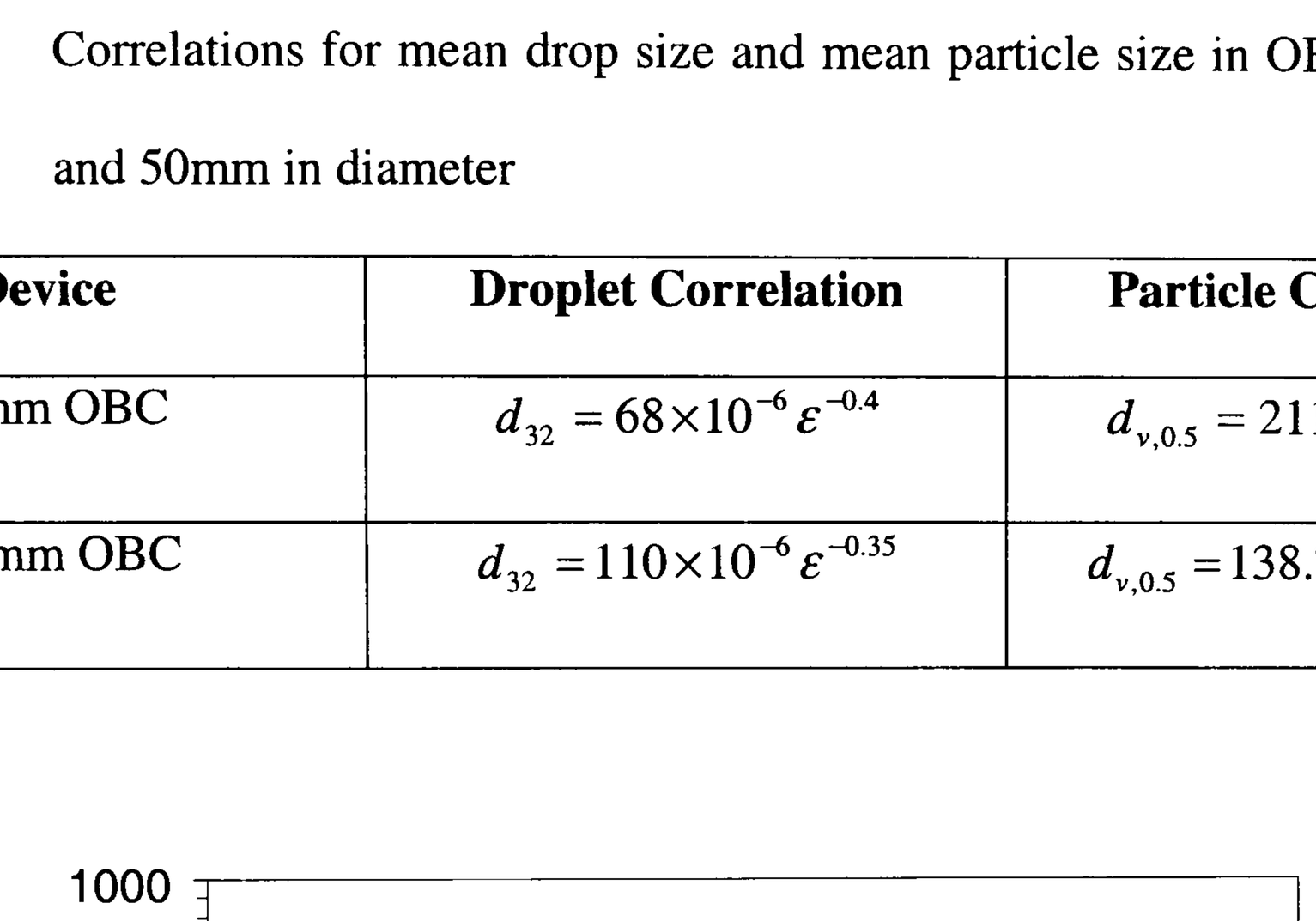

Figure 9.13: Effect of energy dissipation on mean droplet and particle diameter

$$d_{v,0.5} = 3.11 d_{32} \tag{9.6}$$

$$d_{v,0.5} = d_{32} \tag{9.7}$$

The reason for this difference in transient droplet behaviour is not clear but the following two factors may have been influential. Firstly, in the smaller column the oscillation frequencies used were higher. This would result in a more frequent change of direction of the droplet movement and possibly increase the droplet collision frequency. In a reaction environment where breakage is effectively prevented by the high viscosity, a high collision frequency could results in a greater droplet coalescence rate. The second factor is that the two studies used a slightly different recipe as Ineos Acrylics Ltd. modified the formulation between each of these studies being conducted. The difference in surfactant concentrations used would result in different droplet behaviour and could explain why there is better coalescence inhibition in the present case. Overall, however, the difference in droplet and particle sizes is not great between the two devices and in both cases a similar dependence on energy dissipation is observed. This indicates that the energy dissipation rate can be used to control the particle size in any given system, although some variation in size can be expected between different systems. Based on this result it is concluded that larger scale OBR devices than the one used here would again exhibit a similar dependence on energy dissipation although the particle sizes obtained would also depend on the recipe used.

9.3.9 Other Product Properties

9.3.9.1 Molecular Weight Distribution

Molecular weight data are listed in Appendix 4.2. It can be seen that the average molecular weight shows no noticeable dependence on operating conditions and variations are of a somewhat random nature. This can be attributed to the fact that molecular weight is predominantly influenced by reaction temperature. Although temperature profiles were similar for all reaction, slight variations could not be avoided with the experimental set-up used. The molecular weights reported here of between 450,000 and 1,130,000 are however good agreement with those reported by Zhang (1997) (640,000 – 950,000) from a study of suspension polymerisation of MMA in a bench scale OBC and stirred tank reactor. This indicates that the reaction kinetics are not influenced by scale-up provided that good heat transfer and temperature control are maintained. The polydispersity index, which is an important quality control parameter, is also listed in Appendix 4.2. It can be seen that variations are from 2.9 – 6.5 although the majority of values lie within the range 3.0 – 5.0. This is again similar to the results reported by Zhang (1997) who reported a range of 2.8 – 4.1.

9.3.9.2 Residual BPO Content

The residual BPO content is an indicator of the reactivity of the polymer beads and the value of this parameter determines the type of application to which the product is suited. Residual BPO content of approximately 0.75 % or less indicates suitability of the product

for heat curing applications, in which the polymer is mixed with some of its monomer to form a paste, which is then placed in a mould and then heated to reaction temperature, at which point polymerisation occurs and the paste solidifies. A residual BPO content of over 0.75 % indicates suitability of the product for self curing application , in which the added monomer contains a tertiary aromatic amine, which reacts with the BPO (by redox reaction) at room temperature.

A list of residual BPO content for the reactions carried out in this work is given in Appendix 4.3, from which it can be seen that the residual BPO content was always within the range 0.676 – 0.874. This indicates that the product may be suitable for either heat curing or self curing applications although heat curing may be more suitable as self curing processes usually require a low molecular weigh (typically < 500 000). It is also evident that the residual BPO content did not vary much between reactions, which indicates that this parameter is independent of agitation rate and system geometry and also demonstrates the consistency at which the same reaction conditions were achieved.

Previous work by Zhang (1997) has showed that residual BPO contents for the same reaction as that used here were in the range of 0.551 – 0.701 % for a 50 mm diameter OBR and 0.712 % for a stirred tank reactor. These values are in reasonably good agreement with those reported in the present work, indicating that the residual BPO content is unaffected by reactor size and type.

9.4 Fouling Problems

One of the major problems with suspension polymerisation processes is the formation of fouling on the reactor and agitator by surface deposition of polymer material. During a reaction, polymer adheres to and accumulates on internal surfaces and can result in serious build-up if preventative measures are not adopted. Fouling can be reduced by using highly polished surfaces or special coatings or, by adding colloids and surfactants in the correct proportions which helps to keep the polymer in suspension. However, it is not possible to completely eliminate fouling in this type of process, therefore, cleaning is required after a reaction has be completed. This is normally done by employing some form of mechanical cleaning, or by washing the reactor with a solvent (e.g. methylethylketone (MEK)) to dissolve the residual polymer. Industrial size reactors are cleaned using high pressure (>400 bar) water jets after each reaction and periodic washes with solvent.

In the case of the present work, fouling of the internal surfaces of the reactor was observed to occur and could become a significant problem if the reactor was not cleaned sufficiently between reactions. Mechanical cleaning of the reactor was difficult due to accessibility limitations. Therefore, it was decided to wash the reactor MEK after every reaction. The extent to which the fouling was removed depended on the length of the wash cycle and it was found that in order to completely remove fouling, MEK should be left in the reactor overnight followed by a 1 hour long wash at a temperature of 79°C (the boiling point of MEK).

9.5 Conclusions

Results of suspension polymerisation tests have been reported in this chapter. It was found that the particle size distribution was strongly dependent on oscillatory velocity, which could be used to control the mean particle size with a good degree of accuracy at each of the baffle geometries tested. The effect of baffle geometry was weaker with smaller particles being observed at lower baffle free areas and baffle spacing being observed not to have much of an effect. In general, the energy dissipation rate in the system was the governing factor in determining the mean particle size and the data could be fitted with a simple power law relationship, which showed that $d_{v,0.5}$ varied with energy dissipation to the power of –0.51. This dependence is greater than that exhibited by droplet size and this can be attributed to the difference in dispersed phase physical properties between reacting and non-reacting systems. On comparison with the results reported in a smaller scale OBR it was found that coalescence of droplets during the reaction was considerably lower in the present case. The reason for this is not clear but may be due to the slight difference in surfactant concentrations used in the two studies or be a result of the droplet interactions with the eddies of different size that exist in the two systems. Overall, however, particle sizes were not substantially different and a similar dependence on energy dissipation was observed. This indicates that energy dissipation can be used as a guide for scale-up of such processes but accurate prediction of particle size is limited by the complex behaviour of droplets in a suspension polymerisation reaction system. Other product properties such as molecular weight appear not to be affected by scale-up provided that the same reaction conditions are maintained. Overall, therefore, it can be concluded that the oscillatory baffled reactor is a feasible device for the large scale production of polymers by suspension polymerisation. Based on the findings of this study it is recommended that in scaling up

the oscillatory baffled reactor, geometric similarity is maintained and control of the agitation rate is implemented by varying the oscillatory velocity.

10 CONCLUSIONS

It was the objective of this project to determine scale-up rules for the production of polymethylmethacrylate by suspension polymerisation in an oscillatory baffled reactor. These objectives have been met by experimentally investigating the characteristics of mixing, heat transfer, liquid-liquid dispersion and suspension polymerisation using two OBCs, of 380mm diameter and 213mm diameter respectively, and comparing the results with those previously reported for smaller scale devices. The conclusions drawn form this investigation are discussed in the following sub-sections.

10.1 Mixing Characteristics

From a flow visualisation study it was observed that the mixing intensity can be increased by either increasing the oscillation frequency or amplitude or decreasing the baffle orifice diameter, each of which increases the maximum fluid velocity in the system. Oscillation amplitude and baffle spacing were found to be closely related and the fluid mechanical conditions were observed to be optimised when operating with an amplitude of approximately one quarter of the baffle spacing. This finding is in good agreement with results reported in a bench scale OBC that also used oscillating baffles. On comparison with the smaller device in general, it was evident that flow patterns were similar in both columns with only slight differences in the characteristics of bulk fluid motion being observed.

Mixing in the OBC was further assessed by investigating oil-water dispersion characteristics. The minimum frequency for complete dispersion was determined at a

range of amplitudes, baffle geometries and oil phase fractions. It was found that the minimum frequency for complete dispersion decreased with increasing amplitude and decreasing orifice diameter while baffle spacing and phase fraction had little effect. These finding are similar to results reported in a bench scale OBC and a scale-up rule relating the minimum frequency for complete dispersion to the column diameter, based on the effects of oscillatory velocity and energy dissipation, has been derived and is seen to fit the data reasonably well.

From the results of the flow visualisation and oil-water dispersion studies it is evident the characteristics of bulk fluid mixing do not vary substantially between large and small scale oscillatory baffled columns. Based on this result, it can be concluded that the OBC could be scaled up further without modification to geometrical configuration.

10.2 Application of OBC to suspension polymerisation

In order to determine the suitability of OBCs for suspension polymerisation, heat transfer, drop size distribution and suspension polymerisation reaction experiments were carried out.

10.2.1 Heat Transfer Study

Heat transfer rates were determined for a range of oscillatory conditions at a fixed baffle geometry and a correlation was established that relates the tube side Nusselt number to

the oscillatory Reynolds number. The correlation is similar to those previously reported in a small scale OBC and a stirred tank, indicating that the dependence of heat transfer on mixing intensity is similar in each of these devices. A scale-up correlation. relating the tube side heat transfer coefficient to the column diameter, agitation rate and fluid viscosity, has been derived, which provides a good fit to the data obtained from OBCs of both 50 mm and 213 mm in diameter. It is also evident that the heat transfer rates achievable in the OBC are sufficient for the control of temperature during suspension polymerisation.

10.2.2 Droplet Size Distribution

Drop size distributions were determined over a range of oscillation conditions and baffle geometries. The mean drop size was found to vary with the energy dissipation rate to the power of –0.35, which is in good agreement with that predicted by the isotropic turbulence theory. The effects of oscillation frequency and amplitude and baffle free area individually agree with the correlation but the effect of baffle spacing is somewhat different. Although, baffle spacing shows little effect, which is expected, the slight variation in the mean droplet size with changes in baffle spacing cannot be explained in terms of energy dissipation. On comparison with a smaller scale OBC, it is evident that larger droplet are produced in the larger column, which could be a result of the longer droplet circulation times in the larger device.

Further investigation into droplet behaviour was carried out by applying a recently developed model, based on the population balance equation, to experimental DSD data in order to determine droplet breakage and coalescence rates. For a

breakage-only system, a simplified version of the model was used and the calculated breakage rates were found to increase with droplet diameter as well as with the oscillation frequency and amplitude. These results confirmed what was theoretically expected. In the case where both breakage and coalescence were present the accuracy of the model was lost to some extent, which can be attributed to the larger number of parameters in the minimisation process. Although the model performed to a satisfactory level in validation tests that were carried out, scatter was observed in the results when it was applied to the experimental data. Therefore, further development of the model is required. It could be seen, though, that coalescence rates were generally higher than breakage rates and that no particular type of coalescence interaction was dominant, which were expected.

10.2.3 Suspension Polymerisation

Suspension polymerisation reactions were carried out over a range of operating conditions. It was found that the energy dissipation rate was the predominant factor for controlling the particle size distribution and the mean particle size was found to vary with energy dissipation to the power of –0.51. This dependence is greater than that exhibited by the droplet size on energy dissipation and this can be attributed to the difference in physical characteristics between reacting and non-reacting systems. Initial drop size and final particle size are however reported to be close for all conditions tested, which indicates that coalescence was successfully inhibited by the presence of stabilisers. On comparison with result of a similar study in a bench scale device it is evident that droplet and particle sizes exhibit a similar dependence on energy dissipation in both cases although different transient droplet behaviour was observed.

From the results of this investigation it is concluded that the oscillatory baffled column can be used for the large scale production of suspension polymers and that the behaviour of larger scale devices would not differ substantially from that observed in the present case. It is recommended that further scale-up should maintain geometric similarity to the device used here and that of Zhang (1997) and that particle size control should be implemented by varying the oscillatory velocity, which has been shown to provide accurate control over the mean particle size.

11 RECOMMENDATIONS FOR FUTURE WORK

The feasibility of an oscillatory baffled column as reactor for suspension polymerisation has been demonstrated by this work. However, there have been many areas highlighted in which sufficient knowledge relating to a particular process is needed. The areas requiring future research are outlined below.

11.1 Oil-Water Dispersion

The oil-water dispersion study in this work was limited to only one liquid-liquid system, therefore, more work is required to determine the effect of the physical properties of both phases on f_{min} and to incorporate this into the scale-up correlation.

11.2 Heat Transfer

To date, only a limited amount of heat transfer research has been carried out in oscillatory baffled devices. It is therefore recommended that this work be extended to investigate different systems in order to determine the applicability of the correlations that are currently available.

11.3 Drop Size Distribution

The number of reported investigations into drop size distributions in oscillatory baffled devices is very limited. Therefore, it is recommended that more research in this area is carried out. The areas requiring the greatest attention are the determination of all process conditions on drop size and size distribution, investigations into droplet breakage and coalescence rates and scale-up studies.

11.4 Suspension Polymerisation

This study has shown that suspension polymerisation can successfully be carried out in an intermediate-sized oscillatory baffled column. It is therefore recommended that further investigations be performed to study different polymerisation systems as well as the effect of varying parameters such as the surfactant, colloid and initiator concentration in OBRs of various scales in order to gain a broader understanding of such processes.

APPENDIX 1: OIL-WATER DISPERSION RESULTS

Table A1.1: Effect of oscillation time on the relative oil fraction (x_o = 140mm, α = 31%, L = 600mm)

Oscillation time (mins)	Relative oil fraction, f_r			
	f = 0.2Hz	f = 0.3Hz	f = 0.4 Hz	f = 0.5Hz
0	0	0	0	0
0.5	0	0.20	0.60	0.68
1	0	0.27	0.38	0.83
2	0	0.32	0.70	0.87
3	0.05	0.35	0.92	0.95
4	0.03	0.36	0.83	0.93
5	0.03	0.34	0.88	0.93
6	0.03	0.44	0.89	1
7	0.03	0.38	0.85	1
8	0.04	0.39	0.84	1
9	0.05	0.43	0.85	1
10	0.05	0.43	0.89	1

Table A1.2: Effect of oscillation frequency on the relative oil fraction (x_o = 140mm, α = 31%, L = 600mm, oil phase fraction = 20%)

Oscillation frequency (Hz)	Relative oil fraction, f_r
0.2	0.05
0.25	0.3
0.3	0.45
0.4	0.9
0.5	1

Table A1.3: Effect of oscillation amplitude on the relative oil fraction (f = 0.25Hz, α = 31%, L = 600mm, oil phase fraction = 20%)

Oscillation amplitude (mm)	Relative oil fraction, f_r
100	0.01
120	0.06
140	0.3
160	0.55
180	0.75
200	95

Table A1.4: Effect of oscillation frequency and amplitude on the relative oil fraction (α = 25%, L = 600mm, oil phase fraction = 20%)

Oscillation frequency (Hz)	Relative oil fraction, f_r		
	x_o = 100mm	x_o = 140mm	x_o = 180mm
0.15		0.03	0.15
0.2		0.1	0.6
0.25	0.1	0.45	0.85
0.3	0.25	0.75	0.95
0.35	0.65	0.95	1
0.4	0.95	0.95	
0.45		1	
0.5	0.95		
0.55			
0.6	1		

Table A1.5: Effect of oscillation frequency and amplitude on the relative oil fraction (α = 20%, L = 600mm, oil phase fraction = 20%)

Oscillation frequency (Hz)	Relative oil fraction, f_r		
	x_o = 100mm	x_o = 140mm	x_o = 180mm
0.1			0.1
0.15		0.1	0.5
0.2	0.05	0.55	0.95
0.25	0.35	0.9	1
0.3	0.7	1	1
0.35	0.85	1	
0.4	0.9	1	
0.45	0.95		
0.5	1		

Table A1.6: Effect of oscillation frequency and amplitude on the relative oil fraction (α = 25%, L = 500mm, oil phase fraction = 20%)

Oscillation frequency (Hz)	Relative oil fraction, f_r		
	x_o = 100mm	x_o = 140mm	x_o = 180mm
0.15		0.2	0.2
0.2	0.15	0.45	0.85
0.25		0.75	0.9
0.3	0.5	0.93	1
0.35		1	1
0.4	0.85	1	
0.45			
0.5	1		

Table A1.7: Effect of oscillation frequency and amplitude on the relative oil fraction (α = 25%, L = 800mm, oil phase fraction = 20%)

Oscillation frequency (Hz)	Relative oil fraction, f_r		
	x_o = 100mm	x_o = 140mm	x_o = 180mm
0.2	0.15	0.2	0.75
0.25		0.5	0.9
0.3	0.35	0.8	0.95
0.35			1
0.4	0.8	1	
0.45			
0.5	1	1	
0.55			
0.6	1		
0.65			
0.7	1		

Table A1.8: Effect of phase fraction on relative oil fraction (x_o = 140mm, α = 20%, L = 600mm)

Oscillation frequency (Hz)	Relative oil fraction, f_r			
	$\phi = 0.1$	$\phi = 0.2$	$\phi = 0.3$	$\phi = 0.36$
0.2	0.2	0.25	0.24	0.3
0.25	0.7	0.8	0.76	0.75
0.3	0.8	0.8	0.89	0.92
0.35	0.9	1	0.92	0.97
0.4	1	1	1	1

APPENDIX 2: HEAT TRANSFER RESULTS

Appendix 2.1: Experimental and Calculated Results for Continuous Operation

Table A2.1: Effect of shell side flowrate on heat transfer rate

m_c (kg/s)	0.167	0.333	0.5	0.667
Re_s	517.7	1032.3	1550	2067.7
T_{ci} (°C)	6.3	6.4	6.4	6.4
T_{co} (°C)	22	16	13.3	12.1
T_{hi} (°C)	53.8	54.5	54.9	54.8
T_{ho} (°C)	47.8	48.3	47.1	47.2
Q (kW)	10.96	13.36	14.42	15.89
U ($kW/m^2.K$)	0.292	0.323	0.340	0.370

Appendix 2.2: Recorded Temperature Data for Batch Operation

Table A2.2: Recorded temperature data (f = 0.8Hz, x_o = 50mm)

time (s)	T_{in} (°C)	T_{out} (°C)	T_{middle} (°C)	T_{bottom} (°C)
0	12.0	58.4	54.0	51.7
10	8.4	58.7	54.3	51.9
20	7.5	57.8	53.8	51.2
30	7.4	57.5	53.4	51.0
40	7.2	52.9	52.4	50.3
50	7.6	35.5	52.2	49.8
60	7.6	24.8	51.5	49.8
70	7.7	20.2	50.2	48.7
80	7.7	18.7	49.8	48.4
90	7.1	17.2	48.7	47.1
100	7.4	16.6	49.2	46.5
110	6.7	15.2	47.9	45.5
120	7.1	14.5	48.4	46.2
130	7.5	13.7	46.7	45.1
140	7.9	14.0	46.0	44.8
150	7.4	13.4	45.2	43.5
160	7.5	13.7	45.2	42.9
170	7.0	13.1	45.0	42.3
180	7.3	12.8	44.6	42.1
190	7.3	12.1	43.6	42.0
200	7.5	12.7	42.7	41.4
210	7.3	12.9	42.0	40.7
220	7.1	12.4	41.7	39.5
230	6.7	12.2	42.0	39.5
240	6.9	11.3	41.1	39.1
250	7.1	11.5	40.8	39.1
260	7.0	11.7	39.6	38.4
270	7.4	11.7	39.7	38.1
280	7.0	11.8	39.2	36.9
290	7.1	12.2	38.9	36.8
300	5.3	8.8	30.6	28.6

Table A2.3: Recorded temperature data (f = 1.2Hz, x_o = 50mm)

time (s)	T_{in} (°C)	T_{out} (°C)	T_{middle} (°C)	T_{bottom} (°C)
0	13.3	59.0	57.1	54.8
10	8.7	59.6	57.5	55.0
20	7.8	58.4	56.4	54.5
30	7.7	58.3	55.9	54.2
40	7.6	55.8	54.9	53.2
50	8.1	37.9	54.7	52.2
60	7.8	26.6	53.5	51.4
70	7.7	22.0	52.3	50.8
80	7.5	20.0	51.5	50.0
90	7.3	18.4	50.8	48.7
100	7.2	16.9	50.5	48.0
110	7.4	16.1	49.4	47.1
120	7.4	15.8	48.8	46.9
130	7.3	15.0	47.5	45.6
140	7.5	15.3	47.1	45.7
150	7.7	15.1	46.6	44.1
160	7.6	14.0	46.1	43.5
170	7.7	13.9	45.1	43.2
180	7.6	14.1	44.2	42.6
190	7.3	14.0	43.4	41.8
200	7.5	13.5	43.4	41.1
210	7.5	13.3	42.2	39.8
220	7.1	13.0	41.4	39.7
230	7.1	12.7	40.9	38.9
240	7.2	13.0	40.6	38.8
250	6.8	13.0	40.0	37.6
260	7.1	12.2	39.7	37.4
270	7.3	12.2	38.6	36.4
280	7.0	12.3	38.4	36.5
290	6.9	11.8	37.6	36.0
300	6.0	10.2	30.1	29.1

Table A2.4: Recorded temperature data (f = 1.6Hz, x_o = 50mm)

time (s)	T_{in} (°C)	T_{out} (°C)	T_{middle} (°C)	T_{bottom} (°C)
0	11.9	56.6	53.3	50.8
10	8.3	57.1	52.9	51.0
20	7.7	56.8	52.6	49.6
30	7.5	56.9	52.0	50.2
40	7.7	53.7	50.2	48.3
50	7.6	36.4	51.4	48.6
60	8.2	25.8	49.4	46.8
70	7.6	21.7	48.9	46.0
80	7.1	18.5	47.7	45.8
90	7.9	18.7	47.3	44.5
100	6.8	16.4	46.5	43.7
110	7.6	16.4	45.0	42.8
120	6.8	15.0	44.6	42.0
130	7.8	15.2	43.3	41.2
140	6.9	13.9	43.0	40.5
150	8.0	14.5	42.1	40.2
160	7.0	13.9	41.8	39.2
170	7.5	13.8	40.7	38.6
180	6.9	13.3	40.5	37.7
190	7.4	13.4	39.3	37.4
200	7.1	13.4	38.9	36.3
210	7.2	13.3	37.6	36.1
220	7.0	12.7	38.0	35.4
230	7.2	12.8	36.8	35.3
240	6.7	12.3	35.7	33.8
250	7.0	12.2	35.7	34.1
260	6.7	12.1	34.6	32.9
270	7.0	11.8	34.5	33.0
280	6.8	12.2	33.7	31.8
290	7.2	11.9	34.0	32.1
300	5.5	9.4	26.0	24.5

Table A2.5: Recorded temperature data (f = 2.0Hz, x_o = 50mm)

time (s)	T_{in} (°C)	T_{out} (°C)	T_{middle} (°C)	T_{bottom} (°C)
0	9.8	58.7	55.7	53.1
10	8.9	58.4	55.9	53.6
20	8.2	57.8	54.4	52.0
30	7.8	57.0	54.1	50.8
40	7.7	53.3	52.8	50.8
50	7.3	38.2	50.7	48.9
60	7.1	27.1	50.2	47.8
70	6.7	22.9	49.2	47.3
80	6.5	20.1	47.6	45.2
90	6.4	18.6	46.5	44.6
100	6.4	17.2	46.0	43.9
110	6.4	16.8	44.7	42.1
120	6.1	15.9	43.8	41.7
130	6.3	15.1	43.2	40.0
140	6.2	14.7	42.2	39.2
150	6.2	14.1	41.1	38.5
160	6.5	14.2	40.6	38.4
170	6.1	13.0	39.2	37.0
180	6.3	13.1	38.2	36.3
190	5.9	13.0	38.2	35.3
200	5.9	12.5	36.1	34.6
210	6.3	12.7	36.2	34.6
220	6.0	12.4	35.4	33.2
230	6.1	11.7	34.4	31.9
240	6.2	11.7	34.6	32.0
250	6.1	12.4	33.1	31.2
260	6.5	11.7	32.9	30.7
270	6.4	11.7	32.8	29.8
280	6.2	11.2	31.6	29.5
290	6.3	11.6	31.2	28.5
300	4.8	8.7	24.6	22.6

Table A2.6: Recorded temperature data (f = 0.6Hz, x_o = 75mm)

time (s)	T_{in} (°C)	T_{out} (°C)	T_{middle} (°C)	T_{bottom} (°C)
0	24.2	58.8	54.2	52.0
10	12.4	59.3	54.2	52.3
20	11.1	58.6	54.0	52.7
30	10.9	57.5	54.0	52.0
40	10.7	54.8	52.7	50.6
50	11.4	40.4	52.6	50.7
60	11.4	29.0	51.5	49.9
70	10.6	24.1	51.0	49.0
80	9.7	22.1	49.7	48.1
90	9.5	20.1	50.1	47.9
100	9.2	19.5	48.7	46.9
110	7.9	18.3	47.9	46.5
120	7.9	17.2	47.3	45.7
130	8.0	16.9	46.4	45.1
140	7.8	15.4	46.3	45.2
150	7.2	15.1	44.9	43.6
160	7.4	15.2	45.1	43.0
170	8.0	14.9	44.6	42.1
180	7.3	13.7	43.9	41.7
190	7.4	13.7	43.2	40.6
200	7.6	13.2	42.9	40.2
210	7.7	12.9	41.7	40.3
220	7.1	12.6	40.9	39.6
230	7.0	13.0	40.7	39.4
240	6.9	13.1	40.7	38.8
250	6.8	12.4	39.3	38.0
260	6.8	12.8	39.1	37.1
270	7.4	12.3	39.1	36.7
280	6.9	11.7	38.3	35.8
290	7.2	11.6	37.5	35.7
300	7.0	11.2	37.8	35.0

Table A2.7: Recorded temperature data (f = 1.0Hz, x_o = 75mm)

time (s)	T_{in} (°C)	T_{out} (°C)	T_{middle} (°C)	T_{bottom} (°C)
0	20.2	57.6	54.2	52.4
10	10.9	57.5	54.4	52.0
20	10.9	57.5	53.9	52.2
30	10.3	55.8	53.0	51.2
40	9.8	54.3	53.2	50.3
50	9.7	39.1	51.8	49.8
60	9.1	28.3	50.2	47.9
70	9.5	25.4	49.9	47.8
80	9.6	22.1	49.4	46.7
90	9.3	19.9	47.3	45.9
100	9.5	20.0	46.7	45.1
110	9.2	18.0	45.9	44.1
120	9.6	17.2	44.8	42.8
130	9.5	17.5	45.1	42.4
140	8.8	16.5	43.3	41.3
150	8.6	16.3	42.5	41.4
160	8.6	16.4	41.7	40.2
170	8.2	15.4	41.1	38.8
180	8.4	15.6	40.9	38.5
190	7.8	15.3	39.6	37.9
200	7.6	14.3	38.9	36.8
210	7.8	14.5	38.7	36.7
220	7.6	14.2	38.1	36.1
230	7.7	13.7	37.3	35.3
240	7.8	13.8	37.1	34.6
250	7.5	13.0	36.3	33.9
260	7.7	13.0	35.7	33.2
270	7.8	13.4	35.0	33.4
280	7.2	13.1	34.0	32.3
290	7.6	13.3	34.0	32.0
300	7.8	12.9	34.2	31.6

Table A2.8: Recorded temperature data (f = 1.4Hz, x_o = 75mm)

time (s)	T_{in} (°C)	T_{out} (°C)	T_{middle} (°C)	T_{bottom} (°C)
0	14.4	57.3	54.1	51.7
10	8.9	57.0	54.1	51.7
20	7.4	56.2	53.1	51.1
30	7.9	56.8	52.9	50.8
40	7.5	53.3	52.7	50.1
50	7.6	36.6	50.4	48.5
60	7.6	25.7	49.0	47.3
70	7.6	22.1	48.3	46.6
80	7.9	20.4	48.3	45.9
90	7.1	18.3	46.4	44.4
100	7.4	17.8	45.9	43.3
110	7.5	16.8	44.8	43.2
120	7.1	15.1	43.3	41.9
130	7.6	15.5	42.7	41.5
140	7.0	14.8	41.7	40.0
150	6.9	14.0	40.9	38.9
160	7.5	14.1	40.8	38.8
170	7.3	13.8	39.8	37.9
180	7.2	13.5	38.5	36.5
190	7.3	14.2	38.6	36.6
200	7.4	13.6	37.7	35.6
210	7.1	13.3	37.1	35.0
220	7.3	13.7	36.3	34.9
230	6.8	12.5	35.3	33.5
240	7.3	12.7	35.5	33.6
250	7.1	12.5	35.0	32.7
260	7.0	12.2	33.7	31.6
270	6.9	12.2	33.7	31.7
280	6.7	11.6	32.5	30.4
290	6.6	11.5	31.9	29.9
300	7.0	9.9	25.4	23.8

Table A2.9: Recorded temperature data (f = 0.6Hz, x_o = 100mm)

time (s)	T_{in} (°C)	T_{out} (°C)	T_{middle} (°C)	T_{bottom} (°C)
0	13.8	59.3	54.4	52.3
10	7.6	59.5	54.7	52.6
20	6.9	58.3	53.8	51.4
30	6.9	57.6	53.5	51.2
40	6.9	55.2	52.5	50.2
50	6.5	39.5	50.9	49.1
60	6.5	26.7	50.8	48.8
70	6.2	20.9	49.5	47.1
80	6.4	18.7	48.1	46.8
90	6.4	17.1	47.9	45.7
100	6.3	15.4	46.7	45.0
110	6.6	15.4	46.4	44.0
120	5.9	14.3	44.8	42.7
130	6.7	13.7	44.1	42.4
140	6.6	13.2	43.6	41.9
150	6.3	13.4	42.9	41.1
160	6.6	13.0	42.3	40.6
170	6.3	12.3	40.8	39.0
180	6.6	12.6	41.2	39.1
190	6.4	11.9	40.2	38.5
200	6.4	12.1	39.2	37.6
210	6.3	12.0	39.0	36.8
220	6.0	11.8	38.0	35.9
230	6.4	12.2	37.6	36.1
240	5.9	11.6	36.6	34.9
250	6.5	11.7	36.3	34.3
260	6.1	11.3	36.6	34.0
270	6.4	11.2	34.8	33.1
280	6.4	11.4	35.3	33.5
290	6.3	11.0	33.9	32.1
300	5.2	9.4	27.2	25.4

Table A2.10: Recorded temperature data (f = 0.8Hz, x_o = 100mm)

time (s)	T_{in} (°C)	T_{out} (°C)	T_{middle} (°C)	T_{bottom} (°C)
0	22.0	56.6	54.4	52.3
10	7.4	56.1	53.9	52.0
20	6.9	55.6	53.6	51.6
30	6.6	55.3	52.7	50.7
40	6.9	52.9	51.9	50.0
50	6.9	37.6	51.2	49.2
60	6.7	25.3	49.4	47.7
70	6.9	20.9	48.5	46.5
80	6.4	17.3	47.6	45.3
90	7.0	16.7	46.7	44.8
100	6.8	16.3	45.7	43.9
110	6.5	14.9	44.4	42.3
120	6.5	14.4	44.2	42.0
130	6.6	13.9	42.7	40.8
140	6.6	13.6	42.0	40.1
150	6.5	13.3	41.5	39.3
160	6.7	13.4	40.1	38.3
170	6.1	12.2	39.1	37.1
180	6.9	13.3	39.5	37.0
190	6.8	12.8	38.8	36.7
200	6.3	12.1	36.6	34.6
210	6.7	12.4	37.4	35.2
220	6.7	12.0	36.3	34.1
230	6.8	12.5	35.7	33.6
240	6.2	11.3	34.2	32.4
250	6.7	11.6	34.5	32.5
260	6.9	11.8	34.3	32.2
270	6.2	11.2	32.8	30.6
280	6.1	10.8	32.4	30.3
290	6.3	11.0	32.1	30.1
300	5.6	9.0	25.8	23.9

Table A2.11: Recorded temperature data (f = 1.0Hz, x_o = 100mm)

time (s)	T_{in} (°C)	T_{out} (°C)	T_{middle} (°C)	T_{bottom} (°C)
0	17.1	58.0	55.5	53.0
10	8.0	57.9	55.4	52.4
20	7.2	57.1	54.7	52.1
30	7.8	56.1	53.9	51.4
40	7.0	54.7	52.9	50.1
50	7.2	42.1	51.7	49.6
60	7.2	27.4	50.5	47.8
70	7.0	22.5	49.7	46.6
80	6.6	20.2	48.4	45.7
90	6.5	18.4	46.5	44.7
100	6.9	17.5	45.9	44.1
110	6.4	16.4	44.7	43.4
120	6.6	15.4	43.6	41.6
130	6.8	15.1	42.9	41.0
140	6.9	14.1	41.9	39.3
150	7.1	14.5	41.8	39.2
160	7.0	14.7	40.8	38.9
170	6.7	13.4	38.7	37.6
180	7.1	13.3	38.4	36.5
190	7.2	13.2	38.6	35.6
200	7.0	13.2	37.2	35.2
210	6.9	13.0	36.6	34.6
220	6.7	12.2	35.7	33.2
230	6.9	12.7	35.5	32.8
240	6.4	12.6	34.6	32.7
250	6.5	11.8	33.9	31.4
260	6.9	12.2	33.8	31.0
270	6.5	12.0	32.6	30.5
280	6.6	12.2	31.6	30.0
290	6.9	11.4	31.3	29.8
300	5.4	9.0	24.4	22.8

Table A2.12: Recorded temperature data (no oscillation)

time (min)	T_{in} (°C)	T_{out} (°C)	T_{middle} (°C)	T_{bottom} (°C)
0	28.1	57.3	52.0	50.3
1	6.7	26.8	52.5	50.5
2	6.3	12.2	50.2	43.4
3	6.2	9.9	51.0	39.3
4	6.1	9.4	49.9	35.8
5	6.1	9.0	49.0	33.0
6	6.0	8.7	47.2	30.4
7	5.9	8.8	46.4	28.8
8	5.8	8.4	45.5	27.0
9	5.6	8.1	44.3	25.5
10	5.6	8.2	42.9	24.7
11	5.6	8.1	42.2	23.6
12	5.5	7.9	40.6	22.5
13	5.6	8.0	39.7	21.7
14	5.4	7.8	38.0	20.4
15	5.5	7.8	37.6	19.8
16	5.5	7.8	36.5	19.4
17	5.5	7.7	34.7	18.7
18	5.4	7.6	35.2	18.1
19	5.5	7.8	34.2	17.6
20	5.3	7.7	31.1	17.1

Table A2.13: Recorded temperature data (no oscillation, no shell side flow)

time (min)	T_{middle} (°C)	T_{bottom} (°C)
0	49.8	49.8
1	49.5	49.8
2	49.2	49.8
3	49.6	49.8
4	49.4	49.7
5	50.3	50.0
6	49.5	49.6
7	49.9	49.7
8	49.8	49.7
9	49.6	49.5
10	49.5	49.5
11	49.6	49.4
12	49.8	49.2
13	49.9	49.3
14	49.9	49.2
15	49.7	49.0
16	49.5	48.9
17	49.6	48.9
18	49.7	48.9
19	49.8	49.0
20	49.6	49.0
21	49.6	48.9
22	49.6	49.0
23	49.8	49.0
24	49.8	48.8
25	49.7	48.8
26	49.7	48.7
27	49.8	48.5
28	49.5	48.3
29	49.8	48.3
30	49.7	45.8

Appendix 2.3: Calculated Heat Transfer Data

Table A2.14: Heat transfer data for batch experiments

f (Hz)	x_o (mm)	x_of (m/s)	Re_o	T_{in}	T_i	T_f	t (s)	U ($W/m^2.K$)	h_t ($W/m^2.K$)	Nut
0.8	50	0.04	224	7.4	51.7	36.0	290	0.127	0.148	55.29
1.2	50	0.06	336	7.6	54.9	36.3	290	0.145	0.174	65.14
1.6	50	0.08	448	7.4	50.9	31.3	290	0.174	0.218	81.29
2.0	50	0.1	561	6.6	53.3	28.3	290	0.227	0.306	114.2
0.6	75	0.045	252	8.6	52.0	35.4	290	0.139	0.166	61.95
1.0	75	0.075	420	8.9	52.8	32.1	290	0.187	0.237	88.48
1.4	75	0.105	589	7.4	51.6	29.6	290	0.203	0.265	98.89
0.6	100	0.06	336	6.6	52.7	31.9	290	0.175	0.219	81.95
0.8	100	0.08	448	6.9	52.0	30.1	290	0.196	0.252	94.19
1.0	100	0.1	561	7.1	52.7	29.0	290	0.217	0.288	107.7

APPENDIX 3: DROPLET SIZE DISTRIBUTION RESULTS

Appendix 3.1 DSD Data Collected at Various Operating Conditions

Table A3.1: Effect of droplet number on droplet size distribution

d_i (μm)	Number of droplets of diameter d_i				
	75 drops	191 drops	356 drops	487 drops	950 drops
5	3	4	9	12	20
15	15	61	151	213	418
25	20	52	81	105	202
35	18	36	52	72	139
45	10	19	29	38	81
55	6	11	18	20	42
65	2	4	8	12	26
75	1	3	4	6	11
85		0	1	2	3
95		0	0	0	0
105		1	1	1	1
115			0	1	1
125			0	0	0
135			0	0	1
145			0	0	0
155			1	1	1
165			1	3	3
175				1	1

Table A3.2: Results of repeatability tests

d_i (μm)	Number of droplets of diameter d_i		
	day 1	day 2	day 3
5	12	22	15
15	213	215	230
25	105	81	101
35	72	40	62
45	38	23	35
55	20	22	20
65	12	19	13
75	6	11	8
85	2	5	4
95	0	4	3
105	1	2	2
115	1	1	2
125	0	0	1
135	0	1	1
145	0	1	1
155	1	0	1
165	3	1	0
175	1	0	1
185	0	1	0
195			1
d_{32} (μm)	**74.3**	**75.1**	**78.3**

Table A3.3: Effect of sampling location on droplet size distribution

d_i (μm)	Number of droplets of diameter d_i		
	Bottom	Middle	Top
5	35	12	12
15	201	213	198
25	77	105	79
35	53	72	47
45	25	38	23
55	21	20	14
65	17	12	10
75	2	6	3
85	2	2	5
95	2	0	3
105	1	1	2
115	2	1	3
125	2	0	2
135	1	0	1
145	1	0	1
155	0	1	1
165	1	3	0
175		1	
d_{32} (μm)	**69.6**	**74.3**	**73.2**

Table A3.4: Effect of oscillation time on droplet size distribution

d_i (μm)	Number of droplets of diameter d_i			
	t = 15 mins	t = 30 mins	t = 45 mins	t = 60 mins
5	9	13	12	28
15	173	227	206	271
25	132	143	130	149
35	101	73	68	94
45	78	45	49	57
55	42	25	24	36
65	23	11	18	10
75	25	6	12	13
85	13	8	9	10
95	13	4	5	6
105	9	1	3	3
115	6	1	2	2
125	7	1	1	1
135	3	0	1	0
145	5	1	0	1
155	4	0	1	0
165	3	0	0	1
175	3	1	0	0
185	0	0		
195	1			
205	2			
215	0			
225	0			
235	1			
245	2			
255	1			
265	0			
275	1			
285	0			
d_{32} (μm)	**122.6**	**62.4**	**64.4**	**62.8**

Table A3.5: Effect of oscillation frequency and amplitude on droplet size distribution

(α = 20%, L = 315mm)

d_i (μm)	Number of droplets of diameter d_i								
	x_o = 50mm			x_o = 75mm			x_o = 100mm		
	f=0.8 Hz	f=1.2 Hz	f=1.60Hz	f=0.6 Hz	f=1.0 Hz	f=1.4 Hz	f=0.4 Hz	f=0.6 Hz	f=0.8 Hz
5	16	38	23	21	13	17	26	11	23
15	170	173	296	73	243	336	158	196	249
25	73	78	133	132	143	110	105	86	77
35	44	51	67	72	73	48	55	46	43
45	41	29	33	50	45	19	33	30	21
55	18	26	39	35	25	11	23	12	21
65	19	14	8	26	11	3	18	9	6
75	6	10	8	30	6	3	14	4	5
85	10	7	2	12	8	2	3	4	5
95	7	4	2	9	4		9	2	2
105	11	5	2	7	1		7	1	4
115	7	1	0	13	1		5	1	1
125	6	2	5	3	1		2	0	1
135	1	2	1	5	0		2	0	1
145	4	3	2	0	1		2	0	
155	1	2	1	5	0		3	1	
165	2	1	0	1	0		1	0	
175	6	1	1	0	1			0	
185	2	0		1				1	
195	3	1		0					
205	2	0		0					
215	1	1		1					
225	0	0		2					
235	1	1		0					
245	0			0					
255	1			0					
265	1			1					
275	1								
285									
295									
d_{32}	**145**	**106**	**72**	**109**	**62**	**37**	**88**	**67**	**61**

Table A3.6: Effect of oscillation frequency and amplitude on droplet size distribution

(α = 25%, L = 315mm)

d_i (μm)	Number of droplets of diameter d_i									
	x_o = 50mm			x_o = 75mm			x_o = 100mm			
	f=0.8 Hz	f=1.2 Hz	f=1.6 Hz	f=0.6 Hz	f=0.8 Hz	f=1.0 Hz	f=0.4 Hz	f=0.6 Hz	f=0.8 Hz	f=1.0 Hz
5	1	34	14	5	8	12	35	2	15	27
15	174	142	213	161	208	213	119	131	301	348
25	87	46	87	61	130	105	53	125	136	126
35	63	38	84	40	65	72	43	56	80	56
45	38	37	54	38	29	38	33	38	65	47
55	26	20	35	31	19	20	28	22	31	27
65	27	20	24	15	10	12	28	17	30	14
75	18	16	12	11	8	6	27	17	20	8
85	16	12	9	10	3	2	9	9	20	2
95	9	4	10	7	1	0	8	8	3	1
105	11	5	3	7	7	1	8	2	5	4
115	7	7	5	1	2	1	6	1	4	1
125	3	3	4	2	2	0	3	3	3	
135	4	1	2	2	1	0	3	2	0	
145	5	2	1	1	1	0	4	2	1	
155	4	2	0	2	2	1	6	1	1	
165	5	2	1	1	3	3	4	1		
175	4	1	2	0	0	1	2	1		
185	0	0		0	1		2	0		
195	3	1		0	2		1	0		
205	1	1		0			2	0		
215	1			1			1	1		
225	2			0			1			
235	1			1			0			
245	0			0			1			
255	1			0			1			
265	0			1			1			
275	1			0			1			
285	0			1						
295	1									
305	0									
315	1									
325	1									
d_{32}	**156**	**100**	**80**	**131**	**97**	**74**	**140**	**88**	**68**	**50**

Table A3.7: Effect of oscillation frequency and amplitude on droplet size distribution (α = 30%, L = 315mm)

d_i (μm)	Number of droplets of diameter d_i								
	x_o = 50mm			x_o = 75mm			x_o = 100mm		
	f=1.2 Hz	f=1.6 Hz	f=2.0 Hz	f=0.6 Hz	f=1.0 Hz	f=1.4 Hz	f=0.4 Hz	f=0.6 Hz	f=0.8 Hz
5	10	28	16	24	31	50	19	19	21
15	175	122	327	73	215	330	151	286	493
25	73	98	165	33	53	100	81	106	106
35	61	53	87	38	43	74	60	63	72
45	41	43	39	22	37	53	42	32	41
55	31	27	20	25	17	19	37	15	29
65	26	14	5	26	17	15	28	28	19
75	17	8	5	26	21	6	20	17	8
85	16	11	2	24	21	4	16	10	3
95	18	3	2	25	13	2	13	3	5
105	10	6	2	13	13	2	6	5	1
115	4	1	1	9	10	1	8	7	1
125	7	1	2	7	5	2	4	5	1
135	10	3	2	3	6	0	6	3	3
145	6	2	1	6	3	1	4	3	0
155	5	1	2	8	8		2	1	0
165	3	0		3	4		2	1	1
175	0	1		5	4		1		0
185	2	0		3	1		0		0
195	4	1		3	1		1		0
205	8			3			0		1
215	0			2			0		
225	1			2			1		
235				1			1		
245				1			0		
255				1			2		
265				0					
275				1					
285				0					
295				1					
d_{32}	**127**	**85**	**65**	**148**	**111**	**54**	**115**	**107**	**69**

Table A3.8: Effect of oscillation frequency and amplitude on droplet size distribution (α = 25%, L = 263mm)

d_i (μm)	Number of droplets of diameter d_i								
	x_o = 50mm			x_o = 75mm			x_o = 100mm		
	f=1.2 Hz	f=1.6 Hz	f=2.0 Hz	f=0.6 Hz	f=1.0 Hz	f=1.4 Hz	f=0.6 Hz	f=0.8 Hz	f=1.0 Hz
5	4	4	3	4	10	8	5	3	2
15	139	188	214	161	212	168	138	222	264
25	74	102	125	118	100	108	104	82	150
35	52	64	76	51	76	65	76	37	108
45	43	32	40	38	42	45	59	24	42
55	21	35	28	28	24	19	30	18	30
65	20	16	19	20	18	26	30	6	22
75	19	13	9	19	12	15	17	6	16
85	18	11	13	11	9	16	9	13	8
95	9	7	3	7	7	8	8	3	4
105	2	3	4	6	0	3	5	2	0
115	5	3	5	6	2	2	3	2	0
125	8	1	2	9	4	1	3	2	2
135	7	1	0	4	2		2	2	2
145	4	2	1	2	2		2	0	2
155	3	1		4	1		2	2	
165	3			2	0		5	1	
175	2			3	2		2		
185	1			0	2		0		
195	1			0	0		0		
205	1			1	0		1		
215				1	1		0		
225				2			0		
235				1			0		
245				1			0		
255				2			1		
265				1			1		
275				2			0		
285				2			0		
295							0		
305							1		
d_{32}	**107**	**72**	**66**	**158**	**93**	**64**	**123**	**80**	**62**

Table A3.9: Effect of oscillation frequency and amplitude on droplet size distribution

(α = 25%, L = 368mm)

d_i (μm)	**Number of droplets of diameter d_i**								
	x_o = 50mm			x_o = 75mm			x_o = 100mm		
	f=0.8 Hz	f=1.2 Hz	f=1.6 Hz	f=0.6 Hz	f=1.0 Hz	f=1.4 Hz	f=0.6 Hz	f=0.8 Hz	f=1.0 Hz
5	16	23	24	1	12	12	6	33	5
15	161	121	154	110	140	149	259	162	227
25	53	80	109	106	101	142	97	157	84
35	51	58	77	79	58	70	58	68	39
45	48	48	50	62	50	32	38	29	29
55	39	24	43	32	25	15	27	26	12
65	30	40	22	38	14	17	15	25	12
75	21	14	16	25	7	5	15	7	8
85	14	14	12	17	12	5	10	5	1
95	8	9	4	8	11	4	7	5	6
105	7	3	6	28	2	3	4	7	2
115	6	6	4	5	4	1	2	5	2
125	3	4	3	11	3		3	5	
135	9	8	4	12	1		1	1	
145	6	4	2	7	0		1	1	
155	4	3	6	4	0		5	0	
165	0	4	1	4	3		1	0	
175	3	1	2	4	1		3	0	
185	2	1	0	5	0		3	0	
195	3	4	1	3	1		1	1	
205	2	2		2			0		
215	1	2		2			1		
225	3	1		1			1		
235	1			2			0		
245	0			2			0		
255	0			0			1		
265	2			0					
275	0			1					
285	1			1					
295	1			0					
305	1			1					
315	1								
d_{32}	**160**	**122**	**93**	**143**	**86**	**55**	**118**	**77**	**58**

Appendix 3.2 Data Used for Breakage and Coalescence Modelling

Appendix 3.2.1 Data from Breakage-Only Experiments

Table A3.10: Change in DSD with time (f = 0.6 Hz, x_o = 75 mm)

droplet diameter (μm)	Droplet number frequency after a given time				
	10 mins	20 mins	30 mins	40 mins	50 mins
5	28	12	20	19	6
15	108	162	281	115	322
25	56	111	88	110	67
35	54	70	55	64	44
45	35	55	42	45	51
55	28	26	22	34	27
65	24	24	17	19	21
75	17	25	17	19	13
85	17	17	8	9	15
95	14	9	17	8	10
105	12	10	18	7	1
115	10	13	3	7	4
125	9	4	4	3	
135	9	5	2	3	
145	4	6	3	6	
155	2	5	1	1	
165	2	5	1	0	
175	3	1	0	0	
185	6	3	0	0	
195	3	2	1	1	
205	2	1	0	0	
215	1	0	1	1	
225	3	1			
235	1	1			
245	1	0			
255	0	0			
265	0	1			
275	1	1			
285	0				
295	0				
305	0				
315	1				
325	0				
335	1				

Table A3.11: Change in DSD with time (f = 1.0 Hz, x_o = 75 mm)

droplet diameter (μm)	**Droplet number frequency after a given time**				
	10 mins	20 mins	30 mins	40 mins	50 mins
5	5	13	20	10	7
15	158	188	200	184	417
25	125	141	162	169	206
35	62	82	97	107	88
45	45	71	58	67	60
55	42	40	46	28	45
65	27	28	30	35	28
75	10	22	27	23	25
85	17	28	26	22	18
95	12	17	16	17	4
105	10	17	6	9	0
115	2	11	5	2	1
125	2	5	2	2	
135	1	0	1		
145	0	2	2		
155	1	0			
165	0	1			
175	0	1			
185	2				

Table A3.12: Change in DSD with time (f = 1.4 Hz, x_o = 75 mm)

droplet diameter (μm)	**Droplet number frequency after a given time**				
	10 mins	20 mins	30 mins	40 mins	50 mins
5	21	17	14	46	24
15	350	344	232	662	559
25	168	128	143	292	262
35	104	50	67	103	69
45	54	11	27	50	11
55	38	9	17	13	5
65	14	3	6	5	2
75	3	1	3	1	
85	5	1	0	1	
95	2	2	2		
105	0	1	1		
115	0	2			
125	0	1			
135	2				
145	1				

Table A3.13: Change in DSD with time (f = 1.0 Hz, x_o = 50 mm)

droplet diameter (μm)	**Droplet number frequency after a given time**				
	10 mins	20 mins	30 mins	40 mins	50 mins
5	18	13	11	7	1
15	176	160	164	105	85
25	112	116	129	156	154
35	81	78	76	116	92
45	57	57	56	85	57
55	41	30	40	53	49
65	27	29	42	45	29
75	22	21	29	30	26
85	21	17	21	26	19
95	14	12	15	10	5
105	6	13	5	10	6
115	3	6	6	6	2
125	6	5	5	5	1
135	2	3	2	2	2
145	3	7	2	2	3
155	3	4	2	1	
165	4	2	1	1	
175	3	2			
185	5	1			
195	1	1			
205	0	0			
215	1	1			
225	0	1			
235	1				
245	1				
255	0				
265	2				
275	0				
285	1				
295	0				
305	0				
315	1				

Table A3.14: Change in DSD with time (f = 1.0 Hz, x_o = 100 mm)

droplet diameter (μm)	**Droplet number frequency after a given time**				
	10 mins	20 mins	30 mins	40 mins	50 mins
5	17	10	13	17	21
15	240	233	234	294	266
25	192	207	155	153	111
35	112	133	84	85	79
45	61	89	43	40	29
55	40	63	19	4	5
65	25	39	2	1	1
75	13	23	6	0	3
85	6	14	3	0	1
95	5	3	2	0	
105	2	6	2	1	
115	0	5	0		
125	1	4	0		
135	0	1	1		
145	1	1			
155	2	1			

Appendix 3.2.2 Data from Experiments with Breakage and Coalescence

Table A3.15: Change in DSD with time (f = 0.6 Hz, x_o = 75 mm)

droplet diameter (μm)	**Droplet number frequency after a given time**					
	0 mins	10 mins	20 mins	30 mins	40 mins	50 mins
5	33	30	24	53	42	11
15	251	207	366	306	325	114
25	165	131	196	122	128	68
35	68	64	56	57	63	32
45	37	32	37	34	37	19
55	20	26	12	24	24	16
65	6	5	14	10	16	9
75	13	7	6	12	16	8
85	3	7	7	4	5	2
95	3	4	6	3	5	2
105	2	6	2	5	4	3
115	1	1	0	1	3	0
125			0	0	4	1
135			2	0	1	1
145			1	0	0	2
155			1	4	2	1
165				0	0	0
175				0	1	1
185				1	1	0
195					0	0
205					1	0
215						0
225						1
235						

Table A3.16: Change in DSD with time (f = 0.8 Hz, x_o = 75 mm)

droplet diameter (μm)	**Droplet number frequency after a given time**					
	0 mins	10 mins	20 mins	30 mins	40 mins	50 mins
5	34	67	14	24	8	10
15	251	405	223	269	172	168
25	116	192	127	88	175	191
35	67	74	93	46	93	102
45	26	34	37	19	50	56
55	9	18	27	13	23	31
65	6	9	17	2	14	16
75	3	8	7	6	12	11
85	0	2	3	1	6	5
95	2	3	3	2	4	2
105	1	3	3	2	3	7
115	0	1	2	0	2	2
125	1	0	3	1	3	5
135		1	1	1	8	2
145		1	1	1	3	2
155				2	0	0
165					0	0
175					0	0
185					0	0
195					1	0
205						0
215						0
225						1
235						2

Table A3.17: Change in DSD with time (f = 1.0 Hz, x_o = 75 mm)

droplet diameter (μm)	Droplet number frequency after a given time					
	0 mins	10 mins	20 mins	30 mins	40 mins	50 mins
5	48	14	10	6	32	36
15	352	336	417	194	220	238
25	171	174	220	124	155	202
35	74	120	100	73	76	151
45	26	38	46	46	46	71
55	20	25	23	30	20	50
65	9	15	11	14	15	28
75	2	10	7	7	8	14
85	3	7	5	4	3	7
95	2	1	3	3	5	5
105	3	0	0	2	0	4
115	1	1	3	1	0	2
125	1	1	2	0	4	1
135		1	3	1	1	2
145				1	1	2
155				1	1	1
165					1	0
175						1
185						0
195						0
205						1

Table A3.18: Change in DSD with time (f = 0.8 Hz, x_o = 50 mm)

droplet diameter (μm)	**Droplet number frequency after a given time**					
	0 mins	10 mins	20 mins	30 mins	40 mins	50 mins
5	12	33	35	27	11	6
15	125	329	356	242	441	141
25	185	253	234	215	235	175
35	102	134	129	147	122	112
45	61	81	52	93	96	53
55	24	34	21	45	44	36
65	22	23	16	16	12	23
75	6	10	16	13	8	11
85	2	5	9	8	4	7
95	1	7	7	8	7	9
105	2	3	2	4	2	4
115	1	3	2	3	9	5
125		2	0	3	1	1
135		3	4	4	1	4
145		0	4	1	1	2
155		2	1	1	2	3
165			1	0	0	1
175				0	0	1
185				0	3	1
195				0	2	1
205				0	1	0
215				1		1
225				1		0
235						1

Table A3.19: Change in DSD with time (f = 0.8 Hz, x_o = 100 mm)

droplet diameter (μm)	**Droplet number frequency after a given time**					
	0 mins	10 mins	20 mins	30 mins	40 mins	50 mins
5	25	32	15	23	25	12
15	203	280	316	230	272	246
25	91	125	86	107	156	154
35	39	59	36	52	76	69
45	46	25	22	29	38	43
55	21	20	7	30	37	43
65	12	4	14	16	25	24
75	13	4	8	7	16	19
85	3	4	6	9	11	13
95	2	3	1	2	6	7
105	0	3	3	3	1	4
115	0	1	3	2	1	4
125		1	1	1	2	3
135				0	2	3
145				2	1	0
155					2	0
165					1	0
175						0
185						0
195						3
205						1

APPENDIX 4: POLYMERISATION RESULTS

Appendix 4.1: Particle Size Distribution Data

Table A4.1: Effect of oscillation frequency and amplitude on particle size distribution (α=25%, L=315mm)

d_i (μm)	Cumulative Volume Fraction Oversize (%)				
	x_o = 50mm	x_o = 75mm			x_o = 100mm
	f = 1.0 Hz	f = 0.8 Hz	f = 1.0 Hz	f = 1.2 Hz	f = 1.0 Hz
0	100	100	100	100	100
20	100	100	99.5	97.8	96.8
38	100	98.6	97.7	91.9	90.4
50	100	94.8	94.6	83.6	81.3
53	100	93.8	93.9	81.7	79
63	99.9	90.5	91.8	74.6	68.9
75	98.8	84.5	86.6	62.5	50.7
90	96.7	74.3	75.1	44.3	27.2
100	95.1	66.9	65.4	33.5	15.9
106	93.9	62.5	59.2	28.2	11.6
125	88.7	48.2	39.8	16.1	4.49
140	81.4	37.5	27.1	10.7	2.72
150	75.2	30.8	20.3	8.16	1.98
180	51	14.7	7.44	3.43	0.42
200	34.7	7.91	3.47	1.71	0.064
250	7.49	0.7	0.25	0.095	0
300	0.42	0.0054	0.0017	0.00011	0
$d_{v,0.5}$ (μm)	**174.6**	**115.7**	**109.1**	**79.68**	**68.77**
Wt. % O/size	44	28	12	5	2

Table A4.2: Effect of oscillation frequency and amplitude on particle size distribution (α=25%, L=315mm)

volume % > d_i	**d_i (μm)**			
	x_o = 50mm		x_o = 100 mm	
	f = 0.8 Hz	f = 1.2 Hz	f = 0.8 Hz	f = 1.2 Hz
0	339.8	309.6	282.1	234.1
5	270	229.1	178.3	143.6
10	252.6	212.2	157.3	106.2
20	231.2	192.1	131.1	74.41
25	223.3	184.7	121.9	67.72
30	215.4	177.2	114.8	62.65
40	202.1	165.1	102.6	55.35
50	189.4	153.5	92.4	49.73
60	177	142	83.08	45.05
70	163.9	129.7	73.2	40.81
75	156.5	123	67.41	38.72
80	148.5	115.1	60.13	36.59
90	124.8	94.49	42.46	31.15
95	101	79.67	33.37	25.97
$d_{v,0.5}$ (μm)	**181.3**	**146.4**	**86.26**	**52.58**
Wt. % O/size	66	21	6	5

Table A4.3: Effect of oscillation frequency and amplitude on particle size distribution (α=20%, L=315mm)

d_i (μm)	Cumulative Volume Oversize (%)								
	x_o = 50mm			x_o = 75mm			x_o = 100mm		
	f=0.8 Hz	f=1.0 Hz	f=1.2 Hz	f=0.8 Hz	f=1.0 Hz	f=1.2 Hz	f=0.8 Hz	f=1.0 Hz	f=1.2 Hz
0	100	100	100	100	100	100	100	100	100
20	100	99.9	99.2	98.9	100	96.5	94.2	91	84.7
38	100	98.8	96.8	95.8	98	85.1	79.9	65.4	43.7
50	100	97.3	93	91.1	91.2	70.9	64.8	45	23.7
53	100	97	92.2	90.1	89.3	67.5	61.2	40.9	19.4
63	99.9	96	89.6	86.8	81.4	54.7	48.6	29.4	11.4
75	99.3	94.1	83.9	79.5	67	37.3	32.2	19.3	6.46
90	97.9	91	72.3	65.9	45.9	19.7	15.9	11.3	3.47
100	97.1	89	62.9	56.1	33.8	12.5	9.11	7.89	2.39
106	96.6	87.7	56.8	50.3	28.3	9.95	6.53	6.45	1.95
125	93.5	81.2	37.7	33.7	16	5.57	1.78	3.37	1.03
140	87.4	72.3	25	23.3	10.7	4.11	0.44	1.98	0.61
150	81.3	64.8	18.2	17.7	8.22	3.32	0.097	1.26	0.41
180	55.3	38.1	6.15	6.91	3.24	1.27	0	0.1	0.085
200	36.9	22.7	2.73	3.44	1.41	0.52	0	0.004	0.021
250	6.68	2.55	0.12	0.46	.033	0.019	0	0	0
300	0.23	0.025	0	0.076	0	0	0	0	0
$d_{v,0.5}$ (μm)	**180.8**	**153.6**	**105.1**	**99.82**	**86.55**	**61.71**	**61.91**	**46.67**	**35.2**
Wt. % O/size	25.6	15.4	7.5	4.5	3.2	1.5	9.2	4.5	1.0

Table A4.4: Effect of oscillation frequency and amplitude on particle size distribution (α=30%, L=315mm)

d_i (μm)	Cumulative Volume Oversize (%)								
	x_o = 50mm			x_o = 75mm			x_o = 100mm		
	f=0.8 Hz	f=1.0 Hz	f=1.2 Hz	f=0.8 Hz	f=1.0 Hz	f=1.2 Hz	f=0.8 Hz	f=1.0 Hz	f=1.2 Hz
0	100	100	100	100	100	100	100	100	100
20	100	100	100	99.6	99.6	98.9	99.2	96.8	91.8
38	100	100	100	98.9	98.5	96.3	97.4	88.4	72.8
50	100	100	100	98.2	96.4	91.6	94.4	78.8	57
53	100	100	100	98.1	96	90.6	93.8	76.6	53.5
63	100	100	100	97.7	94.6	87.3	91.7	69.4	42.7
75	99.7	99.3	99.3	95.9	90.9	80.4	86.6	58	31.1
90	98.1	96.8	97.4	92.4	83.8	66.6	75.8	41.5	20.4
100	97.3	95.3	95.9	89.9	77.9	55.6	66.6	31.6	15.5
106	96.9	94.5	94.7	88.1	73.6	48.8	60.4	26.6	13.3
125	94.5	91.1	88.6	80	56.6	29	39.5	14.6	8.15
140	89.9	86.5	79.9	69.9	41	17.7	24.4	8.92	5.44
150	85.8	82.7	72.4	61.8	30.8	12.3	16.3	6.18	3.93
180	66.7	65.5	44.9	34.6	8.32	4.29	2.72	1.41	0.76
200	47.3	47.4	28	19.7	1.96	2.35	0.43	0.28	0.11
250	5.43	5.89	3.74	1.79	0.001	0.34	0	0	0
300	0	0	0.046	0.013	0	0.004	0	0	0
$d_{v,0.5}$ (μm)	**188.3**	**184.7**	**169.5**	**152.2**	**121.5**	**97.94**	**106.8**	**73.98**	**53.15**
Wt. % O/size	77	52	24	16	13	6.0	8.1	9.0	7.0

Table A4.5: Effect of oscillation frequency and amplitude on particle size distribution (α=25%, L=368mm)

d_i (μm)	Cumulative Volume Oversize (%)								
	x_o = 50mm			x_o = 75mm			x_o = 100mm		
	f=0.8 Hz	f=1.0 Hz	f=1.2 Hz	f=0.8 Hz	f=1.0 Hz	f=1.2 Hz	f=0.8 Hz	f=1.0 Hz	f=1.2 Hz
0	100	100	100	100	100	100	100	100	100
20	100	100	99.8	99.7	98.6	95.3	97.8	90.9	91.6
38	100	99.5	98.8	98.4	94.9	78.5	93.3	65.5	55.9
50	100	98.4	97.2	96.8	89.3	64	87.5	44.1	29.9
53	100	98.2	96.9	96.4	88.1	60.9	86.3	39.5	25.2
63	100	97.3	95.8	95.4	84.3	50.8	82.3	25.7	14.5
75	99.6	94.8	93	92.9	76.3	37.6	73.2	13.5	7.66
90	97.6	90	87.8	88.1	60.4	23.1	54.7	5.54	3.77
100	96.5	86.4	83.8	84.4	48.1	16.1	41.7	3.09	2.54
106	95.9	84	81.1	81.8	40.8	13.1	34.8	2.2	2.11
125	93	74.9	70.3	71	20.7	6.85	18.3	0.49	1.32
140	88.5	65.3	59.1	59.3	10.1	4.07	11.1	0.077	0.94
150	84.6	58	50.9	50.7	5.37	2.64	8.04	0.006	0.67
180	97	34.3	26.6	25.4	0.26	0.27	3.12	0	0.057
200	48.9	20.9	14.6	13.2	0.008	0.014	1.55	0	0.002
250	6.57	2.65	1.24	0.7	0	0	0.11	0	0
300	0	0.031	0.001	0.003	0	0	0.001	0	0
$d_{v,0.5}$ (μm)	**187.9**	**149.2**	**139.4**	**138.6**	**89.76**	**56.61**	**86.25**	**43.58**	**39.46**
Wt. % O/size	68	29	18	16	14	5	5	7	7

Table A4.6: Effect of oscillation frequency and amplitude on particle size distribution (α=25%, L=263mm)

% > d_i (by vol.)	d_i (μm)								
	x_o = 50mm			x_o = 75mm			x_o = 100mm		
	f=0.8 Hz	f=1.0 Hz	f=1.2 Hz	f=0.8 Hz	f=1.0 Hz	f=1.2 Hz	f=0.8 Hz	f=1.0 Hz	f=1.2 Hz
0	339.8	339.8	309.6	282.1	256.8	282.1	282.1	309.6	256.8
5	270.1	256.2	219.2	209.6	160.2	172.9	174.7	163.9	150.6
10	252.9	241.9	203.5	193.2	139	152	153.2	132.6	115.8
20	232	221.3	182.9	173.6	116	122.6	124.8	98.07	80.86
25	224.5	212.6	174.8	166.2	108.4	111.6	114.9	90.07	71.97
30	216.9	206	168	159.3	102.1	102.9	106.6	83.88	64.78
40	203.8	192.9	155.2	147.1	91.66	89.44	93.45	74.41	53.49
50	191.5	181.2	143.1	136.1	82.38	78.84	82.78	65.79	45.42
60	179.6	169.6	131	125.2	72.95	68.82	72.7	56.69	39.22
70	167	157.4	117.6	113.6	61.91	57.03	61.05	46.86	33.71
75	160.4	150.6	110.1	107.1	55.38	50.29	53.99	42.3	30.78
80	152.3	142.9	101.5	100	48.96	43.97	47	38.01	27.55
90	131	121.1	80.39	81.81	37.98	30.61	34.16	26.9	20.22
95	106.7	94.8	65.32	66.77	30.84	19.39	21.84	19.56	15.8
$d_{v,0.5}$ (μm)	**183.7**	**173**	**133.7**	**128.6**	**75.85**	**71.35**	**75.22**	**62.29**	**46.56**
Wt. % O/size	64	44	16	16	9	3	9	6	7

Appendix 4.2 Molecular Weight Data

Table A4.7: Average molecular weight data (α=20%, L=315mm)

f (Hz)	x_o (mm)	Weight average (Mw)	Number average (Mn)	Weight average peak (Mp)	Polydispersity index D = Mw/Mn
0.8	50	793731	233689	868031	3.397
1.0	50	902391	310479	1029827	2.906
1.2	50	959706	238959	1224797	4.016
0.8	75	667165	223416	396691	2.986
1.0	75				
1.2	75	731438	230980	432458	3.167
0.8	100	988765	305288	1196205	3.239
1.0	100	847158	253875	406877	3.337
1.2	100	729646	143529	365313	5.084

Table A4.8: Average molecular weight data (α=25%, L=315mm)

f (Hz)	x_o (mm)	Weight average (Mw)	Number average (Mn)	Weight average peak (Mp)	Polydispersity index D = Mw/Mn
0.8	50	428506	88137	236677	4.862
1.0	50	510293	116645	302737	4.375
1.2	50	512823	116140	298843	4.416
0.8	75	784449	228916	925577	3.427
1.0	75	755462	221318	986086	3.413
1.2	75	764685	187009	1107625	4.089
0.8	100	487523	102671	266997	4.748
1.0	100	928862	318342	866928	3.087
1.2	100	454928	86402	244722	5.265

Table A4.7: Average molecular weight data (α=30%, L=315mm)

f (Hz)	**x_o (mm)**	**Weight average (Mw)**	**Number average (Mn)**	**Weight average peak (Mp)**	**Polydispersity index D = Mw/Mn**
0.8	50	725742	171618	688565	4.287
1.0	50	735267	182477	374946	4.029
1.2	50	919700	245337	978881	3.749
0.8	75	1129323	301813	1315845	3.742
1.0	75	754395	210933	766931	3.576
1.2	75	906042	240504	1087206	3.767
0.8	100	903378	269426	1058407	3.353
1.0	100	948569	275560	1005397	3.442
1.2	100	1024223	277050	993469	3.697

Table A4.9: Average molecular weight data (α=25%, L=368mm)

f (Hz)	x_o (mm)	Weight average (Mw)	Number average (Mn)	Weight average peak (Mp)	Polydispersity index D = Mw/Mn
0.8	50	706186	137815	251185	5.124
1.0	50	719161	169288	249458	4.248
1.2	50	792470	180032	1023960	4.403
0.8	75	868107	244369	986585	3.552
1.0	75	808079	267258	982451	3.024
1.2	75	755717	215900	895995	3.500
0.8	100	811520	237905	998560	3.411
1.0	100	810718	214906	929251	3.772
1.2	100	815538	246710	952017	3.306

Table A4.10: Average molecular weight data (α=25%, L=263mm)

f (Hz)	**x_o (mm)**	**Weight average (Mw)**	**Number average (Mn)**	**Weight average peak (Mp)**	**Polydispersity index D = Mw/Mn**
0.8	50	546636	126263	323270	4.329
1.0	50	627440	142795	408102	4.394
1.2	50	566838	120589	304842	4.701
0.8	75	601896	125246	339159	4.806
1.0	75	523714	115124	288906	4.549
1.2	75	474842	73518	214359	6.459
0.8	100	494065	84808	268287	5.826
1.0	100	566320	117693	314706	4.812
1.2	100	504417	101107	294712	4.989

Appendix 4.3: Residual BPO Content

Table A4.11: Residual BPO content of polymer beads

f (Hz)	x_o (mm)	α (%)	L (mm)	BPO (%)
0.8	50	20	315	0.705
1.0	50	20	315	0.864
1.2	50	20	315	0.862
0.8	75	20	315	0.728
1.0	75	20	315	0.750
1.2	75	20	315	0.721
0.8	100	20	315	0.874
1.0	100	20	315	0.816
1.2	100	20	315	0.772
0.8	50	25	315	0.800
1.0	50	25	315	
1.2	50	25	315	0.780
0.8	75	25	315	0.750
1.0	75	25	315	0.699
1.2	75	25	315	
0.8	100	25	315	0.790
1.0	100	25	315	0.700
1.2	100	25	315	0.800
0.8	50	30	315	0.770
1.0	50	30	315	0.803
1.2	50	30	315	0.742
0.8	75	30	315	0.790
1.0	75	30	315	0.810
1.2	75	30	315	0.846
0.8	100	30	315	0.747
1.0	100	30	315	0.676
1.2	100	30	315	0.755
0.8	50	25	386	0.701
1.0	50	25	386	0.756
1.2	50	25	386	0.812
0.8	75	25	386	0.745
1.0	75	25	386	0.810
1.2	75	25	386	0.777
0.8	100	25	386	0.780
1.0	100	25	386	0.709
1.2	100	25	386	0.678
0.8	50	25	263	0.788
1.0	50	25	263	0.803
1.2	50	25	263	0.742
0.8	75	25	263	0.801
1.0	75	25	263	0.850
1.2	75	25	263	0.822
0.8	100	25	263	0.790
1.0	100	25	263	0.800
1.2	100	25	263	0.780

REFERENCES

Ahmed, S. M., (1984), Effects of agitation, an the nature of protective colloid on the particle size during suspension polymerization, J. Dispersion Sci. Tech., 5 (3&4), pp. 421-432

Armenante, P. M. and Huang, Y-T., (1992), Experimental determination of the minimum agitation speed for complete liquid-liquid dispersion in mechanically agitated tanks, Ind. Eng. Chem. Res., 31, pp. 1398-1406

Arshady, R., (1992), Suspension, emulsion, and dispersion polymerization: a methodological survey, Colloid Polym Sci., 270, pp. 717-732

Aspostolidou, C. and Stamatopudis, M., (1990), On particle size distribution in suspension polymerisation of styrene, Collect. Czech. Chem. Commun., 55, pp. 2244-2251

Baillagou, P. E. and Soong, D. S., (1985a), Major factors contributing to the nonlinear kinetics of free-radical polymerization, Chem. Engng. Sci., 40 (1), pp. 75-86

Baillagou, P. E. and Soong, D. S., (1985b), Molecular weight distribution of products of free radical nonisothermal polymerization with gel effect. Simulation for the polymerization of poly(methylmethacrylate), Chem. Engng. Sci., 40 (1), pp. 87-104

Baird, M. H. I., Gloyne, A. R., Meghani, A. N., (1986), Solvent extraction in an air-pulsed packed column, Can. J. Chem. Eng., 46, pp. 249-252

Baird, M. H. I. and Lane, S. J., (1973), Drop size and hold-up in a reciprocating plate extraction column, Chem. Engng. Sci., 28, pp. 947-957

Baird, M. H. I. and Rama Rao, N. V., (1995), Power dissipation and flow patterns in reciprocating baffle-plate columns, Can. J. Chem. Eng., 73, pp. 417-425

Baird, M. H. I. and Rama Rao, N. V., (1998), Characteristics of of a countercurrent reciprocating plate bubble column. II. axial mixing and mass transfer, Can. J. Chem. Eng., 66, pp. 222-231

Baird, M. H. I., Rama Rao, N. V., Vijayan, S., (1992), Axial mixing and mass transfer in a vibrating perforated plate extraction column, Can. J. Chem. Eng., 70, pp. 69-76

Baird, M. H. I., and Stonestreet, P., (1995), Energy dissipation in oscillatory flow in a baffled tube, Trans IChemE., 73 (A), pp. 503-511

Baird, M. H. I., Vijayan, S., Rama Rao, N. V., Rohatgi, A., (1989), Extraction and absorption with a vibrating perforated plate, Can. J. Chem. Eng., 67, pp. 787-800

Batchelor, G. K., (1982), The theory of homogeneous turbulence, Cambridge University Press, Cambridge

Bates, R. L., Fondy, P. L., Corpstein, R. R., (1963), An examination of some geometric parameters of impeller power, Ind. Eng. Chem., 2, pp. 310-314

Beckmann, G., (1973), Design of large polymerisation reactors, Advances in Chemistry Series, 128, pp. 37-50

Bellhouse, B. J., Bellhouse, F. H., Curl, C. M., MacMillan, T. I., Gunnin,g A. J., Spratt, E. H., MacMurray, S. B., Nelems J. M., (1973), A high efficiency membrane oxygenaor and and pulsatile pumping system and its application to animal trials, Trans. Amer. Soc. Artif. internal Organs, 19, pp. 72-29

Billingham, N. C., (1989), Molecular weight distributions, in comprehensive polymer science (edited by Geoffrey, A. and Bevington, J. C.), Pergamon, London

Bisenberger, J. A. and Sebastian, D. H., (1983), Principles of polymer engineering, Wiley, New York.

Blondeau, D., Bigan, M., Despres, P., (1995), Ultrasound suspensio polymerisation method for preparation of 2-hydroxyethylmethacrylate macroporous copolymers, Reactive and Fundamental Polymers, 27, pp. 163-173

Bourne, J. R. and Baldyga, J., (1994), Drop break-up in the viscous subrange: a source of possible confusion, Chem. Engng. Sci., 49, pp. 1077-1078

Brandrup, J., Immergut, E. H., Grulke, E. A., (1999), Polymer handbook, 4th edition, Wiley, New York

Brooks, B. W., (1990), Basic aspects and recent developments in suspension polymerisation, Makromol. Chem. Macromol. Symp., 35/36, pp. 121-140

Brown, D. E. and Pitt, K., (1970), Drop break-up in a stirred liquid-liquid contactor, Inst. Chem. Engrgs. Symp. Ser., Chemeca '70, pp. 83-97

Brown, D. E. and Pitt, K., (1972), Drop size distribution of non-coalescing liquid-liquid system, Chem. Engng. Sci., 27, pp.577-583

Brunold, C. R., Hunns, J. C. B., Mackley, M. R. and Thompson, J. W., (1989), Experimental observations of flow patterns and energy losses for oscillatory flow in ducts containing sharp edges, Chem. Engng. Sci., 44, pp. 1227-1244

Calabrese, R. V., Chang, T. P. K., Dang, P. T., (1986), Drop break-up in turbulent stirred tank contactors. Part I: Effect of dispersed phase viscosity, AIChE J., 32 (4), pp. 657-666

Calabrese, R. V., Wang, C. Y., Bryner, N. P., (1986), Drop break-up in turbulent stirred tank contactors. Part III: Correlations for mean size and drop size distribution, AIChE J., 32 (4), pp. 677-681

Chatzi, E. G., Boutris, C. J., Kiparissides, C., (1991a), On-line monitoring of drop size distributions in agitated vessels. 1. Effects of temperature and impeller speed, Ind. Eng. Chem. Res., 30, pp. 536-543

Chatzi, E. G., Boutris, C. J., Kiparissides, C., (1991b), On-line monitoring of drop size distributions in agitated vessels. 2. Effect of stabiliser concentration, Ind. Eng. Chem. Res., 30, pp. 1307-1313

Chen, T. H. and Middleman, S., (1967), Drop size distribution in agitated liquid-liquid systems, AIChE J., 13, pp. 989-995

Church, J. M. and Shinnar, R., (1961), Stabilising liquid-liquid dispersions by agitation, Ind. Engng. Chem., 53 (6), pp. 479-484

Coulaloglou, C. A. and Talvarides, L. L., (1977), Description of interaction processes in agitated liquid-liquid dispersions, Chem. Engng. Sci., 32, pp. 1289-1297

Davidson, J. A. and Witenhafer, B. F., (1980), Particle structure of suspension poly(vinyl chloride) and its origin in the polymerization process, J. Appl. Polym. Sci., 18, pp. 51-69

Dawkins, J. V., (1989) Aqueous suspension polymerisations, in comprehensive polymer science (edited by Geoffrey, A. and Bevington, J. C.), Pergamon, London

Deslandes, Y., (1987), Morphology of hydroxyapatite as suspension stabilizer in the polymerization of poly(styrene-co-butadiene), J. Appl. Polym. Sci., 34, pp. 2249-2257

Dickens, A. W., Mackley, M. R., Williams, H. R., (1989), Experimental residence time distribution measurements for unsteady flow in baffled tubes. Chem. Engng. Sci., 44, pp. 1471-1479

Erbay, E., Bilgic, T., Karali, M., Savasci, O. T., (1992), Polystyrene suspension polymerisation: the effect of polymerisation parameters on particle size distribution, Polym. Plast. Technol. Eng., 31, pp. 598-605

Esch, D. D., D'Angelo, P. J., Pike, R. W., (1971), On the minimum power requirements for emulsification of a two-phase, liquid system, Can. J. Chem. Eng., 49, pp. 872-875

Gough, P., Ni, X. and Symes, K. C., (1997), Experimental flow visualisation in a modified pulsed baffled reactor, J. Chem. Tech. Biotechnol., 69, pp. 321-328

Hazef, M. M., Baird, M. H. I., Nirdosh, I., (1979), Flooding and axial dispersion in reciprocating plate extraction columns, Can. J. Chem. Eng., 57, pp. 150-158

Hazef, M. M., Baird, M. H. I., Nirdosh, I., (1980), A model for reciprocating plate extraction columns, proc. intl. solvent extr. conf.

Hewgill, M. R., Mackley, M. R., Pandit, A. B., Pannu, S. S., (1993), Enhancement of gas-liquid mass transfer using oscillatory flow in a baffled tube, Chem. Engng Sci., 48, pp. 799-809

Hinze, O. J., (1955), Fundamentals of the hydrodynamic mechanism of splitting in dispersion processes, AIChE J., 1, pp. 289-295

Hoffman, F., and Delbruch, K., (1909), Ger. Pat. 250690. Ferbenfabriken Bayer, Germany

Holland, F. A. and Chapman, F. S., (1966), Liquid mixing and processing in stirred tanks, Reinhold Publishing, New York, 147-186

Hopff, H., Lussi, H., Hammer, E., (1964), Zur Kenntnes der perpolymerisation. 2. Mitt Praktische anwendung der dimendionsanalyse auf das system MMA-Mowiol N70/88, Makromol. Chem., 82, pp. 175-183

Horak, D, (1996), Uniform polymer beads of micrometer size, ACTA Polymerica, 47, pp. 20-28

Hosogai, K. and Tanaka, M., (1992a), Effect of impeller diameter on the mean droplet diameter in circular loop reactor, Can. J. Chem. Eng., 70, pp. 6458-653

Hosogai, K. and Tanaka, M., (1992b), Study of suspension polymerization of styrene with a circular loop ractor, Polym. Eng. Sci., 32 (6), pp. 431-437

Hounslow, M. J., (1990), A discretized population balance for continuous steady state systems, AIChE J., 36 (1), pp. 106-116

Hounslow, M. J., Ryall, R. L., Marshall, V. R., (1988), A discretized population balance for nucleation, growth, and aggregation, AIChE J., 34 (11), pp. 1821-1832

Howard, F. R., (1977), Chemical reactor design for process plants. Volume 1: principles and techniques, John Wiley & Sons, New York, pp. 5-12

Howell, J. A., Field, R. W., Wu, D., 1993, Yeast cell microfiltration: flux enhancement in baffled and pulsatile flow systems., J. Membrane Sci., 80, pp. 59-71

Howes, T. and Mackley, M. R., (1990), Experimental axial dispersion for oscillatory flow through a baffled tube, Chem. Engng. Sci., 45, pp. 1349-1358

Howes, T., Mackley, M. R., Roberts, E. P. L., (1991), The simulation of chaotic mixing and dispersion for periodic flows in baffled channels, Chem. Engng. Sci., 46, pp. 1669-1677

Jealous, A. E. and Johnson, H. F., (1955) Power Requirements for Pulse Generation in Pulsed Columns, Ind. Eng. Chem. 47, pp. 1159-1166

Kaflas, G. ands Ray, W. H., (1993a), Modeling and experimental studies of aqueous suspension polymerization processes, 1. Modeling and simulation, Ind. Eng. Chem. Res., 32, pp. 1822-1830

Kaflas, G. ands Ray, W. H., (1993b), Modeling and experimental studies of aqueous suspension polymerization processes, 2. Experiments in batch reactors, Ind. Eng. Chem. Res., 32, pp. 1831-1838

Kamiyama, M., Koyama, K., Matsuda, H., Sano, Y., (1993), Micron-sized polymeric microsphere by suspension polymerization, J. Appl. Polym. Sci., 50, pp. 107-113

Karr, A. E., (1959), Performance of a reciprocating plate extraction column, AIChE J., 5 (4), pp. 446-452

Karr, A. E. and Lo T. C., (1971), Performance and scale-up of a reciprocating plate extraction column, proc intrn solvent extrac conf, 1, pp. 299-320

Kim, S. D. and Baird, M. H. I., (1976) Effect of hole size on hydrodynamics of a reciprocating perforated plate extraction column, Can. J. Chem. Eng., 54, pp. 235-237

Knott, G. F. and Mackley, M.R., (1980), On eddy motions near plates and ducts, induced by water waves and periodic flows, Phil. Trans. R. Soc., 294, pp. 599-628

Kolmogoroff, A., (1941), The local structure of turbulence in incompressible viscous fluids for very large Reynolds numbers, C. R. Acad. Sci. U. R. R. S., 30, pp. 301-305

Konno, M., Aria, K., Saito, S., (1977), The effects of viscous and inertial forces on drop break-up in an agitated tank, J. Chem. Eng. Jpn, 10, pp. 474-477

Konno, M., Aria, K., Saito, S., (1982), The effect of stabilizer on coalescence of dispersed phase drops in suspension polymerisation of styrene, J. Chem. Eng. Jpn, 15 (2), pp. 131-135

Kumar, A. and Gupta, S. K., (1978), Fundamentals of polymer sciance and engineering, McGraw-Hill publishing co. Ltd., New Delhi, pp. 200-215

Langner, F., Moritz, H., Reichert, K., (1979), On particle size of suspension polymers, II. polymerising two-phase systems, Ger. Chem. Eng., 2, pp. 329-336

Laso, M., Steiner, L., Hartland, S., (1987a), Dynamic simulation of liquid-liquid agitated dispersions. I. Derivation of a simple model, Chem. Engng. Sci., 42, pp. 2429-2436

Laso, M., Steiner, L., Hartland, S., (1987b), Dynamic simulation of liquid-liquid agitated dispersions. II. Experimental determination of breakage and coalescence rates in a stirred tank, Chem. Engng. Sci., 42, pp. 2437-2445

Lee, J. C. and Tasakorn, P., (1979), Characteristics of agitated tanks in relation to suspension polymerisation, Proc. 3rd European Conference on Mixing, University of York, U.K., pp. 157-170

Leng, D. E. and Guarderer, G. J., (1982), Drop dispersion in suspension polymerisation, Chem. Eng. Commun., 14, pp. 177-201

Lister, J. D., Smit, D. J., Hounslow, M. J., (1995) Adjustable discretized population balance for growth and aggregation, AIChE J., 41 (3), pp. 591-603

Lo, T.C. and Karr A. E., (1972), Development of a laboratory-scale reciprocating plate extraction column, Ind. Eng. Chem. Process Des. Develop., 11 (4), pp. 495-501

Louie, B. M., Garratt, G. M., Soong, D. S., Modelling the free radical solution and bulk ploymerisation of methyl methacrylate, J. Appl. Polym. Sci., 30, pp. 3985-4012

Mackay, M. E., Mackley, M. R. and Wang, Y., (1991), Oscillatory flow within tubes containing wall or central baffles, Trans. IChemE, 69(A), pp. 506-513

Mackley, M. R., (1987), The use of oscillatory flow to improve performance, The Chemical Engineer, , pp.

Mackley, M. R. and Ni, X., (1991), Mixing and dispersion in a baffled tube for steady laminar and pulsatile flow, Chem. Engng. Sci., 46, pp. 3139-3151

Mackley, M. R. and Ni, X., (1993), Experimental fluid dispersion measurements in periodic baffled tube arrays, Chem. Engng. Sci., 48, pp. 3293-3305

Mackley, M. R., Smith, K. B., Wise N. P., (1993), The mixing and separation of particle suspensions using oscillatory flow in baffled tubes, Trans. IChemE, 71 (A), pp. 649-656

Mackley, M. R. and Stonestreet, P., (1995), Heat transfer and associated energy dissipation for oscillatory flow in baffled tubes, Chem. Engng. Sci., 50, pp. 2211-2224

Mackley, M. R., Stonestreet, P., Thurston, N. C., Wiseman, J. S., (1998), Evaluation of a self-aerating, oscillatory baffled column, Can. J. Chem. Eng., 76, pp. 5-10

Mackley, M. R., Tweddle, G. M., Wyatt, I. D., (1990), Experimental heat transfer measurements for pulsatile flow in baffled tubes, Chem. Engng. Sci., 45, pp. 1237-1242

Madden, A. J. and McCoy, B. J., (1964), On the problem of determining drop size distribution in stirred liquid-liquid systems, Chem. Engng. Sci., 19, pp. 505-507

McCoy, B. J. and Madden, A. J., (1969), Drop size in stirred liquid-liquid systems via encapsulation, Chem. Engng. Sci., 24, pp. 419-421

McDonough, R. J., (1992), Mixing for the process industries, Van Nosrtand Reinhold, New York

Miyanami, K., Tojo, K., Yano, T., (1973), Liquid phase mixing in a MDVC with concurrent gas-liquid flow, J. Chem. Eng. Jpn., 6 (6), pp. 518-522

Miyanami, K., Tojo, K., Yano, T., Miyaji, K., Minami, I., (1975), Drop size and hold-ups in a multistage vibrating disk column, Chem. Engng. Sci., 30, pp. 1415-1420

Mlynek, Y. and Resnick, W., (1972), Drop sizes in agitated liquid-liquid systems, AIChE J., 18, pp. 122-127

Munzer, M., Tromsdorff, E., Rochm, G., (1977), Polymerisation in suspension, in polymerisation processes (edited by Schndknecht, C. E. and Skeist, I.), Wiley, New York, pp. 106-142

Nambiar, D. K. R., Kumar, R., Das, T. R., Gandhi, K. S., (1994), A two-zone model for breakage frequency of drops in stirred dispersions, Chem. Engng. Sci., 49 (13), pp. 2194-2198

Ni, X., (1994), Residence time distribution measurements in a pulsed baffled tube bundle, J. Chem. Tech. Biotechnol., 59, pp. 213-221

Ni, X., (1995), A study of fluid dispersion in oscillatory flow through a baffled tube, J Chem. Tech. Biotechnol., 64, pp. 165-174

Ni, X., Bennette, D. C., Johnstone, J. C., Symes, K. C., Grey, B. D., (2000), Inverse phase suspension polymerisation of acrylamide in a batch oscillatory baffled reactor -- from droplets to particles, submitted to Chem. Eng. Sci.

Ni, X., Brogan, G., Struthers, A., Bennett, D. C., Wilson, S. F., (1998a), A systematic study of the effect of geometrical parameters on the mixing time in oscillatory baffled columns, Trans. IChemE, 76 (A), pp. 635-642

Ni, X. and Gao, S., (1996a), Mass transfer characteristics of a pilot pulsed baffled reactor, J. Chem. Tech. Biotechnol., 65, pp. 65-71

Ni, X. and Gao, S., (1996b), Scale-up correlation for mass transfer in pulsed baffled reactors, Chem. Eng. J., 63, pp. 157-166

Ni, X., Gao, S., Cumming, D. W., (1995), , Biotechnol. Bioeng., pp. 165-

Ni, X., Gao, S., Cumming, R. H. and Pritchard, D. W., (1995), A comparative study of mass transfer in yeast for a batch pulsed baffled bioreactor and a stirred tank fermenter, Chem. Engng. Sci., 50, pp. 2127-2136

Ni, X. and Gough, P., (1997), On the dimensionless groups governing oscillatory flow in a baffled tube, Chem. Engng. Sci., 52, pp. 3209-3212

Ni, X. and Mackley, M. R., (1993), Chemical reaction in batch pulsatile flow and stirred tank reactors, Chem. Eng. J., 52, pp. 107-114

Ni, X. and Pereira, N. E., (2000), Parameters affecting fluid dispersion in a continuous oscillatory baffled tube, AIChE J., 46 (1), pp. 37-45

Ni, X., Zhang, Y., Mustafa, I., (1997), Experimental heat transfer measurement in a batch oscillatory-baffled reactor, AIDIC conf. ser., 2, pp. 271-278

Ni, X., Zhang, Y., Mustafa, I., (1998b), An investigation of droplet size and size distribution in methylmethacrylate suspension in a batch oscillatory-baffled reactor, Chem. Engng. Sci., 53 (16), pp.2903-2919

Ni, X., Zhang, Y., Mustafa, I., (1999), Correlation of polymer particle size with droplet size in suspension polymerisation of methylmethacrylate in a batch oscillatory-baffled reactor, Chem. Engng. Sci., 54, pp.841-850

Okufi, S., Perez de Ortiz, S., Sawistowski, H., (1990), Scale-up of liquid-liquid dispersions in stirred tanks, Can. J. Chem. Eng., 68, pp. 400-406

Omi, S., (1996), Preparation of mondisperse microspheres using Shirasu porous glass emulsification technique, Colloids Surfaces A: Physicochem. Eng. Aspects, 109, pp. 97-107

Omi, S., Katami, K., Yamamoto, A., Iso, M., (1994), Synthesis of polymeric microspheres employing SPG emusification technique, J. Appl. Polym. Sci., 51, pp. 1-11

Pacek, A. W., Moore, I. P. T., Calabrese, R. V., Nienow, A. W., (1993), Evolution of drop size distribution and average drop size in liquid-liquid dispersions before and after phase inversion, Trans. IChemE, 71 (A), pp. 340-341

Pacek, A. W., Moore, I. P. T., Nienow, A. W., Calabrese, R. V., (1994), Video technique for measuring dynamics of liquid-liquid dispersion during phase inversion, AIChE J., 40, pp. 1040-1049

Pacek, A. W. and Nienow, A. W., (1995), Measurement of drop size distributions in concentrated liquid-liquid dispersions: video and capillary techniques, Trans. IChemE, 73 (A), pp. 512-518

Pacek, A. W., Nienow, A. W., Moore, I. P. T., (1994), On the structure of turbulent iquid-liquid dispersed flows in an agitated vessel, Chem. Engng. Sci., 49 (20), pp. 3485-3498

Pantagiotou, T. and Levindis, Y. A., (1991), Generation of spherical and monodispersed particles of poly(styrene) and poly(methylmethacrylate) by atomization of monomers and dissolved polymer precursors, J. Appl. Polym. Sci., 43, pp. 1549-1558

Perry, J., (1997), Crystallisation in a pulsed baffled reactor, BEng (Hons) Final Year Project Thesis, University of Strathclyde, Glasgow, U.K.

Perry, R. H. and Green, D. W., (1998), Perry's chemical engineers' handbook (7th edition), McGraw Hill Publishing

Pla, F., (1995), Main chemical engineering parameters affecting radical polymerization processes in heterogeneous media, Macromol. Symp., 92, pp. 243-252

Polacco, G., Semino, D., Rizzo, C., (1994), Feasibility study of methylmethacrylate polymerization for bone cement by suspension polymerization in a gel phase, J. Mater. Sci. Mater. Medic., 5, pp. 587-591

Ramkrishna, D., (1985), The status of population balances, Reviews in Chem. Eng., 3, 49-95

Richard, L. and Babb, A. L., (1969), Holdup and axial distribution of holdup in a pulsed sieve-plate solvent extraction column, Ind. Eng. Chem. Process Des. Develop., 8 (3), pp. 392-400

Rushton, J. H., Costich, E. W., Everett, H. J., (1950), Power characteristics of mixing impellers, Chem. Eng. Progr., 46, pp.395-404

Saye, B. M. C., (2000), ON the interactions of droplets in oscillatory baffled reactors, M.Phil. Thesis, Heriot-Watt University, Edinburgh, U.K.

Schroder, R. and Bernhard, P., (1982), on particle formation during suspension polymerization of styrene, Ger. Chem. Eng., 5, pp. 139-146

Shinnar, R., (1960), On the behaviour of liquid dispersions in mixing vessels, Fluid Mech., 10, pp. 259-275

Skelland, A. H. P. and Lee, J. M., (1978), Agitator speeds in baffled vessels for uniform liquid-liquid dispersion, Ind. Eng. Chem. Process Des. Develop., 17 (4), pp. 473-478

Skelland, A. H. P. and Kanel, J. S., (1990), Minimum impeller speeds for complete dispersion of non-Newtonian liquid-liquid systems in baffled vessels, Ind. Eng. Chem. Res., 29, pp. 1300-1306

Skelland, A. H. P., and Ramsay, G. G., (1987), Minimum agitator speeds for complete liquid-liquid dispersion, Ind. Eng. Chem. Res., 26, pp. 77-81

Skelland, A. H. P. and Seksaria, R., (1978), Minimum impeller speeds for liquid-liquid dispersion in baffled vessels, Ind. Eng. Chem. Process Des. Develop., 17 (1), pp. 56-61

Smith, T. N., (1974), Measurement of drop size in liquid-liquid dispersions, Chem. Engng. Sci., 29, pp.583-587

Sobey I. J., (1980), On flow through furrowed channels. Part 1. Calculated flow patterns, J. Fluid Mech., 96, pp. 1-26.

Spaay, N. M., Simons, A. J. F., Ten Brink, G. P., (1971), Design and operation of a pulsed packed column for liquid-liquid extraction, Proc. Intl. Solvent Extr. Conf., 1, pp.281-289

Sprow, F. B., (1967a), Drop size distributions in strongly coalescing agitated liquid-liquid systems, AIChE J., 13, pp.995-998

Sprow, F. B., (1967b), Distribution of drop sizes produced in turbulent liquid-liquid dispersion, Chem. Engng. Sci., 22, pp. 435-442

Tanaka, M., Hesagawa, S., O' Shima, E., (1987), Inclusion of gas in the polymer particles in the suspension polymerisation of styrene, Kagaku Kogaku Ronbunshu, 13, pp. 693-697

Tanaka, M. and Hosogai, K., (1990), Suspension polymerization of styrene with a circular loop reactor, J. Appl. Polym. Sci., 39, pp. 955-966

Tanaka, M. and Izumi, T., (1985), Application of a stirred tank reactor equiped with draft tube to suspension polymerization of styrene, J. Chem. Eng. Jpn, 18, pp. 354-358

Tanaka, M. and O' Shima, E., (1988), Dispersing behaviour of droplets in suspension polymerization of styrene in a loop reactor, Can. J. Chem. Eng., 66. pp. 29-35

Tanaka, M., Takahashi, T., Kimaru, I., (1996), Effect of double agitation on particle size in suspension polymerization of styrene with a loop reactor, Chem. Eng. Technol., 19, pp. 97-102

Taylor, G. I., (1934), The information of emulsions in definable field of flow, Proc. Royal Soc. London, A146, pp. 501-512

Tojo, K, Miyanami, K., Yano, T., (1975), The effect of wave form of disk vibration on mass transfer in a MDVC with countercurrent liquid-liquid flow, J. Chem. Eng. Jpn., 8 (2), pp. 165-167

Tojo, K, Miyanami, K., Yano, T., (1976a), Axial mixing in a MDVC with countercurrent liquid-liquid flow, Chem. Eng. J., 11, pp. 101-104

Tojo, K, Miyanami, K., Yano, T., (1976b), Drop size and holdup in a MDVC, Chem. Engng. Sci., 30, pp. 1415-1420

Tojo, K, Miyanami, K., Yano, T., (1980), Design methods and performance characteristics of a MDVC extractor, Ind. Eng. Chem. Process Des. Develop., pp. 459-465

Tromsdorff, E., Koelhe, H., Lagally, P., (1974), Zur polymerisation des nethacrysaueremethlyestrers, Makromolek. Chem., 1, pp. 169-178

Tsouris, C. and Talvarides, L. L., (1994), Breakage and coalescence models for drops in turbulent dispersions, AIChE J., 40 (3), pp. 395-406

Valentas, K. J., Bilous, O., Amundson, N. R., (1966), Analysis of breakage in dispersed phase systems, Ind. Eng. Chem. Fundam., 5 (2), pp. 271-279

Van Dijick, W. J., (1935), US Patent 201186

Van Heuven, J. W., and Beek, W. J., (1971), Power input, drop size and minimum stirrer speed for liquid-liquid dispersion in stirred vessels, Proc. Intl. Solvent Extr. Conf., 1, pp. 70-81

Verhoff, F. H., Ross, S. L., Curl, R. L., (1977), Breakage and coalescence in an agitated dispersion, experimental system and data reduction, Ind. Eng. Chem. Fundam., 16 (3), pp. 371-376

Vivaldo-Lima, E., Wood, P. E., Hamielec, A. E., Penlidis, A., (1997), An updated review on suspension polymerization, Ind. Chem. Eng. Res., 36, pp. 939-965

Wang, C. Y. and Calabrese, R. V., (1986),), Drop break-up in turbulent stirred tank contactors. Part II: Relative influence of viscosity and interfacial tension, AIChE J., 32 (4), pp. 667-676

Wang, Y., Howell, J. A., Field, R .W. and Mackley, M. R., (1994), Oscillatory flow within porous tubes containing wall or central baffles, Trans. IChemE, 72 (A), pp. 686-694

Weinstein, B. and Treybal, R. E., (1973), Liquid-liquid contacting in unbaffled, agitated vessels, AIChE J., 19 (2), pp.304-311

Ventoura, A., (1997), Crystallization in a pulsed baffled reactor, MSc Thesis, University of Strathclyde, Glasgow, U.K.

Yang, N. S., Chen, B. H., McMillan, A. F., (1986a), Axial mixing and mass transfer in gas liquid Karr columns, Ind. Eng. Chem. Process Des. Develop., 25, pp. 776-780

Yang, N. S., Shen, Z-Q., Chen, B. H., McMillan, A. F., (1986b), Pressure drop, Gas holdup and interfacial area for gas-liquid contact in Karr columns, Ind. Eng. Chem. Process Des. Develop., 25 (3), pp. 660-664

Yuan, H. G., Kaflas, G., Ray, W. H., (1991), Suspension polymerisation, Jms-Rev. Macromol. Chem. Phys., C31, pp. 215-299

Zhang, Y., (1998), A study of suspension polymerisation of methylmethacrylate and styrene in an oscillatory baffled reactor, Ph.D. thesis, University of Strathclyde, Glasgow, U.K.

Zhang, Y., Ni, X., Mustafa, I., (1996), A study of oil-water dispersion in a pulsed baffled reactor, J. Chem. Tech. Biotechnol., 66, pp. 305-311

Zeltin, M. A. and Talvarides, L. L., (1972), Fluid-fluid interactions and hydrodynamics in agitated dispersions: a simulation model, Can. J. Chem. Eng., 50, pp. 207-215

Zerfa, M. and Brooks, B. W., (1996), Prediction of vinyl-chloride drop size instabilised liquid-liquid agitated dispersion, Chem. Engng. Sci., 51, pp. 3223-3233